THEORETICAL STUDIES OF THE EXTERNAL VIBRATIONAL CONTROL OF ELECTRONIC EXCITATION TRANSFER AND ITS OBSERVATION USING POLARIZATION- AND OPTICAL PHASE-SENSITIVE ULTRAFAST SPECTROSCOPY

by

JASON DANIEL BIGGS

A DISSERTATION

Presented to the Department of Chemistry
and the Graduate School of the University of Oregon
in partial fulfillment of the requirements
for the degree of
Doctor of Philosophy

December 2010

"Theoretical Studies of the External Vibrational Control of Electronic Excitation Transfer and Its Observation Using Polarization- and Optical Phase-sensitive Ultrafast Spectroscopy," a dissertation prepared by Jason Daniel Biggs in partial fulfillment of the requirements for the Doctor of Philosophy degree in the Department of Chemistry. This dissertation has been approved and accepted by:

_____

Dr. Michael E. Kellman, Chair of the Examining Committee

_____

Date

Commitee in charge:

Dr. Michael E. Kellman, Chair
Dr. Jeffrey A. Cina, Advisor
Dr. David R. Herrick
Dr. Andrew H. Marcus
Dr. Daniel A. Steck

Accepted by:

_____

Dean of the Graduate School

An Abstract of the Dissertation of

Jason D. Biggs for the degree of Doctor of Philosophy

in the Department of Chemistry to be taken December 2010

Title: THEORETICAL STUDIES OF THE EXTERNAL VIBRATIONAL CONTROL OF ELECTRONIC EXCITATION TRANSFER AND ITS OBSERVATION USING POLARIZATION- AND OPTICAL PHASE-SENSITIVE ULTRAFAST SPECTROSCOPY

Approved: _____
Dr. Jeffrey A. Cina

Our theoretical studies involve the control of electronic energy transfer in molecular dimers through the preparation of specific vibrational coherences prior to electronic excitation. Our control strategy is based upon the fact that, following impulsive electronic excitation, nuclear motion acts to change the instantaneous energy difference between site-excited electronic states and thereby influences short-time electronic excitation transfer (EET). By inducing coherent intramolecular vibration in one of the chromophores prior to short-pulse electronic excitation, we exert external control over electronic dynamics.

As a means to monitor this coherent control over EET, we propose using multidimensional wave-packet interferometry (md-WPI). Two pairs of polarized phase-related femtosecond pulses following the control pulse would generate superpositions of coherent nuclear wave packets in optically accessible electronic states. Interference contributions to the time- and frequency-integrated fluorescence signal due to overlaps

among the superposed wave packets provide amplitude-level information on the nuclear and electronic dynamics.

We test both the control strategy and its spectroscopic investigation by calculating pump-probe difference signals for various combinations of pulse polarizations. That signal is the limiting case of the control-influenced md-WPI signal in which the two pulses in the pump pulse-pair coincide, as do the two pulses in the probe pulse-pair. We present calculated pump-probe difference signals for a variety of systems including a simplified model of the covalent dimer dithia-anthracenophane (DTA) in which we treat only the weakly Franck-Condon active ν_{12} anthracene vibration at 385 cm^{-1}. We further present calculated nl-WPI difference signals for an oriented DTA complex, which reveal amplitude-level dynamical information about the interaction of nuclear motion and electronic energy transfer.

We also present pump-probe difference signals from a model system in which a CF_3 group, whose torsional angle is strongly Franck-Condon active, has been added to the anthracene monomers which make up DTA. We make use of electronic structure calculations to find the torsional potential of the monomer, from which we calculate the spectroscopic signals of the dimer. We show that a significant measure of control over short-time EET is achievable in this system.

This dissertation includes previously published coauthored material.

CURRICULUM VITAE

NAME OF AUTHOR: Jason D. Biggs

GRADUATE AND UNDERGRADUATE SCHOOLS ATTENDED:

University of Oregon, Eugene, OR
Indiana University, New Albany, IN

DEGREES AWARDED:

Doctor of Philosophy, University of Oregon, 2010
Master of Science, University of Oregon, 2007
Bachelor of Science, Indiana University, 2005

AREAS OF SPECIAL INTEREST:

Vibrational wave packets
Electronic energy transfer
Quantum dynamics
Vegetable gardening

PROFESSIONAL EXPERIENCE:

Graduate Teaching Fellow, University of Oregon, 2005-2010
Adjunct Professor of Physics, Northwest Christian University, 2010

PUBLICATIONS:

Jason D. Biggs and Jeffrey A. Cina, "Monitoring the External Vibrational Control of Excitation-Energy Transfer Using Pump-Probe Polarization Spectroscopy," Proceedings of the 17th International Conference on Ultrafast Phenomena, Springer, New York (2010).

Jason D. Biggs and Jeffrey A. Cina, "Using Wave-Packet Interferometry to Monitor the External Vibrational Control of Electronic Excitation Transfer," *J. Chem. Phys.* **131**, 224101 (2009).

Jason D. Biggs and Jeffrey A. Cina, "Calculations of Nonlinear Wave-Packet Interferometry Signals in the Pump-Probe Limit as Tests for Vibrational Control over Electronic Excitation Transfer," *J. Chem. Phys.* **131**, 224302 (2009).

ACKNOWLEDGMENTS

I first thank my advisor, Jeff Cina, the guidance he has provided to me over the years. He has shown me the hard work and dedication needed to be a scientist, and helped me to gain the confidence needed to be one myself. I would like to thank the other members of the Cina research group, Craig Chapman, Xiaolu Cheng, and Phil Kovac, for engaging conversations, some of which concerned chemical physics. I also benefited greatly in my time here from the meetings of the Landau and Lifshitz reading group, where I learned so much more than I thought I did at the time.

I would like to thank my wife, Melissa, for all the support she has provided during the writing process and throughout my time in graduate school. It is because of her that I am here today, finishing what I started so many years ago. I also thank my mother, who helped to instill in me a love of learning that has never faded. Finally I would like to thank my daughter Beatrice, who makes me smile.

Laughter and tears are both responses to frustration and exhaustion.
I myself prefer to laugh, since there is less cleaning up to do afterward.
-Kurt Vonnegut

TABLE OF CONTENTS

Chapter Page

LIST OF FIGURES

Figure Page

Figure Page

LIST OF TABLES

Table Page

CHAPTER I

INTRODUCTION

A. Overview

The intramolecular exchange of photoinduced electronic energy is of fundamental importance in natural photosynthetic systems.[1,2] In this process molecular antenna complexes absorb sunlight, which promotes an electron to an excited energy level. This molecular excitation energy is then transferred to a reaction center where it is efficiently converted to chemical energy. This electronic excitation transfer (EET) must be very efficient in order to compete with other energy dissipation mechanisms available.

Early theoretical formulations of EET by Förster[3] focused on the determination of transfer rates between donor and acceptor chromophores. In this theory the EET rate depends on the overlap between donor emission and acceptor absorption spectra, as well as the distance between chromophores and the relative orientation between their transition dipoles. Prior knowledge of the spectra of the isolated chromophores, as well as a model for the distribution of relative orientations, allows for a straightforward determination of inter-chromophore distance using spectroscopic measurements in the presence of EET. The Förster theory has thus been of great utility in interpreting spectra in a wide variety of systems.[4–6]

The rate expressions derived by Förster assume, however, that the inter-chromophore coupling is weak and that the donor and acceptor interact strongly with a collection of vibrational modes, the "baths," and that these baths are independent of each other. This quickly

results in a loss of quantum mechanical coherence between donor- and acceptor-excited states, as the instantaneous transition energies of the donor and acceptor chromophores each fluctuate independently on a timescale fast compared to energy transfer. The picture of EET as an incoherent migration, a "hopping" process, are incompatible with recent experimental evidence[7–10] suggesting that quantum mechanical coherence can be long-lived, even at high temperatures. The extent to which quantum mechanics and nuclear motion play a role in photosynthesis is the subject of much current research and debate. The role of the protein environment in keeping excitation energies correlated even in the presence of thermal fluctuations is thought to be key to this phenomenon.[11]

When the assumption of independent baths is no longer valid, for example when there are nuclear modes common to both chromophores, and the neglect of quantum coherence becomes inadequate to explain the resulting behavior.[12,13] Much effort has gone towards understanding the limits of Förster theory,[14] and extending it to account for electronic coherence,[15,16] and multichromophoric systems.[17]

The interplay between nuclear motion and EET has also been the subject of numerous investigations, and is directly relevant to the subject of this dissertation. Nonequilibrium nuclear motion in Franck-Condon active vibrational modes, which acts to modulate the energy gap between donor- and acceptor-excited states and render the EET "rates" time-dependant, was treated within the framework of Förster theory by Jang, Jung, and Silbey.[18] Cina and Fleming showed[19] that wave-packet motion, coherent between donor- and acceptor-excited states, was consistent with polarized time-resolved fluorescence measurements on the LH-1 antenna of *Rhodobacter sphaeroides*.[20,21] Womick and Moran have investigated EET in light-harvesting dimers in the allophycocyanin protein of cyanobacteria using a variety of ultrafast spectroscopies.[22] They found that the efficient internal conversion between exciton states, a necessary step before the energy is transferred to the reaction center, is facilitated by a Franck-Condon active vibrational mode whose frequency is near in magnitude to the energy gap

between them.

Nuclear motion can also effect EET by modulating the electronic coupling directly. Jang has generalized Förster theory to account for the this effect,[23] deriving rate expressions for the cases where either the donor-acceptor distance or the angle between transition dipoles fluctuate as harmonic oscillators. Asadian *et al.* have recently studied the effect of nuclear motion on energy transfer efficiency in a theoretical model.[24] They considered a linear chain of electronically coupled chromophores, with the electronic excitation initially deposited at one end and a sink at the opposite end. In their treatment the distance between chromophores, of which the electronic coupling is a function, oscillates according to a classical trajectory. They found that for some values of the frequency and initial phase of nuclear motion, the asymptotic sink population was enhanced by nuclear motion relative to a static case in which the electronic couplings take a constant value. In these cases, nuclear motion acted to trap more excitation amplitude in the chromophore nearest to the sink than in the delocalized exciton states found in the static case.

The elucidation of molecular processes on ultrashort timescales has been enabled by the advent of a variety of ultrafast spectroscopic techniques, the interpretation of which has been greatly aided by the unified theoretical framework given by Mukamel.[25] Two-dimensional (2D) heterodyne-detected spectroscopy has proven to be a versatile tool.[26–30] In frequency-domain studies of this kind evidence for electronic coherence can be sought in the analysis of diagonal and anti-diagonal peak widths as a function of waiting time.[31] Mančal *et al.* showed that vibrational coherence manifests in 2D spectra by modulating the relative amplitude of peaks between absolute-value rephasing and non-rephasing signals,[32] as had been observed experimentally by Nemeth *et. al.*[33]

Wave-packet interferometry (WPI), in its linear and multidimensional (md) forms, is another form of ultrafast spectroscopy in which one or more pairs of collinear pulses, whose phase difference is externally manipulated, create superpositions of nuclear wave pack-

ets that evolve on excited-state potential surfaces.[34] The complex-valued interferograms give amplitude-level information on the overlap of these wave packets. Linear WPI, as exemplified by the pioneering studies by Scherer *et al.*,[35,36] directly probe the time-dependant kernel function from which the linear absorption spectrum can be obtained.[37] There is an analogous relationship between md-WPI, as developed theoretically by Humble and Cina,[38] and 2D electronic spectroscopy. WPI is a fluorescence-detected method and does not depend on the creation of a macroscopic polarization, and can therefore be applied to single molecules.[39]

In this dissertation we look at the degree to which EET can be controlled by coherent ground-state nuclear motion induced by an ultrashort laser pulse.[40] In our model this vibrational motion is localized to one monomer, and influences the instantaneous energy transfer rate by changing the instantaneous energy gap between donor- and acceptor-excited states[18,19] rather than changing the coupling strength.[23] The time dependance of the energy transfer "rate" can still be enhanced or diminished using our control strategy, as can its time-averaged value. We look to md-WPI as a means to experimentally observe the vibrational control of EET

B. Outline

In Chapter II we present a scheme in which the vibrational control over EET can be observed experimentally using multidimensional wave-packet interferometry (md-WPI), or the pump-probe limit thereof, and derive the expressions needed to simulate these sixth-order, fluorescence-detected difference signals in terms of the overlap between nuclear wave packets evolving on various electronic surfaces. Chapter III presents numerical simulations of md-WPI difference signals in the pump-probe limit from three different model systems: an equal-energy dimer with moderate excitonic and electron-vibration coupling, a model with weak coupling designed to resemble the covalent dimer dithia(1,5)[3,3]anthracenophane (DTA),

and a model with moderate coupling and unequal site energies so as to explore downhill EET in heterodimers. Chapters II and III have been published as coauthored papers with Jeffrey Cina in *J. Chem. Phys.* **131**, 224101 (2009) and *J. Chem. Phys.* **131**, 224302 (2009), respectively.

Chapter IV treats the issue of whether a lack of direct proportionality between pump-probe and pump-probe difference signals can be taken as evidence of the vibrational control over EET in isotropic samples. We show that, although a polarized control pulse does select an orientational subensemble upon which a pump-probe experiment is performed, in the absence of pulse-induced coherent nuclear motion the signals are largely proportional. This material was coauthored with Jeffrey A. Cina and has been submitted, in revised form, for publication in the *Journal of Chemical Physics*. Chapter V further explores the control strategy presented in Chapter II, examining the effects on subsequent EET of varying the delay between the control pulse and the first electronically resonant pulse, as well as the differences between the cases where the control pulse interacts with the acceptor or donor monomer. Chapter V also presents difference signals, both pump-probe and md-WPI, for DTA using a variety of pulse polarizations and timings. Chapter VI looks at vibrational control in a new model system, Dithia(1,5)[3,3]2-trifluoromethylanthracenophane, or $(\mathrm{TFMA})_2$, in which a CF_3 group, whose torsional angle is strongly coupled to the electronic state of the system, has been added to the anthracene monomers of DTA. Calculated pump-probe difference signals from an oriented $(\mathrm{TFMA})_2$ complex, which demonstrate a significant degree of control over EET, are presented in this chapter.

There are seven appendices to this dissertation. Appendix A gives the direction-cosine prefactors for the various contributions to the sixth-order signals for various polarization schemes, averaged over the random molecular orientations present in solution- or gas-phase measurements, in a straightforward manner equivalent to the method of tensor invariants commonly employed.[41] Appendix B lists all contributions to the md-WPI difference signals

of different phase signatures, while Appendix C catalogues the contributions in the pump-prob limit. Appendix D presents an approximate quantum theory, valid when the electronic coupling is small compared to the vibrational frequency, that seeks to explain the effects on population dynamics of ground-state nuclear motion localized on the acceptor chromophore. Appendix E gives explicit expressions for the second-order pulse propagator matrix elements used in the calculations of Chapter III. Appendix F looks at the initial anisotropy values for the pump-probe difference signals presented in Chapter III. Appendix G compares various excited-state nuclear trajectories in terms of vicinity to the intersection between donor- and acceptor-excited potential surfaces.

Notes

[1] Y.-C. Cheng and G. R. Fleming, Annual Review of Physical Chemistry **60**, 241 (2009).

[2] R. E. Blankenship, *Molecular Mechanisms of Photosynthesis*, Wiley-Blackwell, 2001.

[3] T. Förster, *Delocalized excitation and excitation transfer*, volume 3, pages 93–137, Academic Press, New York, 1965.

[4] D. L. Andrews and A. A. Demidov, *Resonance Energy Transfer*, Wiley, Chichester, UK, 1999.

[5] J. Zheng, *FRET and Its Biological Application as a Molecular Ruler*, Biomedical Applications of Biophysics, Humana Press Inc, 2010.

[6] G. D. Scholes, Annual Review of Physical Chemistry **54**, 57 (2003).

[7] G. S. Engel et al., Nature **446**, 782 (2007).

[8] G. Panitchayangkoon et al., Proceedings of the National Academy of Sciences of the United States of America **107**, 12766 (2010).

[9] A. Ishizaki, T. R. Calhoun, G. S. Schlau-Cohen, and G. R. Fleming, Physical Chemistry Chemical Physics **12**, 7319 (2010).

[10] E. Collini et al., Nature **463**, 644 (2010).

[11] A. Ishizaki and G. R. Fleming, Proceedings of the National Academy of Sciences of the United States of America **106**, 17255 (2009).

[12] T. F. Soules and C. B. Duke, Physical Review B **3**, 262 (1971).

[13] S. Rackovsky and R. Silbey, Molecular Physics **25**, 61 (1973).

[14] D. Beljonne, C. Curutchet, G. D. Scholes, and R. J. Silbey, Journal Of Physical Chemistry B **113**, 6583 (2009).

[15] S. Jang, Y. C. Cheng, D. R. Reichman, and J. D. Eaves, Journal of Chemical Physics **129**, 101104 (2008).

[16] S. Jang, Journal Of Chemical Physics **131**, 164101 (2009).

[17] S. J. Jang, M. D. Newton, and R. J. Silbey, Physical Review Letters **92**, 218301 (2004).

[18] S. Jang, Y. J. Jung, and R. J. Silbey, Chemical Physics **275**, 319 (2002).

[19] J. A. Cina and G. R. Fleming, Journal of Physical Chemistry A **108**, 11196 (2004).

[20] S. E. Bradforth, R. Jimenez, F. Vanmourik, R. van Grondelle, and G. R. Fleming, Journal of Physical Chemistry **99**, 16179 (1995).

[21] R. Monshouwer, A. Baltuska, F. van Mourik, and R. van Grondelle, Journal of Physical Chemistry A **102**, 4360 (1998).

[22] J. M. Womick and A. M. Moran, Journal of Physical Chemistry B **113**, 15747 (2009).

[23] S. Jang, Journal of Chemical Physics **127**, 174710 (2007).

[24] A. Asadian et al., New Journal of Physics **12**, 075019 (2010).

[25] S. Mukamel, *Principles of Nonlinear Optical Spectroscopy*, Oxford University Press, New York, 1995.

[26] D. M. Jonas, Annual Review of Physical Chemistry **54**, 425 (2003).

[27] M. Cho, *Two-Dimensional Optical Spectroscopy*, CRC press, Boca Raton, 2009.

[28] F. Milota, J. Sperling, A. Nemeth, T. Manŏcal, and H. F. Kauffmann, Accounts of Chemical Research **42**, 1364 (2009).

[29] N. Christensson et al., Journal of Physical Chemistry B **113**, 16409 (2009).

[30] D. Abramavicius and S. Mukamel, The Journal of Chemical Physics **133**, 184501 (2010).

[31] Y.-C. Cheng, G. S. Engel, and G. R. Fleming, Chemical Physics **341**, 285 (2007).

[32] T. Manŏcal et al., Journal of Chemical Physics **132**, 184515 (2010).

[33] A. Nemeth et al., The Journal of Chemical Physics **132**, 184514 (2010).

[34] J. A. Cina, Annual Review of Physical Chemistry **59**, 319 (2008).

[35] N. F. Scherer et al., Journal of Chemical Physics **95**, 1487 (1991).

[36] N. F. Scherer et al., Journal of Chemical Physics **96**, 4180 (1992).

[37] E. J. Heller, Accounts of Chemical Research **14**, 368 (1981).

[38] T. S. Humble and J. A. Cina, Journal of Physical Chemistry B **110**, 18879 (2006).

[39] D. Brinks et al., Nature **465**, 905 (2010).

[40] L. Dhar, J. A. Rogers, and K. A. Nelson, Chemical Reviews **94**, 157 (1994).

[41] E. C. Ding, F. Fulmer and M. T. Zanni, Journal of Chemical Physics **123**, 094502 (2005).

CHAPTER II

USING MULTIDIMENSIONAL WAVE-PACKET INTERFEROMETRY TO MONITOR THE COHERENT CONTROL OF ENERGY TRANSFER

A. Introduction

Careful selection of the initial vibrational wave function can dramatically influence excited state dynamics when nuclear motion takes place either on multiple potential surfaces[1–6] or on a single adiabatic potential.[7,8] By controlling the initial state, and thus the subsequent evolution, surface-crossing transitions can, in particular, be hastened or curtailed. Here we propose a method to control the flow of electronic excitation energy (high energy quanta) between coupled chromophores using vibrational motion (low energy quanta). Coherent nuclear motion, imparted by infrared absorption or impulsive stimulated Raman scattering (ISRS)[9–18] in the electronic ground state, acts to influence the instantaneous local resonance between subsequently populated site-excited states and hence the time-course of the surface-crossing transitions corresponding to energy transfer.

To set the stage for theoretical and experimental investigations of this general control strategy, we derive expressions for the fluorescence-detected multidimensional wave-packet

interferometry (md-WPI) signal from a vibrationally excited sample of isotropically oriented energy-transfer dimers of fixed internal geometry. The signal expressions are parametrized by the relevant nuclear Hamiltonians, and should be valid for systems with weak to moderate coupling between site-excited states.

Our basic approach is the common one of describing the molecular system and its environment quantum mechanically, while the laser fields are taken to be classical electromagnetic waves whose interaction with the active chromophores is treated perturbatively. The control processes of interest are most easily visualized in terms of externally driven or freely evolving nuclear wave packets undergoing transfer between different electronic potential energy surfaces under the influence of resonant light pulses or spatially localized EET surface-crossings. The measured quantities are naturally expressed as quantum mechanical overlaps between superposed wave packets that have undergone different sequences of transitions in state space. For these reasons, we find it convenient to organize our calculations in terms of sums over the contributing wave-packet overlaps, each one of which involves a unique sequence of pulse-induced propagation events, free-evolution intervals on a single electronic potential-energy surface, and surface-crossing electronic transitions. The results of our analysis could, however, readily be transcribed to the widely used and formally equivalent notation of time-dependent nonlinear optical response functions, the various contributions to which are often pictured in terms of bra- and ket-sided time diagrams.[19–22]

A.1. Control Scheme

Electronic excitation transfer (EET) involves the inter- or intramolecular redistribution of electronic excitation and competes with other relaxation mechanisms available to the system, such as fluorescence or radiationless decay.[23] In natural photosynthetic systems, the efficiency of EET ensures that the absorbed photon energy is preferentially funnelled towards a

reaction center, where it is converted to chemical energy that can be stored for future use.[24–26] The roles of nuclear motion and molecular structure in these large EET complexes have been the subject of several recent investigations.[27–29] In this subsection, we discuss how the interplay between vibrational and energy-transfer dynamics brought to light by recent work suggests the use of low-frequency vibrational dynamics to influence higher-frequency electronic excitation-transfer dynamics.

A recent theoretical study viewing EET in molecular dimers as an electronic potential energy surface-crossing process,[30,31] showed that the vibrational coherence transfer that naturally accompanies electronic excitation transfer can give rise to quantum beats in time-resolved polarized emission spectra that are in-phase between parallel and perpendicular emission channels, as had been observed in the LH-1 antenna of photosynthetic bacteria.[24,32,33] Those calculations on a model complex composed of two identical chromophores, each supporting a single harmonic vibrational mode, demonstrated that vibrational coherence transfer is a consequence of the nuclear motion resulting from short-pulse excitation to the Franck-Condon point of a site-excited state (the donor-excited state). The periodic return of this localized wave packet to the surface-crossing seam ($q_a = q_b$), where amplitude can be transferred to the acceptor-excited state, results in a stepwise decrease in donor population (see Fig. 2.1 - solid line) and a concomitant transfer of vibrational coherence to the acceptor-excited state. It was shown in Ref. 30 that the resulting coordinated nuclear motion in donor- and acceptor-excited states is manifested by in-phase quantum beats in the polarized pump-probe signals similar to those observed experimentally.

This picture of coherent wave-packet motion accompanying energy transfer suggests a method for controlling the short-time dynamics of energy transfer. If the nuclear wave packet is displaced from the minimum of the ground-state potential along the acceptor vibrational coordinate at the instant of resonant donor excitation (as shown by the dashed trace in the top panel of Fig. 2.1), then the trajectory of the photo-excited wave packet avoids the intersection

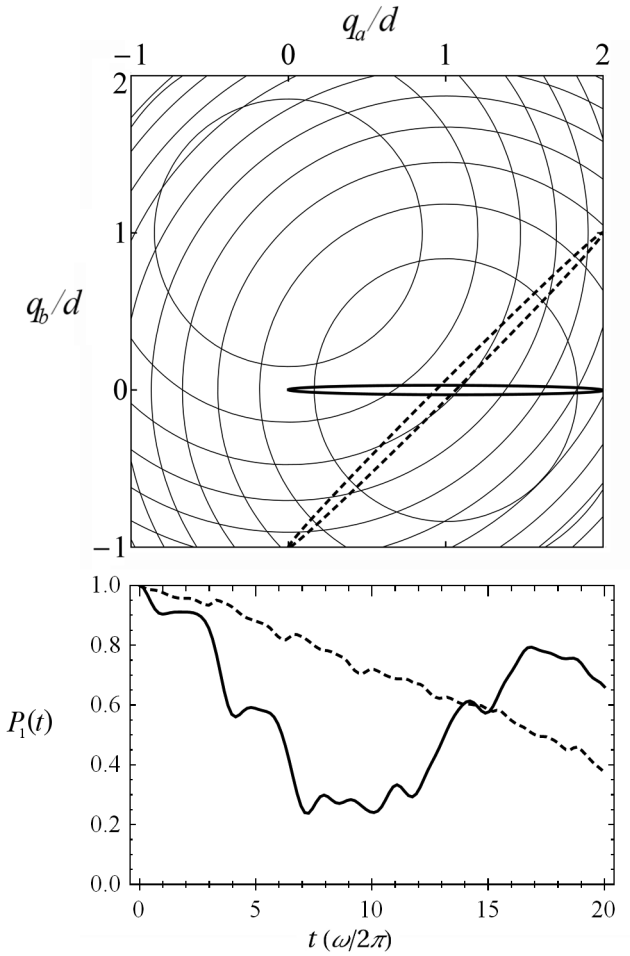

Figure 2.1: Top Panel: Initial trajectories of wave packets launched impulsively to the donor-excited electronic state (shown as elongated ovals for clarity) overlaying contour plots for the harmonic surfaces of two site-excited states, each of which is displaced by d from the ground state potential minimum along the appropriate nuclear coordinate. Bottom Panel: Population $P_1(t)$ of the donor-excited state for the wave packets whose initial trajectories are shown in the left panel; in this simulation any population lost by the donor is gained by the acceptor and vice versa. Shown are the cases in which the wave packet prior to electronic excitation is the vibrational ground state (solid line) or a coherent state executing harmonic motion along the acceptor vibrational coordinate (dashed line).

between the two site-excited potential surfaces, which should significantly curtail short-time EET. We envisage the use of ISRS or coherent infrared absorption to generate this coherent nuclear displacement in the electronic ground state.

A numerical test calculation using the same model system as Ref. 30 shows how this kind of nuclear displacement prior to electronic excitation can alter the ensuing EET. In these simulations, the initial expectation values of the nuclear coordinates are set to $\langle q_a \rangle = 0$ and $\langle q_b \rangle = -d$ at the instant when the system is promoted to the donor-excited state (whose potential-energy minimum is at $(q_a, q_b) = (d, 0)$). The effect on the EET dynamics of this non-stationary initial state is visible in the evolving population of the donor-excited state (bottom panel of Fig. 2.1). Following a vertical transition from the equilibrium geometry at time zero (solid line), EET proceeds in a stepwise fashion, as the local transition energies for the donor-excited→ground and acceptor-excited←ground electronic transitions coincide whenever $t = 2\pi n/\omega$ (where ω is the vibrational frequency).[34] When the initial nuclear wave function is the displaced state (dashed line) on the other hand, the short-time population transfer occurs more slowly and at a steadier rate.

A.2. md-WPI and Pump-Probe Observations of Vibrational Control Over EET

The demonstration calculation of Fig. 2.1 shows that vibrational control can be exerted over EET and motivates our two main goals of outlining a framework for the spectroscopic study of this process (in this chapter) and beginning its detailed numerical simulation (in the following chapter).[35] In a WPI experiment, the system is subjected to one or more pairs of phase-locked (or phase-modulated) ultra-short laser pulses resonant with electronic transitions in the system, and the fluorescence (or some other observable indicative of excited-state population) is measured as a function of the various interpulse delays.[36–41] By cycling the intrapulse-pair phase differences or detecting the third-order signal field traveling in a particu-

lar phase-matched direction, it is sometimes possible to isolate the complex-valued overlap of a target wave packet prepared by one pulse in the sequence with a collection of reference wave packets prepared by the others. Theoretical[22,37,42–48] and experimental[49–64] studies have addressed the application of WPI and the broader methods of multidimensional phase-coherent electronic spectroscopy to a variety of molecular systems. By providing amplitude-level information on nuclear wave packets as they evolve following electronic excitation, wave-packet interferometry should, in particular, provide uniquely detailed records of the nuclear dynamics accompanying surface-crossing processes such as electronic excitation transfer.

Below, we derive the basic expressions for the md-WPI signal from a sample of isotropically oriented EET dimers following prior vibrational excitation through ISRS by a preresonant control pulse. Ideally, the target wave packet-the alteration of whose dynamics by control-pulse-induced vibrational motion we wish to monitor-would be prepared by one of the pulses in the first pulse-pair of the four-pulse WPI sequence, while the remaining WPI pulses would generate a family of three-pulse reference wave packets, whose overlaps with the target constitute the signal (the relevant interference contribution to the one-exciton population). The control pulse and each of the phase-controlled pulse-pairs have independently selected linear polarizations, allowing a measure of external choice-in a statistical sense-of acceptor and donor transition-dipole lab-frame orientations. The control-influenced md-WPI signal proves in general to be more complicated than the ideal situation described above; but the use of polarization selection, choice of pulse center-frequencies, and selection of interpulse delays and optical phase signature, all serve to simplify the observed signal.[42]

Although the full md-WPI signal provides a more complete amplitude-level characterization of the control-influenced energy-transfer dynamics, a relatively simpler polarized fluorescence-detected pump-probe experiment may be sufficient to test the efficacy of vibrational control of EET. Such an experiment reveals the population transfer between monomers (nuclear probability density),[30] but provides less detailed information on the evolution of the

accompanying amplitudes (nuclear wave packets). A md-WPI experiment reduces to a pump-probe experiment when the pulses within each pair arrive simultaneously, and an expression for the pump-induced change in the probe-induced fluorescence is derived from the md-WPI signal by taking this limit.

B. Theory

We consider an energy-transfer dimer and treat each monomer as a system of two electronic levels. The Hamiltonian of the molecular complex is

$$H = |0\rangle H_0 \langle 0| + |1\rangle H_1 \langle 1| + |1'\rangle H_{1'} \langle 1'| + |2\rangle H_2 \langle 2| + J\{|1'\rangle \langle 1| + |1\rangle \langle 1'|\}. \quad (2.1)$$

$H_n(n = 0,\ 1,\ 1',\ 2)$ is the nuclear Hamiltonian in the electronic state $|n\rangle$, where

$$\begin{aligned} |0\rangle &\quad \text{(both chromophores unexcited)} \\ |1\rangle &\quad \text{('first chromophore' excited)} \\ |1'\rangle &\quad \text{('second chromophore' excited)} \\ |1\rangle &\quad \text{(both chromophores excited).} \end{aligned} \quad (2.2)$$

Note that the H_n govern the nuclear motion essential to our control strategy. The energy-transfer coupling J may, in general, depend on nuclear coordinates.

The complex interacts with five independently polarized laser pulses. An electronically non-resonant control pulse, P, comes first; it is responsible for initiating vibrational motion in the electronic ground state by impulsive stimulated Raman scattering* (it could be replaced by a timed sequence of pulses in order to selectively excite a single mode of a partic-

*For present purposes this pulse should perhaps be regarded as pre-resonant with the $1 \leftrightarrow 0$ and $1' \leftrightarrow 0$ transitions, so that effects of interactions with higher-lying electronic states that are absent from our model Hamiltonian can safely be neglected.

ular frequency[12,13,65,66]). The control pulse is followed by a multidimensional WPI sequence comprising a pair of phase-locked (or phase-modulated) electronically resonant pulse-pairs, A-B and C-D (see Fig. 2.2). The laser-molecule interactions are governed by

$$V(t) = -\sum_I \boldsymbol{\mu} \cdot \mathbf{E}_I(t) \qquad I = P, A, B, C, D. \tag{2.3}$$

The dipole moment operator,

$$\boldsymbol{\mu} = \boldsymbol{m} \left(|0\rangle \langle 1| + |1'\rangle \langle 2| \right) + 2\boldsymbol{m'} \left(|0\rangle \langle 1'| + |1\rangle \langle 2| \right) + \text{H.c.}, \tag{2.4}$$

facilitates electronic transitions for the individual chromophores. The dimer complex is assumed to be "rigid" in the sense that the relative angle between $\boldsymbol{m}$ and $\boldsymbol{m}'$ is taken to be a fixed parameter, rather than a dynamical variable. The electric field of the Ith pulse is written as

$$\boldsymbol{E}_I(t) = \boldsymbol{e}_I E_I f_I(t) \cos\left(\Phi_I(t) + \phi_I\right) \ , \tag{2.5}$$

with a well-defined polarization vector, field amplitude, envelope function (peaked at arrival time t_I with duration σ_I), phase function, and constant phase.

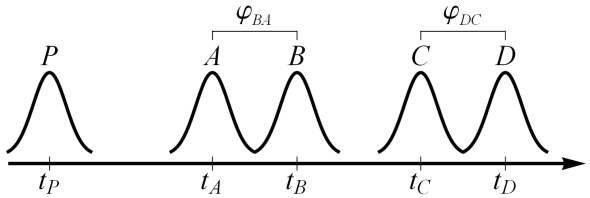

Figure 2.2: Schematic representation of the pulse sequence for the experiments considered here. The pre-resonant control pulse (P) precedes the md-WPI sequence (A–D). The absolute phase of any pulse is considered random, while the phase differences ϕ_{BA} and ϕ_{DC} are precisely controlled.

The two pulse-pairs are assumed to be temporally non-overlapping, and neither overlaps the non-resonant control pulse $t_P \ll t_A, t_B \ll t_C, t_D$ with $t_{BA} \equiv t_B - t_A \geq 0$ and

$t_{DC} \equiv t_D - t_C \geq 0$). We shall account for the possibility that pulses within a pair may overlap in time, so that pulse B (D) may act on the system before pulse A (C). $\phi_{BA} \equiv \phi_B - \phi_A$ and $\phi_{DC} \equiv \phi_D - \phi_C$ are assumed to be externally controlled or modulated, but the absolute phases ϕ_I are unknown and subject to random jitter between successive laser shots. The relative phases between P and A, B, C, and D need not be specified, and those between A or B and C or D are similarly unknown.

The state ket of the system evolves according to

$$i\frac{\partial}{\partial t}\left|\Psi(t)\right\rangle = \left(H + V(t)\right)\left|\Psi(t)\right\rangle \ , \tag{2.6}$$

(we set $\hbar$ equal to 1 throughout) with an initial condition

$$\left|\Psi(t \ll \ t_P)\right\rangle = e^{-i\,H(t-t_A)}\left|0\right\rangle\left|\psi_0\right\rangle \tag{2.7}$$

prior to any of the laser pulses, where $\left|\psi_0\right\rangle$ is an eigenstate of H_0.* Switching to the interaction picture, we evaluate

$$\begin{aligned} i\frac{\partial}{\partial t}e^{i\,H(t-t_A)}\left|\Psi(t)\right\rangle =& e^{i\,H(t-t_A)}\left\{-H + \left(H + V(t)\right)\left|\Psi(t)\right\rangle\right\} \\ =& e^{i\,H(t-t_A)}V(t)\left|\Psi(t)\right\rangle \quad . \end{aligned} \tag{2.8}$$

The formal solution is

$$e^{i\,H(t-t_A)}\left|\Psi(t)\right\rangle = \left|0\right\rangle\left|\psi_0\right\rangle + \frac{1}{i}\int_{-\infty}^{t} dt'\, e^{i\,H(t'-t_A)}\,V(t')\left|\Psi(t')\right\rangle \ , \tag{2.9}$$

*The nuclear degrees of freedom governed by the H_n may comprise any number of molecular and environmental modes. The pure state $\left|g\right\rangle\left|\psi_0\right\rangle$ may, in particular, describe the energy-transfer complex in thermal equilibrium with a surrounding medium at any temperature such that k_BT is much smaller than the monomer electronic excitation energies. For an interesting discussion on this point in a larger context, see Refs. 67 and 68.

or, reverting to the Schrödinger picture,

$$|\Psi(t)\rangle = e^{-i\,H(t-t_A)}\,|0\rangle\,|\psi_0\rangle + \frac{1}{i}\int_{-\infty}^{t} dt' e^{-i\,H(t-t')}V(t')\,|\Psi(t')\rangle \ . \tag{2.10}$$

This standard integral equation is mathematically equivalent to Eq. (2.6). It can be iterated-with the expression for $|\Psi(t)\rangle$ on the RHS being repeatedly substituted into the integral-in order to obtain solutions perturbative to any desired combination of orders of the incident fields.

As the observables of interest we seek all contributions to the one-exciton population $\langle\Psi(t)|\,(|1\rangle\langle 1| + |1'\rangle\langle 1'|)\,|\Psi(t)\rangle$ that are quadratic in E_P ; quadrilinear in E_A, E_B, E_C and E_D ; and carry a specific dependence on the optical phase shifts ϕ_{BA} and ϕ_{DC}. These observables represent the control-pulse-induced change in the md-WPI signals of various phase signatures. Contributions of this kind can be isolated experimentally by optical phase cycling or other fundamentally equivalent procedures.[37,40,49,50,57–64]

In order to keep things relatively simple, we specialize to a complex that does not rotate in the interval t_{DP} between the first and last pulses. We further assume that the time-and-frequency-integrated fluorescence from the one-exciton manifold can be selectively detected without contamination from the two-exciton emission.* As an additional experimentally realizable simplification, we assume that the pulse durations σ_I are significantly shorter than the characteristic timescale, $2\pi/J$, for electronic excitation transfer; this assumption allows us to neglect energy transfer in calculating the action of the individual pulses.†

*This choice of observable differs from that of Ref. 42, where the population of the "acceptor" state was monitored for an oriented complex. If the similarity in emission frequency from the two- and one-exciton states were to make discrimination between them difficult, the theoretical treatment would have to be modified to calculate the expected number of "stored photons," $\langle\Psi(t)|\,(2\,|2\rangle\langle 2| + |1\rangle\langle 1| + |1'\rangle\langle 1'|)\,|\Psi(t)\rangle$.

†Under stronger EET coupling, when the timescale for energy transfer may be less than or on the order of pulse durations, vibrational periods, or both, it can be advantageous to frame the treatment in terms of delocalized exciton states, rather than site-states. See Ref. 29 and Sec. III.C of Ref. 30.

Because contributions to $\langle 1 \mid \Psi(t)\rangle$ and $\langle 1' \mid \Psi(t)\rangle$ come at odd orders in the external fields, we must determine the first-, third-, and fifth-order terms in perturbation theory. Using the notation $[t] = \exp(-i\,H\,t)$ for the free-evolution operator, we can write an expansion of Eq. (2.10) through fifth order,

$$\begin{aligned} |\Psi(t)\rangle = \Big\{ & [t - t_A] + \frac{1}{i} \int_{-\infty}^{t} dt' [t - t'] V(t') [t' - t_A] \\ & + \frac{1}{i^2} \int_{-\infty}^{t} dt'' \int_{-\infty}^{t''} dt' [t - t''] V(t'') [t'' - t'] V(t') \\ & \times [t' - t_A] + \text{through fifth order} \Big\} |0\rangle\, |\psi_0\rangle \ . \end{aligned} \tag{2.11}$$

We define the pulse propagators

$$P_I(t; t') = -\frac{1}{i} \int_{-\infty}^{t} dt' [t_I - t'] \boldsymbol{\mu} \cdot \mathbf{E}_I(t') [t' - t_I] \ , \tag{2.12}$$

where the first argument is the upper limit of integration and the second is the integration variable. With this notation, the perturbed state (2.11) can be re-expressed as

$$\begin{aligned} |\Psi(t)\rangle = \Big\{ & [t - t_A]. + \sum_I [t - t_I] P_I(t; t') [t_{IA}] \\ & + \sum_J \sum_I [t - t_J] P_J(t; t'') [t_{JI}] P_I(t''; t') [t_{IA}] \\ & + \text{through fifth order} \Big\} |0\rangle\, |\psi_0\rangle \quad . \end{aligned} \tag{2.13}$$

We evaluate the necessary electronic matrix elements of the pulse propagators with the help of the rotating wave approximation and neglect energy transfer (but not vibrational motion) during the interaction due to the impulsive nature of the excitation. For an upward

transition such as $1 \leftarrow 0$, we have

$$\begin{aligned}\langle 1|\, P_I(t;t')\,|0\rangle \cong & \frac{iE_I}{2}\int_{-\infty}^{t} dt'[t_I - t']_{11}\,\langle 1|\,\boldsymbol{\mu}\,|0\rangle \\ & \cdot \boldsymbol{e}_I f_I(t')\, e^{-i\,\Phi_I(t')-i\,\phi_I}[t'-t_I]_{00} \\ = & e^{-i\,\phi_I} e_I \frac{iE_I m}{2}\int_{-\infty}^{t} dt'\, f_I(t')\, e^{-i\,\Phi_I(t')}\,[t_I - t']_{11} \\ & \times [t'-t_I]_{00} \equiv e^{-i\,\phi_I} e_I p_I^{(10)}(t;t')\end{aligned} \tag{2.14}$$

where $\boldsymbol{e}_I \cdot \boldsymbol{m} = e_I m$ (i.e. e_I is the component of $\boldsymbol{e}_I$ along $\boldsymbol{m}$).* With the neglect of intrapulse energy transfer, J is to be set to zero when evaluating the free-evolution operators in the integrand, so $[t]_{11} \cong \exp(-iH_1 t)$, $[t]_{1'1'} \cong \exp(-iH_{1'}\,t)$, and $[t]_{1'1} = [t]_{11'} \cong 0$. For a downward transition such as $1 \rightarrow 0$ we have, similarly,

$$\begin{aligned}\langle 0|\, P_I(t;t')\,|1\rangle \cong & e^{i\phi_I} e_I \frac{iE_I m}{2}\int_{-\infty}^{t} dt'\,[t_I - t']_{00} f_I(t')\, e^{i\,\Phi_I(t')}[t'-t_I]_{11} \\ \equiv & e^{i\phi_I} e_I p_I^{(01)}(t;t')\ .\end{aligned} \tag{2.15}$$

Notice the anti-Hermitian property of the reduced pulse propagators

$$p_I^{(01)}(t;t') = -\left(p_I^{(10)}(t;t')\right)^{\dagger}\ . \tag{2.16}$$

The reduced pulse propagators introduced in Eq. (2.15) are purely nuclear operators describing the pulse-dependent distortion of vibrational wave packets accompanying electronic transitions. Extending this notation to the other electronic matrix elements of P_I allows us

*In the analogous matrix elements for a $1' \leftarrow 0$ transition, $\boldsymbol{e}_I \cdot \boldsymbol{m'} \equiv e'_I m'$, and e'_I is the component of $\boldsymbol{e}_I$ along $\boldsymbol{m'}$.

to write

$$\begin{aligned} P_I(t;t') = & e^{-i\phi_I} e_I \left(|1\rangle \langle 0| \, p_I^{(10)}(t;t') + |2\rangle \langle 1'| \, p_I^{(21')}(t;t') \right) \\ & + e^{-i\phi_I} e_I' \left(|1'\rangle \langle 0| \, p_I^{(1'0)}(t;t') + |2\rangle \langle 1| \, p_I^{(21)}(t;t') \right) \\ & + e^{i\phi_I} e_I \left(|0\rangle \langle 1| \, p_I^{(01)}(t;t') + |1'\rangle \langle 2| \, p_I^{(1'2)}(t;t') \right) \\ & + e^{i\phi_I} e_I' \left(|0\rangle \langle 1'| \, p_I^{(01')}(t;t') + |1\rangle \langle 2| \, p_I^{(12)}(t;t') \right) \quad . \end{aligned} \tag{2.17}$$

For the purpose of calculating the non-resonantly pumped md-WPI signal, we need not determine each and every nuclear wave packet linearly superposed to form $\langle 1 \mid \Psi(t) \rangle$ and $\langle 1' \mid \Psi(t) \rangle$. Only those packets linear or trilinear in the WPI-pulse field amplitudes and zeroth- or second-order in the non-resonant control field contribute to the signal (because of its non-resonance, the control pulse cannot make a linear contribution to these nuclear amplitudes alone or in combination with the temporally separated WPI pulses). The relevant first-order contributions to $\langle \varepsilon \mid \Psi(t) \rangle$ ($\varepsilon = 1, 1'$) are

$$|(A)_\varepsilon\rangle \, , \quad |(B)_\varepsilon\rangle \, , \quad |(C)_\varepsilon\rangle \, , \quad |(D)_\varepsilon\rangle \quad . \tag{2.18}$$

The necessary third-order terms are

$$\begin{aligned} & |(APP)_\varepsilon\rangle \, , \quad |(BPP)_\varepsilon\rangle \, , \quad |(CPP)_\varepsilon\rangle \, , \quad |(DPP)_\varepsilon\rangle \\ & |(CBA)_\varepsilon\rangle \, , \quad |(CAB)_\varepsilon\rangle \, , \quad |(DBA)_\varepsilon\rangle \, , \quad |(DAB)_\varepsilon\rangle \\ & |(DCA)_\varepsilon\rangle \, , \quad |(CDA)_\varepsilon\rangle \, , \quad |(DCB)_\varepsilon\rangle \, , \quad |(CDB)_\varepsilon\rangle \ , \end{aligned} \tag{2.19}$$

and contributing fifth-order wave packets consist of

$$\begin{aligned} & |(CBAPP)_\varepsilon\rangle \, , \quad |(CABPP)_\varepsilon\rangle \, , \quad |(DBAPP)_\varepsilon\rangle \, , \quad |(DABPP)_\varepsilon\rangle \\ & |(DCAPP)_\varepsilon\rangle \, , \quad |(CDAPP)_\varepsilon\rangle \, , \quad |(DCBPP)_\varepsilon\rangle \, , \quad |(CDBPP)_\varepsilon\rangle \quad . \end{aligned} \tag{2.20}$$

The meaning of our notation should already be clear. For example,

$$|(APP)_{\varepsilon}\rangle = \langle\varepsilon|\,[t-t_A]P_A(t;t''')[t_{AP}]P_P(t''';t'')P_P(t'';t')[t_{PA}]\,|0\rangle\,|\psi_0\rangle\ . \qquad (2.21)$$

The nuclear state-kets listed in Eqs. (2.18) through (2.20) and discussed extensively in the rest of this paper are the vibrational wave packets referred to in the term "wave-packet interferometry." It is a central feature of our analysis that the sought-after multi-dimensional electronic spectroscopy signals are explicitly expressed and interpreted in terms of the quantum mechanical overlaps between various pairs of these vibrational wave packets.

A special feature of the experimental observable further simplifies the calculation. We are interested in various contributions to the population of the one-exciton manifold at a time $t > t_D$ (i.e. well after the last pulse has acted). Any contribution to the ε-state amplitude continues to evolve during $t - t_D$ and, in particular, amplitude may be gained or lost through excitation transfer. But the Hermitian operator for the one-exciton population $|1\rangle\langle 1| + |1'\rangle\langle 1'|$ commutes with H, so $[-t+t_D]\,(|1\rangle\langle 1| + |1'\rangle\langle 1'|)\,[t-t_D] = |1\rangle\langle 1| + |1'\rangle\langle 1'|$. Without approximation, we may therefore formally set $t = t_D$ in the final free-evolution operator of the contributing first-, third-, and fifth-order nuclear amplitudes used in calculating the one-exciton population.

Each of the first-, third-, and fifth-order nuclear wave packets listed above involves multiple interfering pathways through electronic state space.* For instance, the ε-state wave packet linear in E_A alone has contributions from nuclear amplitudes accompanying the direct

*$|(D)_{\varepsilon}\rangle$ is an exception, however. Because energy transfer during the pulse is presumed negligible, this amplitude involves a single $\varepsilon \leftarrow 0$ excitation pathway.

excitation of both $|1\rangle$ and $|1'\rangle$ states:

$$\begin{aligned} |(A)_{\varepsilon}\rangle &= \langle\varepsilon|\,[t_{DA}]P_A(\infty;t')\,|0\rangle\,|\psi_0\rangle \\ &= e^{-i\phi_A}e_A[t_{DA}]_{\varepsilon 1}p_A^{(10)}(\infty;t')\,|\psi_0\rangle \\ &\quad + e^{-i\phi_A}e'_A[t_{DA}]_{\varepsilon 1'}p_A^{(1'0)}(\infty;t')\,|\psi_0\rangle \quad . \end{aligned} \tag{2.22}$$

The quantities $[t_{DA}]_{\varepsilon 1}$ and $[t_{DA}]_{\varepsilon 1'}$ are nuclear operators that incorporate the energy-transfer events occurring after electronic excitation ($J \neq 0$). The upper integration limit of the reduced pulse propagators in Eq. (2.22) has been set to infinity, since the pulse is assumed to have passed entirely before the excited-state amplitude is reckoned. This assumption is appropriate, because the one-exciton population is to be determined by fluorescence, whose lifetime greatly exceeds the pulse durations.

We can represent this situation with a sketch illustrating the branching pathways through electronic state space that contribute to $|(A)_{\varepsilon}\rangle$,

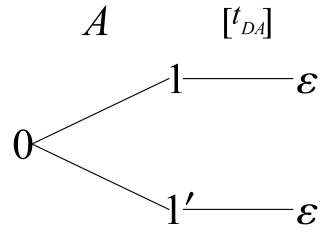

(2.23)

We now introduce a streamlined notation for $|(A)_{\varepsilon}\rangle$ that makes explicit the optical phase-dependence, the polarization-moment direction cosines, and the electronic state-space pathway of each contributing term, rewriting Eq. (2.22) as

$$|(A)_{\varepsilon}\rangle = e^{-i\phi_A}\left[e_A\,|\{a(10)\}_{\varepsilon}\rangle + e'_A\,|\{a(1'0)\}_{\varepsilon}\rangle\right]. \tag{2.24}$$

Both terms carry the same optical phase factor, as both result from an upward electronic transition driven by pulse A. In the case $\varepsilon = 1\,(1')$ the first (second) term is the probability amplitude for the excitation to remain in the $1\,(1')$ state after tDA of evolution in the one-exciton manifold (back-transfer included); the second (first) term is the probability amplitude for energy transfer to have taken place to the $1'\,(1)$ state. This example should illustrate sufficiently the notation we will use to express the other first, third, and fifth-order -state wave packets resulting from multiple interfering pathways through electronic state-space. The other first-order wave packets follow by direct analogy.

The state-space pathways for $|(APP)_{\varepsilon}\rangle$ can be sketched as

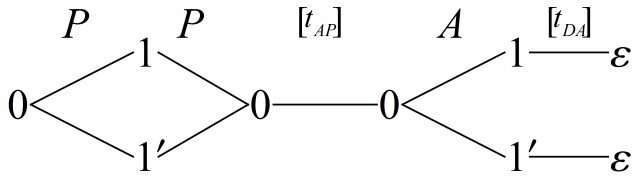

(2.25)

The second-order action of the non-resonant control pulse can return amplitude only to the electronic ground state; transient occupation of the 1 or $1'$ state imparts momentum to Franck-Condon active vibrational modes. We wish to investigate the opportunity this impulsive Raman process offers for vibrational control over the energy transfer that takes place after subsequent resonant excitation to a site-excited electronic state. An expression for $|(APP)_{\varepsilon}\rangle$ can be obtained by applying the second-order action of P along with t_{AP} of ground-state evolution as a "prefix" to $|(A)_{\varepsilon}\rangle$:

$$\begin{aligned}|(APP)_{\varepsilon}\rangle =& e^{-i\,\phi_A}[e_A e_P^2\,|\{a(10)p(01)p(10)\}_{\varepsilon}\rangle + e_A e_P'^2\,|\{a(10)p(01')p(1'0)\}_{\varepsilon}\rangle \\ &+ e_A' e_P^2\,|\{a(1'0)p(01)p(10)\}_{\varepsilon}\rangle + e_A' e_P'^2\,|\{a(1'0)p(01')p(1'0)\}_{\varepsilon}\rangle].\end{aligned} \tag{2.26}$$

Due to the up-and-down action of electronic excitation and de-excitation by the non-resonant control pulse, its optical phase does not appear. The remaining third-order terms which are

quadratic in the non-resonant control pulse, $|(BPP)_\varepsilon\rangle$, $|(CPP)_\varepsilon\rangle$,, and $|(DPP)_\varepsilon\rangle$, can be obtained by simply changing A and a to B and b, C and c, or D and d, respectively, in Eq. (2.26) (but $|(DPP)_\varepsilon\rangle$ reduces to only two nonzero terms for each choice of ε).

The electronic state-space pathways for $|(CBA)_\varepsilon\rangle$ are shown below:

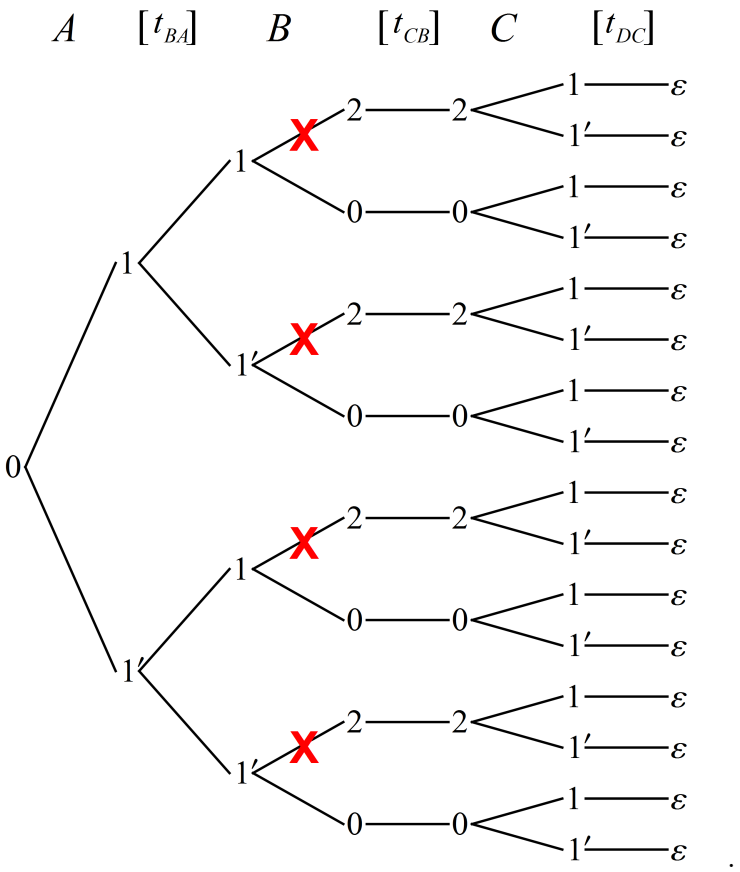

(2.27)

Eight of the sixteen superposed amplitudes in $|(CBA)_\varepsilon\rangle$ cannot contribute in practice to the md-WPI signal. In those marked with an X, both A and B pulses effect upward electronic transitions, $2 \leftarrow 1 \leftarrow 0$ or $2 \leftarrow 1' \leftarrow 0$. In either instance, the overall optical phase factor (including that from a subsequent downward transition under pulse C) is $\exp(-i\phi_A - i\phi_B + i\phi_C)$. Any overlap involving a wave packet of this phase dependence will average to zero over many laser shots, as the uncontrolled phase factor $\exp(-i\phi_A - i\phi_B)$ samples points distributed randomly on a unit circle in the complex plane.

The eight remaining amplitudes in (2.27) carry a phase factor $\exp(-i\phi_A+i\phi_B-i\phi_C)$ resulting from the upward, downward, and upward action of pulses A, B, and C, respectively. Overlaps between these wave packets and those involving an upward transition under pulse D, which carry a phase factor $\exp(-i\phi_D)$, therefore have a phase factor $\exp(i\phi_{BA}+i\phi_{DC})$; since this factor involves only the controlled phase differences, these overlaps do not automatically average to zero and can contribute to the md-WPI signal. The sum of amplitudes forming $|(CBA)_\varepsilon\rangle$ can now be written out from the state-space sketch:

$$\begin{aligned}|(CBA)_\varepsilon\rangle =& e^{i\phi_{BA}-i\phi_C}[e_A e_B e_C\,|\{c(10)b(01)a(10)\}_\varepsilon\rangle \\ &+ e_A e_B e'_C\,|\{c(1'0)b(01)a(10)\}_\varepsilon\rangle + e_A e'_B e_C\,|\{c(10)b(01')a(10)\}_\varepsilon\rangle \\ &+ e_A e'_B e'_C\,|\{c(1'0)b(01')a(10)\}_\varepsilon\rangle + e'_A e_B e_C\,|\{c(10)b(01)a(1'0)\}_\varepsilon\rangle \\ &+ e'_A e_B e'_C\,|\{c(1'0)b(01)a(1'0)\}_\varepsilon\rangle + e'_A e'_B e_C\,|\{c(10)b(01')a(1'0)\}_\varepsilon\rangle \\ &+ e'_A e'_B e'_C\,|\{c(1'0)b(01')a(1'0)\}_\varepsilon\rangle] \quad .\end{aligned} \tag{2.28}$$

A similar expression for $|(DBA)_\varepsilon\rangle$ follows by replacing C and c with D and d, respectively.

In $|(CAB)_\varepsilon\rangle$ the roles of $A(a)$ and $B(b)$ are reversed, despite the fact that the arrival time for the former precedes that for the latter; the B pulse acts first to electronically excite the system before it is de-excited by the A pulse. Because the interval t_{BA} is nonnegative, the expression for $|(CAB)_\varepsilon\rangle$ resulting from a simple substitution in Eq. (2.28) would introduce a slight inconsistency in our treatment. We neglect EET during the short interaction time, and must also do so during backward evolution from t_B to t_A in $|(CAB)_\varepsilon\rangle$, as t_{BA} must be shorter than the pulse duration for this amplitude to be nonzero. This neglect amounts to omitting the four kets whose labels would include either $a(01')b(10)$ or $a(01)b(1'0)$. $|(DAB)_\varepsilon\rangle$ can be obtained from $|(CAB)_\varepsilon\rangle$ by again replacing C with D and c with d.

The next step is to draw the state-space pathways contributing to $|(DCA)_{\varepsilon}\rangle$:

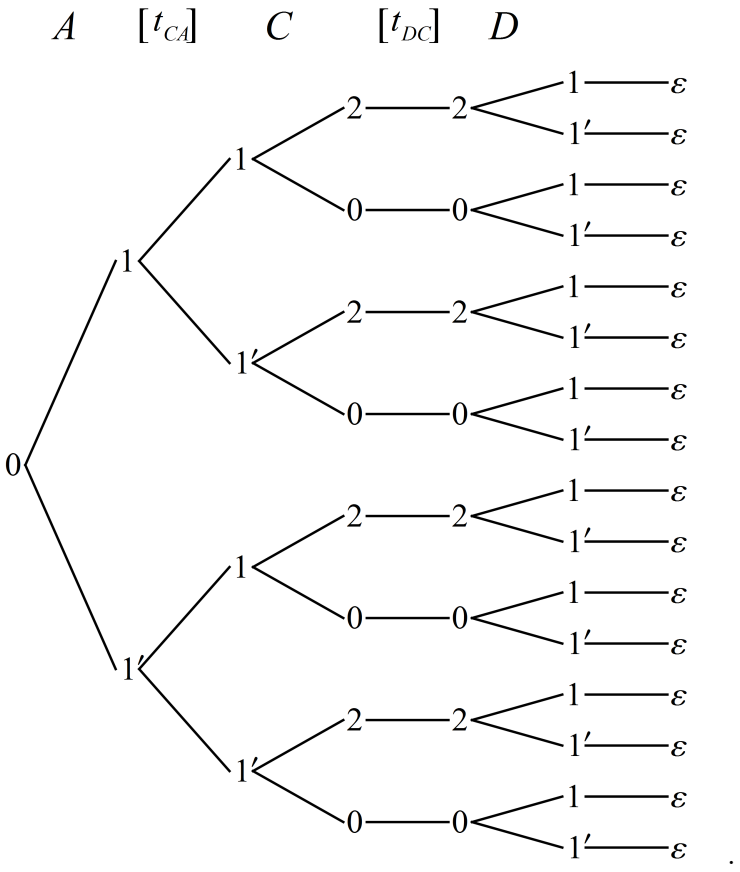

(2.29)

The C and D pulses act in opposite directions in every instance (upwards and downwards, respectively, or vice versa). The optical phase factors accompanying all these amplitudes involve the controlled difference $\phi_D - \phi_C$ rather than the uncontrolled sum $\phi_D + \phi_C$, and none of the signal contributions to which these amplitudes contribute averages to zero due to

shot-to-shot fluctuations in the absolute phase. The corresponding amplitude is

$$
\begin{aligned}
|(DCA)_{\varepsilon}\rangle =& e^{-i\phi_A+i\phi_{DC}}[e_A e'_C e'_D\,|\{d(12)c(21)a(10)\}_{\varepsilon}\rangle \\
&+ e_A e'_C e_D\,|\{d(1'2)c(21)a(10)\}_{\varepsilon}\rangle + e_A e_C e'_D\,|\{d(12)c(21')a(10)\}_{\varepsilon}\rangle \\
&+ e_A e_C e_D\,|\{d(1'2)c(21')a(10)\}_{\varepsilon}\rangle + e'_A e'_C e'_D\,|\{d(12)c(21)a(1'0)\}_{\varepsilon}\rangle \\
&+ e'_A e'_C e_D\,|\{d(1'2)c(21)a(1'0)\}_{\varepsilon}\rangle + e'_A e_C e'_D\,|\{d(12)c(21')a(1'0)\}_{\varepsilon}\rangle \\
&+ e'_A e_C e_D\,|\{d(1'2)c(21')a(1'0)\}_{\varepsilon}\rangle] \\
&+ e^{-i\phi_A-i\phi_{DC}}[e_A e_C e_D\,|\{d(10)c(01)a(10)\}_{\varepsilon}\rangle \\
&+ e_A e_C e'_D\,|\{d(1'0)c(01)a(10)\}_{\varepsilon}\rangle + e_A e'_C e_D\,|\{d(10)c(01')a(10)\}_{\varepsilon}\rangle \\
&+ e_A e'_C e'_D\,|\{d(1'0)c(01')a(10)\}_{\varepsilon}\rangle + e'_A e_C e_D\,|\{d(10)c(01)a(1'0)\}_{\varepsilon}\rangle \\
&+ e'_A e_C e'_D\,|\{d(1'0)c(01)a(1'0)\}_{\varepsilon}\rangle + e'_A e'_C e_D\,|\{d(10)c(01')a(1'0)\}_{\varepsilon}\rangle \\
&+ e'_A e'_C e'_D\,|\{d(1'0)c(01')a(1'0)\}_{\varepsilon}\rangle] \quad .
\end{aligned}
\tag{2.30}
$$

$|(DCB)_{\varepsilon}\rangle$ can be obtained by replacing A with B and a with b in Eq. (2.30). There is no interval of free evolution after the action of pulse D in either $|(DCA)_{\varepsilon}\rangle$ or $|(DCB)_{\varepsilon}\rangle$. Hence eight of the contributing sixteen wave packets-those for which the left index of d differs from ε-vanish identically.

Expressions for $|(CDA)_{\varepsilon}\rangle$ and $|(CDB)_{\varepsilon}\rangle$ can also be obtained by suitable substitutions in the full expression (2.30). Once again, eight of the sixteen terms vanish, in this instance approximately (those for which the left index of c differs from ε). Because we have ignored energy transfer inside the pulse propagators, we must for consistency neglect it as well during forward propagation under $[t_{DC}]$ following the action of the C-pulse propagator and during backward propagation under $[-t_{DC}]$ between D and C, as this interval must be shorter than the pulse duration for C and D to overlap in time.

The fifth-order wave packets listed in Eq. (2.20) incorporate second-order action of the control pulse and can be obtained by inserting the appropriate additional factors in the third-order amplitudes (2.28), (2.30), and their analogs. The pattern is the same as that used to obtain $|(APP)_\varepsilon\rangle$ from $|(A)_\varepsilon\rangle$ (see Eqs. (2.23) and (2.26)).

C. md-WPI Signal

The demonstration calculations of Section A illustrate one possible effect of coherent nuclear displacement on subsequent EET population dynamics (see Figure 1). Experimental verification of this control mechanism and the investigation of others by md-WPI would perhaps be clearest on a molecular complex with a specific orientation in the lab frame.[42] A definite fixed orientation would allow polarization selection of specific "donor" and "acceptor" chromophores. In a liquid-solution or gas-phase sample of many randomly oriented complexes of fixed internal structure, a given laser pulse may instead interact with either or both of the constituent monomers. Vibrational control over EET should still be detectable, however. The polarization of the non-resonant control pulse (P) could, for instance, be set perpendicular to that of the first electronically resonant pulse-pair (A & B). The latter selects the donor in a statistical sense, and the former would therefore preferentially vibrationally excite the acceptor chromophore.* The effect of the control pulse could be sought in the signal anisotropy with respect to the polarization of the second pulse-pair (C & D), chosen parallel to the first (preferentially monitoring the donor-excited $\leftrightarrow$ ground state and acceptor-excited $\leftrightarrow$ two-exciton state transitions) or perpendicular to it (preferentially monitoring the acceptor-excited $\leftrightarrow$ ground state and donor-excited $\leftrightarrow$ two-exciton state transitions).[30]

The signal components of various phase signatures together comprise all control-

*Another possibility would be to set $\boldsymbol{e}_P$, $\boldsymbol{e}_A$ and $\boldsymbol{e}_B$ all parallel to each other and the delay time t_{AP} equal to one quarter of the vibrational period for the mode in question. In this case the ground nuclear state of the donor-excited electronic state is preferentially populated and excited state nuclear motion is essentially quenched.

induced changes in the portion of the one-exciton population that are quadrilinear in the WPI-pulse field strengths (i.e. the quadrilinear one-exciton population with the control pulse minus the quadrilinear one-exciton population without the control pulse). We therefore write the signal as

$$S = S_1 + S_{1'}, \tag{2.31}$$

and denote that portion of ε-state population that is quadratic in E_P and quadrilinear the WPI fields as

$$\begin{aligned} S_\varepsilon =& 2\mathrm{Re}\,[\langle (A)_\varepsilon \mid (DCBPP)_\varepsilon\rangle + \langle (A)_\varepsilon \mid (CDBPP)_\varepsilon\rangle + \langle (B)_\varepsilon \mid (DCAPP)_\varepsilon\rangle \\ &+ \langle (B)_\varepsilon \mid (CDAPP)_\varepsilon\rangle + \langle (C)_\varepsilon \mid (DABPP)_\varepsilon\rangle + \langle (C)_\varepsilon \mid (DBAPP)_\varepsilon\rangle \\ &+ \langle (D)_\varepsilon \mid (CABPP)_\varepsilon\rangle + \langle (D)_\varepsilon \mid (CBAPP)_\varepsilon\rangle + \langle (APP)_\varepsilon \mid (DCB)_\varepsilon\rangle \\ &+ \langle (APP)_\varepsilon \mid (CDB)_\varepsilon\rangle + \langle (BPP)_\varepsilon \mid (DCA)_\varepsilon\rangle + \langle (BPP)_\varepsilon \mid (CDA)_\varepsilon\rangle \\ &+ \langle (CPP)_\varepsilon \mid (DAB)_\varepsilon\rangle + \langle (CPP)_\varepsilon \mid (DBA)_\varepsilon\rangle + \langle (DPP)_\varepsilon \mid (CAB)_\varepsilon\rangle \\ &+ \langle (DPP)_\varepsilon \mid (CBA)_\varepsilon\rangle]\quad . \end{aligned} \tag{2.32}$$

Among the contributions to the signal (2.32) are the overlaps of each of the four single-pulse wave packets (2.18) with its two complementary four-pulse (fifth-order) packets from Eq. (2.20), with the latter differing only in the order of action of the pulses making up a pulse-pair. In addition, there are the overlaps of the four two-pulse (third-order) wave packets from Eq. (2.19), each of which involves a single WPI-pulse, with the two complementary three-pulse (third-order) packets from the same equation, with the latter again differing in the order of action of the pulses making up a pulse-pair.

Phase-sensitive detection methods (see especially the fluorescence-detected phase-modulation technique recently demonstrated by Marcus and co-workers in Refs. 49 and 50) can isolate the (complex-valued) portion of the signal bearing any of the four possible dependen-

cies on the externally controlled phase differences ϕ_{BA} and ϕ_{DC}. We have

$$S_\varepsilon = e^{i(\phi_{BA}+\phi_{DC})}S_\varepsilon^{++}+e^{i(\phi_{BA}-\phi_{DC})}S_\varepsilon^{+-}+e^{i(-\phi_{BA}+\phi_{DC})}S_e^{-+}+e^{i(-\phi_{BA}-\phi_{DC})}S_\varepsilon^{--}, \quad (2.33)$$

in which, for instance,

$$S_\varepsilon^{+-} = \frac{1}{4\pi^2}\int_0^{2\pi} d\phi_{BA}\int_0^{2\pi} d\phi_{DC}\, e^{-i(\phi_{BA}-\phi_{DC})}\, S_\varepsilon \quad (2.34)$$

is the component of S_ε with phase $\phi_{BA}-\phi_{DC}$. We can extend this notation to identify the portion of each wave-packet overlap contributing to the signal component of a given phase signature:

$$\begin{aligned} S_\varepsilon^{++} = {} & \langle (B)_\varepsilon \mid (DCAPP)_\varepsilon \rangle^{++} + \langle (B)_\varepsilon \mid (CDAPP)_\varepsilon \rangle^{++} + \langle (BPP)_\varepsilon \mid (DCA)_\varepsilon \rangle^{++} \\ & + \langle (BPP)_\varepsilon \mid (CDA)_\varepsilon \rangle^{++} + \langle (DCBPP)_\varepsilon \mid (A)_\varepsilon \rangle^{++} + \langle (CDBPP)_\varepsilon \mid (A)_\varepsilon \rangle^{++} \\ & + \langle (DCB)_\varepsilon \mid (APP)_\varepsilon \rangle^{++} + \langle (CDB)_\varepsilon \mid (APP)_\varepsilon \rangle^{++} + \langle (D)_\varepsilon \mid (CBAPP)_\varepsilon \rangle^{++} \\ & + \langle (DPP)_\varepsilon \mid (CBA)_\varepsilon \rangle^{++} + \langle (DABPP)_\varepsilon \mid (C)_\varepsilon \rangle^{++} + \langle (DAB)_\varepsilon \mid (CPP)_\varepsilon \rangle^{++}, \end{aligned} \quad (2.35)$$

$$\begin{aligned} S_\varepsilon^{+-} = {} & \langle (B)_\varepsilon \mid (CDAPP)_\varepsilon \rangle^{+-} + \langle (B)_\varepsilon \mid (DCAPP)_\varepsilon \rangle^{+-} + \langle (BPP)_\varepsilon \mid (CDA)_\varepsilon \rangle^{+-} \\ & + \langle (BPP)_\varepsilon \mid (DCA)_\varepsilon \rangle^{+-} + \langle (CDBPP)_\varepsilon \mid (A)_\varepsilon \rangle^{+-} + \langle (DCBPP)_\varepsilon \mid (A)_\varepsilon \rangle^{+-} \\ & + \langle (CDB)_\varepsilon \mid (APP)_\varepsilon \rangle^{+-} + \langle (DCB)_\varepsilon \mid (APP)_\varepsilon \rangle^{+-} + \langle (C)_\varepsilon \mid (DBAPP)_\varepsilon \rangle^{+-} \\ & + \langle (CPP)_\varepsilon \mid (DBA)_\varepsilon \rangle^{+-} + \langle (CABPP)_\varepsilon \mid (D)_\varepsilon \rangle^{+-} + \langle (CAB)_\varepsilon \mid (DPP)_\varepsilon \rangle^{+-}, \end{aligned} \quad (2.36)$$

$$S_\varepsilon^{-+} = (S_\varepsilon^{+-})^* \quad (2.37)$$

$$S_{\varepsilon}^{--} = (S_{\varepsilon}^{++})^{*} \tag{2.38}$$

Full expressions for the components (2.35) - (2.38) in terms of overlaps between wave packets arising from specified state-space pathways, for an arbitrarily oriented EET complex, are given in Appendix B. Of particular interest is S_{ε}^{+-} (or S_{ε}^{-+}), which may be referred to as echo-like, as it should be the least affected by inhomogeneous dephasing due to differences in the local molecular environment, provided the two site energies of the dimer are positively correlated (see for example Section V.C. of Ref. 42). This distinction may become less significant if md-WPI experiments can eventually be performed on a single-molecule basis,[69] as is possible in principle with fluorescence-detected phase-cycling methods.[49,50,60–62]

D. Pump-Probe Limit

Although md-WPI more fully exposes the amplitude-level nuclear dynamics accompanying electronic excitation transfer, the control scheme proposed here could also be tested with a simpler three-pulse experiment. In such a measurement, the population dynamics following vibrational excitation by the control pulse would be monitored by polarized fluorescence-detected pump-probe spectroscopy. The md-WPI measurement becomes equivalent to a pump-probe experiment in the limit that pulses A and B share the same pulse shape and arrival time (the pump), and pulses C and D have a common pulse shape and arrival time (the probe).

We define $\Theta = \Theta_1 + \Theta_{1'}$ as the change in the pump-probe fluorescence signal caused by the non-resonant control pulse. All four components of the md-WPI signal (2.35) – (2.38) contain identical information when the intrapulse-pair delays are both set to zero. Notice that the Eq. (2.36) can be obtained from Eq. (2.35) simply by interchanging the actions of pulses C and D. Hence $S_{\varepsilon}^{++} = S_{\varepsilon}^{+-}$ (and $S_{\varepsilon}^{--} = S_{\varepsilon}^{-+}$) in the pump-probe limit; and the further

equivalence of pulses A and B then leads to

$$S_{\varepsilon}^{++} = S_{\varepsilon}^{+-} = S_{\varepsilon}^{--} = S_{\varepsilon}^{-+}, \tag{2.39}$$

whence

$$\Theta_{\varepsilon} = 4S_{\varepsilon}^{+-} \quad (t_{BA} = t_{DC} = 0). \tag{2.40}$$

An additional simplification is possible, due to the fact that relationships of the form

$$\langle (CABPP)_{\varepsilon} \mid (D)_{\varepsilon} \rangle^{+-} = \left(\langle (C)_{\varepsilon} \mid (DBAPP)_{\varepsilon} \rangle^{+-} \right)^{*} \tag{2.41}$$

obtain in the pump-probe limit, and we arrive at

$$\begin{aligned} \Theta_{\varepsilon} =& 8\mathrm{Re}\left[\langle (C)_{\varepsilon} \mid (DBAPP)_{\varepsilon} \rangle^{+-} + \langle (CPP)_{\varepsilon} \mid (DBA)_{\varepsilon} \rangle^{+-} \right] \\ &+ 8\mathrm{Re}\left[\langle (B)_{\varepsilon} \mid (CDAPP)_{\varepsilon} \rangle^{+-} + \langle (BPP)_{\varepsilon} \mid (CDA)_{\varepsilon} \rangle^{+-} \right] \\ &+ 8\mathrm{Re}\left[\langle (B)_{\varepsilon} \mid (DCAPP)_{\varepsilon} \rangle^{+-} + \langle (BPP)_{\varepsilon} \mid (DCA)_{\varepsilon} \rangle^{+-} \right] \quad . \end{aligned} \tag{2.42}$$

Grouping wave-packet overlaps based on the nature of their interactions with the resonant pump (A–B) and probe (C–D) pulses leads to the identification of the three terms in Eq. (2.42) as the ground-state bleach, excited-state absorption, and stimulated emission components of the control-induced change in the pump-probe signal, respectively ($\Theta_{\varepsilon} = \Theta_{\varepsilon}^{GSB} + \Theta_{\varepsilon}^{ESA} + \Theta_{\varepsilon}^{SE}$). In the ground-state bleach terms, the A–B pulse acts twice ($0 \leftarrow \varepsilon \leftarrow 0$) to return amplitude to the ground electronic state (and, loosely speaking, thereby cancel ground-state amplitude through destructive interference).[70] In the remaining terms, the C–D pulse acts twice on a wave packet already prepared in an excited electronic state by the A–B pulse ($\varepsilon \leftarrow 2 \leftarrow \varepsilon$ for excited-state absorption and $\varepsilon \leftarrow 0 \leftarrow \varepsilon$ for stimulated emission). Tuning the pulse parameters, such as their duration and center frequency, should

enable the isolation of one or two of these contributions in many cases.[30] Explicit expressions for these contributions to the pump-probe difference signal, in terms of overlaps between nuclear wave packets generated by specific pathways through electronic state-space, can be found in Appendix C. Numerical calculations based on the formulas given in Appendix C are presented in the following chapter.[35]

E. Concluding Discussion

We have proposed a strategy both for influencing the short-time dynamics of electronic excitation transfer by imparting coherent nuclear motion through impulsive vibrational excitation prior to electronic absorption and for monitoring the operation of this control process by multidimensional wave-packet interferometry. The theoretical framework necessary to calculate the polarized multidimensional wave-packet interferometry signal from a randomly oriented EET complex of well-defined internal structure after vibrational excitation by impulsive stimulated Raman scattering is presented in full detail, along with the corresponding expressions in the pump-probe limit of md-WPI. The amplitude-level picture of system dynamics provided by md-WPI will give useful information on surface-crossing dynamics in multi-chromophoric systems. The effect of coherent nuclear motion on molecular processes in excited electronic states could be studied by similar means in the context of internal conversion in large molecules, systems exhibiting Jahn-Teller dynamics, or those with conically intersecting adiabatic electronic potential surfaces generally.[71,72]

Good candidates for experimental and further theoretical study of the control processes envisaged here would be dimer complexes with EET coupling sufficiently strong to compete with other electronic decay mechanisms, yet weak enough to allow the neglect of excitation transfer on the timescale of ultra-short pulse lengths. The linear absorption and fluorescence spectra of such species would be expected to resemble qualitatively those of the

constituent monomers. In order to separately address the internal vibrations (by ISRS) and electronic transitions of the monomers, it will be important that they possess non-parallel electronic transition dipole moments. In the simplest case, allowing single-pulse pre-resonant impulsive excitation of a controlling vibrational mode, the monomer should have a Raman-active low-frequency mode that can be selectively excited by a pulse whose duration is somewhat shorter than the period of that mode, but longer than that of other active modes.

Various anthracene dimers investigated by Yamazaki and co-workers might be appropriate systems in which to study the vibrational control of EET.[73,74] The low-frequency vibrational progression in the $S_1 \leftarrow S_0$ absorption (and $S_1 \rightarrow S_0$ fluorescence) spectrum of anthracene is dominated by the ν_{12} fundamental and its first overtone[75] ($\omega \cong 390$ cm-1), which suggests that this mode could be selectively driven to coherent motion of non-negligible amplitude by pre-resonant ISRS. Dithia-anthracenophane (DTA)[73] is one promising system, with two anthracene monomers held rigidly at an angle of $88.5°$. Other anthracene dimers include ortho- and meta-dianthrylbenzene.[74] All three of these dimer complexes exhibit quantum beats in their time-resolved fluorescence anisotropy indicative of EET. Several naphthalene dimers have recently been synthesized by Johnson and co-workers.[76] DTA is among the model complexes for which calculated pump-probe difference signals are reported in the following chapter.

Notes

[1] P. S. Christopher, M. Shapiro, and P. Brumer, Journal of Chemical Physics **125**, 124310 (2006).

[2] M. Abe, Y. Ohtsuki, Y. Fujimura, and W. Domcke, Journal of Chemical Physics **123**, 144508 (2005).

[3] M. Sugawara, S. Yoshizawa, and S. Yabushita, Chemical Physics Letters **350**, 253 (2001).

[4] T. Buckup, J. Hauer, J. Mohring, and M. Motzkus, Archives of Biochemistry and Biophysics **483**, 219 (2009).

[5] J. Hauer, H. Skenderovic, K. L. Kompa, and M. Motzkus, Chemical Physics Letters **421**, 523 (2006).

[6] J. B. Ballard, H. U. Stauffer, Z. Amitay, and S. R. Leone, Journal of Chemical Physics **116**, 1350 (2002).

[7] B. Amstrup and N. E. Henriksen, Journal of Chemical Physics **97**, 8285 (1992).

[8] N. Elghobashi, P. Krause, J. Manz, and M. Oppel, Physical Chemistry Chemical Physics **5**, 4806 (2003).

[9] L. Dhar, J. A. Rogers, and K. A. Nelson, Chemical Reviews **94**, 157 (1994).

[10] A. M. Walsh and R. F. Loring, Journal of Chemical Physics **93**, 7566 (1990).

[11] U. Banin, A. Bartana, S. Ruhman, and R. Kosloff, Journal of Chemical Physics **101**, 8461 (1994).

[12] T. J. Smith and J. A. Cina, Journal of Chemical Physics **104**, 1272 (1996).

[13] E. M. Hiller and J. A. Cina, Journal of Chemical Physics **105**, 3419 (1996).

[14] C. J. Bardeen, Q. Wang, and C. V. Shank, Journal of Physical Chemistry A **102**, 2759 (1998).

[15] D. Gelman and R. Kosloff, Journal of Chemical Physics **123**, 11 (2005).

[16] S. Fujiyoshi, S. Takeuchi, and T. Tahara, Journal of Physical Chemistry A **107**, 494 (2003).

[17] S. Fujiyoshi, S. Takeuchi, and T. Tahara, Journal of Physical Chemistry A **108**, 5938 (2004).

[18] A. Kahan, O. Nahmias, N. Friedman, M. Sheves, and S. Ruhman, Journal of the American Chemical Society **129**, 537 (2007).

[19] P. N. Butcher and D. Cotter, *The Elements of Nonlinear Optics*, Cambridge University Press, Cambridge, 1991.

[20] S. Mukamel, *Principles of Nonlinear Optical Spectroscopy*, Oxford University Press, New York, 1995.

[21] M. Cho, *Two-Dimensional Optical Spectroscopy*, CRC press, Boca Raton, 2009.

[22] J. Seibt, K. Renziehausen, D. V. Voronine, and V. Engel, Journal of Chemical Physics **130**, 134318 (2009).

[23] J. L. Herek, W. Wohlleben, R. J. Cogdell, D. Zeidler, and M. Motzkus, Nature **417**, 533 (2002).

[24] S. E. Bradforth, R. Jimenez, F. Vanmourik, R. van Grondelle, and G. R. Fleming, Journal of Physical Chemistry **99**, 16179 (1995).

[25] V. Subramanian and D. G. Evans, Journal of Physical Chemistry B **108**, 1085 (2004).

[26] V. Renger, T. May and O. Kuhn, Physics Reports **343**, 137 (2001).

[27] G. S. Engel et al., Nature **446**, 782 (2007).

[28] T. Brixner et al., Nature **434**, 625 (2005).

[29] M. Cho, Bulletin of the Korean Chemical Society **27**, 1940 (2006).

[30] J. A. Cina and G. R. Fleming, Journal of Physical Chemistry A **108**, 11196 (2004).

[31] D. S. Kilin, O. V. Prezhdo, and M. Schreiber, Journal of Physical Chemistry A **111**, 10212 (2007).

[32] V. Novoderezhkin, R. Monshouwer, and R. van Grondelle, Journal of Physical Chemistry B **104**, 12056 (1998).

[33] V. Novoderezhkin, R. Monshouwer, and R. van Grondelle, Journal of Physical Chemistry B **104**, 12056 (2000).

[34] S. Jang, Y. J. Jung, and R. J. Silbey, Chemical Physics **275**, 319 (2002).

[35] J. D. Biggs and J. A. Cina, Journal of Chemical Physics **131**, 224101 (2009).

[36] J. A. Cina, Annual Review of Physical Chemistry **59**, 319 (2008).

[37] T. S. Humble and J. A. Cina, Journal of Physical Chemistry B **110**, 18879 (2006).

[38] T. S. Humble and J. A. Cina, Physical Review Letters **93**, 060402 (2004).

[39] J. A. Cina, Journal of Chemical Physics **113**, 9488 (2000).

[40] N. F. Scherer et al., Journal of Chemical Physics **96**, 4180 (1992).

[41] N. F. Scherer et al., Journal of Chemical Physics **95**, 1487 (1991).

[42] J. A. Cina, D. S. Kilin, and T. S. Humble, Journal of Chemical Physics **118**, 46 (2003).

[43] R. Martinez-Galicia and V. Romero-Rochin, Journal of Chemical Physics **122**, 11 (2005).

[44] S. Ramos-Sanchez and V. Romero-Rochin, Journal of Chemical Physics **121**, 2117 (2004).

[45] P. Kjellberg, B. Bruggemann, and T. Pullerits, Physical Review B **74**, 9 (2006).

[46] A. Donoso, D. Kohen, and C. C. Martens, Journal of Chemical Physics **112**, 7345 (2000).

[47] S. Mukamel, Annual Review of Physical Chemistry **51**, 691 (2000).

[48] D. Egorova, M. F. Gelin, and W. Domcke, Journal of Chemical Physics **126**, 11 (2007).

[49] P. F. Tekavec, T. R. Dyke, and A. H. Marcus, Journal of Chemical Physics **125**, 19 (2006).

[50] P. F. Tekavec, G. A. Lott, and A. H. Marcus, Journal of Chemical Physics **127**, 214307 (2007).

[51] H. Katsuki, H. Chiba, C. Meier, B. Girard, and K. Ohmori, Physical Review Letters **102**, 103602 (2009).

[52] K. Ohmori, Annual Review of Physical Chemistry **60**, 487 (2009).

[53] K. Ohmori et al., Physical Review Letters **96**, 093002 (2006).

[54] K. Ohmori, Y. Sato, E. E. Nikitin, and S. A. Rice, Physical Review Letters **91**, 243003 (2003).

[55] M. A. Bouchene, C. Nicole, and B. Girard, Journal of Physics B-Atomic Molecular and Optical Physics **32**, 5167 (1999).

[56] Y. Cao, L. Zhang, Y. Yang, Z. R. Sun, and Z. G. Wang, Chemical Physics Letters **442**, 53 (2007).

[57] J. C. Vaughan, T. Hornung, K. W. Stone, and K. A. Nelson, Journal of Physical Chemistry A **111**, 4873 (1007).

[58] M. Fushitani, M. Bargheer, M. Guhr, H. Ibrahim, and N. Schwentner, Journal of Physics B-Atomic Molecular and Optical Physics **41**, 074013 (2008).

[59] D. M. Jonas, Annual Review of Physical Chemistry **54**, 425 (2003).

[60] D. Keusters, H. S. Tan, and W. S. Warren, Journal of Physical Chemistry A **103**, 10369 (1999).

[61] P. F. Tian, D. Keusters, Y. Suzaki, and W. S. Warren, Science **300**, 1553 (2003).

[62] C. Q. Li, W. Wagner, M. Ciocca, and W. S. Warren, Journal of Chemical Physics **126**, 164307 (2007).

[63] M. L. Cowan, J. P. Ogilvie, and R. J. D. Miller, Chemical Physics Letters **386**, 184 (2004).

[64] T. Brixner, T. Mančal, I. V. Stiopkin, and G. R. Fleming, Journal of Chemical Physics **121**, 4221 (2004).

[65] A. M. Weiner, D. E. Leaird, G. P. Wiederrecht, and K. A. Nelson, Science **247**, 1317 (1990).

[66] M. M. Wefers, H. Kawashima, and K. A. Nelson, Journal of Chemical Physics **108**, 10248 (1998).

[67] S. Popescu, A. J. Short, and A. Winter, Nature Physics **2**, 754 (2006).

[68] S. Popescu, A. J. Short, and A. Winter, (2006).

[69] J. Hernando et al., Physical Review Letters **97**, 216403 (2006).

[70] T. J. Smith, L. W. Ungar, and J. A. Cina, Journal of Luminescence **58**, 66 (1994).

[71] A. Migani and M. Olivucci, Conical intersections and organic reaction mechanisms, in *Conical Intersections. Electronic Structure, Dynamics, and Spectroscopy*, edited by D. R. Domcke, W. Yarkony and H. Köppel, Singapore, 2004, World Scientific.

[72] D. A. Farrow, W. Qian, E. R. Smith, A. A. Ferro, and D. M. Jonas, Journal of Chemical Physics **128**, 144510 (2008).

[73] I. Yamazaki, S. Akimoto, T. Yamazaki, S. Sato, and Y. Sakata, Journal of Physical Chemistry A **106**, 2122 (2002).

[74] I. Yamazaki, S. Akimoto, N. Aratani, and A. Osuka, Bulletin of the Chemical Society of Japan **77**, 1959 (2004).

[75] W. R. Lambert, P. M. Felker, J. A. Syage, and A. H. Zewail, Journal of Chemical Physics **81**, 2195 (1984).

[76] V. M. Cangelosi, A. C. Sather, L. N. Zakharov, O. B. Berryman, and D. W. Johnson, Inorganic Chemistry **46**, 9278 (2007).

CHAPTER III

CALCULATIONS OF MD-WPI SIGNALS IN THE PUMP-PROBE LIMIT AS TESTS FOR VIBRATIONAL CONTROL OVER ELECTRONIC EXCITATION TRANSFER

A. Background and Setup

Recent theoretical studies of electronic excitation transfer (EET) have explored the influence of coupling between the purely electronic degrees of freedom and "environmental" nuclear motion (both intra- and intermolecular). Making use of experimentally guided choices for bath-mode correlation functions, Aspuru-Guzik and co-workers[1,2] performed computations tracking useful measures for the influence of different environment-induced processes on energy transfer. Plenio *et al.*[3,4] subsequently analyzed the fundamental effects of electronic dephasing, relaxation, and trapping within the context of models relying on a phenomenological Markovian description of the environmental interactions. Both groups have made important headway in elucidating the observed interplay among coherent electronic dynamics, medium-induced decoherence and relaxation, and trapping processes in complex multi-chromophore systems such as the Fenna-Matthews-Olson complex,[5,6] bacterial photosynthetic reaction centers,[7] and conjugated polymers.[8] In the context of these studies, the

electronic degrees of freedom are regarded as the "system," while the "bath" comprises both inter- and intramolecular vibrational degrees of freedom.

Other studies have addressed certain manifestly non-Markovian effects that can occur in the presence of fairly strong coupling between electronic excitations and intramolecular or local vibrations. Jang, Jung, and Silbey[9] formulated a time-dependent generalization of Förster theory accounting for the effects on energy transfer of coherent vibrational motion in a Franck-Condon active mode. Cina and Fleming[10] performed model-system calculations seeking to rationalize the observation of vibrational coherence transfer in time-resolved polarized fluorescence up-conversion measurements on LH-1.[11,12]

In the preceding chapter,[13] we describe a possible means of exerting external influence over the time-course of initial electronic excitation transfer by inducing a coherent intramolecular vibration in the acceptor chromophore prior to short-pulse excitation of the donor. Their strategy builds on the work of Jang, Jung, and Silbey[9] and Cina and Fleming,[10] and seeks to control the instantaneous "rate" of excitation transfer by initiating vibrational motion in a Franck-Condon active acceptor mode in order to render time-dependent the acceptor absorption frequency relative to the emission frequency of the donor.

Motivated by current ultrafast experimental capabilities,[5,8,14–21] this recent theoretical work generalizes Förster's foundational insights on excitation transfer,[22] and builds on other detailed studies of the dynamics of few- or multi-level quantum mechanical systems in condensed media.[23–28]

Chapter II presents general expressions for the md-WPI difference signal from an EET dimer following the action of a control pulse of arbitrary polarization and shape. The signal expressions given there apply to a sample of isotropically distributed dimers, having a specified internal geometry, in which the acceptor vibration can be preferentially driven by impulsive

stimulated Raman excitation with a short, polarized "control" pulse.[29,30*] An electronically resonant, polarized "pump" comprising two optical-phase-related pulses then preferentially excites the donor, and the action of a polarized phase-controlled "probe" pulse-pair enables the detection of a wave-packet interferometry signal. Such control-pulse-influenced md-WPI measurements will provide highly detailed nuclear-amplitude-sensitive records of the effect of the externally induced nuclear motion on the time-course of EET. Here, we perform numerical tests of this approach to the control and observation of short-time EET by applying the previous general treatment to some simplified model systems, and by collapsing the pump and probe pulse-pairs in the WPI sequence each to a single pump or probe pulse.

Chapter II treats a molecular dimer with a field-free Hamiltonian Eq. (2.1). The designation of one molecule as the donor and the other as the acceptor is arbitrary in the case of a homo-dimer of monomers with equal site energy. The signal calculations shown below for such systems treat both chromophores identically; their excitation and de-excitation probabilities depend upon the direction cosines between their individual transition dipole moments and the various field polarizations. In calculations of time-resolved signals from hetero-dimers, the donor (acceptor) will be the monomer having the higher (lower) site energy.

The Hamiltonian Eq. (2.1) is general in form, allowing any number of intramolecular vibrational and bath degrees of freedom-including "mode-sharing" between the monomers-but we specialize here to some simple cases allowing illustrative tests of the basic control strategy and its spectroscopic verification. We ascribe to each chromophore a single internal harmonic vibration whose equilibrium coordinate value is displaced in the monomer's e-state, but whose frequency is the same for both monomers and remains unchanged upon electronic

*As mentioned in Chapter II, similarly effective control over EET may be exercised in some cases by instead coherently displacing the vibrational coordinates of the donor chromophore.

excitation. The nuclear Hamiltonians can then be written as

$$\begin{aligned} H_0 &= \frac{p_a^2 + p_b^2}{2m} + \frac{m\omega^2}{2}\left[q_a^2 + q_b^2\right] \\ H_1 &= \frac{p_a^2 + p_b^2}{2m} + \frac{m\omega^2}{2}\left[(q_a - d)^2 + q_b^2\right] + \varepsilon_1 \\ H_{1'} &= \frac{p_a^2 + p_b^2}{2m} + \frac{m\omega^2}{2}\left[q_b^2 + (q_b - d)^2\right] + \varepsilon_{1'} \\ H_2 &= \frac{p_a^2 + p_b^2}{2m} + \frac{m\omega^2}{2}\left[(q_a - d)^2 + (q_b - d)^2\right] + \varepsilon_2 \ . \end{aligned} \tag{3.1}$$

ω is the common vibrational frequency of both intramolecular modes; ε_1 and $\varepsilon_{1'}$ are the donor and acceptor site energies, respectively; ε_2 is the energy of the two-exciton state (perhaps roughly equal to $\varepsilon_1 + \varepsilon_{1'}$); and d is the displacement of the e-state nuclear potential curves (of importance in the calculations performed below is the dimensionless quantity $\delta = d\sqrt{m\omega/2}$, the coordinate displacement d divided by $2\Delta q_{rms} = \sqrt{2/m\omega}$; $\hbar \equiv 1$ throughout). $q_{a(b)}$ and $p_{a(b)}$ are the position and momentum operators for a vibrational mode localized on the donor (acceptor) chromophore respectively. Extending the Hamiltonian (2.1) to multiple chromophores recovers the Frenkel exciton Hamiltonian widely used to study energy migration in molecular aggregates.[31–33]

Calculations are performed using the eigenbasis of the uncoupled ($J = 0$)) Hamiltonian; $|n\rangle\,|(\nu_a\nu_b)_n\rangle$ denotes the state in which the electronic degrees of freedom are in state n , while the vibrations are in an eigenstate of H_n with ν_a and ν_b quanta in the donor and acceptor, respectively. The basis is truncated beyond states having more than a certain total number of vibrational quanta (between 10 and 24 for the parameter values used here). Free evolution under the EET-coupled Hamiltonian (2.1) is treated by numerical matrix diagonalization to obtain a representation of

$$[t] \equiv e^{-i\,H\,t} = \sum_j |\Psi_j\rangle\, e^{-i\,E_j\,t}\, \langle\Psi_j| \tag{3.2}$$

in our finite basis, where $|\Psi_j\rangle$ is an eigenket of H with energy E_j.

We wish to predict the signals from ultrafast pump-probe difference measurements on the system described by Eq. (2.1). The measured observable is the contribution to the population of the one-exciton manifold (states 1 and 1′) that is simultaneously linear in the intensities (electric field squared) of a nonresonant control pulse (denoted by P), an electronically resonant pump pulse (A), and a resonant probe pulse (C); see Chapter II for more details. The electric field of the pulse I has the form specified by Eq. (2.5), with a Gaussian envelope function

$$f_I(t) = exp\left\{-(t-t_I)^2/2\sigma_I^2\right\} \tag{3.3}$$

and a phase function

$$\Phi_I(t) = \Omega_I \cdot (t - t_I)\ . \tag{3.4}$$

The first- and second-order interactions of the system with each nonzero-duration laser pulse are described by pulse-propagators (see Eqs. (2.12) and (2.17), and further below). These are matrices-whose elements need be calculated only once-which describe a pulse's effect on the state of the system irrespective of the variable arrival time t_I . Calculation of the pulse-propagators is simplified by assuming that the pulse duration σ_I is short compared to the characteristic timescale $2\pi/J$ for excitation transfer, so that EET can be ignored in accounting for the action of a pulse. Using the pulse shape (3.3) and phase function (3.4), we find, for example,

$$\begin{aligned}\left\langle (\nu_a,\nu_b)_1 \left| p_I^{(10)}(\infty)\ |(\bar{\nu}_a,\bar{\nu}_b)_0 \right\rangle =& i\sqrt{\frac{\pi}{2}} E_I m \sigma_I \left\langle (\nu_a)_e \left| (\bar{\nu}_a)_g \right\rangle \delta_{\nu_b,\bar{\nu}_b} \right. \\ & \times \exp\left\{ -\frac{\sigma_I^2}{2}\left(\Omega_I + \omega(\bar{\nu}_a - \nu_a) - \varepsilon_1\right)^2 \right\}\ ,\end{aligned} \tag{3.5}$$

in the notation of Eq. (2.14) in Paper 1; $\delta_{\nu_b\bar{\nu}_b}$ is a Kronecker delta.* Other matrix elements

*The infinity symbol indicates that the upper limit of integration extends past the pulse envelop, as is appro-

of the first-order pulse propagators can be similarly obtained. The Franck-Condon overlap appearing on the RHS of Eq. (3.5) can be calculated straightforwardly using displacement-operator methods.[34]

The second-order action of a pulse (such as the control pulse) includes contributions from matrix elements of the type

$$\begin{aligned}\Big\langle (\nu_a,\nu_b)_0 \Big| p_I^{(01)}(\infty;\, t_2) p_I^{(10)}(t_2;\, t_1) \,|(\bar{\nu}_a,\bar{\nu}_b)_0 \Big\rangle \\ = \left(\frac{iE_I m}{2}\right)^2 \int_{-\infty}^{\infty} dt_2 \int_{-\infty}^{t_2} dt_1 \, f_I(t_2) f_I(t_1) e^{i\Phi_I(t_2) - i\Phi_I(t_1)} \\ \times \Big\langle (\nu_a,\nu_b)_0 \Big| e^{-iH_0(t_I - t_2)} e^{-iH_1(t_2 - t_I)} e^{-iH_1(t_I - t_1)} e^{-iH_0(t_1 - t_I)} \,|(\bar{\nu}_a,\bar{\nu}_b)_0 \Big\rangle \ .\end{aligned} \tag{3.6}$$

Using the eigenenergies of ground and one-exciton vibronic states, along with the Gaussian pulse envelope (3.3) and the phase function (3.4), and making a sequence of integration-variable changes, Eq. (3.6) can be evaluated analytically to give

$$\begin{aligned}\Big\langle (\nu_a,\nu_b)_0 \Big| p_I^{(01)}(\infty;\, t_2) p_I^{(10)}(t_2;\, t_1) \,|(\bar{\nu}_a,\bar{\nu}_b)_0 \Big\rangle \\ = -\frac{\pi}{4}\sigma_I^2 E_I^2 m^2 \delta_{\nu_b,\bar{\nu}_b} \sum_{\bar{\bar{\nu}}_a} \langle (\nu_a)_g |\, (\,\bar{\bar{\nu}}_a)_e \rangle \, \langle (\,\bar{\bar{\nu}}_a)_e |\, (\,\bar{\nu}_a)_g \rangle \\ \times \exp\left\{ -\sigma_I^2 \Delta^2 - \frac{\sigma_I^2 \omega^2}{4} \, (\nu_a - \bar{\nu}_a)^2 \right\} \, \left[1 + \mathrm{erf}(i\sigma_I \Delta)\right] \ ,\end{aligned} \tag{3.7}$$

where

$$\Delta \equiv \Omega_I + \omega \left(\frac{\nu_a + \bar{\nu}_a}{2} - \bar{\bar{\nu}}_a \right) - \varepsilon_1 \ . \tag{3.8}$$

Appendix E details the derivation of Eq. (3.7) and other elements of the second-order pulse propagators. Possession of a compact expression for the second-order action of a pulse propagator-whose identification is a key practical result of this paper-greatly facilitates the calculation of

---

priate for temporally non-overlapping pulses. The second argument of the reduced pulse propagator (compare Eq. (2.14)) can be dropped in this situation.

short-pulse multidimensional optical signals by eliminating the need for repeated numerical evaluation of nested time-integrals like those in Eq. (3.6). Similar expressions can also be derived for linearly chirped Gaussian pulses, whose phase functions are quadratic in time.* Although results of this kind might appear to be limited to displaced harmonic systems, they can also be applied to arbitrary anharmonic potentials by replacing the latter with harmonic approximations whose value, slope, and curvature match those of the actual potential at the instantaneous location of the wave packet on which the propagators act.[36]

B. Calculations

B.1. Model System with Moderate Electronic-Vibrational Coupling

We first consider a model system with moderate vibrational displacements, $\delta = \sqrt{2.5}$, in the site-excited states; a value $J = 0.2\,\omega$ for the energy-transfer parameter; and perpendicular donor and acceptor electronic transition-dipole moments. The monomers are assigned equal site energies, $\varepsilon_1 = \varepsilon_{1'} \equiv \varepsilon$, and $\varepsilon_2 = \varepsilon_1 + \varepsilon_{1'} = 2\varepsilon$.† A numerical search over pulse duration and center frequency, subject to a constraint of less than 5% electronic excitation probability, found that among transform-limited Gaussian control pulses the combination $\sigma_P = 0.140\,(2\pi/\omega)$ and $\Omega_P = \varepsilon - 1.91\,\omega$ generates the largest amplitude of nuclear motion, $0.338\,d = 1.068\,\Delta q_{rms}$, in the electronic ground state. All subsequent calculations ignore the small contribution due to control-induced electronic excitation. In order that the control pulse selectively excite vibrational motion in the "acceptor" chromophore, while the pump and probe pulses excite and probe the "donor," we choose a VHH polarization combination in which the control pulse is perpendicular to the mutually parallel pump and probe.

*See for example Ref. 35

†We make the choice $\varepsilon_2 = \varepsilon_1 + \varepsilon_{1'}$ in the absence of system-specific information on the shift in one monomer's excitation energy due to prior excitation of the other. As mentioned in Chapter II, the presence such a shift would nonetheless be helpful in allowing experimental discrimination between emission signals from the 1- and 2-exciton manifolds.

The pump pulse, with duration $\sigma_A = 0.1\,(2\pi/\omega)$ and center frequency $\Omega_A = \varepsilon + \delta^2\,\omega$, is locally resonant with the $1 \leftarrow 0$ transition along the line $q_a = 0$ and with $1' \leftarrow 0$ along $q_b = 0$. The probe pulse, with $\sigma_C = 0.25\,(2\pi/\omega)$ and $\Omega_C = \varepsilon - 3\delta^2\,\omega$, is resonant with $1 \rightarrow 0$ along the line $q_a = 2d$ and with $1' \rightarrow 0$ along the line $q_b = 2d$. These lines are the loci of vibrational outer turning points in the 1 and 1 states, respectively.

Figure 3.1 shows the fractional population of the one-exciton manifold residing in the donor state (state-1) of an oriented complex (one site transition-dipole vertical, the other horizontal) following A-pulse excitation to that state from the electronic ground state without and with prior impulsive-Raman excitation of coherent vibrational motion in the acceptor chromophore at time $t_P = t_A - 0.56(2\pi/\omega)$ (chosen so that the ground-state wave packet is at its inner turning point, with $\langle q_b \rangle = -\,0.338d$, when the A pulse arrives). Despite the fact that the acceptor-mode displacement achieved by the impulsive Raman process is smaller than the ideal value $\langle q_b \rangle = -\,d$ envisaged in Fig. 2.1, the control pulse evidently slows excitation transfer significantly during the first seven vibrational periods.

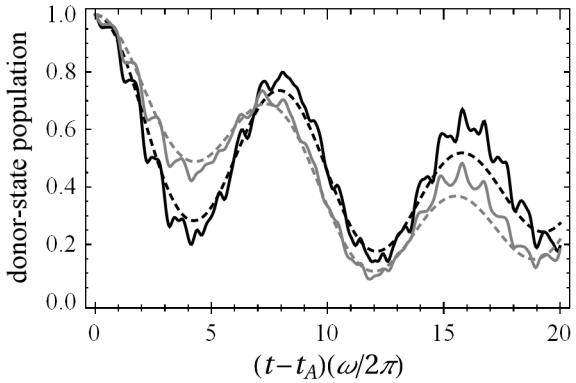

Figure 3.1: Relative population of donor state versus time (in vibrational periods) after electronic excitation from vibrational ground state (solid black curve) and from impulsively displaced vibrational wave packet (solid gray curve). Corresponding dashed curves are semi-analytical predictions of weak EET-coupling theory derived in Appendix D, which depend only on vibronic state populations and miss effects due to vibrational coherence.

Figure 3.2 compares the calculated pump-probe and pump-probe difference signals

for this system in an isotropic sample. In the absence of influence by control-pulse vibrational stimulation on the time-course of excitation transfer, these two signals would be proportional to each other at all times. The lack of simple proportionality between the two curves in Fig. 3.2 therefore demonstrates coherent control of EET. Both the survival probabilities and the pump-probe signals are influenced by vibrational coherences. The latter spectroscopic signals, though, are additionally complicated because the signal selects for nuclear probability density in a specified probe-window region of vibrational configuration space. Thus the pump-probe signals provide detailed views of the nuclear *and* electronic dynamics in this EET system, as they reflect the instantaneous spatial probability density in the probe-window region, rather than just the total population of a specific electronic state.[37,38] In this model system with moderately strong electronic-vibrational coupling, the envelope of the probe-probe signal and the pump-probe difference signal nevertheless roughly resemble the corresponding population traces of Fig. 3.1.* In particular, the envelope of the pump-probe difference signal decreases less precipitously during the first $\sim 5(2\pi/\omega)$ than the envelope of the pump-probe signal without a control pulse.

Because the probe-pulse center frequency is strongly red-shifted from the pump ($\Omega_C - \Omega_A = -4\delta^2\omega$), both signals in Fig. 3.2 are dominated by their stimulated-emission contributions. Those contributions (not shown separately)-specified for the pump-probe difference by Eq. (2.42) and Appendix C -are indistinguishable on the scale of Fig. 3.2 from the total signals including also excited-state absorption and ground-state bleaching.†

*Qualitative agreement between the envelope of the predicted signal and site population dynamics-to be regarded as an abstract "observable," rather than a quantity readily available for spectroscopic determination on the femtosecond timescale-may not obtain in general. Calculations of populations and signals from similar model systems with stronger electronic-vibrational coupling (larger δ, results not shown) exhibited less correspondence between the pump-probe envelope and the donor-excitation survival probability. In the case of stronger electronic-vibrational coupling, the various electronic difference potentials are steeper, and the nuclear probability density in the correspondingly narrowed probe-window regions may become less reflective of the site-state population as a whole.

†$q_a = 2d$ and $q_b = 2d$ are the lines of $1 \rightarrow 0$ and $1' \rightarrow 0$ stimulated-emission resonance, respectively; both lines are visited by significant nuclear probability density in the appropriate singly-excited state. $q_a = 2d$ is also

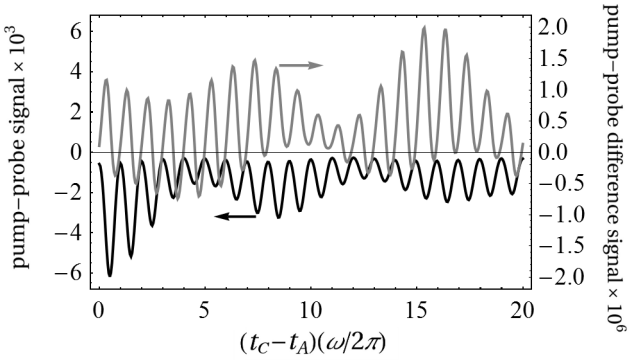

Figure 3.2: Pump-probe signal (black curve, left ordinate in units of $E_A^2 E_C^2 m^4/2^4$) and pump-probe difference signal (gray curve, right ordinate in units of $E_P^2 E_A^2 E_C^2 m^6/2^6$) as a function of delay time between pump and probe pulses. Signals are calculated for an isotropic sample of the model energy-transfer complex with equal-energy monomers having perpendicular transition moments.

The presence of six direction cosines (see Appendix A) suggests that the VHH-polarized pump-probe difference signal from an isotropic sample should be dominated by those terms which would be nonzero if the EET complex were oriented with one transition moment along the vertical axis and the other horizontal. In Figure 3.3 are plotted those portions of the stimulated-emission signals arising from the wave-packet overlaps that would be generated in such ideally oriented complexes.* The handful of overlaps contributing to the signals in Fig. 3.3, which is plotted on the same scale as Fig. 3.2, evidently account a major portion of the pump-probe and pump-probe difference signals from the isotropic sample.

---

the resonance line for $1 \leftarrow 0$ ground-state bleach and $2 \leftarrow 1'$ excited-state absorption, while $q_b = 2d$ is the line for $1' \leftarrow 0$ ground-state bleach and $2 \leftarrow 1$ excited-state absorption; but these regions are never populated by significant nuclear probability density in the electronic state from which the transition would take place.

*The stimulated-emission pump-probe difference signal plotted in Fig. 3 is given by $\Theta_1^{SE} + \Theta_{1'}^{SE}$, where

$$\begin{aligned}\Theta_\varepsilon^{SE} = 8\mathrm{Re}\tfrac{3}{35}\{&\langle\{a(1'0)\}_\varepsilon \mid \{c(1'0)c(01')a(1'0)p(01)p(10)\}_\varepsilon\rangle \\ &+ \langle\{a(10)\}_\varepsilon \mid \{c(10)c(01)a(10)p(01')p(1'0)\}_\varepsilon\rangle \\ &+ \langle\{a(1'0)p(01)p(10)\}_\varepsilon \mid \{c(1'0)c(01')a(1'0)\}_\varepsilon\rangle \\ &+ \langle\{a(10)p(01')p(1'0)\}_\varepsilon \mid \{c(10)c(01)a(10)\}_\varepsilon\rangle\}\end{aligned}$$

(see Appendix C and Table A.1 in Appendix A). Because no further propagation need be carried out after the reduced C-pulse propagator acts, only two of the four terms in this equation can be nonzero for either choice of ε (i.e. the second and fourth (first and third) terms for $\varepsilon = 1$ $(1')$).

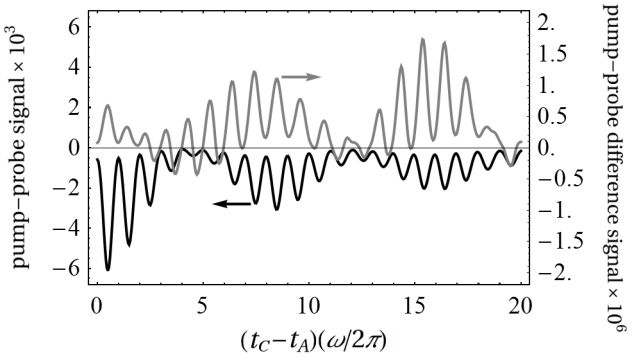

Figure 3.3: Stimulated-emission contributions to the pump-probe and pump-probe difference signals shown in Fig. 3.2 from those wave-packet overlaps that would take nonzero values if one monomer's transition moment were oriented vertically (parallel to the control-pulse polarization) and the other's were oriented horizontally (parallel to the pump and probe polarization).

Although the main focus here is on the energy-transfer dynamics of putatively isolated systems, some indication of the effects of medium-induced dephasing on the calculated signals can be gained by introducing electronic inhomogeneous broadening. To this end, we average the signals over a collection of isotropic dimer systems in which monomer site energies, ε_1 and $\varepsilon_{1'}$, are independently distributed about a common mean value ε. The less rapid decrease in VHH pump-probe difference signal compared to the HH pump-probe signal seen in Fig. 3.2 remains evident in the inhomogeneously broadened signals shown in the upper panel of Figure 3.4.* The corresponding perpendicular-probe cases, VHV and HV are shown there as well, and the resulting signal anisotropies- (VHH-VHV)/(VHH+2VHV) for pump-probe difference and (HH-HV)/(HH+2HV) for pump-probe-are plotted in the lower panel of Fig. 3.4. There is a notably lower initial value in the control-influenced pump-probe difference anisotropy, but it does not appear to decay less rapidly than the pump-probe anisotropy for this system. Appendix F addresses the interesting dependence of the initial pump-probe difference

*The vertical scales are the same in Fig. 3.2 and the upper panel of Fig. 3.4. The signals are larger in the latter case because of the longer pump and probe pulses.

anisoptropy on the duration of pulses A and C. But the findings presented there must be considered approximate because the theory of Chapter II (see its Theory section) and the calculations of this chapter neglect the effects of temporal A–C overlap. Such pump-probe overlap effects are unlikely to be entirely negligible when $t_C - t_A = 0$.

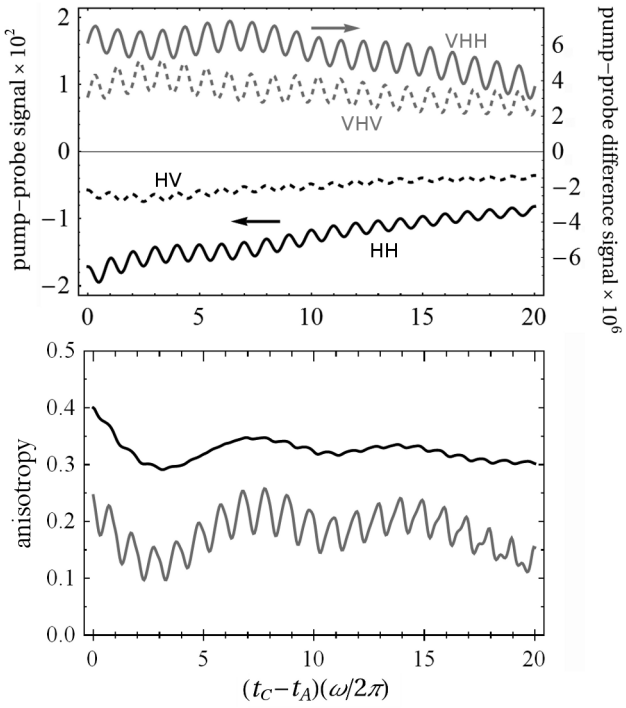

Figure 3.4: Upper panel: Average signals from a collection of 1000 model-system dimers ($\delta = \sqrt{2.5}$, $J = 0.2\,\omega$), whose site energies are chosen from independent normal distributions ($\bar{\varepsilon}_1 = \bar{\varepsilon}_{1'} \equiv \varepsilon$) with FWHM equal to the vibrational frequency. Pulse parameters are the same as in Fig. 3.2, except the temporal widths of the pump and probe pulses are $\sigma_A = 0.25\ (2\pi/\omega)$ and $\sigma_C = 0.5\ (2\pi/\omega)$, respectively. Pump-probe signals are shown for HH and HV polarizations; pump-probe difference signals for VHH and VHV polarizations. Lower panel: Signal anisotropies for the inhomogeneously broadened model system, in black for pump-probe and gray for pump-probe difference.

B.2. Dithia-anthracenophane

Next we examine excitation-transfer dynamics and pump-probe signals from an EET complex with parameter values appropriate to dithia-anthracenophane (DTA), a covalent

anthracene dimer compound that has been studied by Yamazaki and co-workers[39,40*] using time-resolved pump-probe anisotropy measurements. Two vibrational modes of the anthracene monomer, mode-12 at $\omega_{12}/2\pi c = 385\,\mathrm{cm}^{-1}$ and mode-6 at $\omega_6/2\pi c \cong 1400\,\mathrm{cm}^{-1}$, dominate the vibronic progression of its $S_1 \leftarrow S_0$ fluorescence-excitation spectrum within $1500\,\mathrm{cm}^{-1}$ of its origin at $27,695\,\mathrm{cm}^{-1}$.[42] From the jet-spectroscopy data of Lambert *et al.* we abstract a dimensionless displacement $\delta_{12} = \sqrt{0.31}$ for the lower-frequency vibration. We use an effective energy-transfer coupling constant $J = (33.6\,\mathrm{cm}^{-1}/2)\ exp(\delta_{12}^2) = 0.0595\ \omega_{12} = 22.9\mathrm{cm}^{-1}$ obtained by dividing half the population-oscillation frequency reported in Ref. 40 by the estimated Franck-Condon overlap between two mode-12 wave packets separated by their relative displacement ($\sqrt{2}d_{12}$) in the two site-excited potential wells.[†] The two anthracene-monomer transition dipole moments in DTA are known to be approximately, but not exactly, orthogonal;[39] for simplicity, their relative angle is set to $\alpha = \pi/2$ in our calculations.

In the calculations shown here, we have taken chosen pulse widths and center frequencies so that only superpositions of mode-12 vibronic states are prepared upon electronic excitation and only mode-12 is susceptible to impulsive-Raman excitation in the electronic ground state. In particular, mode-6 is quiescent under the action of both the control pulse ($\sigma_P = 0.225(2\pi/\omega_{12}) = 19.5\mathrm{fs}$; $\Omega_P = \varepsilon - 1.53\omega_{12}$) and the vertically resonant pump ($\sigma_A = 0.1(2\pi/\omega_{12}) = 8.66\mathrm{fs}$; $\Omega_A = \varepsilon + \delta_{12}^2\,\omega_{12}$). We therefore report calculations on a simplified model, referred to as DTA-12, in which only this single Franck-Condon active mode is treated explicitly. The probe pulse is longer than the pump and resonant at the outer turning line of nuclear motion in either site-excited state of DTA-12, with $\sigma_C = 0.5\,(2\pi/\omega_{12}) = 43.3\mathrm{fs}$ and $\Omega_C = \varepsilon - 3\delta_{12}^2\,\omega_{12}$. A VHH polarization scheme is

*See also Ref. 41.

†Non-unit Franck-Condon overlaps due to the small relative displacement of other vibrational modes in the two site-excited states presumably contribute to the energy-transfer oscillation frequency observed in Ref. 40 and are therefore implicitly incorporated in our estimated coupling constant J.

adopted (as explained in subsection B.1). The control pulse generates mode-12 nuclear motion in the electronic ground state with amplitude $0.54d_{12} = 0.60\Delta q_{12}$. The delay between the control and pump pulses, $0.56(2\pi/\omega_{12}) = 48.5$ fs,is chosen so that this control-induced wave packet reaches its inner turning point, $\langle q_b \rangle = -0.54d_{12}$, at the arrival time of the pump pulse.

Calculated pump-probe and pump-probe difference signals from an isotropic DTA-12 sample are shown in the upper panel of Figure 3.5. Due to the small δ_{12} value, both excited-state absorption and ground-state bleach, along with stimulated emission, contribute significantly to the calculated signals. One-exciton emission signals very nearly equivalent to the stimulated emission components[43] of the pump-probe and pump-probe difference signals (Fig. 3.5, lower panel) could however be isolated in fluorescence up-conversion measurements.[44]

Despite their general similarity in form, the pump-probe difference and corresponding pump-probe signals in Fig. 3.5 are not constant multiples of each other, so the nuclear motion induced by the control pulse evidently affects to some degree the wave-packet surface-crossing dynamics in the one-exciton manifold. We turn to the population dynamics from an oriented DTA-12 complex to gain further insight. Figure 3.6 plots the donor-state survival probability following the action of the control and pump pulses on a dimer with one site transition-dipole aligned with the control-pulse polarization (vertical) and the other aligned with the pump (horizontal). The control pulse induces small-amplitude motion in the acceptor–$0.54d_{12} = 0.54\delta\sqrt{2/m\omega_{12}} = 0.60/\sqrt{2m\omega_{12}}$, less than the rms width of the wave packet-so the population dynamics in the presence of the control pulse differs only slightly from that in its absence. Moreover, the small-amplitude vibration *accelerates* short-time electronic excitation transfer in DTA-12 rather than forestalling it, by increasing the amplitude of the donor-to-acceptor population oscillation. As explained further in Appendices D and G, this behavior results from the fact that the vibrational displacement in mode-12 is not large

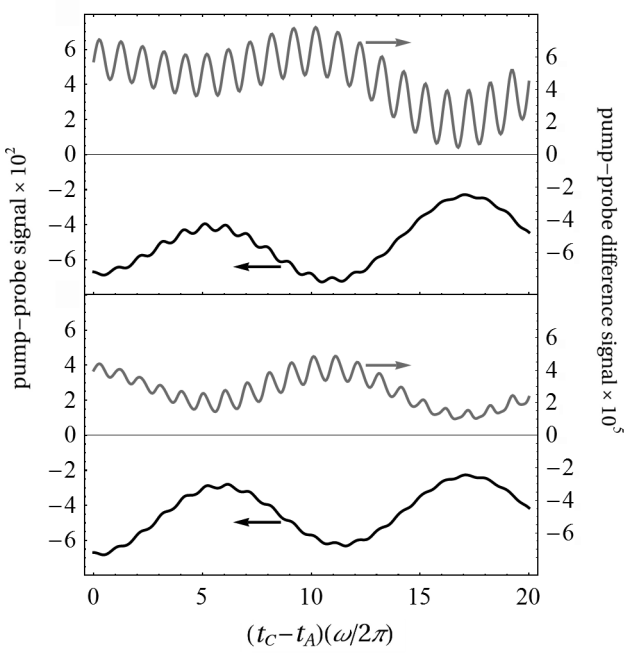

Figure 3.5: Pump-probe signal (black curve, left ordinate) and pump-probe difference signal (gray curve, right ordinate) as function of the delay between pump and probe pulses. Upper panel shows pump-probe and pump-probe difference signals from simplified model of dithiaanthracenophane treating only the dynamics of the low-frequency mode-12. Lower panel plots stimulated-emission contributions from DTA-12.

enough to remove the donor-state wave packet from the region of intersection between the donor-excited and acceptor-excited potential energy surfaces. The quasi-classical argument suggesting that acceptor-mode displacement should impede short-time EET (see Fig. 2.1 of Chapter II and the accompanying explanation) does not apply in this situation.

In an effort to model the effects of electronic inhomogeneous broadening in DTA-12, we can introduce variable monomer site energies (as described in subsection B.1). Figure 3.7 shows the pump-probe and pump-probe difference anisotropies obtained from the inhomogeneously broadened stimulated-emission components. The calculated signals from which these anisotropies were obtained were averaged over 1200 DTA-12 dimers whose site energies were chosen from independent Gaussian distributions with 100-cm-1 FWHM. Pulse parameters are the same as in Fig. 3.5, except $\sigma_A = 0.25\,(2\pi/\omega_{12}) = 21.6$ fs. The slight control-induced acceleration of EET seen in the lower panel of Fig. 3.5 is discernible also in the shorter-period anisotropy oscillation from the pump-probe difference than the pump-probe signal in Fig. 3.7.

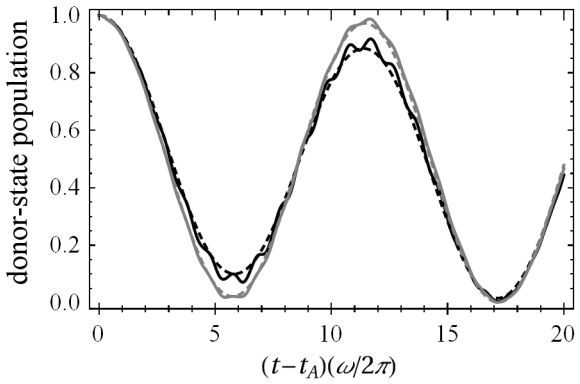

Figure 3.6: Donor-excited-state population dynamics for DTA-12 without (solid black curve) and with (solid gray curve) prior impulsive excitation of mode-12 vibration in acceptor chromophore. Transition dipole moment of acceptor chromophore is aligned with vertical control-pulse polarization. Transition dipole moment of donor is aligned with horizontal pump-pulse polarization. Dashed curves show corresponding predictions of weak EET-coupling approximation (see Appendix D).

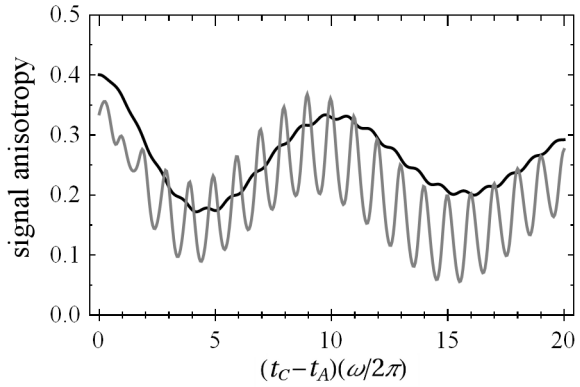

Figure 3.7: Anisotropies calculated from inhomogeneously broadened stimulated emission component of the pump-probe signal (black) and pump-probe difference signal (gray).

B.3. Downhill Energy Transfer

The calculations of subsections B.1 and B.2 focus on homodimers, in which the site excitation energies of the participating monomers are the same. We next investigate the vibrational influence on EET in a heterodimer whose excitation donor has a higher site energy than the acceptor. In order to facilitate comparison with the calculations of subsection 2A, we use the same values of all system parameters except $\varepsilon_{1'} = \varepsilon_1 - 2\omega\delta^2$. This difference in site energies is chosen so that the state-1 potential energy surface passes through the minimum of the state-1 potential located at $(q_a, q_b) = (d, 0)$. The diagonal intersection line between donor-excited and acceptor-excited potentials also passes through the point $(q_a, q_b) = (0, -d)$ corresponding to "ideal" acceptor-mode displacement. In this "downhill" model, it is expected that electronic excitation of the donor chromophore at an instant when the coherently vibrating acceptor mode is at its inner turning point should lead to accelerated short-time energy transfer.

The control pulse used to effect this coherent impulsive excitation has the same vertical polarization and pulse duration ($\sigma_P = 0.140\,(2\pi/\omega)$) as in subsection 2A. Its center frequency is down-shifted by $2\omega\delta^2$ to $\Omega_P = \varepsilon_{1'} - 1.91\,\omega = \varepsilon_1 - 6.91\,\omega$ in keeping with the lower acceptor site energy, and the acceptor-mode wave packet is therefore identical to

that considered previously. The horizontally polarized pump pulse has the same center frequency ($\Omega_A = \varepsilon_1 + \delta^2\,\omega$), duration ($\sigma_A = 0.1\,(2\pi/\omega)$), and arrival time relative to the control pulse as before; it is locally resonant with $1 \leftarrow 0$ along $q_a = 0$ and with $1' \leftarrow 0$ along $q_b = -d$, which is largely unpopulated by nuclear probability amplitude belonging to either the vibrational ground state or the impulsively excited vibrational wave packet in the electronic ground state (given the $0.338\,d$ range of control-induced vibrational motion).

Calculations of the donor-state survival probability for a downhill complex with a vertically (horizontally) aligned acceptor (donor) transition moment are shown in Figure 3.8. The results bear out the expectation that the initial acceptor-mode displacement should accelerate short-time excitation transfer and accentuate oscillatory forward-and-backward EET (of period

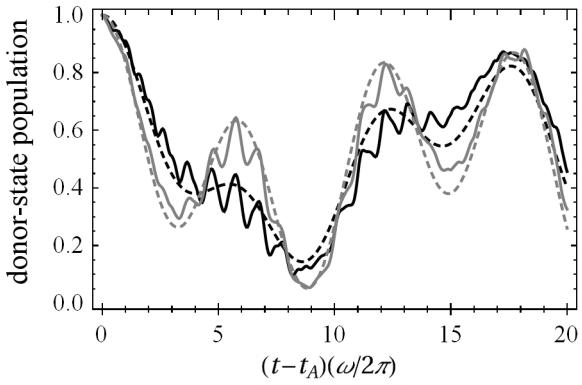

Figure 3.8: Donor-state survival probabilities for oriented downhill EET model without (solid black curves) and with (solid gray curves) prior impulsive excitation of acceptor-mode vibration. Coherent vibrational excitation of acceptor is seen to accelerate short-time EET in this system. Dashed curves give the corresponding predictions under weak EET-coupling approximation.

For the downhill system, we investigate pump-probe and pump-probe difference signals using probe pulses of two different kinds. In order selectively to detect primarily the nuclear probability density in the donor-excited state, we use a horizontally polarized probe pulse of duration $\sigma_C = 0.25\,(2\pi/\omega)$ and center frequency $\Omega_C = \varepsilon_1 - 3\delta^2\,\omega$, which is

resonant for $1 \rightarrow 0$ stimulated emission along the line $q_a = 2d$ and with $1' \rightarrow 0$ stimulated emission along the line $q_b = d$.* To preferentially detect the nuclear probability density in the acceptor-excited state, we use instead a vertically polarized probe, with duration $\sigma_C = 0.25\,(2\pi/\omega)$ and frequency $\Omega_C = \varepsilon_{1'} - 3\delta^2\,\omega$. This pulse is locally resonant with $1' \rightarrow 0$ stimulated emission near the line $q_b = 2d$.†

The pump-probe and pump-probe difference signals from an isotropic sample of the downhill dimer in the donor-detection case are plotted in Figure 9. The absence of even rough proportionality between the two signals attests to the effective influence of the control pulse on the time-course of short-time excitation transfer. A discernible correspondence exists between the envelope of each of these signals and the corresponding donor-population trace in Fig. 3.8. But the hastening of excitation transfer during the first several vibrational periods by the action of the control pulse is not immediately obvious from the pump-probe difference signal.

Interpretation of the pump-probe and pump-probe difference signals is complicated in the donor-detection case of Fig. 3.9 by the presence of significant excited-state absorption and some ground-state bleach, in addition to stimulated emission. These three contributions to both signals are shown separately in Figure 3.10. Stimulated emission (top panel) makes the largest contribution to both the pump-probe and pump-probe difference signals, and in

*When $\Omega_C = \varepsilon_1 - 3\delta^2\,\omega$, the spatial band $q_a = 2d$ is also the locus of resonant $1 \leftarrow 0$ ground-state bleach and $2 \leftarrow 1'$ excited-state absorption. This region is largely inaccessible in the electronic ground state, so ground-state bleaching should be very slight. It may be accessible to some degree following EET to the acceptor-excited state, especially from a wave packet displaced along the acceptor mode by control-induced ISRS before excitation to the donor-state. The band along $q_b = d$ is also the locus of $1' \leftarrow 0$ ground-state bleach and $2 \leftarrow 1$ excited-state absorption with this same probe frequency. The former process should again be weak, but the latter may occur to some degree in the presence of control-induced acceptor-mode displacement, despite being discriminated against by the horizontally polarized probe in the VHH scheme. These qualitative predictions are consistent with the significant signal contributions from excited-state absorption shown in the middle panel of Fig. 3.10.

†With $\Omega_C = \varepsilon_{1'} - 3\delta^2\,\omega$, $q_b = 2d$ is also the line of resonance for $1' \leftarrow 0$ ground-state bleach and $2 \leftarrow 1$ excited-state absorption, both of which should be negligible. $q_a = 3d$ is the line of resonance for $1 \rightarrow 0$ stimulated emission, $1 \leftarrow 0$ ground-state bleach, and $2 \leftarrow 1'$ excited-state absorption with this probe frequency, all which are expected to be essentially undetectable.

both instances has a form similar to the overall signal. The excited-state absorption contribution to the pump-probe (pump-probe difference) signal has a maximum amplitude about 14% (49%) as large as stimulated emission, and is rather different in form. The ground-state bleach contribution to the pump-probe signal (bottom panel) is negligible, that to the pump-probe difference signal largely so. The relative sizes of these three contributions to the signals are consistent with the anticipated presence or absence of nuclear probability density in the vicinity of the line of local resonance on the potential energy surface or surfaces from which each transition originates.

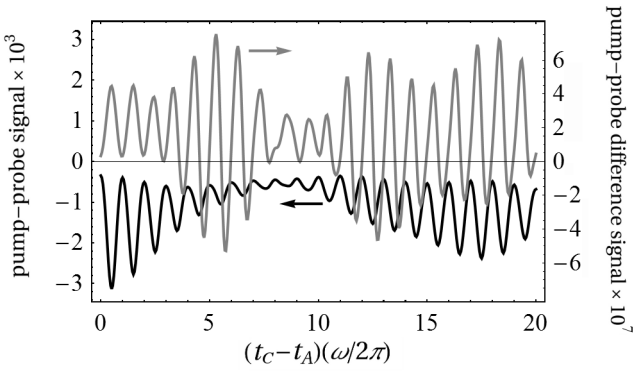

Figure 3.9: Pump-probe signal (black curve) and pump-probe difference signal (gray curve) for isotropic sample of downhill EET dimer using VHH polarization scheme and probe-pulse center frequency which select primarily for nuclear probability density in the donor-excited state.

The calculated pump-probe and pump-probe difference signals from an isotropic sample of the downhill dimer in the alternative, acceptor-detection case are shown in Figure 3.11. The strong influence of control-pulse-induced nuclear motion on the excitation-transfer process is again manifested by a lack of proportionality between the two signals. In this case, the envelopes of the two signals are very similar in form to the corresponding acceptor-state population (one minus the donor-state population plotted in Fig. 3.8). Comparison of the stimulated-emission, excited-state absorption, and ground-state bleach contributions (not shown) shows that both the pump-probe and the pump-probe difference are entirely

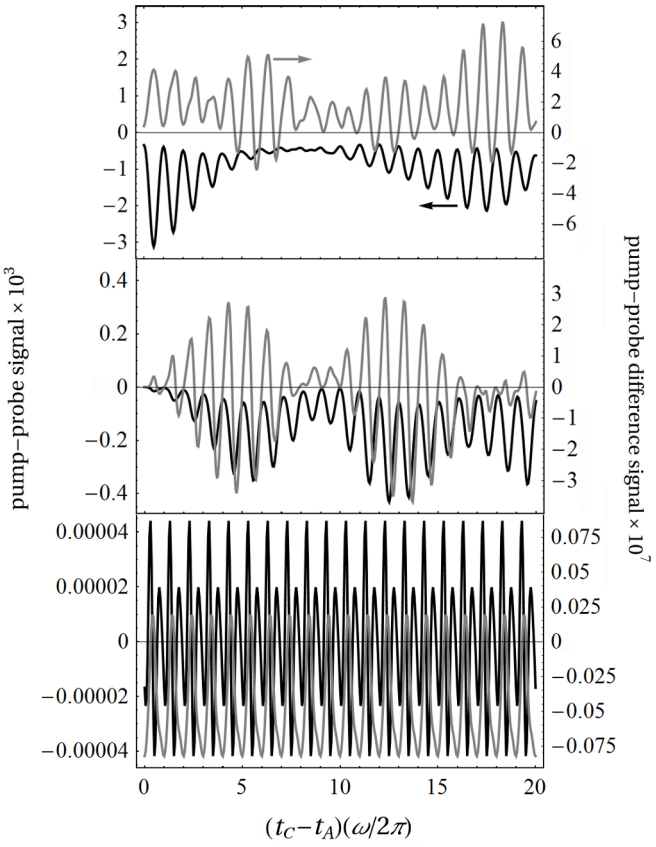

Figure 3.10: Contributions from stimulated-emission (top panel), excited-state absorption (middle), and ground-state bleach (bottom) to pump-probe (black curves) and pump-probe difference (gray curves) to signals shown in Fig. 3.9.

dominated by the first of these, as is consistent with arguments based on wave-packet access to the lines of local resonance.

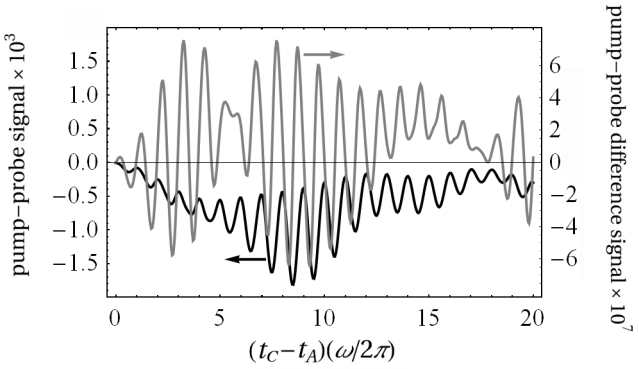

Figure 3.11: Same as Fig. 3.9, but with VHV polarization and probe-pulse center frequency selecting for nuclear probability density in the acceptor-excited state.

C. Discussion and Future Prospects

The calculations of donor-state survival probability, shown in Section B for three different EET dimers, demonstrate that impulsive excitation of coherent vibrational motion in the acceptor chromophore can significantly alter the time-course of population transfer between donor- and acceptor-excited states. The pronounced effect of an externally driven acceptor vibration in impeding (or accelerating) short-time EET in the presence of moderately strong electronic-vibrational coupling in an equal-energy (or downhill) dimer is demonstrated in subsection B.1 (B.3). The diminished effect of a coherent vibration on electronic population transfer under weak electronic-vibrational coupling is illustrated for DTA-12 by the results of subsection B.2. These illustrative results provide the motivation for our more extensive investigation of the various corresponding spectroscopic pump-probe difference signals.

The at-best indirect correspondence between the nominally observable *total population* of the donor-excited state and the spectroscopic *signals* that would actually be measured in

an ultrafast pump-probe or pump-probe difference experiment suggest that detailed system-specific calculations will generally be required to assist in the interpretation of future experiments along the lines proposed here and in Chapter II.

On the other hand, the calculations of subsection B.1 demonstrate that the pump-probe difference signal (for appropriately chosen pulse center frequencies) can be dominated by its stimulated-emission component and that this signal component from an isotropic sample does not differ greatly from that for an oriented complex (which comprises just two wave-packet overlaps). These findings suggest that similar simplifications should be possible in the calculation and analysis of the full md-WPI difference signals for which the general expressions are given in the preceding paper. Domination of md-WPI difference signals from EET systems by a small number of overlaps should greatly facilitate their interpretation in terms of the amplitude-level dynamics of surface-crossing wave packets.

The signal calculations presented here focus mainly on isolated model systems most closely representing energy-transfer dimers in the gas phase. Neglect of rotational motion is reasonable given the nanosecond-to-picosecond rotational periods estimated for molecules such as dithia-anthracenophane.* But following the strategy of Ref. 10, the effects of medium-induced inhomogeneous broadening were mimicked in some cases by averaging calculations from EET systems having variable independent monomer site energies selected from a Gaussian distribution. Dynamical effects of embedding EET dimers in a liquid or crystalline environment could be simulated by combining Redfield[46–51] or other relaxation theories with explicit dynamical treatment of strongly driven nuclear degrees of freedom, or perhaps by semiclassical wave-packet methods.† The full md-WPI signals considered in Paper 1 depend on the preservation of electronic coherence over the relevant intrapulse-pair delays. But pump-

*For a recent demonstration of coherent control and state reconstruction of rotational wave packets, se Ref. 45

†See Ref. 52

probe difference measurements of impulsive vibrational control should be primarily sensitive to vibrational dephasing, and should therefore be applicable to condensed-phase systems on a timescale of tens of picoseconds.

The control strategy investigated here is motivated by the semiclassical notion that a Gaussian wave packet displaced from the $q_a = q_b$ line of intersection between donor- and acceptor-excited electronic states of equal site energy should be less susceptible to energy transfer than one sitting astride that line. As seen in subsections B.1, this strategy is effective under fairly strong electronic-vibrational coupling. On the other hand, subsection B.2 shows that this simple displacement method is ineffective under weak electronic-vibrational coupling, where the spatial width of the wave packet is smaller than the excited-state shift in the equilibrium value of the vibrational coordinate, and the semiclassical picture of EET breaks down.

This failure under weak electronic-vibrational coupling does not, however, preclude the exertion of vibrational control over excitation transfer in such systems. With reference to Appendix D, we note, for instance, that the Franck-Condon overlap for DTA-12,

$$\langle (2_A)_{1'} |\, (2_A)_1 \rangle = -\,0.03506\,,$$

happens to take a very small value. This small overlap should lead to slow excitation transfer from any state of the form $|1\rangle\,|\psi_1\rangle$ with $|\psi_1\rangle = U_S \otimes I_A\,|(0_S\,2_A)_1\rangle = U_S \otimes I_A \{\frac{1}{2}\,|(2_a\,0_b)_1\rangle - \frac{1}{\sqrt{2}}\,|(1_a\,1_b)_1\rangle + \frac{1}{2}\,|(0_a\,2_b)_1\rangle\}$.* The donor-state survival probability following the preparation of such an initial state in DTA-12 is plotted in Figure 12. For the example shown, we have imagined displacing the wave packet $|\psi_0\rangle = |(0_S\,2_A)_0\rangle$ by $-\,d$ along q_b prior to short-pulse absorption to the donor-excited state, so that $|\psi_1\rangle = e^{ip_b d}\,|(0_S 2_A)_0\rangle = e^{i\sqrt{2}P_S d}\,|(0_S\,2_A)_1\rangle$. Although this illustration defers the question of how the initial state $|0\rangle\,|(0_S\,2_A)_0\rangle$ could be

*U_S is an arbitrary unitary transformation in the symmetric degrees of freedom, and I_A is the antisymmetric-mode identity operator.

prepared in practice, the greatly diminished initial decay of the donor-state population observed in Fig. 3.12 suggests that effective vibrational control over EET might well be possible even in the presence of weak electronic-vibrational coupling.

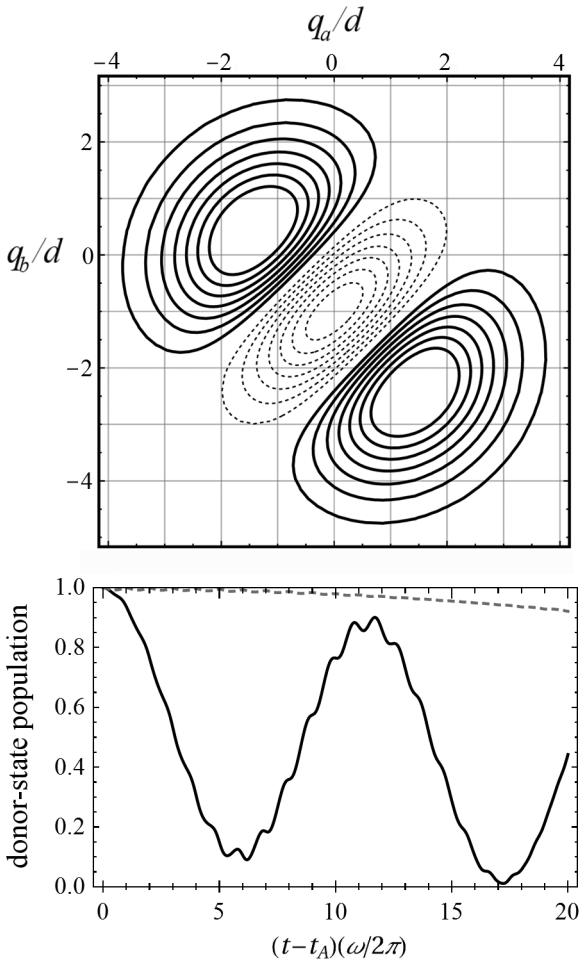

Figure 3.12: Illustration of possible vibrational-control strategy for the DTA-12 model with its weak electronic-vibrational coupling. Upper panel shows spatially translated $\nu_A = 2$ vibrational wave function at instant of transfer to donor-excited state. Lower panel compares subsequent donor-state survival probability (gray dashed line) to that following direct excitation from vibrational ground state (solid black line).

Notes

[1] M. Mohseni, P. Rebentrost, S. Lloyd, and A. Aspuru-Guzik, Journal of Chemical Physics **129**, 174106 (2008).

[2] P. Rebentrost, M. Mohseni, and A. Aspuru-Guzik, Journal of Physical Chemistry B **113**, 9942 (2009).

[3] F. Caruso, A. W. Chin, A. Datta, S. F. Huelga, and M. B. Plenio, Journal of Chemical Physics **131**, 105106 (2009).

[4] M. B. Plenio and S. F. Huelga, New Journal of Physics **10**, 113019 (2008).

[5] T. Brixner et al., Nature **434**, 625 (2005).

[6] G. S. Engel et al., Nature **446**, 782 (2007).

[7] H. Lee, Y. C. Cheng, and G. R. Fleming, Science **316**, 1462 (2007).

[8] E. Collini and G. D. Scholes, Journal of Physical Chemistry A **113**, 4223 (2009).

[9] S. Jang, Y. J. Jung, and R. J. Silbey, Chemical Physics **275**, 319 (2002).

[10] J. A. Cina and G. R. Fleming, Journal of Physical Chemistry A **108**, 11196 (2004).

[11] S. E. Bradforth, R. Jimenez, F. Vanmourik, R. van Grondelle, and G. R. Fleming, Journal of Physical Chemistry **99**, 16179 (1995).

[12] R. Monshouwer, A. Baltuska, F. van Mourik, and R. van Grondelle, Journal of Physical Chemistry A **102**, 4360 (1998).

[13] J. D. Biggs and J. A. Cina, Journal of Chemical Physics **131**, 224302 (2009).

[14] I. P. Mercer et al., Physical Review Letters **102**, 057402 (2009).

[15] D. M. Jonas, Annual Review of Physical Chemistry **54**, 425 (2003).

[16] T. Brixner, T. Mančal, I. V. Stiopkin, and G. R. Fleming, Journal of Chemical Physics **121**, 4221 (2004).

[17] P. F. Tekavec, G. A. Lott, and A. H. Marcus, Journal of Chemical Physics **127**, 214307 (2007).

[18] S. Mukamel, Annual Review of Physical Chemistry **51**, 691 (2000).

[19] M. Cho, Bulletin of the Korean Chemical Society **27**, 1940 (2006).

[20] S. Mukamel, *Principles of Nonlinear Optical Spectroscopy*, Oxford University Press, New York, 1995.

[21] M. Cho, *Two-Dimensional Optical Spectroscopy*, CRC press, Boca Raton, 2009.

[22] T. Förster, *Delocalized excitation and excitation transfer*, volume 3, pages 93–137, Academic Press, New York, 1965.

[23] S. Rackovsky and R. Silbey, Molecular Physics **25**, 61 (1973).

[24] T. F. Soules and C. B. Duke, Physical Review B **3**, 262 (1971).

[25] R. A. Harris and R. Silbey, Journal of Chemical Physics **78**, 7330 (1983).

[26] R. Silbey and R. A. Harris, Journal of Physical Chemistry **93**, 7062 (1989).

[27] A. J. Leggett et al., Reviews of Modern Physics **59**, 1 (1987).

[28] P. Anderson, Physical Review **109**, 1492 (1958).

[29] A. M. Weiner, D. E. Leaird, G. P. Wiederrecht, and K. A. Nelson, Science **247**, 1317 (1990).

[30] L. Dhar, J. A. Rogers, and K. A. Nelson, Chemical Reviews **94**, 157 (1994).

[31] M. Hoffmann and Z. G. Soos, Physical Review B **66**, 024305 (2002).

[32] F. C. Spano, Journal of Chemical Physics **116**, 5877 (2002).

[33] F. C. Spano, Journal of Chemical Physics **118**, 981 (2003).

[34] C. Cohen-Tannoudji, B. Diu, and F. Laloë, *complement* G_V, volume 1, page 559, John Wiley & Sons, New York, 1977.

[35] Y. C. Shen and J. A. Cina, Journal of Chemical Physics **110**, 9793 (1999).

[36] T. J. Smith, L. W. Ungar, and J. A. Cina, Journal of Luminescence **58**, 66 (1994).

[37] Y. J. Yan and S. Mukamel, Physical Review A **41**, 6485 (1990).

[38] D. Egorova, M. F. Gelin, and W. Domcke, Journal of Chemical Physics **122**, 9793 (2005).

[39] I. Yamazaki, S. Akimoto, T. Yamazaki, S. Sato, and Y. Sakata, Journal of Physical Chemistry A **106**, 2122 (2002).

[40] I. Yamazaki, S. Akimoto, N. Aratani, and A. Osuka, Bulletin of the Chemical Society of Japan **77**, 1959 (2004).

[41] R. Kishi et al., Journal of Physical Chemistry A **113**, 5455 (2009).

[42] W. R. Lambert, P. M. Felker, J. A. Syage, and A. H. Zewail, Journal of Chemical Physics **81**, 2195 (1984).

[43] L. W. Ungar and J. A. Cina, Advances in Chemical Physics **100**, 171 (1997).

[44] H. Rhee et al., Journal of Chemical Physics **125**, 8 (2006).

[45] H. Hasegawa and Y. Ohshima, Physical Review Letters **101**, 4 (2008).

[46] W. T. Pollard, A. K. Felts, and R. A. Friesner, **93**, 77 (1996).

[47] A. Matro and J. A. Cina, Journal of Physical Chemistry **99**, 2568 (1995).

[48] L. W. Ungar and J. A. Cina, Journal of Physical Chemistry A **102**, 7382 (1998).

[49] D. Egorova and W. Domcke, Chemical Physics Letters **384**, 157 (2004).

[50] M. Yang and G. R. Fleming, Chemical Physics **282**, 163 (2002).

[51] W. M. Zhang, T. Meier, V. Chernyak, and S. Mukamel, Journal of Chemical Physics **108**, 7763 (1998).

[52] C. T. Chapman and J. A. Cina, Journal of Chemical Physics **127**, 10 (2007).

CHAPTER IV

SPECTROSCOPIC SIGNATURES OF THE COHERENT CONTROL OF ENERGY TRANSFER

This chapter has been submitted, in revised form, for publication in the *Journal of Chemical Physics*. This material was coauthored with Dr. Jeff Cina.

In Chapter III, we investigated the influence of externally induced coherent vibrational motion on electronic excitation transfer (EET) in chromophore dimers and its observation using pump-probe polarization spectroscopy. Coherent ground-state vibrational motion is to be imparted by an impulsive Raman process, and the effect of this motion on EET following excitation by a resonant ultrashort pump pulse is monitored in the pump-probe difference signal. In such an experiment, the measured quantity is the polarized pump-probe signal with prior Raman excitation minus the signal without. We calculated the signals for several model systems as the pump-probe limit of a multidimensional wave-packet interferometry (md-WPI) experiment, in which the time-delay between pulses within a phase-locked (or phase-modulated) pair is set to zero. The signals are written as sums of several contributing overlaps between excited-state vibronic wave packets (see Chapter II for details). Evidence of vibrational control of EET is sought in the lack of direct proportionality between corresponding pump-probe difference and pump-probe signals. In this chapter, we elaborate upon

and further investigate that basic point, which will play an important role in unambiguously identifying the successful exertion of vibrational control over electronic energy transfer.

We begin by examining the basic expression for the pump-probe signal in the absence of a control pulse. Contributions to this signal come from three processes, denoted ground-state bleach (GSB), excited state absorption (ESA), and stimulated emission (SE). Here, we focus solely on the SE contributions, but similar analyses apply to the other signal components. Our approach views the pump-probe and pump-probe difference signals as limiting cases of the md-WPI signal and its alteration by control-pulse-induced stimulated Raman excitation, respectively. In an md-WPI description, the pump and probe pulses each comprise two pulses (A and B for the pump and C and D for the probe) with a definite intrapulse-pair optical phase relationship. In notation that makes clear the order of interaction with the pulses, as well as the phase dependence of the signal, the SE component of the pump-probe signal can be written as the sum of two terms:

$$\Xi^{SE} = \sum_{\varepsilon=1,1'} 8\mathrm{Re}\left\langle (B)_\varepsilon \mid (DCA)_\varepsilon \right\rangle^{+-} \quad . \tag{4.1}$$

Each term in Eq. (4.1) is the overlap between two nuclear wave packets in a given site-excited electronic state (1 or $1'$) that have interacted with the pulses in a definite order. The bras in Eq. (4.1) have undergone a single electronic excitation initiated by the pump pulse, while, after excitation by the pump, the kets have been de-excited then re-excited by the probe pulse. The $+-$ superscript distinguishes this overlap from one carrying a $++$ phase signature in which the probe excites the system to the doubly-excited state before de-excitation to a one-exciton state.

Expression (4.1) for the pump-probe signal experiment in the absence of a control pulse is derived in a manner analogous to that used in Sec. D of Chapter II, which deals with the pump-probe difference signal. An unstated assumption behind Eq. (2.40) of that

chapter is that in the pump-probe limit of an md-WPI experiment, the intrapulse-pair phase differences ϕ_{BA} and ϕ_{DC} go to zero in addition to the time delays t_{BA} and t_{DC}. Alternatively, one could maintain the phase differences while setting the time delays to zero and view any single signal component, e.g. S_{ε}^{+-}, as the pump-probe signal. Expressions for the signals in the latter case are the same as those presented here divided by four.

In an HH polarization scheme, the pump and probe are both polarized in the horizontal direction. With the probe polarization parallel to the pump, one monitors the population of the initially accessed site-excited electronic state (in a statistical sense for an isotropic sample). Averaging the contributions from a collection of randomly oriented dimers within which, for the sake of definiteness, the angle between the chromophores' transition dipole moments is fixed at $\pi/2$,, we find,

$$\begin{aligned}\Xi_{HH}^{SE} =& \frac{8}{15}\mathrm{Re}\,(3\,\langle\{a(10)\}_1 \mid \{c(10)c(01)a(10)\}_1\rangle \\ &+ 3\,\langle\{a(1'0)\}_{1'} \mid \{c(1'0)c(01')a(1'0)\}_{1'}\rangle \\ &+ \langle\{a(10)\}_{1'} \mid \{c(1'0)c(01')a(10)\}_{1'}\rangle \\ &+ \langle\{a(1'0)\}_1 \mid \{c(10)c(01)a(1'0)\}_1\rangle \\ &+ \langle\{a(10)\}_1 \mid \{c(10)c(01')a(1'0)\}_1\rangle \\ &+ \langle\{a(1'0)\}_{1'} \mid \{c(1'0)c(01)a(10)\}_{1'}\rangle \\ &+ \langle\{a(10)\}_{1'} \mid \{c(1'0)c(01)a(1'0)\}_{1'}\rangle \\ &+ \langle\{a(1'0)\}_1 \mid \{c(10)c(01')a(10)\}_1\rangle)\ .\end{aligned} \tag{4.2}$$

This expression is written in terms of reduced pulse propagators, each of which describes a single excitation or de-excitation event without reference to the phase of the pulse or its polarization. The content of the notation in Eq. (4.2) can be illustrated by examining the first overlap on the RHS. The bra is the portion of a wave packet that was excited from the

ground electronic state (state 0) to the "donor-excited" state (state 1) by the pump pulse, and still resides in state 1 when the probe pulse arrives. The ket follows the same state-space path until the arrival of the probe pulse, which de-excites the wave packet to state 0 and then re-excites it to state 1. In carrying out the summation indicated in Eq. (4.1), only the reduced overlaps in which ε is the same as the state to which the probe excites the ket survive. This simplification is possible because any energy transfer taking place after interaction with the probe pulse does not influence the total population of the one-exciton manifold (which is regarded as the measured quantity in Chapters II and III). The system is a homo-dimer, so the value of an overlap does not change upon interchange of the labels 1 and $1'$. The first two terms of Eq. (4.2) are therefore equal to each other, as are the third and fourth terms, and so on, and Eq. (4.2) reduces to

$$\begin{aligned}\Xi_{HH}^{SE} =& \frac{16}{15}\mathrm{Re}\,(3\,\langle\{a(10)\}_1 \mid \{c(10)c(01)a(10)\}_1\rangle \\ &+ \langle\{a(10)\}_{1'} \mid \{c(1'0)c(01')a(10)\}_{1'}\rangle \\ &+ \langle\{a(10)\}_1 \mid \{c(10)c(01')a(1'0)\}_1\rangle \\ &+ \langle\{a(10)\}_{1'} \mid \{c(1'0)c(01)a(1'0)\}_{1'}\rangle)\quad .\end{aligned} \tag{4.3}$$

HV is another polarization scheme of interest, in which the pump (H) and probe (V) are perpendicularly polarized. In this case, the probe pulse preferentially monitors the population of the site state that was not initially excited by the pump pulse:

$$\begin{aligned}\Xi_{HV}^{SE} =& \frac{8}{15}\mathrm{Re}\,(2\,\langle\{a(10)\}_1 \mid \{c(10)c(01)a(10)\}_1\rangle \\ &+ 4\,\langle\{a(10)\}_{1'} \mid \{c(1'0)c(01')a(10)\}_{1'}\rangle \\ &- \langle\{a(10)\}_1 \mid \{c(10)c(01')a(1'0)\}_1\rangle \\ &- \langle\{a(10)\}_{1'} \mid \{c(1'0)c(01)a(1'0)\}_{1'}\rangle)\quad .\end{aligned} \tag{4.4}$$

In Eq. (4.4), we have again invoked the symmetry with respect to the interchange of 1 and $1'$.

We can now compare Eqs. (4.3) and (4.4) with the corresponding pump-probe difference signal expressions and ask to what extent a lack of direct proportionality between them (as seen, for example, in Figs. 3.2 and 3.5) is unequivocal evidence for vibrational control over EET. As an extreme example, we imagine a control pulse that is largely ineffective at generating nuclear motion in the electronic ground state (while retaining the criterion that this pulse not promote substantial population to the excited electronic state). Such a control pulse fails to exert vibrational control over EET. But because its polarization selects an anisotropic sub-ensemble of the overall orientational distribution, the possibility exists that it could nonetheless give rise to a pump-probe difference signal that is not directly proportional to the original pump-probe signal.

Recall that nuclear motion in the electronic ground state is to be imparted to the system by the control pulse through an impulsive stimulated Raman scattering process (ISRS). This control pulse is somewhat shorter than the timescale of nuclear motion ($2\pi/\omega$ where ω is the vibrational frequency of the mode in question), so that the transient occupation of an excited electronic state during the pulse generates a momentum kick to the ground-electronic state nuclear wave function in the direction of the minimum of the upper potential surface. Ordinarily, the center frequency of the control pulse would be set just far enough below resonance ($\Omega_P < \varepsilon_1, \varepsilon_{1'}$) with the electronic transition that electronic absorption is negligible (in the calculations of Chapter III electronic population loss is kept below 5%). A control pulse could be rendered ineffective by making its duration so short that a momentum kick is not delivered, while red-shifting its center frequency so as to keep its broadened power spectrum away from electronic resonance.

The SE contribution to the pump-probe difference signal is written

$$\Theta^{SE} = \sum_{\varepsilon=1,1'} 8\mathrm{Re}\left(\langle (B)_\varepsilon \mid (DCAPP)_\varepsilon\rangle + \langle (BPP)_\varepsilon \mid (DCA)_\varepsilon\rangle\right) \ . \tag{4.5}$$

For any orientation of the complex, and any fixed interchromophore angle, the wave-packet overlaps constituting the SE signal consist of equally-weighted sums of corresponding reduced overlaps. From Eqs. (C.9) and (C.10) of Appendix C, we can identify one such combination of corresponding overlaps, with the sum over ε carried out, as

$$\begin{aligned}\langle \{a(10)\}_{1'} \mid \{c(1'0)c(01)a(10)p(01')p(1'0)\}_{1'}\rangle \\ + \langle \{a(10)p(01')p(1'0)\}_{1'} \mid \{c(1'0)c(01)a(10)\}_{1'}\rangle \, .\end{aligned} \tag{4.6}$$

Analysis of this combination serves to illustrate the sums of other pairs of corresponding overlaps in the SE signal (and in fact in the GSB and ESA signals as well). In Eq. (4.6) we have deliberately chosen a pair of corresponding overlaps that do not contribute to the pump-probe difference signal from an isotropic sample in order to emphasize the generality of the argument that follows. In more explicit notation, the illustrative terms are

$$\begin{aligned}\langle\psi_0|\,(p_A^{(10)})^\dagger[-t_{CA}]_{11'}p_C^{(1'0)}p_C^{(01)}[t_{CA}]_{11}p_A^{(10)}[t_{AP}]_{00}p_P^{(01')}p_P^{(1'0)}[-t_{AP}]_{00}\,|\psi_0\rangle \\ + \langle\psi_0|\,[t_{AP}]_{00}(p_P^{(01')}p_P^{(1'0)})^\dagger[-t_{AP}]_{00}(p_A^{(10)})^\dagger[-t_{CA}]_{11'}p_C^{(1'0)}p_C^{(01)}[t_{CA}]_{11}p_A^{(10)}\,|\psi_0\rangle \, .\end{aligned} \tag{4.7}$$

Contiguous propagators for the same pulse are nested.

We define the projection operators $\mathscr{P}_0 \equiv |\psi_0\rangle\langle\psi_0|$ and $\mathscr{Q}_0 \equiv 1 - \mathscr{P}_0$, and insert

$1 = \mathscr{Q}_0 + \mathscr{P}_0$ into Eq. (4.7), which becomes

$$\begin{aligned}
&\beta \langle\psi_0| (p_A^{(10)})^\dagger [-t_{CA}]_{11'} p_C^{(1'0)} p_C^{(01)} [t_{CA}]_{11} p_A^{(10)} |\psi_0\rangle \\
&+ \beta^* \langle\psi_0| (p_A^{(10)})^\dagger [-t_{CA}]_{11'} p_C^{(1'0)} p_C^{(01)} [t_{CA}]_{11} p_A^{(10)} |\psi_0\rangle \\
&+ \langle\psi_0| (p_A^{(10)})^\dagger [-t_{CA}]_{11'} p_C^{(1'0)} p_C^{(01)} [t_{CA}]_{11} p_A^{(10)} \mathscr{Q}_0 [t_{AP}]_{00} p_P^{(01')} p_P^{(1'0)} [-t_{AP}]_{00} |\psi_0\rangle \\
&+ \langle\psi_0| [t_{AP}]_{00} (p_P^{(01')} p_P^{(1'0)})^\dagger [-t_{AP}]_{00} \mathscr{Q}_0 (p_A^{(10)})^\dagger [-t_{CA}]_{11'} p_C^{(1'0)} p_C^{(01)} [t_{CA}]_{11} p_A^{(10)} |\psi_0\rangle \ .
\end{aligned} \tag{4.8}$$

Here, $\beta = \beta' + i\beta'' \equiv \langle\psi_0| [t_{AP}]_{00} p_P^{(01')}(\infty; t_2) p_P^{(1'0)}(t_2; t_1) [-t_{AP}]_{00} |\psi_0\rangle$. The third and fourth terms in Eq. (4.8), which include $\mathscr{Q}_0$, are those in which the second-order action of the control pulse induces stimulated-Raman transitions to vibrational eigenstates other than ψ_0 (taken here and in Chapter III to be the vibrational ground state of the complex). The first and second terms in Eq. (4.8) sum to give

$$2\beta' \langle \{a(10)\}_{1'} \mid \{c(1'0)c(01)a(10)\}_{1'} \rangle \,, \tag{4.9}$$

and this is the only remaining contribution in the absence of impulsive Raman transitions. This term is proportional to the real part of β, which accounts for the depletion of population in ψ_0 due to residual electronic absorption of the control pulse. This situation is general, as it applies to all pairs of corresponding overlaps in the stimulated emission signal, and to the ground-state bleach and excited-state absorption signals.

An explicit expression for the parameter β, defined below Eq. (4.8), is obtained from the matrix elements of the second-order pulse propagator as (see online Appendix E for a detailed derivation).

$$\beta = -\frac{\sqrt{\pi}}{2} \sigma_P^2 E_P^2 m'^2 e^{-\delta^2} \sum_{\nu_b} \frac{\delta^{2\nu_b}}{\nu_b!} K_{\nu_b}, \tag{4.10}$$

with

$$\begin{aligned} K_{\nu_b} \equiv & \int_0^\infty dt \exp\left\{-t^2 + 2\,i\,\sigma_P\Delta\cdot t\right\} \\ = & \frac{\sqrt{\pi}}{2} e^{-\sigma_P^2\Delta^2} + i\,e^{-\sigma_P^2\Delta^2} \int_0^{\sigma_P\Delta} dt\, e^{t^2} \;= K'_{\nu_b} + i\,K''_{\nu_b},. \end{aligned} \tag{4.11}$$

Here, δ is the dimensionless displacement of the potential minimum of the monomer upon electronic excitation, and $\Delta = \Omega_P - \varepsilon_{1'} - \omega\nu_b$ is the "resonance offset." For small values of the dimensionless resonance offset, $\sigma_P\Delta$, K'' can be approximated by its Taylor series,

$$K'' = \sum_n \frac{(-2)^n(\sigma_P\Delta)^{2n+1}}{(2n+1)!!}\ . \tag{4.12}$$

For large values of $\sigma_P\Delta$, an asymptotic series (truncated at some finite order) is more appropriate and is given by

$$K'' = \sum_n \frac{(2n-1)!!}{2^{n+1}(\sigma_P\Delta)^{2n+1}}[1 - e^{-\sigma_P^2\Delta^2}\sum_{m=0}^{n}\frac{(\sigma_P\Delta)^{2m}}{m!}] \tag{4.13}$$

The difference-signal polarization corresponding to HH is VHH, where a vertically polarized control pulse precedes the HH pump-probe sequence. This polarization sequence would be chosen in order to monitor the effect of acceptor-mode nuclear motion on the donor-excited electronic population. The pump-probe difference signal with an ineffectual control pulse (under which $\mathscr{Q}_0$-including terms vanish in Eq. (4.8) and its analogs) under VHH polarization is written, again taking advantage of the symmetry with respect to inter-

change of 1 and $1'$ labels,

$$\begin{aligned}\Theta_{VHH}^{SE} =& \frac{128}{105}\beta' \mathrm{Re}\,(3\,\langle\{a(10)\}_1 \mid \{c(10)c(01)a(10)\}_1\rangle \\ &+ \langle\{a(10)\}_{1'} \mid \{c(1'0)c(01')a(10)\}_{1'}\rangle \\ &+ \langle\{a(10)\}_1 \mid \{c(10)c(01')a(1'0)\}_1\rangle \\ &+ \langle\{a(10)\}_{1'} \mid \{c(1'0)c(01)a(1'0)\}_{1'}\rangle)\,,\end{aligned} \tag{4.14}$$

which is in fact proportional to the HH pump-probe signal (4.3). Under VHV polarization (a V-polarized control pulse followed by an HV pump-probe sequence) we find

$$\begin{aligned}\Theta_{VHV}^{SE} =& \frac{32}{105}\beta' \mathrm{Re}\,(5\,\langle\{a(10)\}_1 \mid \{c(10)c(01)a(10)\}_1\rangle \\ &+ 11\,\langle\{a(10)\}_{1'} \mid \{c(1'0)c(01')a(10)\}_{1'}\rangle \\ &- 3\,\langle\{a(10)\}_1 \mid \{c(10)c(01')a(1'0)\}_1\rangle \\ &- 3\,\langle\{a(10)\}_{1'} \mid \{c(1'0)c(01)a(1'0)\}_{1'}\rangle)\,.\end{aligned} \tag{4.15}$$

In this case, the pump-probe difference signal is not quite proportional to the HV pump-probe signal (4.4). The lack of proportionality under arbitrary polarization is not unexpected, as the second-order action of the control pulse - while failing to excite coherent nuclear motion - interacts with a subset of the total isotropic sample, and it is this subset upon which a pump-probe experiment is conducted.

Figure 4.1 shows pump-probe and pump-probe difference signals from the same model system studied in Sec. B.2 of Chapter III, for the two polarizations considered here. The system features moderate excitonic coupling ($J = 0.2\omega$), moderate vibrational displacement ($\delta = \sqrt{2.5}$), equal site energies, and perpendicular transition dipole moments. As in the calculations of Chapter III, the pump pulse is short and vertically resonant ($\sigma_A = 0.1(2\pi/\omega)$ and $\Omega_A = \varepsilon + \delta^2\omega$), while the probe is longer and resonant at the outer turning point for

nuclear motion in the excited state ($\sigma_C = 0.25(2\pi/\omega)$ and $\Omega_C = \varepsilon - 3\delta^2\omega$). Inhomogeneous broadening is not simulated in the present calculations. The control pulse is now chosen to be ineffective at generating nuclear motion: it is very short and well off resonance ($\sigma_P = 0.01(2\pi/\omega)$ and $\Omega_P = \varepsilon - 15\omega$), and precedes the pump by roughly half a vibrational period ($t_{AP} = 0.56(2\pi/\omega)$. The signals have been divided by their maximum value (and, in the case of the pump-probe signals, multiplied by -1) in order to compare them. On this scale the HH and VHH signals are virtually indistinguishable, with the difference resulting from the small but non-zero contribution from terms containing $\mathscr{Q}_0$. The HV and VHV signals, however, are visibly disproportionate. Under both VHH and VHV, the pump-probe difference signals plotted in Fig. 4.1 are dominated by the very slight vibrational-coordinate independent (but orientationally selective) depletion of the ground-state nuclear wave function. We have verified that this portion of the signal is independent of the control-pump delay, t_{AP}, in each case, unlike the similarly miniscule contribution due to control-pulse-induced population in the one-exciton manifold (which is not included in our simulations).

Pump-probe difference spectroscopy is a potentially powerful technique for assessing the extent to which externally induced nuclear motion can influence short-time energy-transfer dynamics. It is important to establish that any significant alteration to the pump-probe signal following the control pulse results from pulse-induced nuclear motion, and is not simply due to the orientational selectivity of the control pulse. We conclude that the lack of direct proportionality between pump-probe and pump-probe difference signals from chromophore dimers can be taken as evidence of vibrational control over EET. When a VHH polarization scheme is used, such evidence is entirely unequivocal. When a VHV polarization is used, the pump-probe difference signal does differ slightly from the pump-probe signal even in the absence of control-pulse-induced nuclear motion. But this intrinsic difference between HV and VHV signals is minor compared with the expected differences brought about by an effective control pulse (see Figs. 3.2 and 3.11).

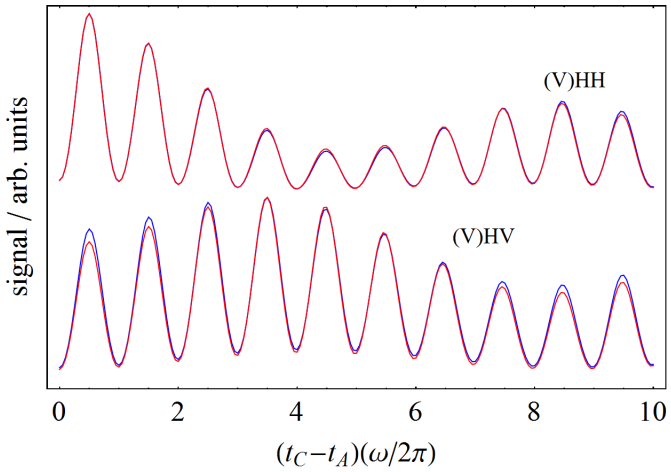

Figure 4.1: Pump-probe difference signals in the presence of an ineffective control pulse. Upper traces: Pump-probe (blue) and pump-probe difference (red) signals when pump and probe pulses are both polarized horizontally (HH) and control pulse is polarized vertically (V). Lower traces (vertically displaced for clarity): The same but for a vertically polarized probe pulse (HV and VHV). Signals have been scaled to highlight the proportionality (or lack thereof) between two- and three-pulse signals when the control pulse is ineffective at driving nuclear motion.

CHAPTER V

OBSERVING THE COHERENT VIBRATIONAL CONTROL OVER ENERGY TRANSFER IN DITHIA-ANTHRACENOPHANE USING MULTIDIMENSIONAL WAVE-PACKET INTERFEROMETRY

A. Introduction and Setup

In Chapter II we put forth a method by which coherent nuclear motion could control the time course of electronic excitation transfer. In Chapter III we presented calculated pump-probe difference signals for DTA-12 for two different polarization conditions, VHH and VHV, as a means of monitoring that coherent control. Evidence for the coherent vibrational control over EET was sought in the lack of direct proportionality between pump-probe and pump-probe difference signals. Here we show that, by comparing difference signals from the polarizations HHH and VHH for two different values of t_{AP}, those corresponding to maximal negative *and* positive displacement, we obtain direct evidence not only of the existence of vibrational control but also the direction of that control.

A.1. Control Scheme Revisited

We consider an electronically-coupled molecular dimer, where each monomer possesses a Franck-Condon active nuclear mode. When one monomer is electronically excited, marking it as the excitation donor, wave packet motion ensues due to the displacement of

the potential minimum in the excited electronic state, as depicted in the purple line in Figure 5.1. When the wave packet is at its outer turning point in the 1-state, the donor $e \rightarrow g$ and acceptor $e \leftarrow g$ transitions are out of resonance by $4\delta^2\omega$ (as can be seen in the purple traces of Figure 5.2), which hinders energy transfer. The donor's instantaneous emission spectrum is rendered time dependant, while the acceptor's absorption spectrum remains constant. The overlap between the two is maximal at the Franck-Condon point, and it is at this point when the probability of a surface crossing is maximized.

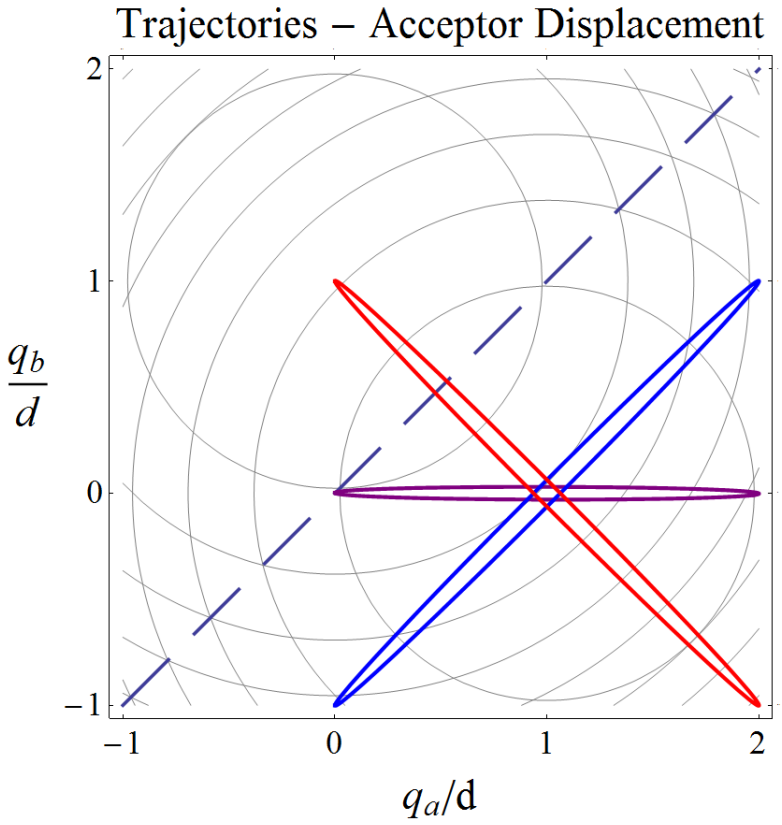

Figure 5.1: Classical trajectories for nuclear wave packets in the 1-state. The purple line shows the trajectory for the unperturbed case, in which nuclear motion is initially confined to the electronically excited donor. The blue line is the case of ideal acceptor displacement, where the nuclear wave packet is at $(q_a, q_b) = (0, -d)$ at the instant of electronic excitation (assuming an oriented sample). If the electronically resonant pulse arrives one half period later, the wave packet is at $(q_a, q_b) = (0, d)$ and follows the trajectory shown in red.

When the acceptor nuclear mode is displaced to $q_b = -d$ prior to electronic excita-

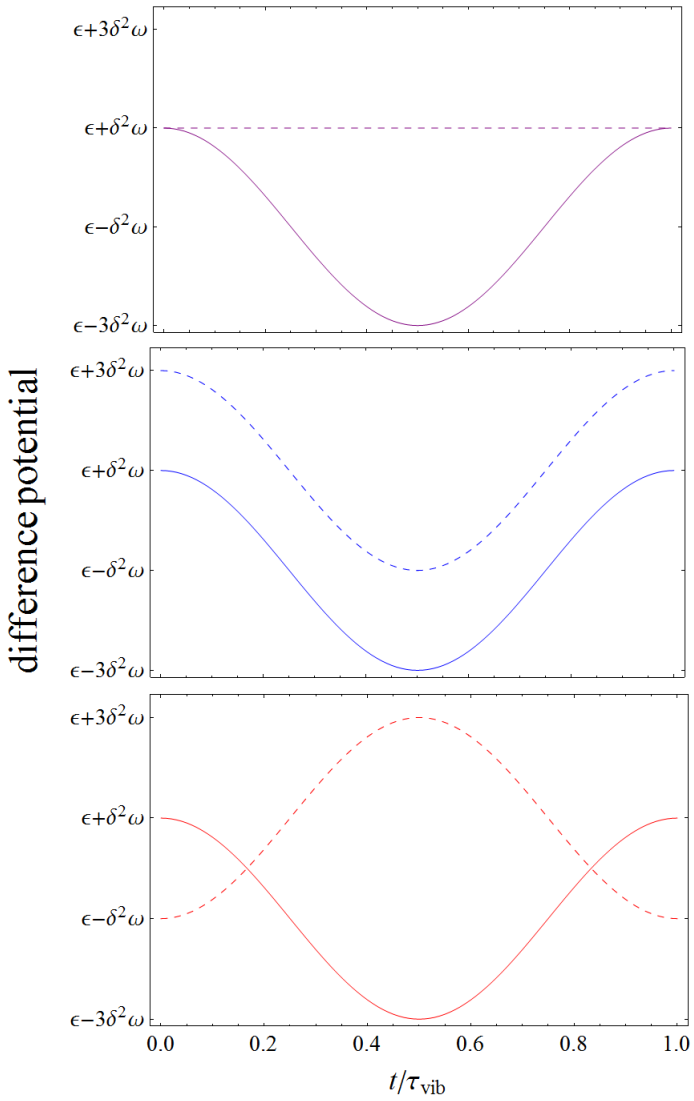

Figure 5.2: Instantaneous transition frequencies for donor-emission (solid lines) and acceptor-absorption (dashed lines) for the classical trajectories depicted in Fig. 5.1.

tion of the donor, as described in Section A of Chapter II and depicted by the blue line in Fig. 5.1, the gap between donor-emission and acceptor-absorption is constant in time. The difference potential for the acceptor and donor, related to the instantaneous absorption and emission frequencies, are shown for this trajectory in the middle panel of Fig. 5.2. From this figure we see that the energy gap between donor- and acceptor-excited states is a constant $2\delta^2\omega$. In Chapter II it was assumed that since this trajectory keeps the wave packet away from the intersection of donor- and acceptor-excited potential surfaces, short time EET would be diminished relative to the unperturbed case. The calculations of Subsection B.2 of Chapter III on the model system DTA-12 showed that EET was enhanced when the acceptor vibrational mode was displaced in the negative direction at the instant of donor electronic-excitation, seemingly in contradiction to the semiclassical prediction. Quantum calculations of Appendix D, in which we ignore coupling between non-isoenergetic nuclear states in the 1 and $1'$ electronic states, showed that when the displacement of the potential minimum upon electronic excitation is small compared with the width of the ground-state nuclear wave packet, EET is indeed predicted to be enhanced for negative acceptor displacement. As we show in Appendix G, this is also consistent with the semiclassical idea that a wave packet that spends more time near the potential-surface intersection is more likely to transfer amplitude between states.

Another possibility for the vibrational control over EET is possible when the acceptor is vibrationally perturbed as described above. If the electronically resonant pulse arrives later by one half of a vibrational period, the excited-state nuclear trajectory will be similar to that depicted by the red line in Fig. 5.1. Here the center of the wave packet crosses the intersection twice each vibrational period, rather than avoiding it, as is the case for the blue trajectory in that same figure. However, at the point of crossing the intersection line the wave packet has significant momentum and spends less time with its center directly on the intersection than it does in the case of vertical excitation (purple trajectory). The difference potentials for

the donor and acceptor are shown for this trajectory in the lower panel of Fig. 5.2. Note that when the wave packet reaches its turning point, at $(q_a, q_b) = (2d, -d)$, the energy gap between site-excited states is $6\delta^2\omega$, six times the Franck-Condon energy. We therefore expect short-time EET to be diminished (relative to vertical excitation) when the acceptor is displaced in the positive direction prior to electronic excitation, while it is enhanced for negative displacement.* As the control-pulse influenced wave packet samples both of these spatial regions over the course of a single vibrational period, changes in pump-probe and WPI difference signals as a function of the control-pulse delay time, t_{AP}, could be sought as further evidence of coherent vibrational control over EET.

However, when these signals come from an isotropic distribution of dimer orientations, contributions to the signal where the control pulse and the pump pulse (or pump pulse-pair) interact with different monomers are combined with contributions where they interact with the same monomer. These two cases are referred to herein as acceptor-displaced and donor-displaced, respectively. When a VHH polarization is used on an isotropic sample, the orientational averaging weights the direction-cosine prefactors $\langle e_A e_B e_C e_D {e'_P}^2 \rangle$ and $\langle e_A e_B e_C e_D {e_P}^2 \rangle$ by a ratio of 3:1 (assuming perpendicular transition dipole moments). Signal contributions from donor-displaced dimers will therefore be non-negligible for isotropic VHH signals.† Furthermore, one could directly probe the effect of donor-displacement on EET by using an HHH polarization scheme. In this case the ratio of $\langle e_A e_B e_C e_D {e'_P}^2 \rangle$ and $\langle e_A e_B e_C e_D {e_P}^2 \rangle$ is 1:5, so the HHH signal from an isotropic sample will bear even more resemblance to the same signal from an oriented sample.

We therefore will need to understand the effect of donor-displacement on short-time

*While this model predicts that the average short-time EET is diminished for positive acceptor displacement, we expect the vibrational period fluctuations in the instantaneous EET to be enhanced.

†They could, in principle, be spectrally selected against by using a longer, still vertically resonant, pump pulse as the $1 \leftarrow 0$ transition energy varies for donor-displacement but not acceptor-displacement. However, using a longer, and thus more spectrally narrow, pump pulse contrasts with our control strategy of creating a moving ground-state wave packet and copying it to the excited state with an impulsive pump.

EET, and how this effect changes as a function of t_{AP}, in order to fully understand isotropic pump-probe difference signals. If the A pulse arrives while the ground-state wave packet is at its outer turning point $(q_a, q_b) = (d, 0)$, the resulting nuclear wave packet is essentially stationary in the 1-state. This is represented by the red circle in Fig. 5.3.* Following electronic excitation, the donor $e \rightarrow g$ and acceptor $e \leftarrow g$ transition energies are out of resonance by a constant amount equal to $2\delta^2\omega$, as can be seen in the red traces of Fig. 5.4. This is the same constant amount that we see when the acceptor is displaced to its *inner* turning point, and we therefore expect short time electronic dynamics to be identical for these two cases. If the A pulse arrives a half-period later, the 1-state nuclear wave packet will follow the blue trajectory in Fig. 5.3. The wave packet crosses the potential-surface intersection twice each vibrational period, with nonzero momentum, and the gap between donor and acceptor transition energies oscillates between $2\delta^2\omega$ and $6\delta^2\omega$ (see the blue traces of Fig. 5.4). Thus we expect short-time EET to be diminished for the donor displaced in the negative direction.

The similarity between donor positive displacement and acceptor negative displacement, and vice versa, is due to the fact that these trajectories are identical, when projected onto the antisymmetric axis defined in Fig. D.1. The difference between the acceptor- and donor-displaced cases suggests another means of experimentally monitoring and verifying the effectiveness of our control strategy. By comparing the VHH and HHH signals for values of t_{AP} which correspond to maximum negative and positive displacement, one should see evidence of control.

In the following sections we show the VHH and HHH pump-probe difference signals for DTA, for both an oriented sample and an isotropic distribution. We see that clear and unambiguous evidence of vibrational control can be found by comparing pump-probe

*The coloring of the trajectories in Figs. 5.1 and 5.3 is such that the same control-pulse delay time gives rise to trajectories of the same color in the donor- and acceptor-displaced cases. Corresponding colors are used in Figs. 5.2 and 5.4.

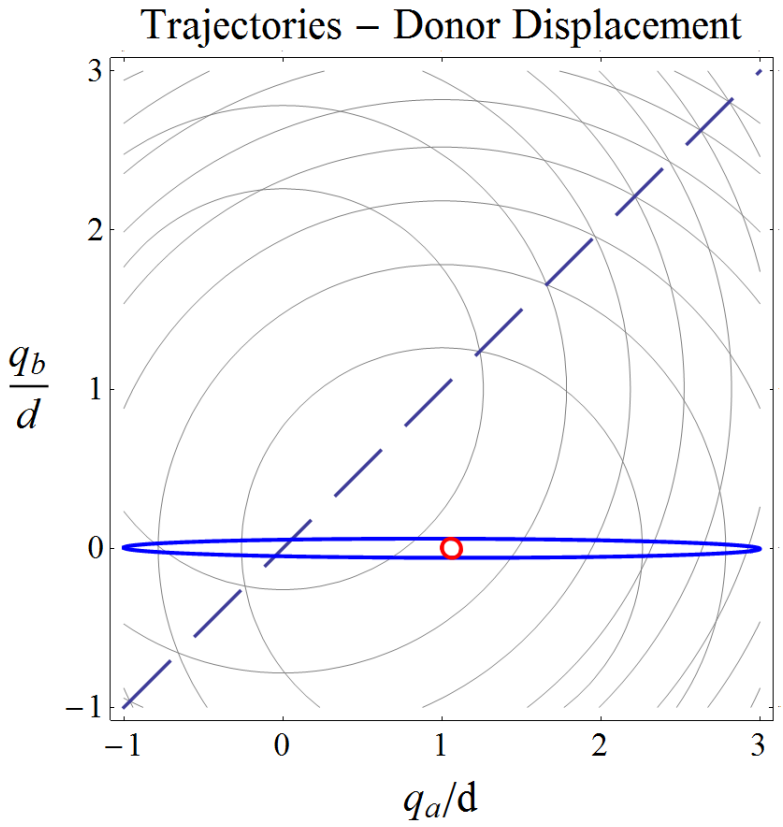

Figure 5.3: Classical trajectories for nuclear wave packets in the 1-state for the case of donor-displacement. The blue line is the case where the nuclear wave packet is at $(q_a, q_b) = (-d, 0)$ at the instant of electronic excitation (assuming an oriented sample). If the electronically resonant pulse arrives one half period later, the wave packet is at $(q_a, q_b) = (0, d)$ and will stay put as it is at the excited-state minimum. The coloring of the trajectories mirrors that in Fig. 5.1.

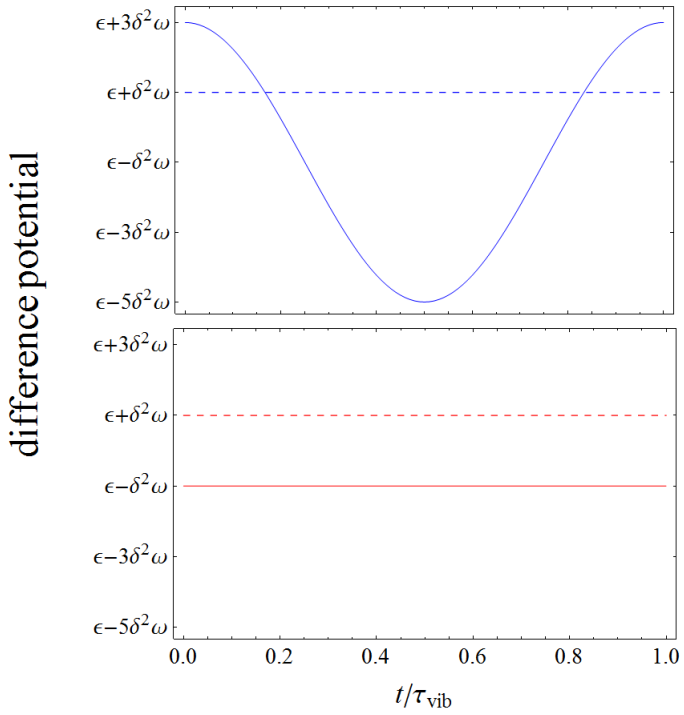

Figure 5.4: Instantaneous transition frequencies for donor-emission (solid lines) and acceptor-absorption (dashed lines) for the classical trajectories depicted in Fig. 5.3.

difference signals from DTA at different values of t_{AP}. We further show that this clear evidence is present not only in the stimulated emission from an oriented sample, which directly probes the donor-excited state without any other contribution, but is also present in the total pump-probe difference signal from an isotropic sample.

A.2. Chirped Pulse Vibrational Excitation

As has been shown previously,[1] introducing a linear frequency chirp can increase the range of nuclear motion induced by an ultrashort laser pulse in the electronic ground state. For displaced harmonic oscillator systems, such as DTA-12 and the other model systems considered in Chapter III, the difference potential is a linear function of the nuclear coordinate with a negative slope. Therefore using a control pulse with a negative linear chirp selects for nuclear amplitude that has moved toward the excited state minimum during its transient occupation of the excited electronic state.

A chirped pulse can be created by sending a transform-limited pulse through a dispersive medium, which introduces a second-order frequency-dependant phase shift. The resulting electric field is written as[2]

$$E_I(t) = \frac{\boldsymbol{e}_I E_I \sigma_I}{2} f_I(t) \left[\frac{\exp\left(-i\Phi_I(t)\right)}{\left(\sigma_I^2 + i\alpha_I\right)^{1/2}} + \frac{\exp\left(i\Phi_I(t)\right)}{\left(\sigma_I^2 - i\alpha_I\right)^{1/2}} \right], \tag{5.1}$$

where σ_I is the duration of the unchirped pulse (equal to the full width at half maximum in intensity divided by $2\sqrt{\ln 2}$), and α_I is the linear chirp rate. The pulse envelope and phase function are written

$$f_I(t) = exp\left(-\frac{(t - t_I)^2}{2(\sigma_I^2 + \alpha_I^2/\sigma_I^2)} \right), \tag{5.2}$$

and

$$\Phi_I(t) = \Omega_I(t - t_I) + i\frac{\alpha_I}{2(\sigma_I^4 + \alpha_I^2)}(t - t_I)^2. \tag{5.3}$$

The resulting chirped pulse is therefore longer in duration than the transform-limited pulse from which it is made, with an effective duration $\sigma_I' \equiv \sqrt{\sigma_I^2 + \alpha_I^2/\sigma_I^2}$.

In the calculations presented here we only consider chirp for the control pulse, and consider all electronically-resonant pulses to be transform-limited. We therefore need matrix elements of the second-order pulse propagator, as seen in Eq. (3.7), with the effects of chirp included. The required matrix element is written

$$\begin{aligned}\left\langle (\nu_a,\nu_b)_0 \left| p_I^{(01)}(\infty;\, t_2) p_I^{(10)}(t_2;\, t_1) \right| (\bar{\nu}_a,\bar{\nu}_b)_0 \right\rangle \\ = -\frac{\pi}{4}\sigma_I^2 E_I^2 m^2 \delta_{\nu_b,\bar{\nu}_b} \sum_{\bar{\bar{\nu}}_a} \langle (\nu_a)_g |\, (\,\bar{\bar{\nu}}_a)_e\rangle \,\langle (\,\bar{\bar{\nu}}_a)_e |\, (\,\bar{\nu}_a)_g\rangle \\ \times \exp\left(-\frac{1}{2}\Delta_1^2\left(\sigma^2 + i\alpha\right) - \frac{1}{2}\Delta_2^2\left(\sigma^2 - i\alpha\right)\right) \\ \times \left[1 + \mathrm{erf}\left(i\frac{\Delta_1\left(\sigma^2 + i\alpha\right) + \Delta_2\left(\sigma^2 - i\alpha\right)}{2\sigma}\right)\right],\end{aligned} \tag{5.4}$$

where

$$\Delta_1 = \Omega_I - \varepsilon + (\nu_a - \bar{\bar{\nu}}_a)\omega \tag{5.5}$$

and

$$\Delta_2 = \Omega_I - \varepsilon + (\bar{\nu}_a - \bar{\bar{\nu}}_a)\omega \tag{5.6}$$

are the effective resonance offsets for the downward and upward transitions, respectively. Eq. (5.4) reduces to Eq. (3.7) when the chirp rate α_I is set equal to zero.

B. Calculations

B.1. Survival Probabilities

A numerical search over pulse duration, center frequency, and linear chirp rate, subject to the constraint that the squared norm of the first-order wave packet in the excited

electronic state be less than 5% the size of the norm of the second-order wave packet, found that the largest amplitude motion occurs for $\Omega_P = \varepsilon - 1.58\,\omega_{12}$, $\sigma_P = 0.217\,\tau_{vib} = 18.9\,\text{fs}$, and $\alpha_P = -0.031\,\tau_{vib}^2 = -234\,\text{fs}^2$.* The effective duration of the chirped pulse is slightly longer, with $\sigma_I' = 22.6\,\text{fs}$. Following interaction with the control pulse, the affected monomer achieves a maximum negative displacement of $\langle q_{b(a)} \rangle = -0.63\,d$ at $t - t_P = 0.47\,\tau_{vib}$ (and a half-vibrational period later the wave packet has this same displacement in the positive direction). Therefore the introduction of chirp to the control pulse increases the maximum nuclear displacement in DTA-12 by 12%.

In Fig. 5.5 we present survival probabilities† for an oriented DTA-12 complex, where the donor and acceptor transition dipoles are aligned with the lab-frame H and V axes, respectively. The control pulse is either V or H polarized, and the A pulse is H polarized. The A pulse is the same as was used in subsection B.2 of Chapter III , (with duration $\sigma_A = 0.1\tau_{vib} = 8.66\text{fs}$ and center frequency $\Omega_A = \varepsilon + \delta_{12}^2\,\omega_{12}$). The top panel shows contour plots of the survival probabilities for $0 \leq t_{AP} \leq \tau_{vib}$, and the bottom panel shows slices of constant t_{AP} corresponding to maximum negative and positive displacement. When $t_{AP} = 0.47\ \tau_{vib}$, maximum negative displacement occurs (blue traces in the lower panel), and maximum positive displacement occurs at $t_{AP} = 0.97\ \tau_{vib}$ (red traces). These results show that when the donor is negatively (positively) displaced, energy transfer is diminished (enhanced), and the opposite is true when the acceptor is displaced. As we will see in the next subsection, this opposite behavior for V- and H-polarized control pulse is evident in VHH and HHH signals from both oriented and isotropic samples.

---

*This value of α_P is lower than the chirp rate which gives rise to the greatest rate of change in the "instantaneous frequency", $\dot{\omega}_{\text{max}} = \pm 1/(2\sigma_P^2)$.

†The survival probability is defined as the fractional population of the one-exciton manifold residing in the donor state (state-1) following A-pulse excitation to that state from the electronic ground state.

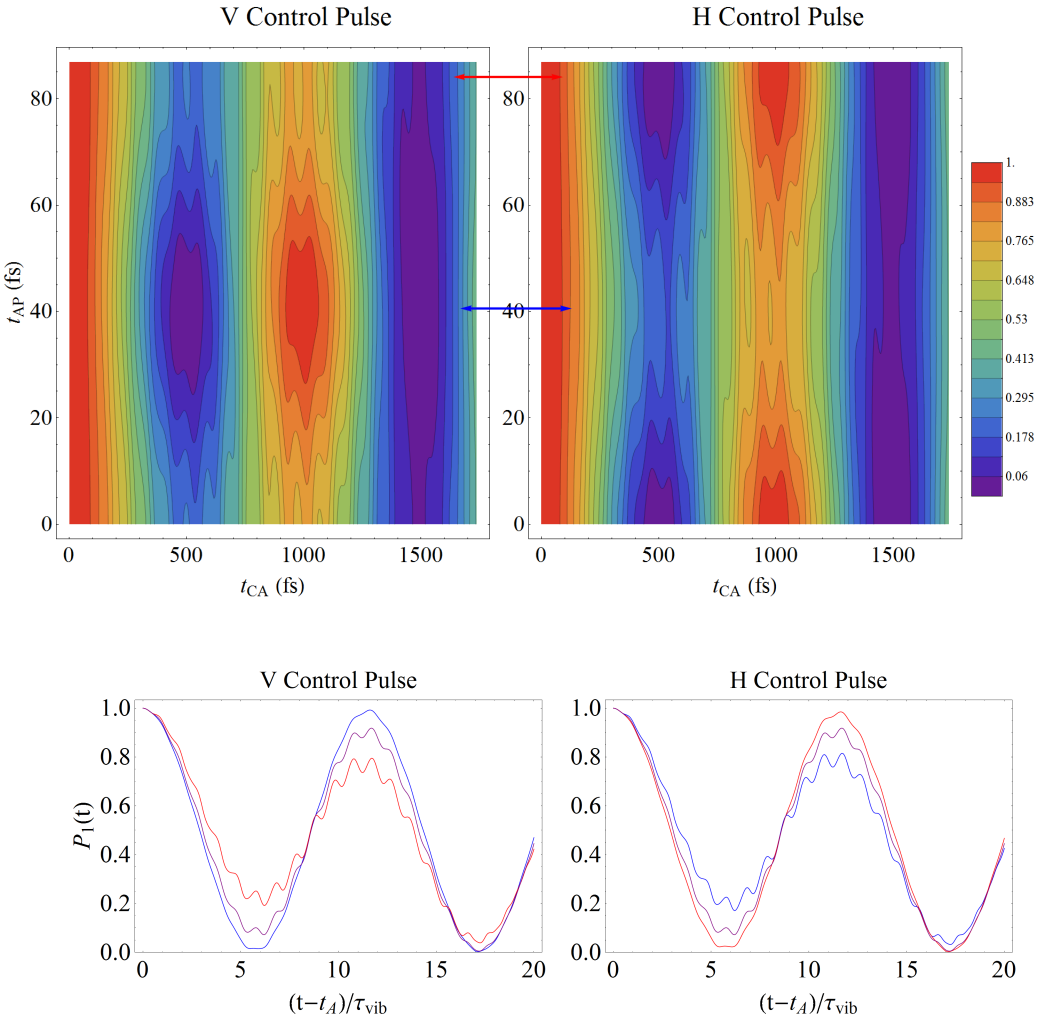

Figure 5.5: Survival probabilities for an oriented DTA-12 complex which has interacted with either a V- or H-polarized control pulse, and therefore have had the acceptor or donor vibrationally perturbed. (Top) Contour plots for $0 \leq t_{AP} \leq \tau_{vib}$. (Bottom) Slices of the contour plots above at $t_{AP} = 0.47\ \tau_{vib}$ (blue) and $t_{AP} = 0.97\ \tau_{vib}$ (red). Arrows on the top correspond to the traces in the bottom panel, as well as to the idealized trajectories shown in Figs. 5.1 and 5.3. Note that when $t_{AP} = 0.47\ \tau_{vib}$ (when the wave packet is at its inner turning point), EET is enhanced with a V control pulse and diminished for an H control pulse. The reverse is true at $t_{AP} = 0.97\ \tau_{vib}$.

B.2. Pump-Probe Difference Signals

First we examine the stimulated emission signal component from an oriented DTA-12 sample. Under these conditions, the HHH and VHH signals are proportional to the real parts of

$$\begin{aligned}\langle\{b(10)p(01)p(10)\}_1|\{d(10)c(01)a(10)\}_1\rangle \\ + \langle\{b(10)\}_1|\{d(10)c(01)a(10)p(01)p(10)\}_1\rangle\end{aligned} \tag{5.7}$$

and

$$\begin{aligned}\langle\{b(10)p(01')p(1'0)\}_1|\{d(10)c(01)a(10)\}_1\rangle \\ + \langle\{b(10)\}_1|\{d(10)c(01)a(10)p(01')p(1'0)\}_1\rangle\end{aligned} \tag{5.8}$$

respectively. These signals most closely monitor the population of the 1-state. Specifically they monitor local spatial interference in the region of probe-pulse resonance. The pump and probe pulses are the same as described in Subsection B.2 of Chapter III. The pump is short and vertically resonant ($\sigma_A = 0.1\tau_{\text{vib}} = 8.66$fs; $\Omega_A = \varepsilon + \delta^2\,\omega$), while the probe is longer (and hence more spectrally selective) and resonant at the outer turning point for nuclear motion in the excited state($\sigma_C = 0.5\tau_{\text{vib}} = 43.3$fs; $\Omega_C = \varepsilon - 3\delta^2\,\omega$). The control pulse is the chirped pulse described above.

Figure 5.6 shows the HHH and VHH signals for t_{AP} values between 0 and t_{vib}.* We showed in Chapter IV that a lack of direct proportionality between pump-probe and pump-probe difference signals can be taken as evidence of the coherent vibrational control over EET, and therefore any change of the signal shape as a function of t_{AP} can itself be taken as evidence of control. As can be seen in Fig. 5.6, there is significant variation of the

*As we do not consider overlap between control and pump pulses, these should be taken to represent values of t_{AP} for one period of ground-state evolution.

signal along the t_{AP} axis. The signal maxima and minima occur for the values of t_{AP} at which the ground-state wave packet ($|\{p(01')p(1'0)\}_0\rangle$ or $|\{p(01')p(1'0)\}_0\rangle$) is near the origin with considerable momentum in the positive or negative direction. These are the values which lead to the greatest momentum mismatch between the kets and bras of Eqs. 5.7 and 5.8, while the greatest change in the survival probabilities of Fig. 5.5 occurs for values of t_{AP} where the ground-state wave packet is at a turning point, and thus has no momentum.

In Fig. 5.7 we show stimulated-emission HHH and HHV signals, from an oriented complex, for single values of t_{AP}. These plots are horizontal slices of the contour plots in Fig. 5.6. The control pulse delay time is set to either $t_{AP} = 0.47\tau_{\text{vib}} = 40.8$ fs (or $t_{AP} = 0.97\tau_{\text{vib}} = 84.3$ fs), so that the control-induced wave packet is at $\langle q_b \rangle = -0.63d_{12}$, (or $0.63d_{12}$), when the A pulse arrives. The vibrational-period beating is a result of the excite-state wave packet coming in and out of resonance with the C pulse once a period. The longer-period oscillation is due electronic energy transfer. The VHH signals (solid lines) show that the dominant electronic oscillation period is longer, by more than one vibrational period, for positive acceptor displacement (at $t_{AP} = 0.97\tau_{\text{vib}}$) than it is for negative acceptor displacement (at $t_{AP} = 0.47\tau_{\text{vib}}$). This is in perfect agreement with the arguments put forth in Subsection A.1 of this chapter and in Appendix G concerning the effects of acceptor displacement on EET. As expected, we see the opposite in the HHH signals (dashed lines), which probe the effects of donor-displacement. Here the electronic oscillation period is discernably longer at $t_{AP} = 0.47\tau_{\text{vib}}$ than it is a half vibrational period later.

In Fig. 5.8 we see contour plots of the total HHH and VHH signals, including the effects of ground-state bleach and excited-state absorption, for isotropic samples of DTA-12. There is still considerable signal variation along t_{AP}, though many of the features seen in the oriented stimulated-emission signals are absent or diminished by the other contributions present. Fig. 5.9 shows slices of the total HHH and VHH signals for the two values of t_{AP} considered above. These signals only approximately probe the effects of acceptor (VHH) or

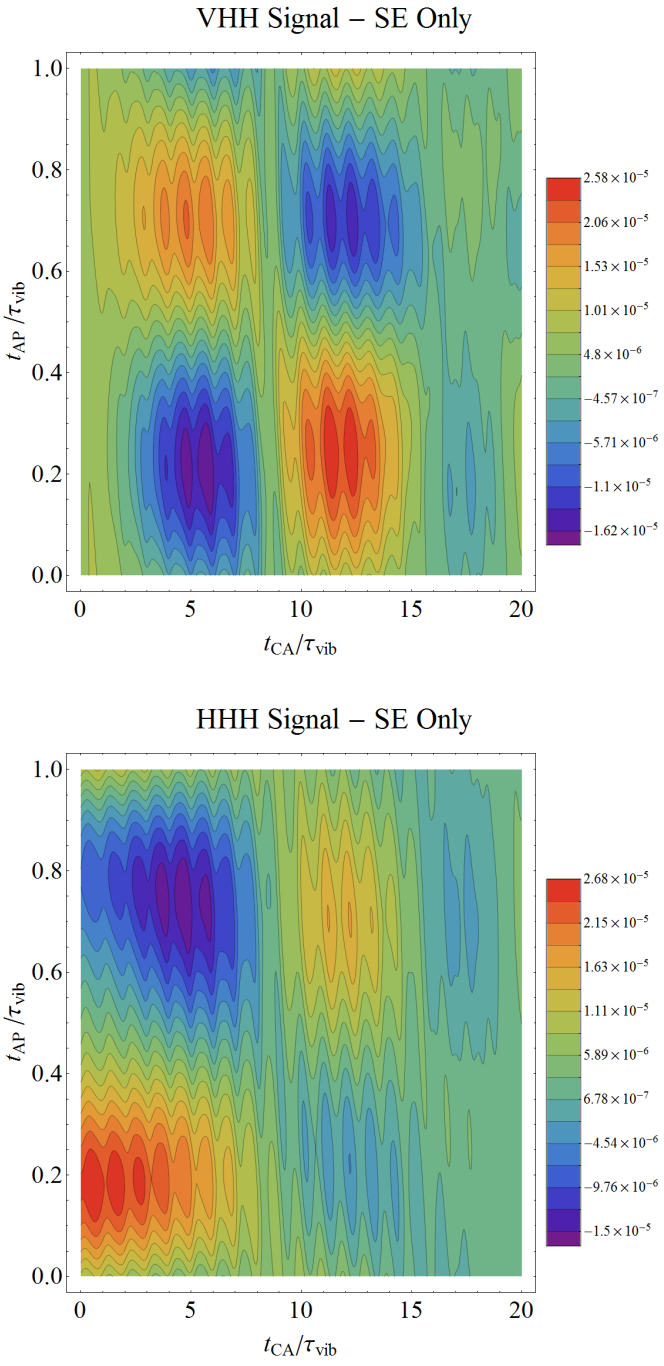

Figure 5.6: Stimulated-emission contributions to the VHH and HHH pump-probe difference signals from an oriented DTA-12 complex, as a function of the control pulse delay time, t_{AP}. The presence of signal variation along the vertical axis is evidence of the vibrational control over EET. Two horizontal slices of these signals are found in Fig. 5.7.

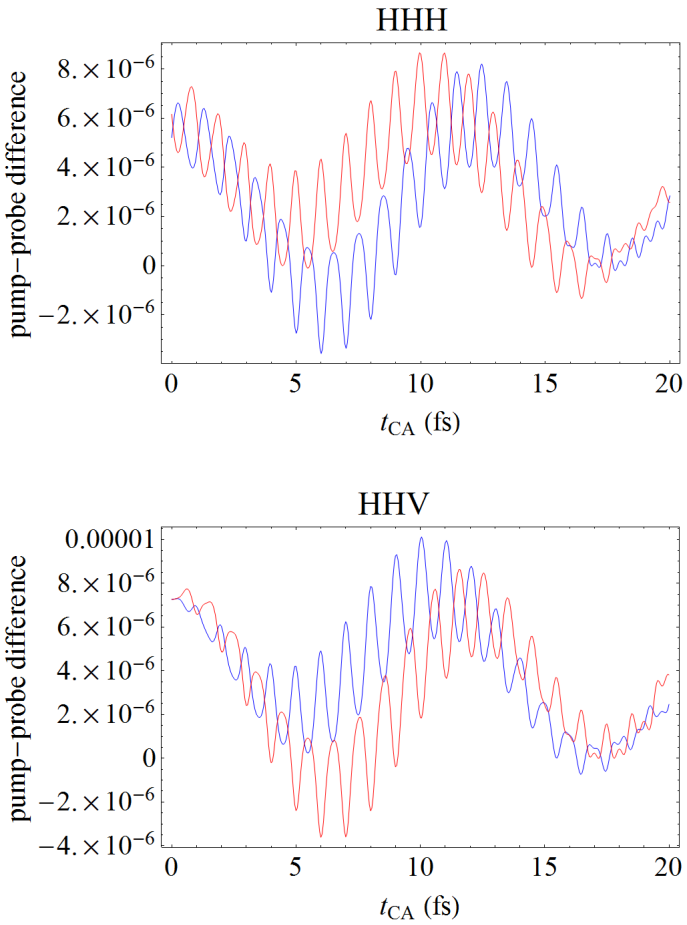

Figure 5.7: Stimulated-emission contributions to the HHH (top panel) and VHH (bottom panel) pump-probe difference signals from an oriented DTA-12 complex for two different values of t_{AP}. The control pulse delay has been set to $t_{AP} = 0.47\ \tau_{vib}$ (blue traces) or $t_{AP} = 0.97\ \tau_{vib}$ (red traces). We see the opposite behavior here for VHH and HHH concerning the directionality of the control over EET in these plots.

donor (HHH) displacement on subsequent EET dynamics, as each contains contributions from both donor- and acceptor-displaced wave packets. However, in Fig. 5.9 it is clear that at $t_{AP} = 0.47\ \tau_{vib}$ the dominant electronic oscillation period is shorter for VHH than for HHH, and at $t_{AP} = 0.97\ \tau_{vib}$ the reverse is true. This is clear evidence of the vibrational control over EET in DTA-12.

B.3. WPI Difference Signals

In this section we present complex-valued md-WPI signals from an oriented DTA-12 dimer, both with and without a control pulse. We show that the md-WPI difference signals from HHH and VHH polarizations* are not directly proportional to the HH signal, and point to this as further evidence for the vibrational control of electronic energy transfer. We defer to a later date, however, a detailed analysis of the fringe structure in the difference interferograms, and the amplitude-level information on EET that they contain.

Here we look at that portion of the total frequency- and time-integrated fluorescence which bears the optical phase $\phi_{BA} - \phi_{DC}$ and is, in the case of the difference measurement, quadratic in the control-pulse amplitude. The signal is therefore S_{ε}^{+-}, as defined in Eq. 2.35 and Appendix B. The molecular system is the same as in the last section, DTA-12. For simplicity we make all four of the md-WPI pulses, pulses A–D, to be transform-limited and short in duration ($\sigma_I = 0.1\tau_{\text{vib}}$. The center frequencies of the WPI pulses are set to be vertically resonant ($\Omega_I = \varepsilon + \delta^2\omega$), in contrast to the pump-probe results of the preceding section where the probe pulse was redshifted with respect to the pump. The interferogram is aliased to remove high-frequency oscillations by multiplying it by a reference wave of the form $e^{i\Omega_L(t_{BA}-t_{DC})}$, where Ω_L is the locking frequency, taken to be the common center frequency

*In all of the calculated md-WPI signals presented here, pulses within a phase-related pulse pair share the same polarization. We therefore use the same polarization designations used for the pump-probe difference signals, i.e. we write VHH instead of VHHHH to indicate that the control pulse is V polarized and the WPI pulses are all H polarized.

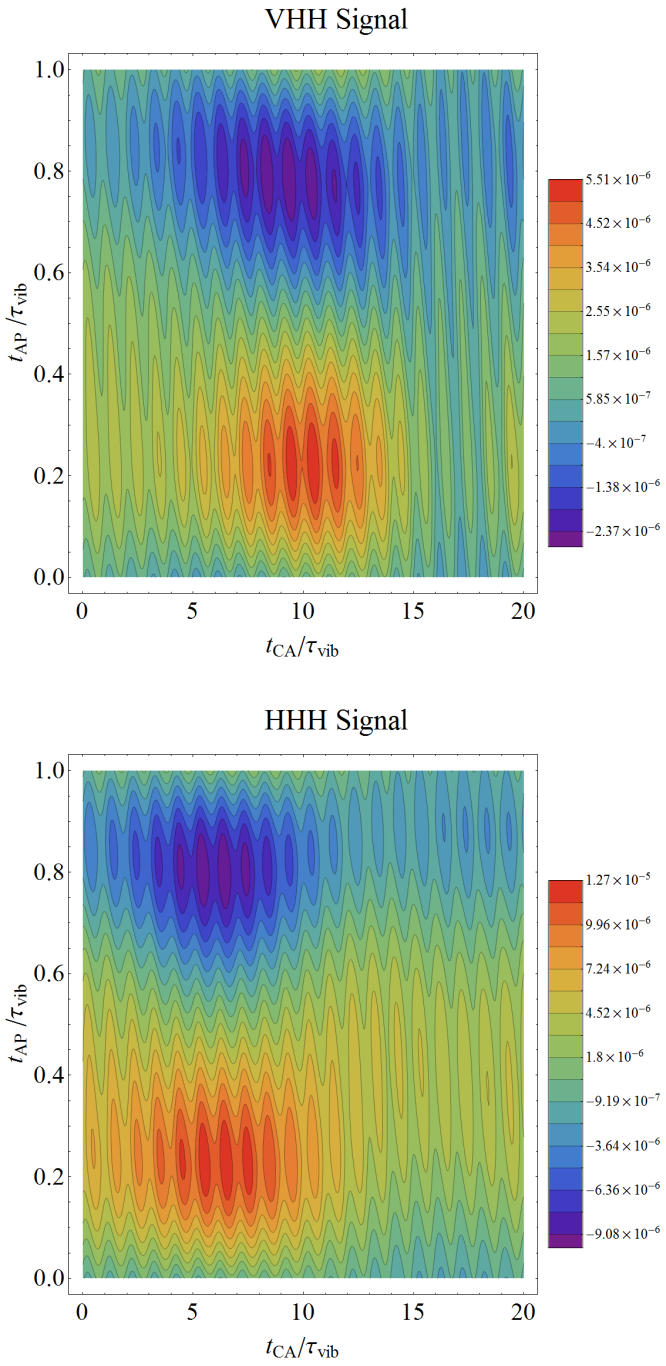

Figure 5.8: Total VHH and HHH pump-probe difference signals, including stimulated emission, excited-state absorption, and ground-state bleach, from an isotropic DTA-12 sample. Two horizontal slices of these signals are found in Fig. 5.9.

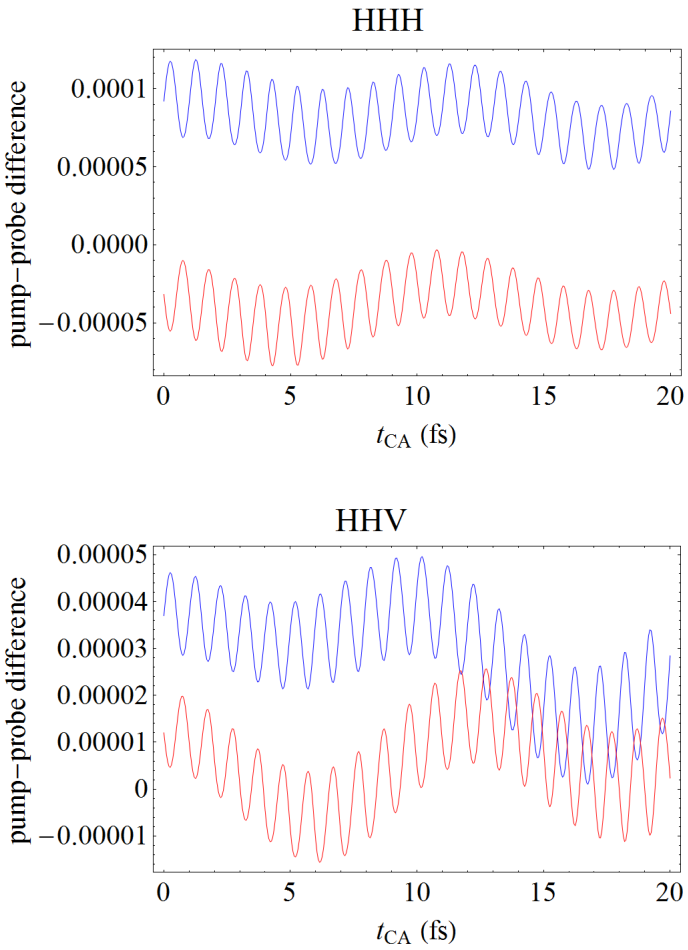

Figure 5.9: The same as Fig. 5.7, but here we have the full signal (including GSB and ESA contributions) from an isotropic sample. The evidence of the opposite directionality of control is still evident, although less pronounced than it was from an oriented sample.

of the WPI pulses. We set the waiting time, t_{CB}, equal to a half vibrational period. This allows us to safely neglect overlap between the B and C pulses, yet ensures that little to no EET occurs during the waiting time. Here we also neglect overlap between pulses within a phase-locked pulse pair, and accordingly we also neglect contributions from wave packets where the pulses within a pair act out of sequence.

The total md-WPI signal in the absence of the control pulse is

$$\begin{aligned} T_{HH}^{+-} = &\langle \{b(10)\}_1 | \{d(10)c(01)a(10)\}_1 \rangle \\ &+ \langle \{d(1'2)c(21')b(10)\}_{1'} | \{a(10)\}_{1'} \rangle \\ &+ \langle \{c(10)\}_1 | \{d(10)b(01)a(10)\}_1 \rangle . \end{aligned} \tag{5.9}$$

The signal components listed in Eq. 5.9 reduce to the stimulate emission (SE), excited-state absorption (ESA), and ground-state bleach signals, respectively, in the pump-probe limit. The ESA contribution to the total signal is proportional to the amplitude transferred from the 1 to the $1'$ states during t_{CB}, and therefore does not contribute significantly to the signals presented here, where t_{CB} is small. The SE and GSB contributions are similar in form and magnitude. In going from the SE to the GSB terms, t_{CB} of free evolution is transferred from the one-exciton manifold to the 0 state for both the bra and ket. With a small t_{CB}, the differences are minor, and the two contributions resemble each other and the total signal resembles these two terms.

In Fig. 5.10 we show the absolute value of the total HH signal from an oriented sample. The molecule is again oriented so that the acceptor transition dipole is aligned with the lab-frame V axis, and the donor transition dipole is aligned with the lab-frame V axis. Both vibrational and electronic motion is clearly visible in this interferogram. At early times, before energy transfer has taken place to a significant degree, the fringe structure resembles that from a simple displaced harmonic oscillator system. The signal is maximized when $t_{BA} + t_{DC}$ is

equal to an integer multiple of the vibrational frequency. At later times, after back-and-forth EET has occurred, the vibrational beating is less pronounced. Fig. 5.11 shows the real and imaginary parts of the interferogram from Fig. 5.10.

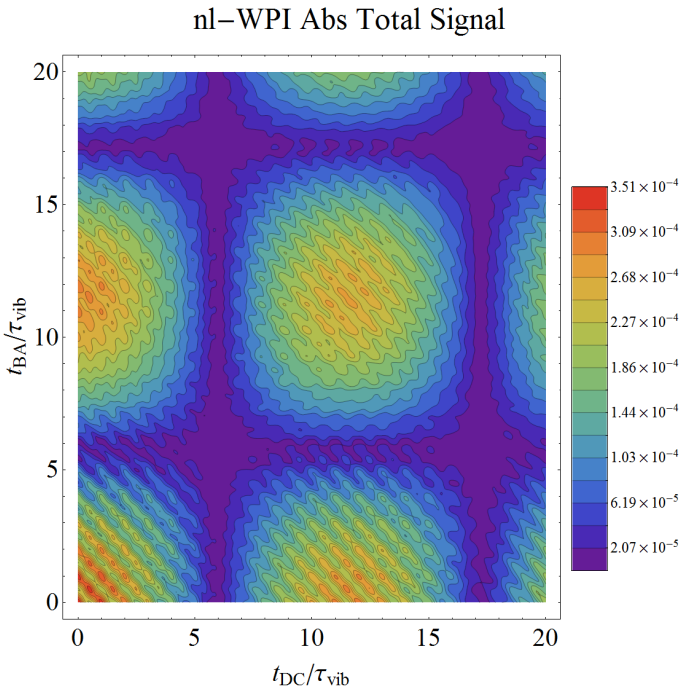

Figure 5.10: Absolute value +− WPI signal from an oriented DTA-12 complex, with HH polarization.

The md-WPI difference signal from this oriented complex, for HHH polarization, is

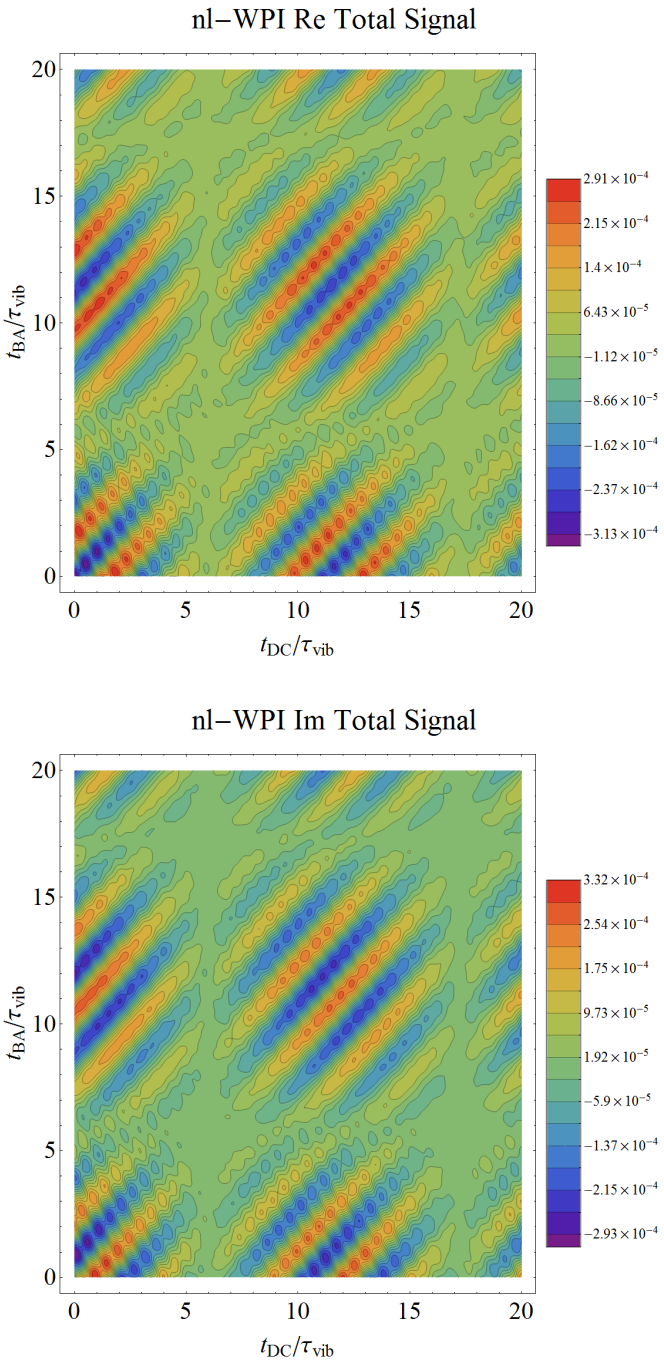

Figure 5.11: Real (top) and imaginary (bottom) parts of the md-WPI signal from Fig. 5.10.

written

$$\begin{aligned} S^{+-}_{HHH} = &\langle\{b(10)\}_1|\{d(10)c(01)a(10)p(01)p(10)\}_1\rangle \\ &+ \langle\{b(10)p(01)p(10)\}_1|\{d(10)c(01)a(10)\}_1\rangle \\ &+ \langle\{d(1'2)c(21')b(10)\}_{1'}|\{a(10)p(01)p(10)\}_{1'}\rangle \\ &+ \langle\{d(1'2)c(21')b(10)p(01)p(10)\}_{1'}|\{a(10)\}_{1'}\rangle \\ &+ \langle\{c(10)\}_1|\{d(10)b(01)a(10)p(01)p(10)\}_1\rangle \\ &+ \langle\{c(10)p(01)p(10)\}_1|\{d(10)b(01)a(10)\}_1\rangle\,. \end{aligned} \tag{5.10}$$

The middle two terms, which reduce to the ESA contribution in the pump-probe limit, are small compared with the other terms for the same reason as described above (namely that they are proportional to the small amount of amplitude transferred during t_{CB}). We can immediately see from Eq. (5.10) that watching for signal variation as a function of t_{AP} is not as strait forward as it is for pump-probe difference signals. Setting a single value of t_{AP} fixes the initial displacement of the $|\{a(10)p(01)p(10)\}_1\rangle$ wave packet, however the initial displacement of the $|\{b(10)p(01)p(10)\}_1\rangle$ wave packet varies with t_{BA}. The interferogram fringe structure therefore depends on t_{AP} in an entirely different way than the pump-probe difference signal. In the difference signals presented here, we set $t_{AP} = 0.47\tau_{\text{vib}}$ such that the ground state wave packet $|\{p(01)p(10)\}_0\rangle$ is at its inner turning point when the A pulse arrives. For this t_{AP} value, we saw enhanced (diminished) EET for the VHH (HHH) pump-

probe difference signal. The md-WPI difference signal for VHH polarization is written

$$\begin{aligned} S^{+-}_{VHH} = &\langle\{b(10)\}_1|\{d(10)c(01)a(10)p(01')p(1'0)\}_1\rangle \\ &+ \langle\{b(10)p(01')p(1'0)\}_1|\{d(10)c(01)a(10)\}_1\rangle \\ &+ \langle\{d(1'2)c(21')b(10)\}_{1'}|\{a(10)p(01')p(1'0)\}_{1'}\rangle \\ &+ \langle\{d(1'2)c(21')b(10)p(01')p(1'0)\}_{1'}|\{a(10)\}_{1'}\rangle \\ &+ \langle\{c(10)\}_1|\{d(10)b(01)a(10)p(01')p(1'0)\}_1\rangle \\ &+ \langle\{c(10)p(01')p(1'0)\}_1|\{d(10)b(01)a(10)\}_1\rangle\,. \end{aligned} \tag{5.11}$$

Fig. 5.12 shows the absolute value interferogram for the HHH and VHH polarizations. The real and imaginary HHH signals are shown in Fig. 5.13, while Fig. 5.14 is the same for VHH. We can see from these results that the vibrational-period interferences are made stronger by the action of the control pulse, just as they were in the pump-probe difference signals.* We also see that the VHH signal starts out small, and only grows in as t_{BA} or t_{DC} gets larger, i.e. after back-and-forth energy transfer has taken place.

To understand the behavior of the VHH signal, we look closer at those contributions to the VHH signal which reduce to GSB in the pump-probe limit. They are,

$$\begin{aligned} &\langle\{c(10)\}_1|\{d(10)b(01)a(10)p(01')p(1'0)\}_1\rangle \\ &\qquad + \langle\{c(10)p(01')p(1'0)\}_1|\{d(10)b(01)a(10)\}_1\rangle\,. \end{aligned} \tag{5.12}$$

For small interpulse delays, the sum written above is close to zero, meaning that the overlaps are equal and opposite in magnitude to each other. This is always the case when the control pulse is ineffective at generating nuclear motion, as we learned in Chapter IV. However in the case considered here, the control pulse *is* effective at generating nuclear motion but

*See Fig. 3.5 for a direct comparison between pump-probe and pump-probe difference signals in DTA-12.

this nuclear motion is located entirely in the acceptor mode for the VHH signal. The sum in Eq. (5.11) only gains in magnitude after either of the interpulse delays reaches the time for back energy transfer. As t_{AB} gets larger, the wave packet $|\{d(10)b(01)a(10)\}_1\rangle$ begins to acquire momentum in the acceptor vibrational mode and can therefore overlap with the $|\{c(10)p(01')p(1'0)\}_1\rangle$ wave packet. As t_{DC} gets larger, the wave packet $|\{c(10)\}_1\rangle$ likewise begins to acquire momentum in the acceptor vibrational mode and can overlap with the $|\{d(10)b(01)a(10)p(01')p(1'0)\}_1\rangle$ wave packet. For an HHH difference signal, the momentum generated by the control pulse is entirely in the donor vibrational mode, and overlap is maximum before EET takes place.

As evidence of vibrational control over EET, we point to the fact that the electronic revival appears to come in at earlier times in the VHH signal than for the HHH signal. This is consistent with the pump-probe difference results presented in the preceding section.

Notes

[1] E. M. Hiller and J. A. Cina, Journal of Chemical Physics **105**, 3419 (1996).

[2] Y. C. Shen and J. A. Cina, Journal of Chemical Physics **110**, 9793 (1999).

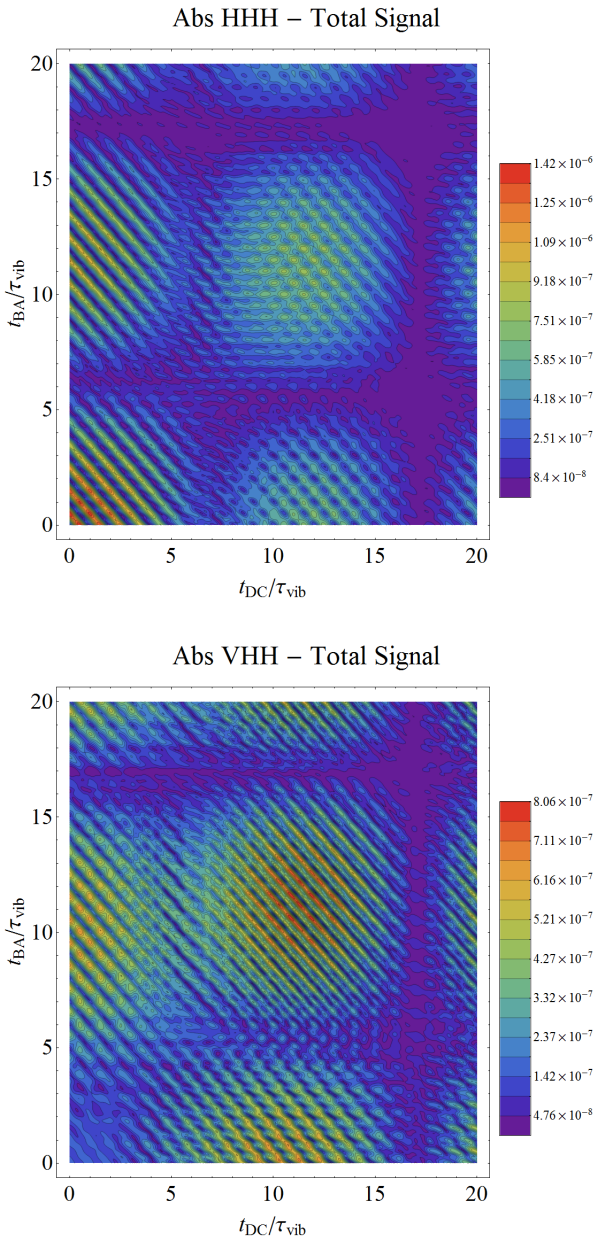

Figure 5.12: Absolute value interferograms for the HHH (top) and VHH (bottom) md-WPI difference signals, with $t_{AP} = 0.47\tau_{\text{vib}}$.

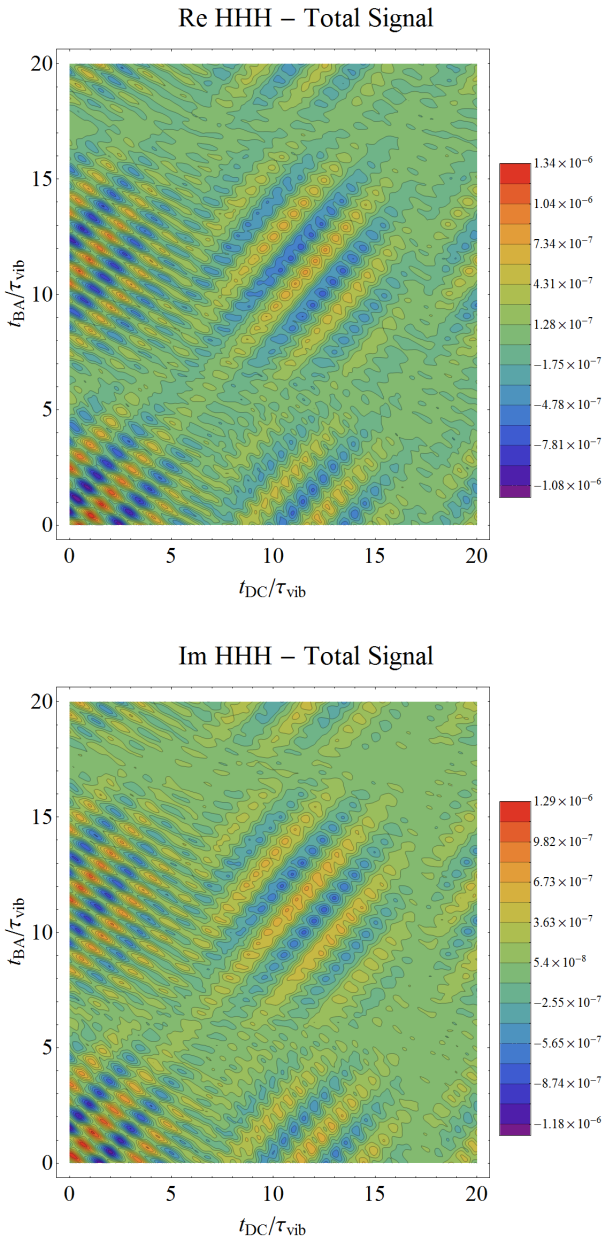

Figure 5.13: Complex-valued interferograms for the HHH md-WPI difference signals, with $t_{AP} = 0.47\tau_{\text{vib}}$.

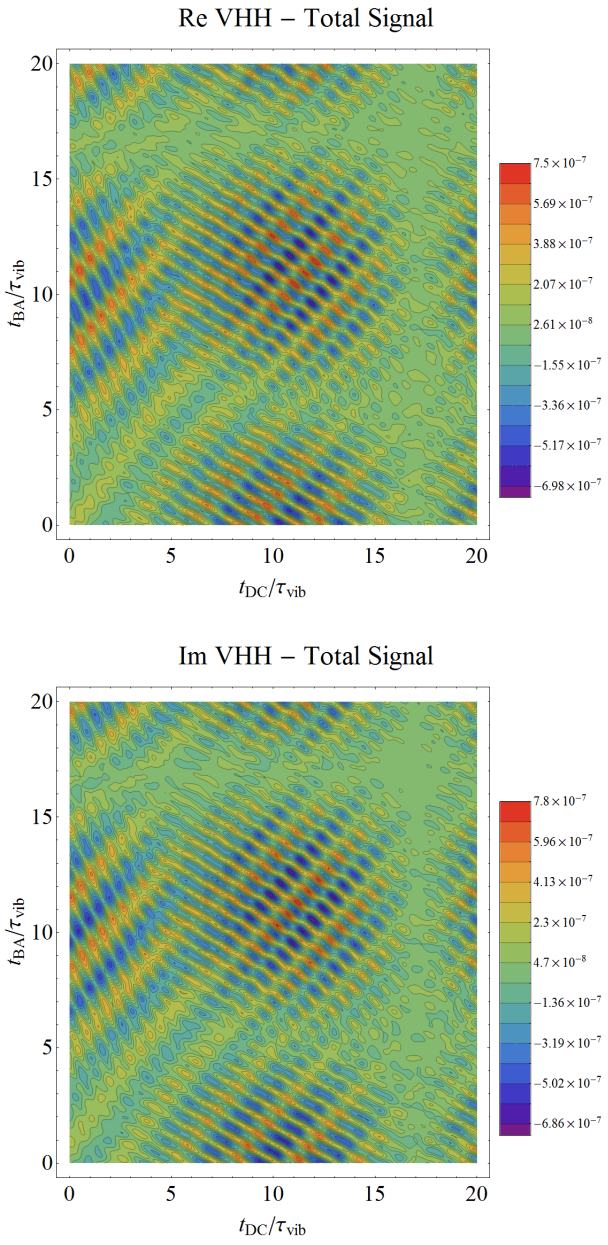

Figure 5.14: Complex-valued interferograms for the VHH md-WPI difference signals, with $t_{AP} = 0.47\tau_{\text{vib}}$.

CHAPTER VI

MONITORING THE TORSIONAL CONTROL OVER ENERGY TRANSFER USING PUMP-PROBE POLARIZATION SPECTROSCOPY

A. Motivation

In the preceding chapter, we saw that coherent intramolecular vibrational motion can alter the time-course of electronic energy transfer (EET) in dithia-anthracenophane (DTA). We performed calculations on DTA-12, our model dimer which includes only the low frequency ν_{12} vibrational mode of each anthracene monomer. In those calculations, nuclear motion is induced via an impulsive Raman process. As shown in Appendices D and G, for harmonic systems with a small excited-state displacement, where $\delta < 1$, the effect of this nuclear motion on subsequent EET is small in magnitude and the direction of control is dependant on the displacement direction. DTA-12, for which the dimensionless excited state displacement δ^* is equal to $\sqrt{0.31}$, exemplifies the amount of control that is possible in such a system. However, the demonstration calculations of presented in Fig. 2.1 show that a much greater degree of control is available for systems with larger δ (i.e. systems with larger nuclear reorganization energy). We will now investigate the control of energy transfer in a system with a much larger displacement ($\delta \approx 6$), and see that a considerable degree of control over

*δ is defined as the displacement of the nuclear potential minimum divided by twice the RMS width of the ground-state wave function.

EET is possible in this case.

We wish to use the structural framework provided by DTA by modifying the anthracene monomer through the introduction of a highly Franck-Condon active vibrational mode. Werst *et al.*[1] found, using gas-phase laser-induced fluorescence (LIF) measurements, that the addition of a phenyl- or 2-naphthyl- group to the 9-position in anthracene introduces just such a mode. In the ground state, the aromatic substituent is orthogonal to the anthracene plane, while in the excited state the torsional minima are displaced to $55°$ or $125°$. Introduction of a phenyl or naphthyl substituent to the equivalent position on the anthracene monomers of DTA, however, would likely change these angles considerably, as the perpendicular geometry would bring hydrogen atoms from the substituent very close to the opposing anthracene monomer. Addition of the phenyl group to the 2-position in anthracene, which would be less sterically challenged in a DTA-like dimer, did not result in such strong coupling between nuclear and electronic degrees of freedom.

The internal rotation of a methyl group at the 2-position of anthracene is highly coupled to the electronic state of the system. Gas-phase LIF studies by Lin *et al.*[2] and Nakagaki *et al.*,[3] as well as dispersed fluorescence measurements by the latter, show that the minimum of the torsional potential in this system undergoes a $60°$ phase shift upon excitation to the S_1 electronic state. This was consistent with electronic structure calculations performed by Nakagaki *et al.*[3] In those calculations, they show that interaction between π molecular orbitals in the anthracene ring and σ^* orbitals in the out-of-plane hydrogen acts to stabilize the ground electronic state when the torsional angle is $0°$. In the first-excited state a similar interaction between π^* and σ^* orbitals has a stabilizing effect for a torsional angle of $60°$. This covalent-like interaction between methyl hydrogens and the π cloud of the aromatic rings was described as a hyperconjugation effect.

A DTA-like dimer of 2-methylanthracene is therefore one good candidate system for testing the vibrational control over EET, as it features strong coupling between electronic

and nuclear degrees of freedom. We choose to modify this system by replacing the methyl hydrogens with fluorine atoms. By increasing the mass, and therefore the moment of inertia for this internal rotator, we create a system with a much more compact torsional ground-state. Since δ is defined as the excited-state potential displacement divided by twice the RMS width of the ground-state wave function, the substitution of fluorine for hydrogen atoms effectively increases δ.

In this chapter we present electronic structure calculations on the torsional dependence of the S_0 and S_1 states of 2-trifluoromethylanthracene (TFMA). In the top panel of Fig. 6.1, we show the optimized ground-state geometry for TFMA (see Subsection B.2 for details). We develop a model dimer system based on TFMA, in which each monomer is a two-level electronic system with one nuclear degree of freedom. This dimer model is denoted $(\mathrm{TFMA})_2$, and a schematic picture of what such a dimer might look like is shown in the lower panel of Fig. 6.1. We investigate the use of torsional motion, induced by an impulsive Raman process, to control energy transfer in $(\mathrm{TFMA})_2$. We further present pump-probe and pump-probe difference signals for $(\mathrm{TFMA})_2$, and show that this control is observable in the differences between these signals.

B. Setup

B.1. Torsional Control Strategy

In Fig. 6.2 we show the potential curves for the S_0 and S_1 states of TFMA, see the following subsections for details concerning its calculation. The ground-state potential barriers, at $\theta = -60^\circ$, 60°, and 180°, are more than four times the size of the barriers in the excited electronic state, which are shifted by 60° with respect to the ground state. Note the flatness of the excited-state potential near its minima, while the ground-state potential is very nearly harmonic near its minima. The potential energy surfaces for the 1 and $1'$ states of

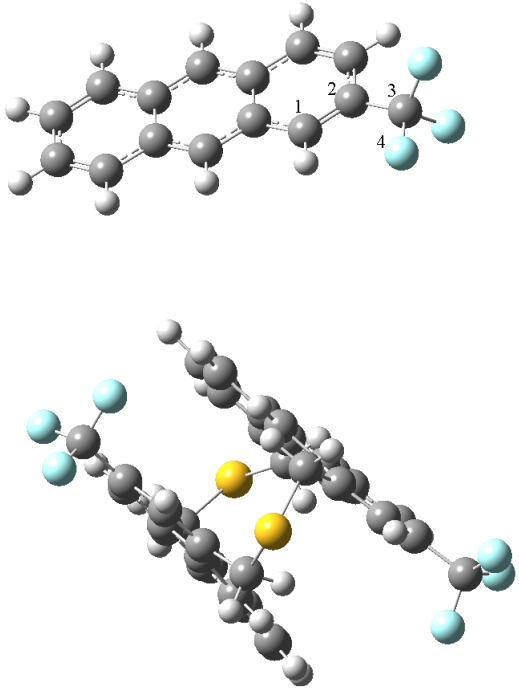

Figure 6.1: (Top) Optimized S_0 geometry for TFMA, as determined by DFT calculations at the B3LYP/6-31+G(d,p) level. The nuclear coordinate in the calculations of this chapter is the dihedral angle between the atoms labeled 1-2-3-4.(Bottom) Schematic representation of a TFMA dimer, not optimized. Sulfur atoms are shown in yellow, and fluorine atoms in teal.

$(\mathrm{TFMA})_2$ are shown in Fig. 6.3, where the intersection lines between the two are indicated with dashed lines.

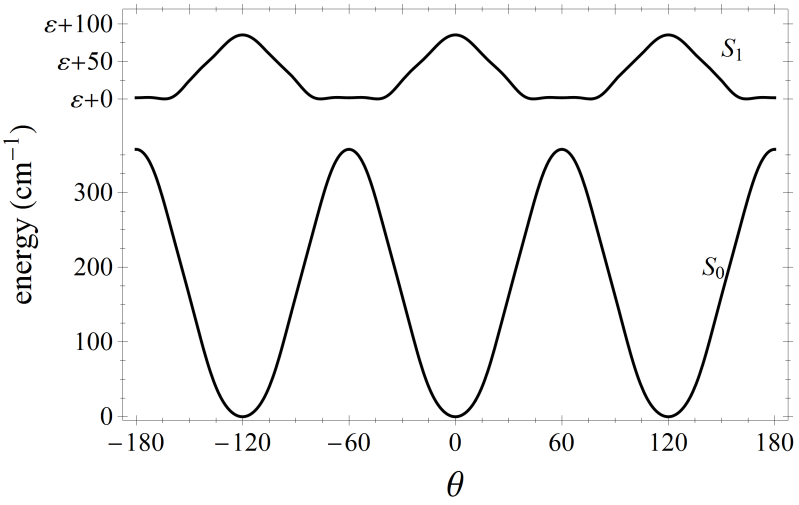

Figure 6.2: Torsional potentials for the S_0 and S_1 electronic states of 2-trifluoromethylanthracene (TFMA), as derived from density functional calculations, in which all other nuclear degrees of freedom are held fixed in their equilibrium positions.

The interplay between nuclear and electronic dynamics in $(\mathrm{TFMA})_2$ is inherently different from DTA-12, yet the control strategy put forth in Chapters II and V is applicable. In the case of vertical excitation of a ground-state nuclear wave packet initially localized at $(\theta_a, \theta_b) = (0°, 0°)$ to the 1 state*, nuclear motion is initially slow due to small slope of the excited-state potential in this region. As the wave packet acquires momentum in both the positive and negative directions, it spreads considerably and will, in the absence of dissipation, eventually cover the range $-\pi \leq \langle\theta_a\rangle \leq \pi$.

In the presence of energy transfer there is surface crossing when the wave packet is near the intersection of 1- and $1'-$potentials, such as at the Franck-Condon point. Away from the intersection, the energy gap between donor-emission and acceptor-absorption grows quickly:

*The dynamics are similar when the initial state a the delocalized ground state, with equal probability amplitude in all three potential wells.

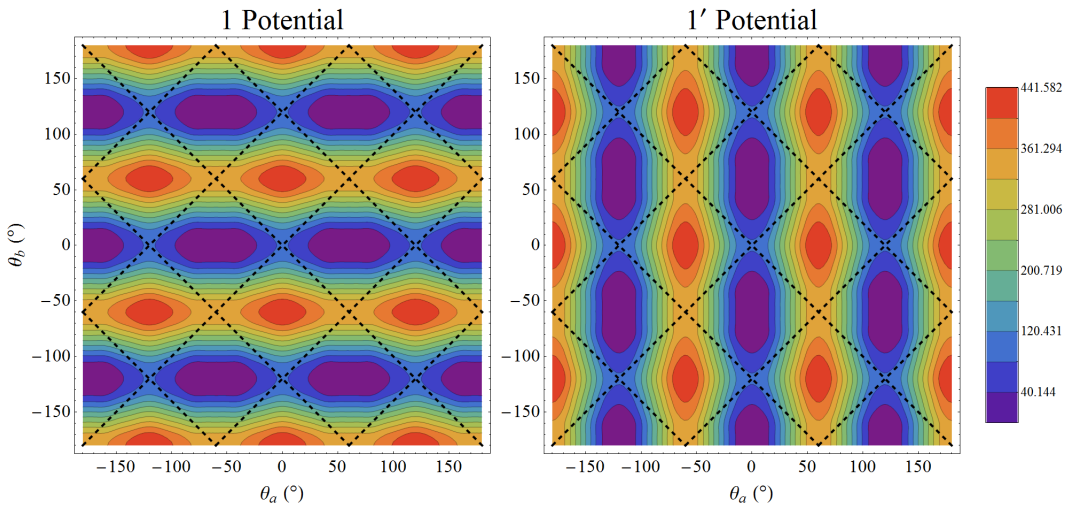

Figure 6.3: Torsional potentials for the 1 and 1′ states of the dimer model $(\mathrm{TFMA})_2$, in which two TFMA monomers are aligned in a DTA-like covalent dimer. In the 1 electronic state the a-monomer is electronically excited and the b-monomer is in the ground state, and the reverse is true for the 1′ state. Energies are given in cm^{-1}

at the origin this energy gap is zero, while at $(\theta_a, \theta_b) = (60°, 0°)$ it is equal to 441 cm^{-1}. During the time it takes for the vertically excited nuclear wave packet to move away from the origin, which occurs on a time-scale comparable to $2\pi/J$, EET will occur. EET is effectively shut down in regions away from the intersection

However, as before, one could use impulsive stimulated Raman scatting (ISRS) to generate nuclear motion in the ground state prior to electronic excitation. In this process, a pre-resonant pulse that is shorter than the vibrational period transiently promotes nuclear amplitude to the excited state, before bringing it back to the ground electronic state. The nuclear wave packet, having propagated under the excited- state Hamiltonian during the interaction, has acquired momentum in the direction of the excited-state minimum. In $(\mathrm{TFMA})_2$, unlike the displaced harmonic oscillators considered previously, the slope of the excited-state potential is zero at the Franck-Condon point and small in the region near it. The wave packet will therefore spread slowly in both directions during the interaction with the field. Momentum

will be generated in both directions simultaneously, while the total momentum remains zero. The effect is to move nuclear amplitude away from the origin, effectively creating two wave packets rotating in opposite directions in phase space, passing each other at the origin.

If the maximum displacement of theses smaller wave packets was large when an electronically-resonant pulse arrives, they would be excited directly into the upper-state potential well - far away from the intersection. This is analogous to the control strategy put forth in Chapter V, in which the donor is positively displaced. In this case EET would be diminished, as we are in the high-δ limit. In Fig. 6.4 we demonstrate the extent to which control over EET is possible, by plotting the survival probabilities* for several nuclear states. Here we take the initial nuclear state to be two copies of the ground-state wave function centered at $(\theta_a, \theta_b) = (\phi, 0^\circ)$ and $(\theta_a, \theta_b) = (-\phi, 0^\circ)$, respectively. These results confirm that the farther the wave packet is from the intersection, the less energy transfer takes place. When $\phi = 0^\circ$, we recover the ground state, and when $\phi = 60^\circ$ we excite directly to the minimum of the upper-state potential. We see that displacing the wave packet from the intersection in the excited state, while insuring that it lacks the momentum get to the intersection subsequently, significantly reduces the amount of population transferred to the $1'$ state. If one could populate the ground torsional state in the 1 state, there would be virtually no loss of population. However, the vanishingly small Franck-Condon factor for the transition makes this strategy quite difficult. The calculations of Fig. 6.4 are intended merely as a demonstration, analogous to that shown in Fig. 2.1, of the extent to which control is possible in $(\mathrm{TFMA})_2$. The actual displacement of the ground-state wave packet through ISRS is small, and its influence over subsequent EET is transient, as we show below.

*Recall that the survival probability is defined as the fractional population of the one-exciton manifold residing in the donor state (state-1) following A-pulse excitation to that state from the electronic ground state.

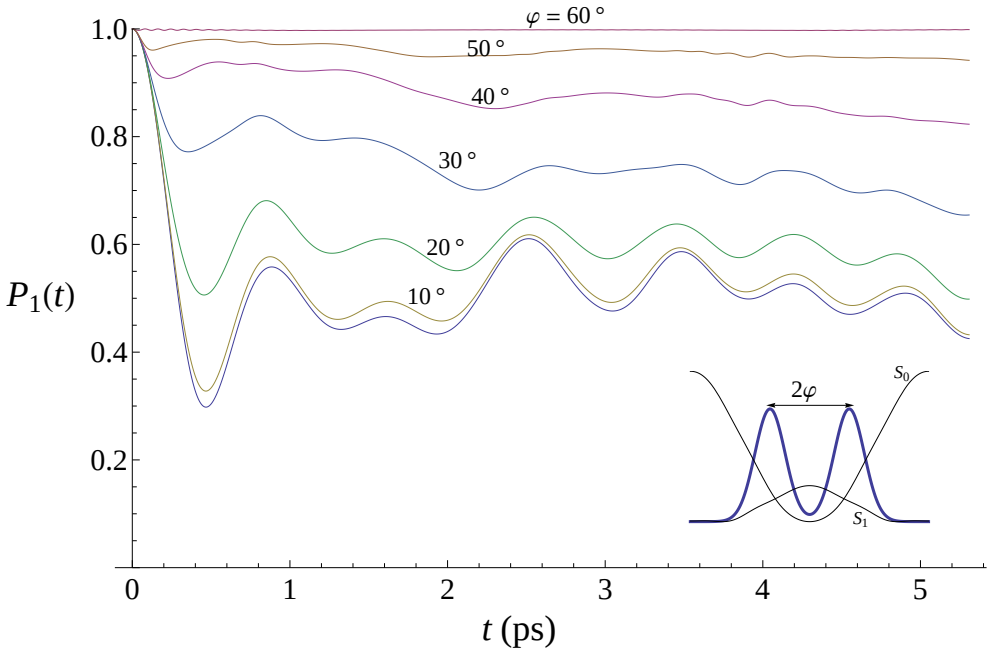

Figure 6.4: Survival probabilities for nuclear wave packets in $(\mathrm{TFMA})_2$ placed on the 1-state potential at $t = 0$. The form of the wave packet in the b-mode is the localized ground state, a Gaussian centered at $\theta_b = 0°$. The a-mode wave packet is the normalized sum of two such Gaussians centered at $\theta_a = \pm\varphi$, for values of φ between $0°$ and $60°$(putting off for now the question of how such a state might be created). The inset shows the amplitude of such an a-mode wave packet superimposed on the potentials for the ground and excited electronic states of the monomer.

B.2. Quantum Chemical Calculations

Electronic structure calculations were performed using the GAUSSIAN09 software package.[4] First the geometry of TFMA was optimized in the ground state using density functional theory (DFT).[5] We used the hybrid functional B3LYP,[6] combined with the 6-31+G(d,p) basis set. This minimum energy geometry, slightly modified, defines the torsional origin, $\theta = 0$. In order that our model potential reflect the physical system, we enforce a three-fold symmetry on the rotational group by setting each C-F bond and F-C-F bond angle equal to the average value in the equilibrium geometry. The imposed change in bond length is smaller than the zero-point oscillation for typical C-F vibrations, in support of this approximation. The torsional angle was then varied between $0°$ and $120°$ in steps of $10°$, holding all other molecular parameters constant. At each point, the S_0 and S_1 energies were found, the latter using time dependant density functional theory (TD-DFT). The torsional angle did not appreciably change the direction or magnitude of the calculated $S_1 \leftarrow S_0$ transition dipole moment.

The energy transfer coupling constant, J, in $(\text{TFMA})_2$ is approximated here by multiplying the spectroscopically derived constant for DTA[7] by the ratio of the squared norms of the transition dipoles for TFMA and anthracene, calculated at the same level of theory. That is,

$$\begin{aligned} J_{(\text{TFMA})_2} =& J_{\text{DTA}} \frac{\boldsymbol{\mu}_{\text{TFMA}} \cdot \boldsymbol{\mu}_{\text{TFMA}}}{\boldsymbol{\mu}_{\text{anth}} \cdot \boldsymbol{\mu}_{\text{anth}}} \\ =& 16.8\,\text{cm}^{-1} \times 0.907 \\ =& 15.2\,\text{cm}^{-1}. \end{aligned} \tag{6.1}$$

We treat TFMA as a one-dimensional system, a rather drastic approximation. It is likely that the rotation of the CF_3 group is coupled to other nuclear modes, in particular there is a 55 cm^{-1} CF_3-rocking mode in the ground state. In Ref. 3, the torsional poten-

tial for 2-methylanthracene was found in a similar manner to that used here, except that at each rotational angle the other degrees of freedom were optimized. They justified this by the fact that the rotational motion is slow compared to other modes. However, the inherently multidimensional nature of these 'relaxed' potentials, in which the other nuclear degrees of freedom respond adiabatically to changes in the torsional coordinate, is outside the scope of this work. The quantum-dynamical calculations presented below include only the torsional motion of the CF_3 group.

B.3. Model Hamiltonian

We model the torsional potentials for the S_0 and S_1 electronic states as

$$V^{(j)}(\theta) = \sum_n \frac{V_n^{(j)}}{2}(1 - \cos n(\theta - \phi_j)) \qquad n = 3, 6, 9.... \tag{6.2}$$

The expansion coefficients up to V_{18} are obtained by a least squares fit to the quantum chemical data, with $\phi_e = 60°$, The S_0 and S_1 potentials are shown in Fig. 6.2, and the results of the least squares fit are given in Table 6.1.

Table 6.1: Potential parameters for the S_0 and S_1 states of TFMA, from Eq. (6.2), obtained via a least-squares fit to the quantum chemical results in units of cm^{-1}.

Term	S_0	S_1
V_3	357.4	84.4
V_6	-18.6	-20.5
V_9	2.3	-2.9
V_{12}	-4.2	-4.0
V_{15}	-2.2	2.6
V_{18}	1.5	1.6

We write the TFMA monomer Hamiltonian as

$$H = |g\rangle\, H_g\, \langle g| + |e\rangle\, H_e\, \langle e|\,. \tag{6.3}$$

The vibrational Hamiltonians for the ground and first-excited electronic states are written as one-dimensional hindered rotors

$$\begin{aligned} H_g &= -\frac{1}{2I}\frac{\partial^2}{\partial\theta^2} + V^{(g)}(\theta_a) \\ H_e &= -\frac{1}{2I}\frac{\partial^2}{\partial\theta^2} + V^{(e)}(\theta_a) + \varepsilon, \end{aligned} \tag{6.4}$$

(we set $\hbar = 1$ throughout). Here I is the moment of inertia for rotation around the C-C single bond, equal to

$$\frac{I_{\mathrm{CF_3}} I_{\mathrm{TFMA}}}{I_{\mathrm{CF_3}} + I_{\mathrm{TFMA}}}.$$

We take $I_{\mathrm{TFMA}} \gg I_{\mathrm{CF_3}}$, and set I equal to $I_{\mathrm{CF_3}} = 97.19\,\mathrm{amu}\,\mathring{\mathrm{A}}^2$. Working in the basis of the free rotor, $|m\rangle$, defined by

$$|\theta\rangle\, \langle\theta|m\rangle = e^{im\theta}(2\pi)^{-1/2} \qquad\qquad -m_{max} \le m \le m_{max}, \tag{6.5}$$

we can easily find the matrix elements for operators by

$$\langle m'|\hat{x}|m\rangle = \int_{-\pi}^{\pi} d\theta e^{i(m-m')\theta}\, \langle\theta|\, \hat{x}\, |\theta\rangle\,. \tag{6.6}$$

In particular the matrix elements for the ground and excited state nuclear Hamiltonians (6.4) are

$$\langle m'|H_g|m\rangle = \frac{m^2}{2I}\delta_{m',m} + \sum_n \frac{V_n^{(g)}}{2}\left(\delta_{m',m} - \frac{1}{2}(\delta_{m',m+n} + \delta_{m',m-n})\right), \tag{6.7}$$

and

$$\langle m'|H_e|m\rangle = \frac{m^2}{2I}\delta_{m',m} + \sum_n \frac{V_n^{(e)}}{2}\left(\delta_{m',m} - \frac{1}{2}(e^{-in\pi/3}\delta_{m',m+n} + e^{in\pi/3}\delta_{m',m-n})\right) + \varepsilon, \tag{6.8}$$

respectively. The monomer eigenstates and eigenenergies of are found by numerically diagonalizing the nuclear Hamiltonians, constructed in this basis, and are defined by

$$\begin{aligned} H_g\,|(n)_g\rangle &= \xi_n^{(g)}\,|(n)_g\rangle \\ H_e\,|(n)_e\rangle &= \xi_n^{(e)}\,|(n)_e\rangle\,. \end{aligned} \tag{6.9}$$

The first seventy eigenergies of the ground and excited electronic states are shown in Table 6.2. The expansion coefficients $\chi_{m,n}^{(j)} \equiv \langle m|(n)_j\rangle$ allow us to cast any operator whose elements can be found by Eq. (6.6) in the energy eigenbasis. The Franck-Condon overlaps between ground and excited nuclear states can now be written as

$$\begin{aligned} \langle(n)_g|(n')_e\rangle &= \sum_{m=-m_{\max}}^{m_{\max}} \left(\chi_{m,n}^{(g)}\right)^* \chi_{m,n'}^{(e)} \\ \langle(n)_e|(n')_g\rangle &= \sum_{m=-m_{\max}}^{m_{\max}} \left(\chi_{m,n}^{(e)}\right)^* \chi_{m,n'}^{(g)}. \end{aligned} \tag{6.10}$$

The dimer Hamiltonian (2.1) is, again, general in form. The nuclear Hamiltonians are

$$\begin{aligned} H_0 &= -\frac{1}{2I}\left(\frac{\partial^2}{\partial\theta_a^2} + \frac{\partial^2}{\partial\theta_b^2}\right) + V^{(g)}(\theta_a) + V^{(g)}(\theta_b) \\ H_1 &= -\frac{1}{2I}\left(\frac{\partial^2}{\partial\theta_a^2} + \frac{\partial^2}{\partial\theta_b^2}\right) + V^{(e)}(\theta_a) + V^{(g)}(\theta_b) + \varepsilon_1 \\ H_{1'} &= -\frac{1}{2I}\left(\frac{\partial^2}{\partial\theta_a^2} + \frac{\partial^2}{\partial\theta_b^2}\right) + V^{(g)}(\theta_a) + V^{(e)}(\theta_b) + \varepsilon_{1'} \\ H_2 &= -\frac{1}{2I}\left(\frac{\partial^2}{\partial\theta_a^2} + \frac{\partial^2}{\partial\theta_b^2}\right) + V^{(e)}(\theta_a) + V^{(e)}(\theta_b) + \varepsilon_2\,. \end{aligned} \tag{6.11}$$

Table 6.2: The first seventy nuclear eigenenergies for the S_0 and S_1 states of $(\mathrm{TFMA})_2$, in units of cm^{-1}. Due to the symmetry of the system, the nuclear states are three-fold degenerate (or nearly so) for energies below the potential barriers.

n	$\xi_n^{(g)}$	$\xi_n^{(e)} - \varepsilon$	n	$\xi_n^{(g)}$	$\xi_n^{(e)} - \varepsilon$
1	9.84	1.52	36	229.82	92.48
2	9.84	1.52	37	247.42	93.60
3	9.84	1.52	38	247.42	98.85
4	29.84	6.01	39	247.42	98.85
5	29.84	6.01	40	264.63	105.17
6	29.84	6.01	41	264.63	105.17
7	50.44	13.82	42	264.63	111.93
8	50.44	13.82	43	281.42	112.00
9	50.44	13.82	44	281.42	119.19
10	71.45	23.36	45	281.42	119.19
11	71.45	23.36	46	297.75	126.84
12	71.45	23.36	47	297.75	126.84
13	92.59	32.81	48	297.76	134.88
14	92.59	32.81	49	313.47	134.88
15	92.59	32.81	50	313.49	143.32
16	113.61	42.05	51	313.49	143.32
17	113.61	42.05	52	328.34	152.13
18	113.61	42.05	53	328.34	152.13
19	134.31	50.72	54	328.58	161.33
20	134.31	50.73	55	341.61	161.33
21	134.31	50.73	56	342.46	170.90
22	154.54	58.98	57	342.46	170.90
23	154.54	58.98	58	353.14	180.83
24	154.54	59.02	59	353.14	180.83
25	174.21	66.96	60	356.65	191.14
26	174.21	67.15	61	361.53	191.14
27	174.21	67.15	62	366.90	201.81
28	193.28	74.66	63	366.90	201.81
29	193.28	74.66	64	375.39	212.85
30	193.28	75.45	65	375.39	212.85
31	211.80	80.89	66	385.17	224.24
32	211.80	82.80	67	385.47	224.24
33	211.80	82.80	68	395.20	236.00
34	229.82	88.06	69	395.20	236.00
35	229.82	88.06	70	405.72	248.12

As in Chapters III – V, we perform dimer calculations using the eigenbasis of the uncoupled ($J = 0$) Hamiltonian; $|n\rangle\,|(\nu_a\nu_b)_n\rangle$ denotes the state in which the electronic degrees of freedom are in state n , while the vibrations are in an eigenstate of H_n with ν_a and ν_b quanta in the donor and acceptor, respectively. The basis is truncated beyond states having more than a certain total number of vibrational quanta. Setting this energetic cutoff at 101 total vibrational quanta results in 5,050 vibrational states per electronic state. As before, the system is propagated in time by projecting onto the global eigenstates of H, by*

$$[t] \equiv e^{-i\,H\,t} = \sum_k |\Psi_k\rangle\, e^{-i\,E_k\,t}\, \langle\Psi_k| \,. \tag{6.12}$$

This introduces an effective limit to the basis size, as we must diagonalize the Hamiltonian in the one-exciton manifold, an inherently memory-intensive calculation.

Armed with the eigenenergies and Franck-Condon overlaps for the TFMA monomer, Eqs. (6.9) and (6.10), we can easily find the matrix elements of the first- and second-order pulse propagators by direct substitution into Eqs. (3.5) and (3.7). The resulting expressions are

$$\begin{aligned}\left\langle (\nu_a,\nu_b)_1 \left| p_I^{(10)}(\infty)\, |(\bar\nu_a,\bar\nu_b)_0 \right\rangle =& i\sqrt{\frac{\pi}{2}} E_I m \sigma_I \left\langle (\nu_a)_e \left| (\bar\nu_a)_g \right\rangle \delta_{\nu_b,\bar\nu_b} \right. \\ & \times \exp\left\{ -\frac{\sigma_I^2}{2}\left(\Omega_I + \xi_{\bar\nu_a}^{(g)} - \xi_{\nu_a}^{(e)}\right)^2 \right\} \quad ,\end{aligned} \tag{6.13}$$

and

$$\begin{aligned}&\left\langle (\nu_a,\nu_b)_0 \left| p_I^{(01)}(\infty;\, t_2) p_I^{(10)}(t_2;\, t_1)\, |(\bar\nu_a,\bar\nu_b)_0 \right\rangle \right. \\ &\qquad = -\frac{\pi}{4}\sigma_I^2 E_I^2 m^2 \delta_{\nu_b,\bar\nu_b} \sum_{\bar{\bar\nu}_a} \langle (\nu_a)_g|\, (\,\bar{\bar\nu}_a)_e\rangle\, \langle (\,\bar{\bar\nu}_a)_e|\, (\,\bar\nu_a)_g\rangle \\ &\qquad\quad \times \exp\left(-\frac{1}{2}\sigma^2 \left(\Delta_1^2 + \Delta_2^2\right)\right) \left[1 + \mathrm{erf}\left(i\sigma \frac{\Delta_1 + \Delta_2}{2} \right) \right],\end{aligned} \tag{6.14}$$

*Here $|\Psi_j\rangle$ is an eigenket of H with energy E_j.

where

$$\Delta_1 = \Omega_I + \xi_{\nu_a}^{(g)} - \xi_{\bar{\nu}_a}^{(e)} \tag{6.15}$$

and

$$\Delta_2 = \Omega_I + \xi_{\bar{\nu}_a}^{(g)} - \xi_{\bar{\nu}_a}^{(e)} \tag{6.16}$$

are the effective resonance offsets for the downward and upward transitions, respectively.

C. Results and Discussion

C.1. Energy Transfer Dynamics in $(\mathrm{TFMA})_2$.

Nuclear dynamics in TFMA is quite slow. The S_0 potential is nearly harmonic near the origin, with an effective frequency $\omega/2\pi c = 20.0$ cm^{-1} (corresponding to a librational period of 1.67 ps). The RMS width of the ground-state wave function is found to be $5.5°$, (which makes $\delta = 5.4$, placing $(\mathrm{TFMA})_2$ clearly in the large-displacement regime). In the excited state, near the origin the dynamics occur even more slowly. The classical round-trip time for a particle placed on the S_1 potential at $\theta = 7.7°$* is 4.4 ps. Therefore, for vertical excitation, we expect to see back-and-forth EET in the survival probability before the wave packet has entirely left the Franck-Condon region.

As in Chapters III and V, the control pulse is chosen through a numerical search over pulse duration and center frequency subject to the constraint that the squared norm of the first-order wave packet in the excited electronic state be less than 5% the size of the norm of the second-order wave packet. The transform-limited pulse that creates the most energetic second-order wave packet has a duration $\sigma_P = 183$ fs, and a center frequency 83.5 cm^{-1} below vertical resonance. The second-order ground-state wave packet created by the control

*$\theta = 7.7°$ is the classical turning point for a particle in the ground state possessing energy equal to the zero-point energy in that state, $\xi_1^{(g)} = 9.8\,\mathrm{cm}^{-1}$.

pulse is more energetic than the zeroth order wave packet by 29%. The RMS width of the second-order wave packet oscillates between $3.8°$ and $7.6°$. Fig. 6.5 shows the control pulse wave packet, $|\{p(01)p(10)\}_0\rangle$, for the two different values of t_{AP} that correspond to maximal and minimal extension. The ground-state wave function is shown for comparison.

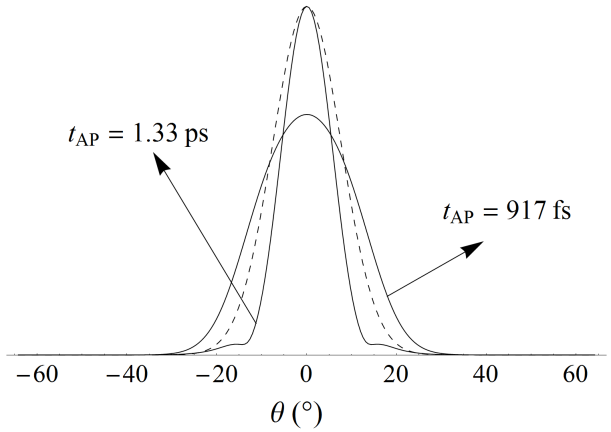

Figure 6.5: Wave packet amplitude for $|\{p(01)p(10)\}_0\rangle$, at $t = t_A$ for two values of the control pulse delay time t_{AP} (solid traces). Shown for reference is the amplitude of the librational ground state, scaled down(dashed trace). The values of t_{AP} shown here correspond to the maximum and minimum values of θ_{RMS}, i.e. at $t_{AP} = 917$fs $(1.33$ps$)$ the wave packet is at its widest (most compact).

In Fig. 6.6, we show the survival probability for $|\{a(10)p(01)p(10)\}_1\rangle$ as a function of the for many different values of t_{AP}. Also shown in the thick blue trace is the survival probability for $|\{a(10)\}_1\rangle$, as a comparison. In these, and all subsequent calculations, the system is assumed oriented with the donor transition dipole along the lab-frame H axis and the acceptor dipole along the lab-frame V axis. The A pulse has a duration of $\sigma_A = 147$ fs, and is resonant at $\theta_a = \pm 7.4°$ (i.e. it is resonant at the classical outer turning point for a particle possessing the zero-point energy).

We can see in Fig. 6.6 that there is considerable population loss, and back-transfer within the first picosecond after electronic excitation in all cases. Subsequent population oscillations, however, are much less complete than the first. We can also see from Fig. 6.6

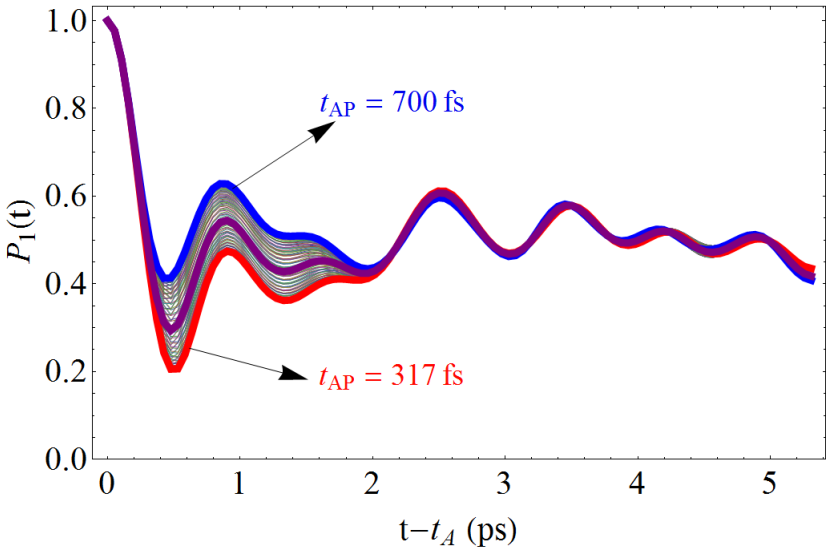

Figure 6.6: Survival probabilities for nuclear wave packets in an oriented $(\mathrm{TFMA})_2$ dimer excited to the 1-state potential at t_A. The form of the wave packet in the b-mode is the localized ground state, a Gaussian centered at $\theta_b = 0°$. The a-mode wave packet prior to the arrival of the A pulse is either the librational ground state (thick purple trace) or $|\{p(01)p(10)\}_0\rangle$ for values of the control pulse delay time t_{AP} spanning one ground-state librational period (multi-colored traces). Some degree of control over population transfer is evident for short times following resonant excitation, however after 2 ps this difference is gone as the wave packets spread out over the entire two-dimensional space (θ_a, θ_b). The red and blue trace indicates the survival probability when EET is the most enhanced or diminished, respectively, relative to vertical excitation.

that a deal of control is achieved by the addition of a control pulse, and that this control is only significant for the first couple of electronic oscillation cycles. After this point, the survival probability in the presence of the control pulse is nearly indistinguishable from that in the absence of the control pulse.

Fig. 6.7 shows a contour plot of the survival probability for the control-pulse induced wave packet ($|\{a(10)p(01)p(10)\}_1\rangle$) as a function of t_{AP}, alongside a plot of the RMS width of this same wave packet in the ground-state prior to electronic excitation($|\{p(01)p(10)\}_0\rangle$). From this figure, we can see that the greatest change in the survival probability, enhancing *or* diminishing EET, comes when the RMS width is at its mean value (at 317 and 700 fs)- not when it is at a maximum or minimum as expected (at 917 fs and 1.33 ps). This is in contrast to the case of DTA-12, where the greatest degree of control happened at the turning points for nuclear motion.

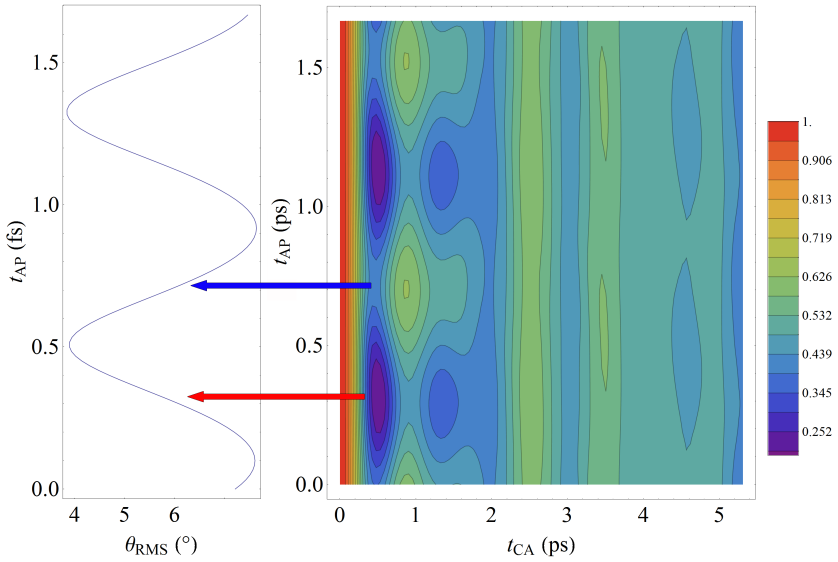

Figure 6.7: Left panel: θ_{RMS} for the control-pulse induced ground state wave packet as a function of t_{AP}. Right panel: Survival probabilities from Fig. 6.6 presented as a contour plot. Here we see that the maximum enhancement (diminishment) of energy transfer occurs not when θ_{RMS} is at its minimum (maximum) value, but when it is moving towards that point.

In the cycle of contraction and expansion of $|\{p(01)p(10)\}_0\rangle$ depicted in Fig. 6.5, the ideal time to excite to the 1 state, if the goal is to diminish short time EET, is when the wave packet resembles the ground-state and is expanding. The resulting excited-state wave packet, $|\{a(10)p(01)p(10)\}_1\rangle$, takes less time to leave the Franck-Condon point in this case. If the goal is to enhance short-time EET, ideal time to excite is when the wave packet resembles the ground-state and is contracting as this increases the amount of time it takes to leave the area around the potential intersection.

C.2. Pump-Probe Signals

Here we present pump-probe and pump-probe difference signals from $(\mathrm{TFMA})_2$. As shown in Chapter IV, a lack of proportionality between the two can be taken as evidence for the vibrational control over EET. The control and pump pulses are as described above, i.e. the control pulse is H polarized and has a duration of $\sigma_P = 183$ fs, and a center frequency 83.5 cm^{-1} below vertical resonance. The pump pulse is H polarized, $\sigma_A = 147$ fs, and is resonant at $\theta_a = \pm 7.4^\circ$ The probe pulse is significantly shorter, $\sigma_C = 24.2$ fs, and resonant with the $e \rightarrow g$ transition in TFMA at the bottom of the excited state potential.

Fig. 6.8 shows the stimulated-emission (SE) contribution to the HH and HV polarized pump-probe signals from an oriented $(\mathrm{TFMA})_2$ complex, which are proportional to the real parts of $\langle\{b(10)\}_1|\{d(10)c(01)a(10)\}_1\rangle$ and $\langle\{b(10)\}_{1'}|\{d(1'0)c(01')a(10)\}_{1'}\rangle$, respectively. The SE contribution can be isolated by monitoring the time-resolved fluorescence following A pulse excitation, and the C pulse acts as the gate pulse in this case. The HH signal is largely proportional to the survival probability (with a negative constant of proportionality), while the HV signal is proportional to one minus the survival probability. In our previous pump-probe difference studies on DTA-12, the time-scales for nuclear and electronic motion were well separated, and clearly discernable in the signals. The vibrational-period beats of Fig.

3.5, for example, are due to nuclear motion while the longer period oscillations are due to EET. In $(\mathrm{TFMA})_2$, as opposed to DTA-12, the nuclear and electronic motions happen on similar time-scales and are highly coupled, i.e. EET *only* happens when nuclear amplitude is near the intersection regions. In Fig. 6.9, we show the SE component to the pump-probe

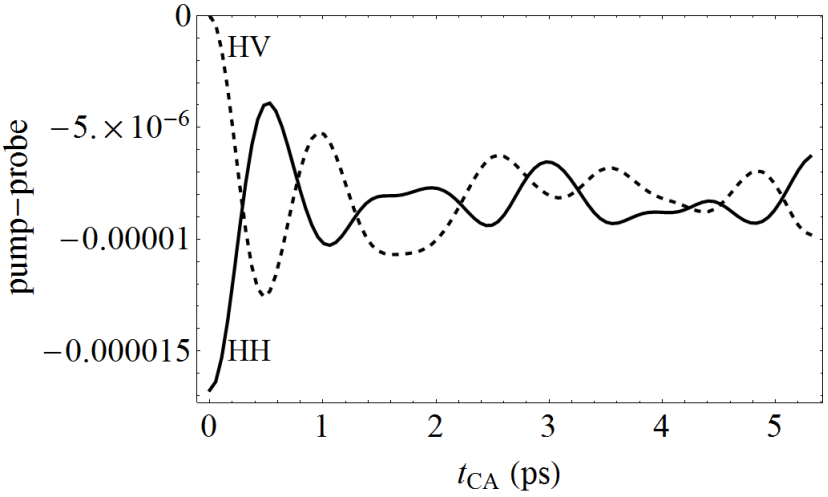

Figure 6.8: Stimulated emission contributions to the HH (solid trace) and HV (dashed trace) polarized pump-probe signals from oriented $(\mathrm{TFMA})_2$ dimers. The HH signal is roughly proportional to the survival probability in the absence of the control pulse, shown as the blue trace in Fig. 6.6 (the proportionality constant contains i^2), while the HV signal monitors the acceptor-excited population and is roughly proportional to one minus the survival probability.

difference signals (from an oriented complex) for the HHH and HHV polarizations. The HHH and HHV signals are proportional to the real parts of

$$\begin{aligned}\langle\{b(10)p(01)p(10)\}_1|\{d(10)c(01)a(10)\}_1\rangle \\ + \langle\{b(10)\}_1|\{d(10)c(01)a(10)p(01)p(10)\}_1\rangle\end{aligned} \tag{6.17}$$

and

$$\begin{aligned}\langle\{b(10)p(01)p(10)\}_{1'}|\{d(1'0)c(01')a(10)\}_{1'}\rangle \\ + \langle\{b(10)\}_{1'}|\{d(1'0)c(01')a(10)p(01)p(10)\}_{1'}\rangle\end{aligned} \tag{6.18}$$

respectively. As in DTA-12, there is significant variation in the shape of the signals as a function of t_{AP}, which we take as evidence of the vibrational control over EET in $(\mathrm{TFMA})_2$. The maximum and minimum in the HHH signal roughly corresponds to the values of t_{AP} that lead to the greatest change in the survival probability, as indicated by the red and blue arrows (the red arrow is at $t_{AP} = 317$ fs when EET is enhanced, while the blue arrow is at $t_{AP} = 700$ fs when EET is diminished). The HHV signal, however, has its maximum (minimum) values for those t_{AP} which give a maximum (minimum) RMS width in the ground-state wave packet. In Fig. 6.10 we show the HHH signals from Fig. 6.9 for $t_{AP} = 317$ fs and 700 fs. There is a discernable difference in the shape of these signals, as well as between these signals and the HH signal in Fig. 6.8. The bottom panel of Fig. 6.10 shows the same plots, only they have been divided by their initial value to more clearly show their different shapes. Note that the directionality of the control at these control delay times which was evident in the survival probabilities of Fig. 6.6 is not clear in the pump-probe difference signals. In fact, the apparent change in control direction evident in these signals is the reverse from what is seen in the survival probabilities. The blue trace in the bottom panel of Fig. 6.10 (corresponding to $t_{AP} = 700fs$) appears to show more EET than the red trace of that same figure (corresponding to $t_{AP} = 317fs$), while the reverse is evidently true in Fig. 6.6. We must remember that the pump-probe difference signal is sensitive to the local interference, within the of probe resonance window, between wave packets that are zeroth and second-order in the control pulse field, and is therefore inherently more complicated than the survival probabilities.

In Fig. 6.11 we show the HHV signals from Fig. 6.9 for $t_{AP} = 317$ fs and 700 fs. Again, we note a discernable difference in the shape of these signals, as well as the fact that they are both visibly different from the HV signal of Fig. 6.8 which can be taken as direct evidence of the vibrational control over EET.

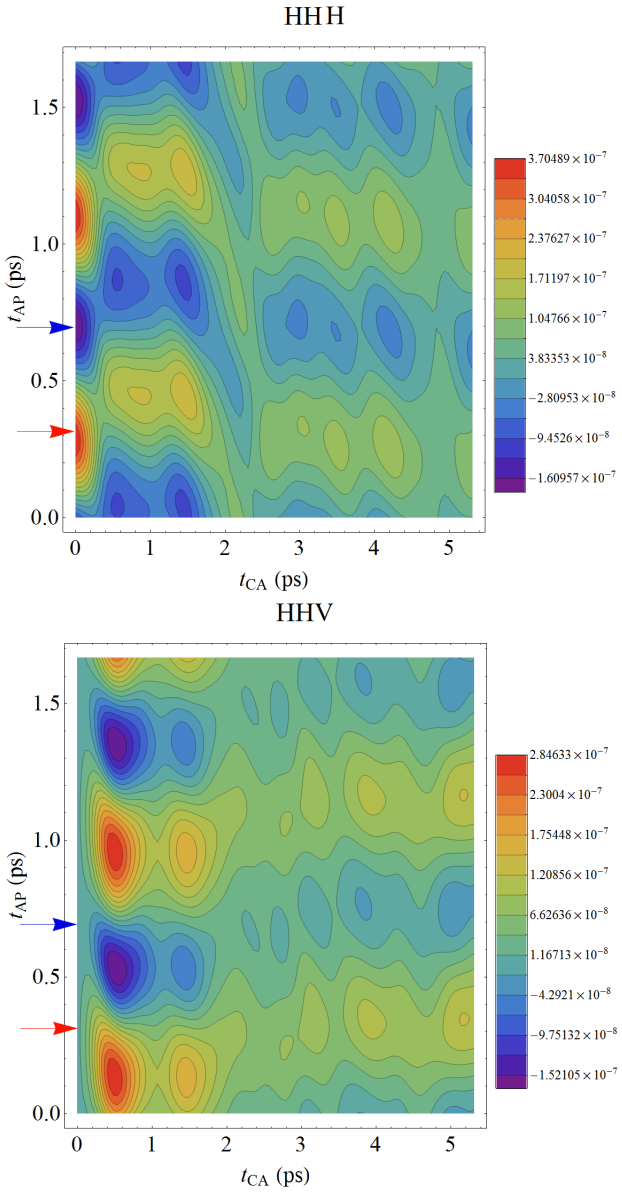

Figure 6.9: Stimulated emission contributions to the HHH (top) and HHV (bottom) polarized pump-probe signals from oriented $(TFMA)_2$ dimers, as a function of the control-pulse delay time. As in Chapter V, the presence of signal variation along the vertical axis here is taken to be evidence of the influence of externally-induced vibrational motion on subsequent EET.

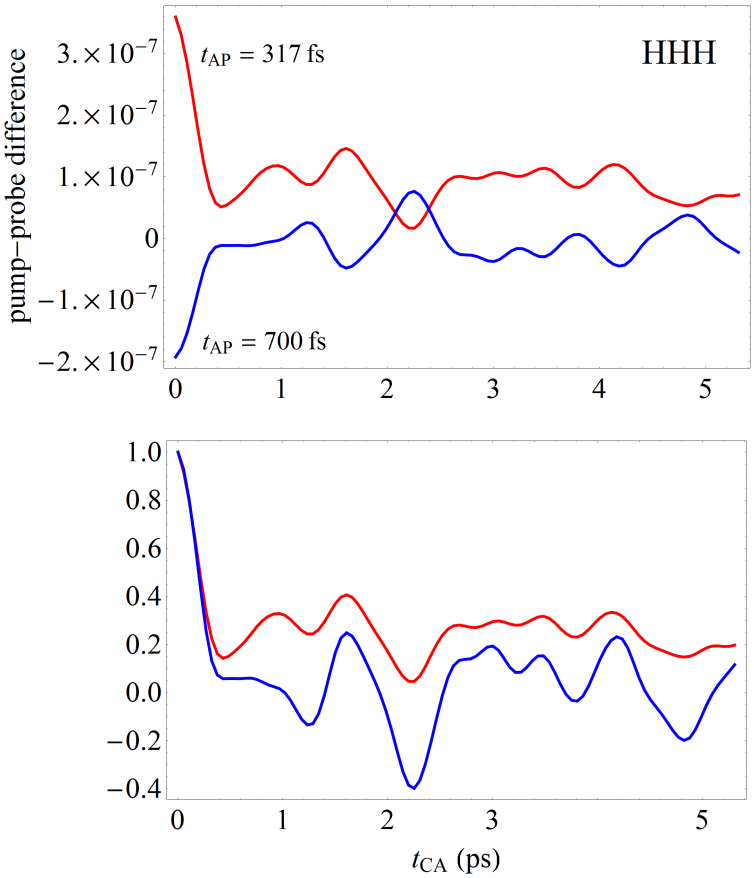

Figure 6.10: Stimulated emission contributions to the HHH polarized pump-probe difference signals from oriented $(TFMA)_2$ dimers, for two different values of t_{AP}. From the survival probabilities shown in Figs. 6.6 and 6.7 we know that when t_{AP} is equal to 317 ps (700 ps), short-time EET is enhanced (diminished). The HHH pump-probe difference signals at these control-pulse delays are discernably disproportional to the HH pump-probe signal shown in Fig. 6.8. The lower panel shows the HHH signals from the top panel, divided by their initial value, to highlight their differences.

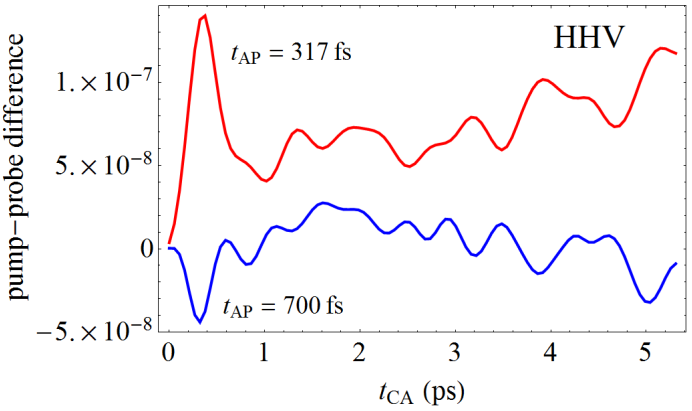

Figure 6.11: Stimulated emission contributions to the HHV polarized pump-probe difference signals from oriented $(TFMA)_2$ dimers, for two different values of t_{AP}. From the survival probabilities shown in Figs. 6.6 and 6.7 we know that when t_{AP} is equal to 317 ps (700 ps), short-time EET is enhanced (diminished). The HHV pump-probe difference signals at these control-pulse delays are discernably disproportional to the HV pump-probe signal shown in the Fig. 6.8.

D. Discussion and Future Prospects

In this chapter, we have presented a model dimer system, $(TFMA)_2$, where each monomer features a three-fold symmetric rotational group whose periodic nuclear potential undergoes significant change in shape as well as a 60° phase shift upon electronic excitation. We used DFT calculations to find the torsional potentials for the ground and first-excited states of the monomer, TFMA, which we used to create a dimer Hamiltonian. We explore the relationship between nuclear motion and energy transfer in $(TFMA)_2$, and show that it is remarkably dissimilar to that in DTA-12.

We have presented a modified version of our control strategy, and shown how externally induced nuclear motion can, in principle, drastically alter the time-course and overall extent of energy transfer. We used ISRS to generate a non-stationary wave packet in the ground state of $(TFMA)_2$, and showed how this nuclear motion influences short-time EET but that this alteration is transient in time. We presented calculated pump-probe and pump-probe difference stimulated emission signals, as could be collected using a fluorescence upconver-

sion process. As evidence for the vibrational control over EET, we point to the lack of strict proportionality between pump-probe and pump-probe difference signals.

In Chapter V we explored the use of a linearly chirped control pulse to increase the extent of vibrational motion in DTA-12. We are currently investigating whether this is worthwhile in $(\mathrm{TFMA})_2$, though it is not immediately clear that this is the case. The arguments for using a negative linear chirp for harmonic systems, namely that the difference potential is also linear in those systems with a negative slope, does not apply to the periodic potential under consideration here, where the difference potential has no slope at the Franck-Condon point and grows in in a nonlinear fashion in that region. The addition of a linear frequency was effective at increasing the total energy of the second-order ground-state wave packet, however. The effect of chirp on the ground-state was to give portions of that wave packet significant momentum, enough to surmount the potential barriers in the ground state. Fig. 6.12 shows the effects of introducing a linear frequency chirp to the control pulse in $(\mathrm{TFMA})_2$. The control pulse in this case has a duration and chirp rate of $\sigma_P = 34.2$ fs, and $\alpha_P = 16.0\mathrm{fs}^2$, and has a frequency 356 cm^{-1} below vertical resonance. This control pulse creates a ground state wave packet with portions that have significant momentum in both the positive and negative directions, and if the A pulse arrives 1.02 ps later (and has been redshifted in frequency so as to be resonant at the excited-state minimum), the survival probability is greatly affected. However, the portion of the second-order wave packet that gets excited to the upper state potential, and can contribute to the signal, is small compared to the full second-order wave packet. Furthermore, the A pulse in this case would be unable to excite the ground-state wave packet due to a frequency mismatch, and therefore the highly-energetic second-order wave packet will not contribute significantly to a pump-probe measurement. We are, however, pursuing whether such wave packets can contribute to wave-packet interferometry signals from $(\mathrm{TFMA})_2$.

In this dissertation, we have put forth a method by which nuclear motion can ef-

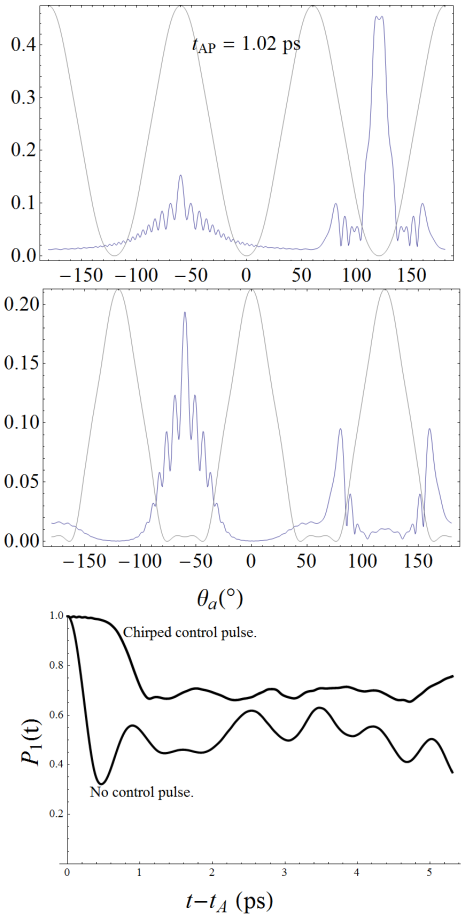

Figure 6.12: Ground and excited state wave packets in TFMA resulting from chirped-pulse excitation. (Top panel) Superposed on top of the ground state torsional potential is the amplitude of the a-mode nuclear wave packet second-order in the control pulse field. The chirped control pulse creates two high-energy sub- wave packets which propagate in opposite directions from the origin (here taken to be at $\theta_a = 120°$ for clarity). These smaller wave packets meet 1.02 ps after the control pulse has passed at $\theta_a = -60°$, i.e. in the region corresponding to an excited-state minimum. At this point the A pulse, whose center frequency has been shifted to be resonant at $\theta_a = -60°$, arrives. The middle panel shows the amplitude of the resulting excited state wave packet in the a-mode, at the arrival time of the A pulse, superposed on top of the S_1 potential. Once excited to the 1-state, the wave packet does not remain trapped in the upper-state potential as it still possesses significant momentum. It is not until nearly a picosecond after excitation that the wave packet comes into contact with the potential intersection and EET commences, as is evident from the survival probabilities in the lower panel.

fect the time-course of EET in molecular dimers. By changing the excited-state wave-packet trajectory, we can increase or decrease the probability amplitude near the intersection of 1 and 1′ potential surfaces. In Chapter II, we derived the expressions needed to simulate md-WPI signals following a pre-resonant control pulse, using a pulse-propagator formalism. In this way we take advantage of the brevity of ultrashort pulses to focus on the dynamical aspects of the molecular processes under consideration, rendering the field-matter interactions as arrival-time independent operators. The signal contributions are calculated straightforwardly as products of pulse propagators and time-evolution operators, the order of which is indicated by our intuitive notation.

We have presented calculated signals from a variety of model systems. In this Chapter and Subsections B.1 and B.3 of Chapter III, we look at models featuring strong coupling between electronic and vibrational degrees of freedom. Under this condition coherent nuclear motion has the potential to dramatically reduce short-time EET, as indicated by Figs. 2.1 and 6.4. Although we do not achieve these optimal results using a pre-resonant transform-limited control pulse, we can still exert a significant degree of control over short-time EET, see Figs. 3.1 and 6.6. In Chapter V and Subsection B.2 of Chapter III we look at a model system with weak electron-vibration coupling, and find that EET can be diminished or enhanced by ground-state nuclear motion, depending on the phase of the motion at the arrival time of the electronically resonant control pulse. We see that including a linear chirp in the control pulse increases the range of ground state motion induced by the control pulse in DTA-12. We also show that there are interesting differences in this phase-dependence depending on whether the donor or acceptor was vibrationally perturbed.

In Chapters III, V, and VI we present calculated pump-probe difference signals, taken as the limiting case of a md-WPI signal where intrapair delays are set equal to zero. We point to the lack of direct proportionality between pump-probe and pump-probe difference signals as experimentally verifiable evidence of the vibrational control over EET, an assumption which

is verified in Chapter IV. In Chapter V we present md-WPI difference signals for DTA-12, and see interesting differences between these and the corresponding signals without control pulse.

In these investigations, we have limited the search for an effective control pulse to transform-limited and linearly chirped pulses. Recent advances in ultrafast pulse-shaping and characterization have greatly impacted the field of coherent optical control.[8] Using a variational approach,[9,10] one could find, theoretically, the specifically tailored control pulse that creates a ground-state wave packet that maximizes some fitness parameter while minimizing electronic absorption. That fitness parameter could involve the overlap with some target state, so as to realize the "ideal control" case from Figs. 2.1 and 6.4, or, more directly, the donor-excited survival probability at some specified time after resonant excitation.

Notes

[1] D. W. Werst, A. M. Brearley, W. R. Gentry, and P. F. Barbara, Journal of the American Chemical Society **109**, 32 (1987).

[2] H. Lin, J. A. Hunter, and J. Pfab, Chemical Physics Letters **210**, 38 (1993).

[3] M. Nakagaki et al., Chemical Physics **316**, 178 (2005).

[4] M. J. Frisch et al., Gaussian 09 Revision A.2, Gaussian Inc. Wallingford CT 2009.

[5] R. G. Parr and W. Yang, *Density-Functional Theory of Atoms and Molecules in Chemistry*, Springer, New York, 1991.

[6] A. D. Becke, Journal of Chemical Physics **98**, 5648 (1993).

[7] I. Yamazaki, S. Akimoto, T. Yamazaki, S. Sato, and Y. Sakata, Journal of Physical Chemistry A **106**, 2122 (2002).

[8] S. A. Rice and M. Zhao, *Optical Control of Molecular Dynamics*, John Wiley and Sons, New York, 2000.

[9] Y. Ohtsuki, H. Kono, and Y. Fujimura, The Journal of Chemical Physics **109**, 9318 (1998).

[10] J. Werschnik and E. K. U. Gross, Journal of Physics B: Atomic Molecular and Optical Physics **40**, R175 (2007).

APPENDIX A

ORIENTATIONAL AVERAGING

If the experiment is performed on a sample in solution, then we must average the direction cosine terms like $e_A e_B e_C e_D {e_P}^2$ to account for this isotropic distribution. While the ideal system to demonstrate our control mechanism will have perpendicular transition dipole moments, any system whose chromophores are held rigidly and non-parallel should the effect of control. Our signal expression is for the total fluorescence from the one exciton manifold, and is therefore insensitive to molecular rotations following the last acting pulse.

We model the system as two transition dipoles whose relative orientation is fixed while the absolute orientation of the system is random. Setting the inter-chromophore angle as a, we define the molecular dipoles in the the lab frame (*X,Y,Z*) in terms of the azimuthal angle ψ, polar angle θ, and azimuthal angle ϕ.

$$\begin{aligned} \boldsymbol{m} &= m\boldsymbol{R}_Z(\phi)\boldsymbol{R}_Y(\theta)\boldsymbol{R}_Z(\psi)\hat{\boldsymbol{Z}} \\ \boldsymbol{m}' &= m'\boldsymbol{R}_Z(\phi)\boldsymbol{R}_Y(\theta)\boldsymbol{R}_Z(\psi)\boldsymbol{R}_Y(\alpha)\hat{\boldsymbol{Z}} \end{aligned} \tag{A.1}$$

While the number of possible polarization schemes is large, we restrict this treatment to three possible polarization schemes. In order for the non-resonant pump pulse to control EET most efficiently it should excite coherent motion on the chromophore on the chromophore that is *not* electronically excited by the first pulse-pair (A and B), thus setting $\boldsymbol{e}_P$ perpendicular to $\boldsymbol{e}_A$ and $\boldsymbol{e}_B$. We now consider the cases where the second pulse-pair (C and

D) is polarized either parallel (VHH) or perpendicular (VHV) to the first pulse-pair. We also consider the case where all pulses are polarized parallel to each other, denoted as HHH. Defining the orientational average as

$$\langle F \rangle = \frac{1}{8\pi^2} \int_0^{2\pi} d\varphi \int_0^{\pi} \sin\theta d\theta \int_0^{2\pi} d\psi F \,, \tag{A.2}$$

we can obtain values for the direction cosine terms parameterized by the inter-chromophore angle α.

Table A.1: Orientationally averaged direction cosine terms for VHH polarization.

Term	Value
$\langle e_A e_B e_C e_D {e_P}^2 \rangle$,$\langle e'_A e'_B e'_C e'_D {e'_P}^2 \rangle$	$1/35$
$\langle e'_A e_B e_C e_D {e_P}^2 \rangle$,$\langle e_A e'_B e_C e_D {e_P}^2 \rangle$ $\langle e_A e_B e'_C e_D {e_P}^2 \rangle$,$\langle e_A e_B e_C e'_D {e_P}^2 \rangle$ $\langle e'_A e'_B e'_C e_D {e'_P}^2 \rangle$,$\langle e'_A e_B e'_C e'_D {e'_P}^2 \rangle$ $\langle e'_A e'_B e_C e'_D {e'_P}^2 \rangle$,$\langle e_A e'_B e'_C e'_D {e'_P}^2 \rangle$	$(\cos\alpha)/35$
$\langle e'_A e'_B e_C e_D {e_P}^2 \rangle$,$\langle e'_A e_B e'_C e_D {e_P}^2 \rangle$ $\langle e'_A e_B e_C e'_D {e_P}^2 \rangle$,$\langle e_A e'_B e'_C e_D {e_P}^2 \rangle$ $\langle e_A e_B e'_C e'_D {e_P}^2 \rangle$,$\langle e_A e'_B e_C e'_D {e_P}^2 \rangle$ $\langle e'_A e'_B e_C e_D {e'_P}^2 \rangle$,$\langle e'_A e_B e'_C e_D {e'_P}^2 \rangle$ $\langle e'_A e_B e_C e'_D {e'_P}^2 \rangle$,$\langle e_A e'_B e'_C e_D {e'_P}^2 \rangle$ $\langle e_A e_B e'_C e'_D {e'_P}^2 \rangle$,$\langle e_A e'_B e_C e'_D {e'_P}^2 \rangle$	$(5+\cos 2\alpha)/210$
$\langle e'_A e'_B e'_C e_D {e_P}^2 \rangle$, $\langle e'_A e_B e'_C e'_D {e_P}^2 \rangle$ $\langle e'_A e'_B e_C e'_D {e_P}^2 \rangle$,$\langle e_A e'_B e'_C e'_D {e_P}^2 \rangle$ $\langle e'_A e_B e_C e_D {e'_P}^2 \rangle$,$\langle e_A e'_B e_C e_D {e'_P}^2 \rangle$ $\langle e_A e_B e'_C e_D {e'_P}^2 \rangle$,$\langle e_A e_B e_C e'_D {e'_P}^2 \rangle$	$(5\cos\alpha - \cos 3\alpha)/140$
$\langle e'_A e'_B e'_C e'_D {e_P}^2 \rangle$,$\langle e_A e_B e_C e_D {e'_P}^2 \rangle$	$(2-\cos 2\alpha)/35$

Table A.2: Orientationally averaged direction cosine terms for VHV polarization.

Term	Parallel Probing
$\langle e_A e_B e_C e_D {e_P}^2\rangle$,$\langle e'_A e'_B e'_C e'_D {e'_P}^2\rangle$	$1/35$
$\langle e'_A e'_B e_C e_D {e_P}^2\rangle$,$\langle e_A e'_B e_C e_D {e_P}^2\rangle$ $\langle e_A e_B e'_C e_D {e_P}^2\rangle$,$\langle e_A e_B e_C e'_D {e_P}^2\rangle$ $\langle e'_A e'_B e'_C e_D {e'_P}^2\rangle$,$\langle e'_A e_B e'_C e'_D {e'_P}^2\rangle$ $\langle e'_A e'_B e_C e'_D {e'_P}^2\rangle$,$\langle e_A e'_B e'_C e'_D {e'_P}^2\rangle$	$(\cos\alpha)/35$
$\langle e'_A e'_B e_C e_D {e_P}^2\rangle$,$\langle e_A e_B e'_C e'_D {e'_P}^2\rangle$	$(2-\cos 2\alpha)/35$
$\langle e'_A e_B e'_C e_D {e_P}^2\rangle$,$\langle e'_A e_B e_C e'_D {e_P}^2\rangle$ $\langle e_A e'_B e'_C e_D {e_P}^2\rangle$,$\langle e_A e'_B e_C e'_D {e_P}^2\rangle$ $\langle e'_A e_B e'_C e_D {e'_P}^2\rangle$,$\langle e'_A e_B e_C e'_D {e'_P}^2\rangle$ $\langle e_A e'_B e'_C e_D {e'_P}^2\rangle$,$\langle e_A e'_B e_C e'_D {e'_P}^2\rangle$	$(1+3\cos 2\alpha)/140$
$\langle e'_A e'_B e'_C e_D {e_P}^2\rangle$,$\langle e'_A e'_B e_C e'_D {e_P}^2\rangle$ $\langle e_A e_B e'_C e_D {e'_P}^2\rangle$,$\langle e_A e_B e_C e'_D {e'_P}^2\rangle$	$(5\cos\alpha-\cos 3\alpha)/140$
$\langle e'_A e_B e'_C e'_D {e_P}^2\rangle$, $\langle e_A e'_B e'_C e'_D {e_P}^2\rangle$ $\langle e'_A e_B e_C e_D {e'_P}^2\rangle$,$\langle e_A e'_B e_C e_D {e'_P}^2\rangle$	$(2\cos\alpha+\cos 3\alpha)/105$
$\langle e'_A e'_B e'_C e'_D {e_P}^2\rangle$,$\langle e_A e_B e'_C e'_D {e_P}^2\rangle$ $\langle e_A e_B e_C e_D {e'_P}^2\rangle$,$\langle e'_A e'_B e_C e_D {e'_P}^2\rangle$	$(5+\cos 2\alpha)/210$

Table A.3: Orientationally averaged direction cosine terms for HHH polarization.

Term	Value
$\langle e_A e_B e_C e_D {e_P}^2\rangle$,$\langle e'_A e'_B e'_C e'_D {e'_P}^2\rangle$	$1/7$
$\langle e'_A e_B e_C e_D {e_P}^2\rangle$,$\langle e_A e'_B e_C e_D {e_P}^2\rangle$ $\langle e_A e_B e'_C e_D {e_P}^2\rangle$,$\langle e_A e_B e_C e'_D {e_P}^2\rangle$ $\langle e'_A e'_B e'_C e_D {e'_P}^2\rangle$,$\langle e'_A e_B e'_C e'_D {e'_P}^2\rangle$ $\langle e'_A e'_B e_C e'_D {e'_P}^2\rangle$,$\langle e_A e'_B e'_C e'_D {e'_P}^2\rangle$	$(\cos\alpha)/7$
$\langle e'_A e'_B e_C e_D {e_P}^2\rangle$,$\langle e'_A e_B e'_C e_D {e_P}^2\rangle$ $\langle e'_A e_B e_C e'_D {e_P}^2\rangle$,$\langle e_A e'_B e'_C e_D {e_P}^2\rangle$ $\langle e_A e'_B e_C e'_D {e_P}^2\rangle$,$\langle e_A e_B e'_C e'_D {e_P}^2\rangle$ $\langle e'_A e_B e_C e_D {e'_P}^2\rangle$,$\langle e_A e'_B e_C e_D {e'_P}^2\rangle$ $\langle e'_A e_B e'_C e'_D {e'_P}^2\rangle$,$\langle e_A e'_B e'_C e_D {e'_P}^2\rangle$ $\langle e'_A e_B e_C e'_D {e'_P}^2\rangle$,$\langle e_A e'_B e_C e'_D {e'_P}^2\rangle$ $\langle e_A e_B e'_C e'_D {e'_P}^2\rangle$,$\langle e_A e_B e_C e_D {e'_P}^2\rangle$	$(3+2\cos 2\alpha)/35$
$\langle e'_A e'_B e'_C e_D {e_P}^2\rangle$, $\langle e'_A e_B e'_C e'_D {e_P}^2\rangle$ $\langle e'_A e'_B e_C e'_D {e_P}^2\rangle$,$\langle e_A e'_B e'_C e'_D {e_P}^2\rangle$ $\langle e'_A e_B e_C e_D {e'_P}^2\rangle$,$\langle e_A e'_B e_C e_D {e'_P}^2\rangle$ $\langle e_A e_B e'_C e_D {e'_P}^2\rangle$,$\langle e_A e_B e_C e'_D {e'_P}^2\rangle$	$(9\cos\alpha+\cos 3\alpha)/70$
$\langle e'_A e'_B e'_C e'_D {e_P}^2\rangle$,$\langle e_A e_B e_C e_D {e'_P}^2\rangle$	$(3+2\cos 2\alpha)/35$

APPENDIX B

MD-WPI SIGNAL FOLLOWING CONTROL PULSE

Here we provide detailed expressions for the multidimensional wave-packet interferometry signal from an energy transfer complex subjected to a pre-resonant control pulse (derived in Section C of Chapter II). The signal is decomposed into four components of different phase signature,

$$\begin{aligned} S_\varepsilon = & \, e^{i(\phi_{BA}+\phi_{DC})} S_\varepsilon^{++} + e^{i(\phi_{BA}-\phi_{DC})} S_\varepsilon^{+-} \\ & + e^{i(-\phi_{BA}+\phi_{DC})} S_\varepsilon^{-+} + e^{i(-\phi_{BA}-\phi_{DC})} S_\varepsilon^{--} \, , \end{aligned} \tag{B.1}$$

the first two of which are written out in detail below. The other components are easily obtained from the relations $S_\varepsilon^{--} = (S_\varepsilon^{++})^*$ and $S_\varepsilon^{-+} = (S_\varepsilon^{+-})^*$.

$$\begin{aligned} S_\varepsilon^{++} = & \langle (B)_\varepsilon | (DCAPP)_\varepsilon \rangle^{++} + \langle (B)_\varepsilon | (CDAPP)_\varepsilon \rangle^{++} + \langle (BPP)_\varepsilon | (DCA)_\varepsilon \rangle^{++} \\ & + \langle (BPP)_\varepsilon | (CDA)_\varepsilon \rangle^{++} + \langle (DCBPP)_\varepsilon | (A)_\varepsilon \rangle^{++} + \langle (CDBPP)_\varepsilon | (A)_\varepsilon \rangle^{++} \\ & + \langle (DCB)_\varepsilon | (APP)_\varepsilon \rangle^{++} + \langle (CDB)_\varepsilon | (APP)_\varepsilon \rangle^{++} + \langle (D)_\varepsilon | (CBAPP)_\varepsilon \rangle^{++} \\ & + \langle (DPP)_\varepsilon | (CBA)_\varepsilon \rangle^{++} + \langle (DABPP)_\varepsilon | (C)_\varepsilon \rangle^{++} + \langle (DAB)_\varepsilon | (CPP)_\varepsilon \rangle^{++} \end{aligned} \tag{B.2}$$

$$
\begin{aligned}
S_{\varepsilon}^{+-} = &\langle (B)_{\varepsilon} | (DCAPP)_{\varepsilon} \rangle^{+-} + \langle (B)_{\varepsilon} | (CDAPP)_{\varepsilon} \rangle^{+-} + \langle (BPP)_{\varepsilon} | (DCA)_{\varepsilon} \rangle^{+-} \\
&+ \langle (BPP)_{\varepsilon} | (CDA)_{\varepsilon} \rangle^{+-} + \langle (DCBPP)_{\varepsilon} | (A)_{\varepsilon} \rangle^{+-} + \langle (CDBPP)_{\varepsilon} | (A)_{\varepsilon} \rangle^{+-} \\
&+ \langle (DCB)_{\varepsilon} | (APP)_{\varepsilon} \rangle^{+-} + \langle (CDB)_{\varepsilon} | (APP)_{\varepsilon} \rangle^{+-} + \langle (C)_{\varepsilon} | (DBAPP)_{\varepsilon} \rangle^{+-} \\
&+ \langle (CPP)_{\varepsilon} | (DBA)_{\varepsilon} \rangle^{+-} + \langle (CABPP)_{\varepsilon} | (D)_{\varepsilon} \rangle^{+-} + \langle (CAB)_{\varepsilon} | (DPP)_{\varepsilon} \rangle^{+-}
\end{aligned}
\tag{B.3}
$$

$$
\begin{aligned}
\langle (B)_{\varepsilon} | (DCAPP)_{\varepsilon} \rangle^{++} = &\, e_A e_B e_C e_D {e_P}^2 \langle \{b(10)\}_{\varepsilon} | \{d(1'2)c(21')a(10)p(01)p(10)\}_{\varepsilon} \rangle \\
&+ e'_A e_B e_C e_D {e_P}^2 \langle \{b(10)\}_{\varepsilon} | \{d(1'2)c(21')a(1'0)p(01)p(10)\}_{\varepsilon} \rangle \\
&+ e'_A e'_B e_C e_D {e_P}^2 \langle \{b(1'0)\}_{\varepsilon} | \{d(1'2)c(21')a(1'0)p(01)p(10)\}_{\varepsilon} \rangle \\
&+ e'_A e_B e'_C e_D {e_P}^2 \langle \{b(10)\}_{\varepsilon} | \{d(1'2)c(21)a(1'0)p(01)p(10)\}_{\varepsilon} \rangle \\
&+ e'_A e_B e_C e'_D {e_P}^2 \langle \{b(10)\}_{\varepsilon} | \{d(12)c(21')a(1'0)p(01)p(10)\}_{\varepsilon} \rangle \\
&+ e'_A e'_B e'_C e_D {e_P}^2 \langle \{b(1'0)\}_{\varepsilon} | \{d(1'2)c(21)a(1'0)p(01)p(10)\}_{\varepsilon} \rangle \\
&+ e'_A e_B e'_C e'_D {e_P}^2 \langle \{b(10)\}_{\varepsilon} | \{d(12)c(21)a(1'0)p(01)p(10)\}_{\varepsilon} \rangle \\
&+ e'_A e'_B e_C e'_D {e_P}^2 \langle \{b(1'0)\}_{\varepsilon} | \{d(12)c(21')a(1'0)p(01)p(10)\}_{\varepsilon} \rangle \\
&+ e'_A e'_B e'_C e'_D {e_P}^2 \langle \{b(1'0)\}_{\varepsilon} | \{d(12)c(21)a(1'0)p(01)p(10)\}_{\varepsilon} \rangle \\
&+ e_A e'_B e_C e_D {e_P}^2 \langle \{b(1'0)\}_{\varepsilon} | \{d(1'2)c(21')a(10)p(01)p(10)\}_{\varepsilon} \rangle \\
&+ e_A e_B e'_C e_D {e_P}^2 \langle \{b(10)\}_{\varepsilon} | \{d(1'2)c(21)a(10)p(01)p(10)\}_{\varepsilon} \rangle \\
&+ e_A e_B e_C e'_D {e_P}^2 \langle \{b(10)\}_{\varepsilon} | \{d(12)c(21')a(10)p(01)p(10)\}_{\varepsilon} \rangle \\
&+ e_A e'_B e'_C e_D {e_P}^2 \langle \{b(1'0)\}_{\varepsilon} | \{d(1'2)c(21)a(10)p(01)p(10)\}_{\varepsilon} \rangle \\
&+ e_A e_B e'_C e'_D {e_P}^2 \langle \{b(10)\}_{\varepsilon} | \{d(12)c(21)a(10)p(01)p(10)\}_{\varepsilon} \rangle \\
&+ e_A e'_B e_C e'_D {e_P}^2 \langle \{b(1'0)\}_{\varepsilon} | \{d(12)c(21')a(10)p(01)p(10)\}_{\varepsilon} \rangle
\end{aligned}
$$

$$
\begin{aligned}
&+ e_A e'_B e'_C e'_D e_P{}^2 \langle \{b(1'0)\}_\varepsilon | \{d(12)c(21)a(10)p(01)p(10)\}_\varepsilon \rangle \\
&+ e_A e_B e_C e_D e'_P{}^2 \langle \{b(10)\}_\varepsilon | \{d(1'2)c(21')a(10)p(01')p(1'0)\}_\varepsilon \rangle \\
&+ e'_A e_B e_C e_D e'_P{}^2 \langle \{b(10)\}_\varepsilon | \{d(1'2)c(21')a(1'0)p(01')p(1'0)\}_\varepsilon \rangle \\
&+ e'_A e'_B e_C e_D e'_P{}^2 \langle \{b(1'0)\}_\varepsilon | \{d(1'2)c(21')a(1'0)p(01')p(1'0)\}_\varepsilon \rangle \\
&+ e'_A e_B e'_C e_D e'_P{}^2 \langle \{b(10)\}_\varepsilon | \{d(1'2)c(21)a(1'0)p(01')p(1'0)\}_\varepsilon \rangle \\
&+ e'_A e_B e_C e'_D e'_P{}^2 \langle \{b(10)\}_\varepsilon | \{d(12)c(21')a(1'0)p(01')p(1'0)\}_\varepsilon \rangle \\
&+ e'_A e'_B e'_C e_D e'_P{}^2 \langle \{b(1'0)\}_\varepsilon | \{d(1'2)c(21)a(1'0)p(01')p(1'0)\}_\varepsilon \rangle \\
&+ e'_A e_B e'_C e'_D e'_P{}^2 \langle \{b(10)\}_\varepsilon | \{d(12)c(21)a(1'0)p(01')p(1'0)\}_\varepsilon \rangle \\
&+ e'_A e'_B e_C e'_D e'_P{}^2 \langle \{b(1'0)\}_\varepsilon | \{d(12)c(21')a(1'0)p(01')p(1'0)\}_\varepsilon \rangle \\
&+ e'_A e'_B e'_C e'_D e'_P{}^2 \langle \{b(1'0)\}_\varepsilon | \{d(12)c(21)a(1'0)p(01')p(1'0)\}_\varepsilon \rangle \\
&+ e_A e'_B e_C e_D e'_P{}^2 \langle \{b(1'0)\}_\varepsilon | \{d(1'2)c(21')a(10)p(01')p(1'0)\}_\varepsilon \rangle \\
&+ e_A e_B e'_C e_D e'_P{}^2 \langle \{b(10)\}_\varepsilon | \{d(1'2)c(21)a(10)p(01')p(1'0)\}_\varepsilon \rangle \\
&+ e_A e_B e_C e'_D e'_P{}^2 \langle \{b(10)\}_\varepsilon | \{d(12)c(21')a(10)p(01')p(1'0)\}_\varepsilon \rangle \\
&+ e_A e'_B e'_C e_D e'_P{}^2 \langle \{b(1'0)\}_\varepsilon | \{d(1'2)c(21)a(10)p(01')p(1'0)\}_\varepsilon \rangle \\
&+ e_A e_B e'_C e'_D e'_P{}^2 \langle \{b(10)\}_\varepsilon | \{d(12)c(21)a(10)p(01')p(1'0)\}_\varepsilon \rangle \\
&+ e_A e'_B e_C e'_D e'_P{}^2 \langle \{b(1'0)\}_\varepsilon | \{d(12)c(21')a(10)p(01')p(1'0)\}_\varepsilon \rangle \\
&+ e_A e'_B e'_C e'_D e'_P{}^2 \langle \{b(1'0)\}_\varepsilon | \{d(12)c(21)a(10)p(01')p(1'0)\}_\varepsilon \rangle
\end{aligned}
\tag{B.4}
$$

$$
\begin{aligned}
\langle (B)_\varepsilon | (CDAPP)_\varepsilon \rangle^{++} = {} & e_A e_B e_C e_D e_P{}^2 \langle \{b(10)\}_\varepsilon | \{c(10)d(01)a(10)p(01)p(10)\}_\varepsilon \rangle \\
&+ e'_A e_B e_C e_D e_P{}^2 \langle \{b(10)\}_\varepsilon | \{c(10)d(01)a(1'0)p(01)p(10)\}_\varepsilon \rangle \\
&+ e'_A e'_B e_C e_D e_P{}^2 \langle \{b(1'0)\}_\varepsilon | \{c(10)d(01)a(1'0)p(01)p(10)\}_\varepsilon \rangle
\end{aligned}
$$

$$
\begin{aligned}
&+ e'_A e_B e'_C e_D {e_P}^2 \langle \{b(10)\}_\varepsilon | \{c(1'0)d(01)a(1'0)p(01)p(10)\}_\varepsilon \rangle \\
&+ e'_A e_B e_C e'_D {e_P}^2 \langle \{b(10)\}_\varepsilon | \{c(10)d(01')a(1'0)p(01)p(10)\}_\varepsilon \rangle \\
&+ e'_A e'_B e'_C e_D {e_P}^2 \langle \{b(1'0)\}_\varepsilon | \{c(1'0)d(01)a(1'0)p(01)p(10)\}_\varepsilon \rangle \\
&+ e'_A e_B e'_C e'_D {e_P}^2 \langle \{b(10)\}_\varepsilon | \{c(1'0)d(01')a(1'0)p(01)p(10)\}_\varepsilon \rangle \\
&+ e'_A e'_B e_C e'_D {e_P}^2 \langle \{b(1'0)\}_\varepsilon | \{c(10)d(01')a(1'0)p(01)p(10)\}_\varepsilon \rangle \\
&+ e'_A e'_B e'_C e'_D {e_P}^2 \langle \{b(1'0)\}_\varepsilon | \{c(1'0)d(01')a(1'0)p(01)p(10)\}_\varepsilon \rangle \\
&+ e_A e'_B e_C e_D {e_P}^2 \langle \{b(1'0)\}_\varepsilon | \{c(10)d(01)a(10)p(01)p(10)\}_\varepsilon \rangle \\
&+ e_A e_B e'_C e_D {e_P}^2 \langle \{b(10)\}_\varepsilon | \{c(1'0)d(01)a(10)p(01)p(10)\}_\varepsilon \rangle \\
&+ e_A e_B e_C e'_D {e_P}^2 \langle \{b(10)\}_\varepsilon | \{c(10)d(01')a(10)p(01)p(10)\}_\varepsilon \rangle \\
&+ e_A e'_B e'_C e_D {e_P}^2 \langle \{b(1'0)\}_\varepsilon | \{c(1'0)d(01)a(10)p(01)p(10)\}_\varepsilon \rangle \\
&+ e_A e_B e'_C e'_D {e_P}^2 \langle \{b(10)\}_\varepsilon | \{c(1'0)d(01')a(10)p(01)p(10)\}_\varepsilon \rangle \\
&+ e_A e'_B e_C e'_D {e_P}^2 \langle \{b(1'0)\}_\varepsilon | \{c(10)d(01')a(10)p(01)p(10)\}_\varepsilon \rangle \\
&+ e_A e'_B e'_C e'_D {e_P}^2 \langle \{b(1'0)\}_\varepsilon | \{c(1'0)d(01')a(10)p(01)p(10)\}_\varepsilon \rangle \\
&+ e_A e_B e_C e_D {e'_P}^2 \langle \{b(10)\}_\varepsilon | \{c(10)d(01)a(10)p(01')p(1'0)\}_\varepsilon \rangle \\
&+ e'_A e_B e_C e_D {e'_P}^2 \langle \{b(10)\}_\varepsilon | \{c(10)d(01)a(1'0)p(01')p(1'0)\}_\varepsilon \rangle \\
&+ e'_A e'_B e_C e_D {e'_P}^2 \langle \{b(1'0)\}_\varepsilon | \{c(10)d(01)a(1'0)p(01')p(1'0)\}_\varepsilon \rangle \\
&+ e'_A e_B e'_C e_D {e'_P}^2 \langle \{b(10)\}_\varepsilon | \{c(1'0)d(01)a(1'0)p(01')p(1'0)\}_\varepsilon \rangle \\
&+ e'_A e_B e_C e'_D {e'_P}^2 \langle \{b(10)\}_\varepsilon | \{c(10)d(01')a(1'0)p(01')p(1'0)\}_\varepsilon \rangle \\
&+ e'_A e'_B e'_C e_D {e'_P}^2 \langle \{b(1'0)\}_\varepsilon | \{c(1'0)d(01)a(1'0)p(01')p(1'0)\}_\varepsilon \rangle \\
&+ e'_A e_B e'_C e'_D {e'_P}^2 \langle \{b(10)\}_\varepsilon | \{c(1'0)d(01')a(1'0)p(01')p(1'0)\}_\varepsilon \rangle \\
&+ e'_A e'_B e_C e'_D {e'_P}^2 \langle \{b(1'0)\}_\varepsilon | \{c(10)d(01')a(1'0)p(01')p(1'0)\}_\varepsilon \rangle \\
&+ e'_A e'_B e'_C e'_D {e'_P}^2 \langle \{b(1'0)\}_\varepsilon | \{c(1'0)d(01')a(1'0)p(01')p(1'0)\}_\varepsilon \rangle \\
&+ e_A e'_B e_C e_D {e'_P}^2 \langle \{b(1'0)\}_\varepsilon | \{c(10)d(01)a(10)p(01')p(1'0)\}_\varepsilon \rangle
\end{aligned}
$$

$$
\begin{aligned}
&+ e_A e_B e'_C e_D {e'_P}^2 \langle \{b(10)\}_\varepsilon | \{c(1'0)d(01)a(10)p(01')p(1'0)\}_\varepsilon \rangle \\
&+ e_A e_B e_C e'_D {e'_P}^2 \langle \{b(10)\}_\varepsilon | \{c(10)d(01')a(10)p(01')p(1'0)\}_\varepsilon \rangle \\
&+ e_A e'_B e'_C e_D {e'_P}^2 \langle \{b(1'0)\}_\varepsilon | \{c(1'0)d(01)a(10)p(01')p(1'0)\}_\varepsilon \rangle \\
&+ e_A e_B e'_C e'_D {e'_P}^2 \langle \{b(10)\}_\varepsilon | \{c(1'0)d(01')a(10)p(01')p(1'0)\}_\varepsilon \rangle \\
&+ e_A e'_B e_C e'_D {e'_P}^2 \langle \{b(1'0)\}_\varepsilon | \{c(10)d(01')a(10)p(01')p(1'0)\}_\varepsilon \rangle \\
&+ e_A e'_B e'_C e'_D {e'_P}^2 \langle \{b(1'0)\}_\varepsilon | \{c(1'0)d(01')a(10)p(01')p(1'0)\}_\varepsilon \rangle
\end{aligned} \tag{B.5}
$$

$$
\begin{aligned}
\langle (BPP)_\varepsilon | (DCA)_\varepsilon \rangle^{++} = {} & e_A e_B e_C e_D {e_P}^2 \langle \{b(10)p(01)p(10)\}_\varepsilon | \{d(1'2)c(21')a(10)\}_\varepsilon \rangle \\
&+ e'_A e_B e_C e_D {e_P}^2 \langle \{b(10)p(01)p(10)\}_\varepsilon | \{d(1'2)c(21')a(1'0)\}_\varepsilon \rangle \\
&+ e'_A e'_B e_C e_D {e_P}^2 \langle \{b(1'0)p(01)p(10)\}_\varepsilon | \{d(1'2)c(21')a(1'0)\}_\varepsilon \rangle \\
&+ e'_A e_B e'_C e_D {e_P}^2 \langle \{b(10)p(01)p(10)\}_\varepsilon | \{d(1'2)c(21)a(1'0)\}_\varepsilon \rangle \\
&+ e'_A e_B e_C e'_D {e_P}^2 \langle \{b(10)p(01)p(10)\}_\varepsilon | \{d(12)c(21')a(1'0)\}_\varepsilon \rangle \\
&+ e'_A e'_B e'_C e_D {e_P}^2 \langle \{b(1'0)p(01)p(10)\}_\varepsilon | \{d(1'2)c(21)a(1'0)\}_\varepsilon \rangle \\
&+ e'_A e_B e'_C e'_D {e_P}^2 \langle \{b(10)p(01)p(10)\}_\varepsilon | \{d(12)c(21)a(1'0)\}_\varepsilon \rangle \\
&+ e'_A e'_B e_C e'_D {e_P}^2 \langle \{b(1'0)p(01)p(10)\}_\varepsilon | \{d(12)c(21')a(1'0)\}_\varepsilon \rangle \\
&+ e'_A e'_B e'_C e'_D {e_P}^2 \langle \{b(1'0)p(01)p(10)\}_\varepsilon | \{d(12)c(21)a(1'0)\}_\varepsilon \rangle \\
&+ e_A e'_B e_C e_D {e_P}^2 \langle \{b(1'0)p(01)p(10)\}_\varepsilon | \{d(1'2)c(21')a(10)\}_\varepsilon \rangle \\
&+ e_A e_B e'_C e_D {e_P}^2 \langle \{b(10)p(01)p(10)\}_\varepsilon | \{d(1'2)c(21)a(10)\}_\varepsilon \rangle \\
&+ e_A e_B e_C e'_D {e_P}^2 \langle \{b(10)p(01)p(10)\}_\varepsilon | \{d(12)c(21')a(10)\}_\varepsilon \rangle \\
&+ e_A e'_B e'_C e_D {e_P}^2 \langle \{b(1'0)p(01)p(10)\}_\varepsilon | \{d(1'2)c(21)a(10)\}_\varepsilon \rangle \\
&+ e_A e_B e'_C e'_D {e_P}^2 \langle \{b(10)p(01)p(10)\}_\varepsilon | \{d(12)c(21)a(10)\}_\varepsilon \rangle
\end{aligned}
$$

$$
\begin{aligned}
&+ e_A e'_B e_C e'_D e_P{}^2 \langle\{b(1'0)p(01)p(10)\}_\varepsilon|\{d(12)c(21')a(10)\}_\varepsilon\rangle \\
&+ e_A e'_B e'_C e'_D e_P{}^2 \langle\{b(1'0)p(01)p(10)\}_\varepsilon|\{d(12)c(21)a(10)\}_\varepsilon\rangle \\
&+ e_A e_B e_C e_D e'_P{}^2 \langle\{b(10)p(01')p(1'0)\}_\varepsilon|\{d(1'2)c(21')a(10)\}_\varepsilon\rangle \\
&+ e'_A e_B e_C e_D e'_P{}^2 \langle\{b(10)p(01')p(1'0)\}_\varepsilon|\{d(1'2)c(21')a(1'0)\}_\varepsilon\rangle \\
&+ e'_A e'_B e_C e_D e'_P{}^2 \langle\{b(1'0)p(01')p(1'0)\}_\varepsilon|\{d(1'2)c(21')a(1'0)\}_\varepsilon\rangle \\
&+ e'_A e_B e'_C e_D e'_P{}^2 \langle\{b(10)p(01')p(1'0)\}_\varepsilon|\{d(1'2)c(21)a(1'0)\}_\varepsilon\rangle \\
&+ e'_A e_B e_C e'_D e'_P{}^2 \langle\{b(10)p(01')p(1'0)\}_\varepsilon|\{d(12)c(21')a(1'0)\}_\varepsilon\rangle \\
&+ e'_A e'_B e'_C e_D e'_P{}^2 \langle\{b(1'0)p(01')p(1'0)\}_\varepsilon|\{d(1'2)c(21)a(1'0)\}_\varepsilon\rangle \\
&+ e'_A e_B e'_C e'_D e'_P{}^2 \langle\{b(10)p(01')p(1'0)\}_\varepsilon|\{d(12)c(21)a(1'0)\}_\varepsilon\rangle \\
&+ e'_A e'_B e_C e'_D e'_P{}^2 \langle\{b(1'0)p(01')p(1'0)\}_\varepsilon|\{d(12)c(21')a(1'0)\}_\varepsilon\rangle \\
&+ e'_A e'_B e'_C e'_D e'_P{}^2 \langle\{b(1'0)p(01')p(1'0)\}_\varepsilon|\{d(12)c(21)a(1'0)\}_\varepsilon\rangle \\
&+ e_A e'_B e_C e_D e'_P{}^2 \langle\{b(1'0)p(01')p(1'0)\}_\varepsilon|\{d(1'2)c(21')a(10)\}_\varepsilon\rangle \\
&+ e_A e_B e'_C e_D e'_P{}^2 \langle\{b(10)p(01')p(1'0)\}_\varepsilon|\{d(1'2)c(21)a(10)\}_\varepsilon\rangle \\
&+ e_A e_B e_C e'_D e'_P{}^2 \langle\{b(10)p(01')p(1'0)\}_\varepsilon|\{d(12)c(21')a(10)\}_\varepsilon\rangle \\
&+ e_A e'_B e'_C e_D e'_P{}^2 \langle\{b(1'0)p(01')p(1'0)\}_\varepsilon|\{d(1'2)c(21)a(10)\}_\varepsilon\rangle \\
&+ e_A e_B e'_C e'_D e'_P{}^2 \langle\{b(10)p(01')p(1'0)\}_\varepsilon|\{d(12)c(21)a(10)\}_\varepsilon\rangle \\
&+ e_A e'_B e_C e'_D e'_P{}^2 \langle\{b(1'0)p(01')p(1'0)\}_\varepsilon|\{d(12)c(21')a(10)\}_\varepsilon\rangle \\
&+ e_A e'_B e'_C e'_D e'_P{}^2 \langle\{b(1'0)p(01')p(1'0)\}_\varepsilon|\{d(12)c(21)a(10)\}_\varepsilon\rangle
\end{aligned}
\tag{B.6}
$$

$$
\begin{aligned}
\langle(BPP)_\varepsilon|(CDA)_\varepsilon\rangle^{++} &= e_A e_B e_C e_D e_P{}^2 \langle\{b(10)p(01)p(10)\}_\varepsilon|\{c(10)d(01)a(10)\}_\varepsilon\rangle \\
&+ e'_A e_B e_C e_D e_P{}^2 \langle\{b(10)p(01)p(10)\}_\varepsilon|\{c(10)d(01)a(1'0)\}_\varepsilon\rangle
\end{aligned}
$$

$$
\begin{aligned}
&+ e'_A e'_B e_C e_D e_P{}^2 \langle \{b(1'0)p(01)p(10)\}_\varepsilon | \{c(10)d(01)a(1'0)\}_\varepsilon \rangle \\
&+ e'_A e_B e'_C e_D e_P{}^2 \langle \{b(10)p(01)p(10)\}_\varepsilon | \{c(1'0)d(01)a(1'0)\}_\varepsilon \rangle \\
&+ e'_A e_B e_C e'_D e_P{}^2 \langle \{b(10)p(01)p(10)\}_\varepsilon | \{c(10)d(01')a(1'0)\}_\varepsilon \rangle \\
&+ e'_A e'_B e'_C e_D e_P{}^2 \langle \{b(1'0)p(01)p(10)\}_\varepsilon | \{c(1'0)d(01)a(1'0)\}_\varepsilon \rangle \\
&+ e'_A e_B e'_C e'_D e_P{}^2 \langle \{b(10)p(01)p(10)\}_\varepsilon | \{c(1'0)d(01')a(1'0)\}_\varepsilon \rangle \\
&+ e'_A e'_B e_C e'_D e_P{}^2 \langle \{b(1'0)p(01)p(10)\}_\varepsilon | \{c(10)d(01')a(1'0)\}_\varepsilon \rangle \\
&+ e'_A e'_B e'_C e'_D e_P{}^2 \langle \{b(1'0)p(01)p(10)\}_\varepsilon | \{c(1'0)d(01')a(1'0)\}_\varepsilon \rangle \\
&+ e_A e'_B e_C e_D e_P{}^2 \langle \{b(1'0)p(01)p(10)\}_\varepsilon | \{c(10)d(01)a(10)\}_\varepsilon \rangle \\
&+ e_A e_B e'_C e_D e_P{}^2 \langle \{b(10)p(01)p(10)\}_\varepsilon | \{c(1'0)d(01)a(10)\}_\varepsilon \rangle \\
&+ e_A e_B e_C e'_D e_P{}^2 \langle \{b(10)p(01)p(10)\}_\varepsilon | \{c(10)d(01')a(10)\}_\varepsilon \rangle \\
&+ e_A e'_B e'_C e_D e_P{}^2 \langle \{b(1'0)p(01)p(10)\}_\varepsilon | \{c(1'0)d(01)a(10)\}_\varepsilon \rangle \\
&+ e_A e_B e'_C e'_D e_P{}^2 \langle \{b(10)p(01)p(10)\}_\varepsilon | \{c(1'0)d(01')a(10)\}_\varepsilon \rangle \\
&+ e_A e'_B e_C e'_D e_P{}^2 \langle \{b(1'0)p(01)p(10)\}_\varepsilon | \{c(10)d(01')a(10)\}_\varepsilon \rangle \\
&+ e_A e'_B e'_C e'_D e_P{}^2 \langle \{b(1'0)p(01)p(10)\}_\varepsilon | \{c(1'0)d(01')a(10)\}_\varepsilon \rangle \\
&+ e_A e_B e_C e_D e'_P{}^2 \langle \{b(10)p(01')p(1'0)\}_\varepsilon | \{c(10)d(01)a(10)\}_\varepsilon \rangle \\
&+ e'_A e_B e_C e_D e'_P{}^2 \langle \{b(10)p(01')p(1'0)\}_\varepsilon | \{c(10)d(01)a(1'0)\}_\varepsilon \rangle \\
&+ e'_A e'_B e_C e_D e'_P{}^2 \langle \{b(1'0)p(01')p(1'0)\}_\varepsilon | \{c(10)d(01)a(1'0)\}_\varepsilon \rangle \\
&+ e'_A e_B e'_C e_D e'_P{}^2 \langle \{b(10)p(01')p(1'0)\}_\varepsilon | \{c(1'0)d(01)a(1'0)\}_\varepsilon \rangle \\
&+ e'_A e_B e_C e'_D e'_P{}^2 \langle \{b(10)p(01')p(1'0)\}_\varepsilon | \{c(10)d(01')a(1'0)\}_\varepsilon \rangle \\
&+ e'_A e'_B e'_C e_D e'_P{}^2 \langle \{b(1'0)p(01')p(1'0)\}_\varepsilon | \{c(1'0)d(01)a(1'0)\}_\varepsilon \rangle \\
&+ e'_A e_B e'_C e'_D e'_P{}^2 \langle \{b(10)p(01')p(1'0)\}_\varepsilon | \{c(1'0)d(01')a(1'0)\}_\varepsilon \rangle \\
&+ e'_A e'_B e_C e'_D e'_P{}^2 \langle \{b(1'0)p(01')p(1'0)\}_\varepsilon | \{c(10)d(01')a(1'0)\}_\varepsilon \rangle \\
&+ e'_A e'_B e'_C e'_D e'_P{}^2 \langle \{b(1'0)p(01')p(1'0)\}_\varepsilon | \{c(1'0)d(01')a(1'0)\}_\varepsilon \rangle
\end{aligned}
$$

$$
\begin{aligned}
&+ e_A e'_B e_C e_D {e'_P}^2 \langle\{b(1'0)p(01')p(1'0)\}_\varepsilon|\{c(10)d(01)a(10)\}_\varepsilon\rangle \\
&+ e_A e_B e'_C e_D {e'_P}^2 \langle\{b(10)p(01')p(1'0)\}_\varepsilon|\{c(1'0)d(01)a(10)\}_\varepsilon\rangle \\
&+ e_A e_B e_C e'_D {e'_P}^2 \langle\{b(10)p(01')p(1'0)\}_\varepsilon|\{c(10)d(01')a(10)\}_\varepsilon\rangle \\
&+ e_A e'_B e'_C e_D {e'_P}^2 \langle\{b(1'0)p(01')p(1'0)\}_\varepsilon|\{c(1'0)d(01)a(10)\}_\varepsilon\rangle \\
&+ e_A e_B e'_C e'_D {e'_P}^2 \langle\{b(10)p(01')p(1'0)\}_\varepsilon|\{c(1'0)d(01')a(10)\}_\varepsilon\rangle \\
&+ e_A e'_B e_C e'_D {e'_P}^2 \langle\{b(1'0)p(01')p(1'0)\}_\varepsilon|\{c(10)d(01')a(10)\}_\varepsilon\rangle \\
&+ e_A e'_B e'_C e'_D {e'_P}^2 \langle\{b(1'0)p(01')p(1'0)\}_\varepsilon|\{c(1'0)d(01')a(10)\}_\varepsilon\rangle
\end{aligned}
\tag{B.7}
$$

$$
\begin{aligned}
\langle(DCBPP)_\varepsilon|(A)_\varepsilon\rangle^{++} = {} & e_A e_B e_C e_D {e_P}^2 \langle\{d(10)c(01)b(10)p(01)p(10)\}_\varepsilon|\{a(10)\}_\varepsilon\rangle \\
&+ e'_A e_B e_C e_D {e_P}^2 \langle\{d(10)c(01)b(10)p(01)p(10)\}_\varepsilon|\{a(1'0)\}_\varepsilon\rangle \\
&+ e'_A e'_B e_C e_D {e_P}^2 \langle\{d(10)c(01)b(1'0)p(01)p(10)\}_\varepsilon|\{a(1'0)\}_\varepsilon\rangle \\
&+ e'_A e_B e'_C e_D {e_P}^2 \langle\{d(10)c(01')b(10)p(01)p(10)\}_\varepsilon|\{a(1'0)\}_\varepsilon\rangle \\
&+ e'_A e_B e_C e'_D {e_P}^2 \langle\{d(1'0)c(01)b(10)p(01)p(10)\}_\varepsilon|\{a(1'0)\}_\varepsilon\rangle \\
&+ e'_A e'_B e'_C e_D {e_P}^2 \langle\{d(10)c(01')b(1'0)p(01)p(10)\}_\varepsilon|\{a(1'0)\}_\varepsilon\rangle \\
&+ e'_A e_B e'_C e'_D {e_P}^2 \langle\{d(1'0)c(01')b(10)p(01)p(10)\}_\varepsilon|\{a(1'0)\}_\varepsilon\rangle \\
&+ e'_A e'_B e_C e'_D {e_P}^2 \langle\{d(1'0)c(01)b(1'0)p(01)p(10)\}_\varepsilon|\{a(1'0)\}_\varepsilon\rangle \\
&+ e'_A e'_B e'_C e'_D {e_P}^2 \langle\{d(1'0)c(01')b(1'0)p(01)p(10)\}_\varepsilon|\{a(1'0)\}_\varepsilon\rangle \\
&+ e_A e'_B e_C e_D {e_P}^2 \langle\{d(10)c(01)b(1'0)p(01)p(10)\}_\varepsilon|\{a(10)\}_\varepsilon\rangle \\
&+ e_A e_B e'_C e_D {e_P}^2 \langle\{d(10)c(01')b(10)p(01)p(10)\}_\varepsilon|\{a(10)\}_\varepsilon\rangle \\
&+ e_A e_B e_C e'_D {e_P}^2 \langle\{d(1'0)c(01)b(10)p(01)p(10)\}_\varepsilon|\{a(10)\}_\varepsilon\rangle \\
&+ e_A e'_B e'_C e_D {e_P}^2 \langle\{d(10)c(01')b(1'0)p(01)p(10)\}_\varepsilon|\{a(10)\}_\varepsilon\rangle
\end{aligned}
$$

$$
\begin{aligned}
&+ e_A e_B e'_C e'_D e_P{}^2 \langle\{d(1'0)c(01')b(10)p(01)p(10)\}_\varepsilon|\{a(10)\}_\varepsilon\rangle \\
&+ e_A e'_B e_C e'_D e_P{}^2 \langle\{d(1'0)c(01)b(1'0)p(01)p(10)\}_\varepsilon|\{a(10)\}_\varepsilon\rangle \\
&+ e_A e'_B e'_C e'_D e_P{}^2 \langle\{d(1'0)c(01')b(1'0)p(01)p(10)\}_\varepsilon|\{a(10)\}_\varepsilon\rangle \\
&+ e_A e_B e_C e_D e'_P{}^2 \langle\{d(10)c(01)b(10)p(01')p(1'0)\}_\varepsilon|\{a(10)\}_\varepsilon\rangle \\
&+ e'_A e_B e_C e_D e'_P{}^2 \langle\{d(10)c(01)b(10)p(01')p(1'0)\}_\varepsilon|\{a(1'0)\}_\varepsilon\rangle \\
&+ e'_A e'_B e_C e_D e'_P{}^2 \langle\{d(10)c(01)b(1'0)p(01')p(1'0)\}_\varepsilon|\{a(1'0)\}_\varepsilon\rangle \\
&+ e'_A e_B e'_C e_D e'_P{}^2 \langle\{d(10)c(01')b(10)p(01')p(1'0)\}_\varepsilon|\{a(1'0)\}_\varepsilon\rangle \\
&+ e'_A e_B e_C e'_D e'_P{}^2 \langle\{d(1'0)c(01)b(10)p(01')p(1'0)\}_\varepsilon|\{a(1'0)\}_\varepsilon\rangle \\
&+ e'_A e'_B e'_C e_D e'_P{}^2 \langle\{d(10)c(01')b(1'0)p(01')p(1'0)\}_\varepsilon|\{a(1'0)\}_\varepsilon\rangle \\
&+ e'_A e_B e'_C e'_D e'_P{}^2 \langle\{d(1'0)c(01')b(10)p(01')p(1'0)\}_\varepsilon|\{a(1'0)\}_\varepsilon\rangle \\
&+ e'_A e'_B e_C e'_D e'_P{}^2 \langle\{d(1'0)c(01)b(1'0)p(01')p(1'0)\}_\varepsilon|\{a(1'0)\}_\varepsilon\rangle \\
&+ e'_A e'_B e'_C e'_D e'_P{}^2 \langle\{d(1'0)c(01')b(1'0)p(01')p(1'0)\}_\varepsilon|\{a(1'0)\}_\varepsilon\rangle \\
&+ e_A e'_B e_C e_D e'_P{}^2 \langle\{d(10)c(01)b(1'0)p(01')p(1'0)\}_\varepsilon|\{a(10)\}_\varepsilon\rangle \\
&+ e_A e_B e'_C e_D e'_P{}^2 \langle\{d(10)c(01')b(10)p(01')p(1'0)\}_\varepsilon|\{a(10)\}_\varepsilon\rangle \\
&+ e_A e_B e_C e'_D e'_P{}^2 \langle\{d(1'0)c(01)b(10)p(01')p(1'0)\}_\varepsilon|\{a(10)\}_\varepsilon\rangle \\
&+ e_A e'_B e'_C e_D e'_P{}^2 \langle\{d(10)c(01')b(1'0)p(01')p(1'0)\}_\varepsilon|\{a(10)\}_\varepsilon\rangle \\
&+ e_A e_B e'_C e'_D e'_P{}^2 \langle\{d(1'0)c(01')b(10)p(01')p(1'0)\}_\varepsilon|\{a(10)\}_\varepsilon\rangle \\
&+ e_A e'_B e_C e'_D e'_P{}^2 \langle\{d(1'0)c(01)b(1'0)p(01')p(1'0)\}_\varepsilon|\{a(10)\}_\varepsilon\rangle \\
&+ e_A e'_B e'_C e'_D e'_P{}^2 \langle\{d(1'0)c(01')b(1'0)p(01')p(1'0)\}_\varepsilon|\{a(10)\}_\varepsilon\rangle
\end{aligned}
\tag{B.8}
$$

$$
\langle(CDBPP)_\varepsilon|(A)_\varepsilon\rangle^{++} = e_A e_B e_C e_D e_P{}^2 \langle\{c(1'2)d(21')b(10)p(01)p(10)\}_\varepsilon|\{a(10)\}_\varepsilon\rangle
$$

$$
\begin{aligned}
&+ e'_A e_B e_C e_D {e_P}^2 \langle \{c(1'2)d(21')b(10)p(01)p(10)\}_\varepsilon | \{a(1'0)\}_\varepsilon \rangle \\
&+ e'_A e'_B e_C e_D {e_P}^2 \langle \{c(1'2)d(21')b(1'0)p(01)p(10)\}_\varepsilon | \{a(1'0)\}_\varepsilon \rangle \\
&+ e'_A e_B e'_C e_D {e_P}^2 \langle \{c(12)d(21')b(10)p(01)p(10)\}_\varepsilon | \{a(1'0)\}_\varepsilon \rangle \\
&+ e'_A e_B e_C e'_D {e_P}^2 \langle \{c(1'2)d(21)b(10)p(01)p(10)\}_\varepsilon | \{a(1'0)\}_\varepsilon \rangle \\
&+ e'_A e'_B e'_C e_D {e_P}^2 \langle \{c(12)d(21')b(1'0)p(01)p(10)\}_\varepsilon | \{a(1'0)\}_\varepsilon \rangle \\
&+ e'_A e_B e'_C e'_D {e_P}^2 \langle \{c(12)d(21)b(10)p(01)p(10)\}_\varepsilon | \{a(1'0)\}_\varepsilon \rangle \\
&+ e'_A e'_B e_C e'_D {e_P}^2 \langle \{c(1'2)d(21)b(1'0)p(01)p(10)\}_\varepsilon | \{a(1'0)\}_\varepsilon \rangle \\
&+ e'_A e'_B e'_C e'_D {e_P}^2 \langle \{c(12)d(21)b(1'0)p(01)p(10)\}_\varepsilon | \{a(1'0)\}_\varepsilon \rangle \\
&+ e_A e'_B e_C e_D {e_P}^2 \langle \{c(1'2)d(21')b(1'0)p(01)p(10)\}_\varepsilon | \{a(10)\}_\varepsilon \rangle \\
&+ e_A e_B e'_C e_D {e_P}^2 \langle \{c(12)d(21')b(10)p(01)p(10)\}_\varepsilon | \{a(10)\}_\varepsilon \rangle \\
&+ e_A e_B e_C e'_D {e_P}^2 \langle \{c(1'2)d(21)b(10)p(01)p(10)\}_\varepsilon | \{a(10)\}_\varepsilon \rangle \\
&+ e_A e'_B e'_C e_D {e_P}^2 \langle \{c(12)d(21')b(1'0)p(01)p(10)\}_\varepsilon | \{a(10)\}_\varepsilon \rangle \\
&+ e_A e_B e'_C e'_D {e_P}^2 \langle \{c(12)d(21)b(10)p(01)p(10)\}_\varepsilon | \{a(10)\}_\varepsilon \rangle \\
&+ e_A e'_B e_C e'_D {e_P}^2 \langle \{c(1'2)d(21)b(1'0)p(01)p(10)\}_\varepsilon | \{a(10)\}_\varepsilon \rangle \\
&+ e_A e'_B e'_C e'_D {e_P}^2 \langle \{c(12)d(21)b(1'0)p(01)p(10)\}_\varepsilon | \{a(10)\}_\varepsilon \rangle \\
&+ e_A e_B e_C e_D {e'_P}^2 \langle \{c(1'2)d(21')b(10)p(01')p(1'0)\}_\varepsilon | \{a(10)\}_\varepsilon \rangle \\
&+ e'_A e_B e_C e_D {e'_P}^2 \langle \{c(1'2)d(21')b(10)p(01')p(1'0)\}_\varepsilon | \{a(1'0)\}_\varepsilon \rangle \\
&+ e'_A e'_B e_C e_D {e'_P}^2 \langle \{c(1'2)d(21')b(1'0)p(01')p(1'0)\}_\varepsilon | \{a(1'0)\}_\varepsilon \rangle \\
&+ e'_A e_B e'_C e_D {e'_P}^2 \langle \{c(12)d(21')b(10)p(01')p(1'0)\}_\varepsilon | \{a(1'0)\}_\varepsilon \rangle \\
&+ e'_A e_B e_C e'_D {e'_P}^2 \langle \{c(1'2)d(21)b(10)p(01')p(1'0)\}_\varepsilon | \{a(1'0)\}_\varepsilon \rangle \\
&+ e'_A e'_B e'_C e_D {e'_P}^2 \langle \{c(12)d(21')b(1'0)p(01')p(1'0)\}_\varepsilon | \{a(1'0)\}_\varepsilon \rangle \\
&+ e'_A e_B e'_C e'_D {e'_P}^2 \langle \{c(12)d(21)b(10)p(01')p(1'0)\}_\varepsilon | \{a(1'0)\}_\varepsilon \rangle \\
&+ e'_A e'_B e_C e'_D {e'_P}^2 \langle \{c(1'2)d(21)b(1'0)p(01')p(1'0)\}_\varepsilon | \{a(1'0)\}_\varepsilon \rangle
\end{aligned}
$$

$$
\begin{aligned}
&+ e'_A e'_B e'_C e'_D {e'_P}^2 \langle\{c(12)d(21)b(1'0)p(01')p(1'0)\}_\varepsilon|\{a(1'0)\}_\varepsilon\rangle \\
&+ e_A e'_B e_C e_D {e'_P}^2 \langle\{c(1'2)d(21')b(1'0)p(01')p(1'0)\}_\varepsilon|\{a(10)\}_\varepsilon\rangle \\
&+ e_A e_B e'_C e_D {e'_P}^2 \langle\{c(12)d(21')b(10)p(01')p(1'0)\}_\varepsilon|\{a(10)\}_\varepsilon\rangle \\
&+ e_A e_B e_C e'_D {e'_P}^2 \langle\{c(1'2)d(21)b(10)p(01')p(1'0)\}_\varepsilon|\{a(10)\}_\varepsilon\rangle \\
&+ e_A e'_B e'_C e_D {e'_P}^2 \langle\{c(12)d(21')b(1'0)p(01')p(1'0)\}_\varepsilon|\{a(10)\}_\varepsilon\rangle \\
&+ e_A e_B e'_C e'_D {e'_P}^2 \langle\{c(12)d(21)b(10)p(01')p(1'0)\}_\varepsilon|\{a(10)\}_\varepsilon\rangle \\
&+ e_A e'_B e_C e'_D {e'_P}^2 \langle\{c(1'2)d(21)b(1'0)p(01')p(1'0)\}_\varepsilon|\{a(10)\}_\varepsilon\rangle \\
&+ e_A e'_B e'_C e'_D {e'_P}^2 \langle\{c(12)d(21)b(1'0)p(01')p(1'0)\}_\varepsilon|\{a(10)\}_\varepsilon\rangle
\end{aligned}
\tag{B.9}
$$

$$
\begin{aligned}
\langle(DCB)_\varepsilon|(APP)_\varepsilon\rangle^{++} &= e_A e_B e_C e_D {e_P}^2 \langle\{d(10)c(01)b(10)\}_\varepsilon|\{a(10)p(01)p(10)\}_\varepsilon\rangle \\
&+ e'_A e_B e_C e_D {e_P}^2 \langle\{d(10)c(01)b(10)\}_\varepsilon|\{a(1'0)p(01)p(10)\}_\varepsilon\rangle \\
&+ e'_A e'_B e_C e_D {e_P}^2 \langle\{d(10)c(01)b(1'0)\}_\varepsilon|\{a(1'0)p(01)p(10)\}_\varepsilon\rangle \\
&+ e'_A e_B e'_C e_D {e_P}^2 \langle\{d(10)c(01')b(10)\}_\varepsilon|\{a(1'0)p(01)p(10)\}_\varepsilon\rangle \\
&+ e'_A e_B e_C e'_D {e_P}^2 \langle\{d(1'0)c(01)b(10)\}_\varepsilon|\{a(1'0)p(01)p(10)\}_\varepsilon\rangle \\
&+ e'_A e'_B e'_C e_D {e_P}^2 \langle\{d(10)c(01')b(1'0)\}_\varepsilon|\{a(1'0)p(01)p(10)\}_\varepsilon\rangle \\
&+ e'_A e_B e'_C e'_D {e_P}^2 \langle\{d(1'0)c(01')b(10)\}_\varepsilon|\{a(1'0)p(01)p(10)\}_\varepsilon\rangle \\
&+ e'_A e'_B e_C e'_D {e_P}^2 \langle\{d(1'0)c(01)b(1'0)\}_\varepsilon|\{a(1'0)p(01)p(10)\}_\varepsilon\rangle \\
&+ e'_A e'_B e'_C e'_D {e_P}^2 \langle\{d(1'0)c(01')b(1'0)\}_\varepsilon|\{a(1'0)p(01)p(10)\}_\varepsilon\rangle \\
&+ e_A e'_B e_C e_D {e_P}^2 \langle\{d(10)c(01)b(1'0)\}_\varepsilon|\{a(10)p(01)p(10)\}_\varepsilon\rangle \\
&+ e_A e_B e'_C e_D {e_P}^2 \langle\{d(10)c(01')b(10)\}_\varepsilon|\{a(10)p(01)p(10)\}_\varepsilon\rangle \\
&+ e_A e_B e_C e'_D {e_P}^2 \langle\{d(1'0)c(01)b(10)\}_\varepsilon|\{a(10)p(01)p(10)\}_\varepsilon\rangle
\end{aligned}
$$

$$
\begin{aligned}
&+ e_A e'_B e'_C e_D e_P{}^2 \langle \{d(10)c(01')b(1'0)\}_\varepsilon | \{a(10)p(01)p(10)\}_\varepsilon \rangle \\
&+ e_A e_B e'_C e'_D e_P{}^2 \langle \{d(1'0)c(01')b(10)\}_\varepsilon | \{a(10)p(01)p(10)\}_\varepsilon \rangle \\
&+ e_A e'_B e_C e'_D e_P{}^2 \langle \{d(1'0)c(01)b(1'0)\}_\varepsilon | \{a(10)p(01)p(10)\}_\varepsilon \rangle \\
&+ e_A e'_B e'_C e'_D e_P{}^2 \langle \{d(1'0)c(01')b(1'0)\}_\varepsilon | \{a(10)p(01)p(10)\}_\varepsilon \rangle \\
&+ e_A e_B e_C e_D e'_P{}^2 \langle \{d(10)c(01)b(10)\}_\varepsilon | \{a(10)p(01')p(1'0)\}_\varepsilon \rangle \\
&+ e'_A e_B e_C e_D e'_P{}^2 \langle \{d(10)c(01)b(10)\}_\varepsilon | \{a(1'0)p(01')p(1'0)\}_\varepsilon \rangle \\
&+ e'_A e'_B e_C e_D e'_P{}^2 \langle \{d(10)c(01)b(1'0)\}_\varepsilon | \{a(1'0)p(01')p(1'0)\}_\varepsilon \rangle \\
&+ e'_A e_B e'_C e_D e'_P{}^2 \langle \{d(10)c(01')b(10)\}_\varepsilon | \{a(1'0)p(01')p(1'0)\}_\varepsilon \rangle \\
&+ e'_A e_B e_C e'_D e'_P{}^2 \langle \{d(1'0)c(01)b(10)\}_\varepsilon | \{a(1'0)p(01')p(1'0)\}_\varepsilon \rangle \\
&+ e'_A e'_B e'_C e_D e'_P{}^2 \langle \{d(10)c(01')b(1'0)\}_\varepsilon | \{a(1'0)p(01')p(1'0)\}_\varepsilon \rangle \\
&+ e'_A e_B e'_C e'_D e'_P{}^2 \langle \{d(1'0)c(01')b(10)\}_\varepsilon | \{a(1'0)p(01')p(1'0)\}_\varepsilon \rangle \\
&+ e'_A e'_B e_C e'_D e'_P{}^2 \langle \{d(1'0)c(01)b(1'0)\}_\varepsilon | \{a(1'0)p(01')p(1'0)\}_\varepsilon \rangle \\
&+ e'_A e'_B e'_C e'_D e'_P{}^2 \langle \{d(1'0)c(01')b(1'0)\}_\varepsilon | \{a(1'0)p(01')p(1'0)\}_\varepsilon \rangle \\
&+ e_A e'_B e_C e_D e'_P{}^2 \langle \{d(10)c(01)b(1'0)\}_\varepsilon | \{a(10)p(01')p(1'0)\}_\varepsilon \rangle \\
&+ e_A e_B e'_C e_D e'_P{}^2 \langle \{d(10)c(01')b(10)\}_\varepsilon | \{a(10)p(01')p(1'0)\}_\varepsilon \rangle \\
&+ e_A e_B e_C e'_D e'_P{}^2 \langle \{d(1'0)c(01)b(10)\}_\varepsilon | \{a(10)p(01')p(1'0)\}_\varepsilon \rangle \\
&+ e_A e'_B e'_C e_D e'_P{}^2 \langle \{d(10)c(01')b(1'0)\}_\varepsilon | \{a(10)p(01')p(1'0)\}_\varepsilon \rangle \\
&+ e_A e_B e'_C e'_D e'_P{}^2 \langle \{d(1'0)c(01')b(10)\}_\varepsilon | \{a(10)p(01')p(1'0)\}_\varepsilon \rangle \\
&+ e_A e'_B e_C e'_D e'_P{}^2 \langle \{d(1'0)c(01)b(1'0)\}_\varepsilon | \{a(10)p(01')p(1'0)\}_\varepsilon \rangle \\
&+ e_A e'_B e'_C e'_D e'_P{}^2 \langle \{d(1'0)c(01')b(1'0)\}_\varepsilon | \{a(10)p(01')p(1'0)\}_\varepsilon \rangle
\end{aligned}
\tag{B.10}
$$

$$
\begin{aligned}
\langle (CDB)_\varepsilon | (APP)_\varepsilon \rangle^{++} = {} & e_A e_B e_C e_D {e_P}^2 \langle \{c(1'2)d(21')b(10)\}_\varepsilon | \{a(10)p(01)p(10)\}_\varepsilon \rangle \\
& + e'_A e_B e_C e_D {e_P}^2 \langle \{c(1'2)d(21')b(10)\}_\varepsilon | \{a(1'0)p(01)p(10)\}_\varepsilon \rangle \\
& + e'_A e'_B e_C e_D {e_P}^2 \langle \{c(1'2)d(21')b(1'0)\}_\varepsilon | \{a(1'0)p(01)p(10)\}_\varepsilon \rangle \\
& + e'_A e_B e'_C e_D {e_P}^2 \langle \{c(12)d(21')b(10)\}_\varepsilon | \{a(1'0)p(01)p(10)\}_\varepsilon \rangle \\
& + e'_A e_B e_C e'_D {e_P}^2 \langle \{c(1'2)d(21)b(10)\}_\varepsilon | \{a(1'0)p(01)p(10)\}_\varepsilon \rangle \\
& + e'_A e'_B e'_C e_D {e_P}^2 \langle \{c(12)d(21')b(1'0)\}_\varepsilon | \{a(1'0)p(01)p(10)\}_\varepsilon \rangle \\
& + e'_A e_B e'_C e'_D {e_P}^2 \langle \{c(12)d(21)b(10)\}_\varepsilon | \{a(1'0)p(01)p(10)\}_\varepsilon \rangle \\
& + e'_A e'_B e_C e'_D {e_P}^2 \langle \{c(1'2)d(21)b(1'0)\}_\varepsilon | \{a(1'0)p(01)p(10)\}_\varepsilon \rangle \\
& + e'_A e'_B e'_C e'_D {e_P}^2 \langle \{c(12)d(21)b(1'0)\}_\varepsilon | \{a(1'0)p(01)p(10)\}_\varepsilon \rangle \\
& + e_A e'_B e_C e_D {e_P}^2 \langle \{c(1'2)d(21')b(1'0)\}_\varepsilon | \{a(10)p(01)p(10)\}_\varepsilon \rangle \\
& + e_A e_B e'_C e_D {e_P}^2 \langle \{c(12)d(21')b(10)\}_\varepsilon | \{a(10)p(01)p(10)\}_\varepsilon \rangle \\
& + e_A e_B e_C e'_D {e_P}^2 \langle \{c(1'2)d(21)b(10)\}_\varepsilon | \{a(10)p(01)p(10)\}_\varepsilon \rangle \\
& + e_A e'_B e'_C e_D {e_P}^2 \langle \{c(12)d(21')b(1'0)\}_\varepsilon | \{a(10)p(01)p(10)\}_\varepsilon \rangle \\
& + e_A e_B e'_C e'_D {e_P}^2 \langle \{c(12)d(21)b(10)\}_\varepsilon | \{a(10)p(01)p(10)\}_\varepsilon \rangle \\
& + e_A e'_B e_C e'_D {e_P}^2 \langle \{c(1'2)d(21)b(1'0)\}_\varepsilon | \{a(10)p(01)p(10)\}_\varepsilon \rangle \\
& + e_A e'_B e'_C e'_D {e_P}^2 \langle \{c(12)d(21)b(1'0)\}_\varepsilon | \{a(10)p(01)p(10)\}_\varepsilon \rangle \\
& + e_A e_B e_C e_D {e'_P}^2 \langle \{c(1'2)d(21')b(10)\}_\varepsilon | \{a(10)p(01')p(1'0)\}_\varepsilon \rangle \\
& + e'_A e_B e_C e_D {e'_P}^2 \langle \{c(1'2)d(21')b(10)\}_\varepsilon | \{a(1'0)p(01')p(1'0)\}_\varepsilon \rangle \\
& + e'_A e'_B e_C e_D {e'_P}^2 \langle \{c(1'2)d(21')b(1'0)\}_\varepsilon | \{a(1'0)p(01')p(1'0)\}_\varepsilon \rangle \\
& + e'_A e_B e'_C e_D {e'_P}^2 \langle \{c(12)d(21')b(10)\}_\varepsilon | \{a(1'0)p(01')p(1'0)\}_\varepsilon \rangle \\
& + e'_A e_B e_C e'_D {e'_P}^2 \langle \{c(1'2)d(21)b(10)\}_\varepsilon | \{a(1'0)p(01')p(1'0)\}_\varepsilon \rangle
\end{aligned}
$$

$$
\begin{aligned}
&+ e'_A e'_B e'_C e_D e'_P{}^2 \langle\{c(12)d(21')b(1'0)\}_\varepsilon|\{a(1'0)p(01')p(1'0)\}_\varepsilon\rangle \\
&+ e'_A e_B e'_C e'_D e'_P{}^2 \langle\{c(12)d(21)b(10)\}_\varepsilon|\{a(1'0)p(01')p(1'0)\}_\varepsilon\rangle \\
&+ e'_A e'_B e_C e'_D e'_P{}^2 \langle\{c(1'2)d(21)b(1'0)\}_\varepsilon|\{a(1'0)p(01')p(1'0)\}_\varepsilon\rangle \\
&+ e'_A e'_B e'_C e'_D e'_P{}^2 \langle\{c(12)d(21)b(1'0)\}_\varepsilon|\{a(1'0)p(01')p(1'0)\}_\varepsilon\rangle \\
&+ e_A e'_B e_C e_D e'_P{}^2 \langle\{c(1'2)d(21')b(1'0)\}_\varepsilon|\{a(10)p(01')p(1'0)\}_\varepsilon\rangle \\
&+ e_A e_B e'_C e_D e'_P{}^2 \langle\{c(12)d(21')b(10)\}_\varepsilon|\{a(10)p(01')p(1'0)\}_\varepsilon\rangle \\
&+ e_A e_B e_C e'_D e'_P{}^2 \langle\{c(1'2)d(21)b(10)\}_\varepsilon|\{a(10)p(01')p(1'0)\}_\varepsilon\rangle \\
&+ e_A e'_B e'_C e_D e'_P{}^2 \langle\{c(12)d(21')b(1'0)\}_\varepsilon|\{a(10)p(01')p(1'0)\}_\varepsilon\rangle \\
&+ e_A e_B e'_C e'_D e'_P{}^2 \langle\{c(12)d(21)b(10)\}_\varepsilon|\{a(10)p(01')p(1'0)\}_\varepsilon\rangle \\
&+ e_A e'_B e_C e'_D e'_P{}^2 \langle\{c(1'2)d(21)b(1'0)\}_\varepsilon|\{a(10)p(01')p(1'0)\}_\varepsilon\rangle \\
&+ e_A e'_B e'_C e'_D e'_P{}^2 \langle\{c(12)d(21)b(1'0)\}_\varepsilon|\{a(10)p(01')p(1'0)\}_\varepsilon\rangle
\end{aligned}
\tag{B.11}
$$

$$
\begin{aligned}
\langle(D)_\varepsilon|(CBAPP)_\varepsilon\rangle^{++} = {} & e_A e_B e_C e_D e_P{}^2 \langle\{d(10)\}_\varepsilon|\{c(10)b(01)a(10)p(01)p(10)\}_\varepsilon\rangle \\
&+ e'_A e_B e_C e_D e_P{}^2 \langle\{d(10)\}_\varepsilon|\{c(10)b(01)a(1'0)p(01)p(10)\}_\varepsilon\rangle \\
&+ e'_A e'_B e_C e_D e_P{}^2 \langle\{d(10)\}_\varepsilon|\{c(10)b(01')a(1'0)p(01)p(10)\}_\varepsilon\rangle \\
&+ e'_A e_B e'_C e_D e_P{}^2 \langle\{d(10)\}_\varepsilon|\{c(1'0)b(01)a(1'0)p(01)p(10)\}_\varepsilon\rangle \\
&+ e'_A e_B e_C e'_D e_P{}^2 \langle\{d(1'0)\}_\varepsilon|\{c(10)b(01)a(1'0)p(01)p(10)\}_\varepsilon\rangle \\
&+ e'_A e'_B e'_C e_D e_P{}^2 \langle\{d(10)\}_\varepsilon|\{c(1'0)b(01')a(1'0)p(01)p(10)\}_\varepsilon\rangle \\
&+ e'_A e_B e'_C e'_D e_P{}^2 \langle\{d(1'0)\}_\varepsilon|\{c(1'0)b(01)a(1'0)p(01)p(10)\}_\varepsilon\rangle \\
&+ e'_A e'_B e_C e'_D e_P{}^2 \langle\{d(1'0)\}_\varepsilon|\{c(10)b(01')a(1'0)p(01)p(10)\}_\varepsilon\rangle \\
&+ e'_A e'_B e'_C e'_D e_P{}^2 \langle\{d(1'0)\}_\varepsilon|\{c(1'0)b(01')a(1'0)p(01)p(10)\}_\varepsilon\rangle
\end{aligned}
$$

$$
\begin{aligned}
&+ e_A e'_B e_C e_D {e_P}^2 \langle \{d(10)\}_\varepsilon | \{c(10)b(01')a(10)p(01)p(10)\}_\varepsilon \rangle \\
&+ e_A e_B e'_C e_D {e_P}^2 \langle \{d(10)\}_\varepsilon | \{c(1'0)b(01)a(10)p(01)p(10)\}_\varepsilon \rangle \\
&+ e_A e_B e_C e'_D {e_P}^2 \langle \{d(1'0)\}_\varepsilon | \{c(10)b(01)a(10)p(01)p(10)\}_\varepsilon \rangle \\
&+ e_A e'_B e'_C e_D {e_P}^2 \langle \{d(10)\}_\varepsilon | \{c(1'0)b(01')a(10)p(01)p(10)\}_\varepsilon \rangle \\
&+ e_A e_B e'_C e'_D {e_P}^2 \langle \{d(1'0)\}_\varepsilon | \{c(1'0)b(01)a(10)p(01)p(10)\}_\varepsilon \rangle \\
&+ e_A e'_B e_C e'_D {e_P}^2 \langle \{d(1'0)\}_\varepsilon | \{c(10)b(01')a(10)p(01)p(10)\}_\varepsilon \rangle \\
&+ e_A e'_B e'_C e'_D {e_P}^2 \langle \{d(1'0)\}_\varepsilon | \{c(1'0)b(01')a(10)p(01)p(10)\}_\varepsilon \rangle \\
&+ e_A e_B e_C e_D {e'_P}^2 \langle \{d(10)\}_\varepsilon | \{c(10)b(01)a(10)p(01')p(1'0)\}_\varepsilon \rangle \\
&+ e'_A e_B e_C e_D {e'_P}^2 \langle \{d(10)\}_\varepsilon | \{c(10)b(01)a(1'0)p(01')p(1'0)\}_\varepsilon \rangle \\
&+ e'_A e'_B e_C e_D {e'_P}^2 \langle \{d(10)\}_\varepsilon | \{c(10)b(01')a(1'0)p(01')p(1'0)\}_\varepsilon \rangle \\
&+ e'_A e_B e'_C e_D {e'_P}^2 \langle \{d(10)\}_\varepsilon | \{c(1'0)b(01)a(1'0)p(01')p(1'0)\}_\varepsilon \rangle \\
&+ e'_A e_B e_C e'_D {e'_P}^2 \langle \{d(1'0)\}_\varepsilon | \{c(10)b(01)a(1'0)p(01')p(1'0)\}_\varepsilon \rangle \\
&+ e'_A e'_B e'_C e_D {e'_P}^2 \langle \{d(10)\}_\varepsilon | \{c(1'0)b(01')a(1'0)p(01')p(1'0)\}_\varepsilon \rangle \\
&+ e'_A e_B e'_C e'_D {e'_P}^2 \langle \{d(1'0)\}_\varepsilon | \{c(1'0)b(01)a(1'0)p(01')p(1'0)\}_\varepsilon \rangle \\
&+ e'_A e'_B e_C e'_D {e'_P}^2 \langle \{d(1'0)\}_\varepsilon | \{c(10)b(01')a(1'0)p(01')p(1'0)\}_\varepsilon \rangle \\
&+ e'_A e'_B e'_C e'_D {e'_P}^2 \langle \{d(1'0)\}_\varepsilon | \{c(1'0)b(01')a(1'0)p(01')p(1'0)\}_\varepsilon \rangle \\
&+ e_A e'_B e_C e_D {e'_P}^2 \langle \{d(10)\}_\varepsilon | \{c(10)b(01')a(10)p(01')p(1'0)\}_\varepsilon \rangle \\
&+ e_A e_B e'_C e_D {e'_P}^2 \langle \{d(10)\}_\varepsilon | \{c(1'0)b(01)a(10)p(01')p(1'0)\}_\varepsilon \rangle \\
&+ e_A e_B e_C e'_D {e'_P}^2 \langle \{d(1'0)\}_\varepsilon | \{c(10)b(01)a(10)p(01')p(1'0)\}_\varepsilon \rangle \\
&+ e_A e'_B e'_C e_D {e'_P}^2 \langle \{d(10)\}_\varepsilon | \{c(1'0)b(01')a(10)p(01')p(1'0)\}_\varepsilon \rangle \\
&+ e_A e_B e'_C e'_D {e'_P}^2 \langle \{d(1'0)\}_\varepsilon | \{c(1'0)b(01)a(10)p(01')p(1'0)\}_\varepsilon \rangle \\
&+ e_A e'_B e_C e'_D {e'_P}^2 \langle \{d(1'0)\}_\varepsilon | \{c(10)b(01')a(10)p(01')p(1'0)\}_\varepsilon \rangle
\end{aligned}
$$

$$+ e_A e'_B e'_C e'_D {e'_P}^2 \langle \{d(1'0)\}_\varepsilon | \{c(1'0)b(01')a(10)p(01')p(1'0)\}_\varepsilon \rangle \tag{B.12}$$

$$\begin{aligned}
\langle (DPP)_\varepsilon | (CBA)_\varepsilon \rangle^{++} = {} & e_A e_B e_C e_D {e_P}^2 \langle \{d(10)p(01)p(10)\}_\varepsilon | \{c(10)b(01)a(10)\}_\varepsilon \rangle \\
& + e'_A e_B e_C e_D {e_P}^2 \langle \{d(10)p(01)p(10)\}_\varepsilon | \{c(10)b(01)a(1'0)\}_\varepsilon \rangle \\
& + e'_A e'_B e_C e_D {e_P}^2 \langle \{d(10)p(01)p(10)\}_\varepsilon | \{c(10)b(01')a(1'0)\}_\varepsilon \rangle \\
& + e'_A e_B e'_C e_D {e_P}^2 \langle \{d(10)p(01)p(10)\}_\varepsilon | \{c(1'0)b(01)a(1'0)\}_\varepsilon \rangle \\
& + e'_A e_B e_C e'_D {e_P}^2 \langle \{d(1'0)p(01)p(10)\}_\varepsilon | \{c(10)b(01)a(1'0)\}_\varepsilon \rangle \\
& + e'_A e'_B e'_C e_D {e_P}^2 \langle \{d(10)p(01)p(10)\}_\varepsilon | \{c(1'0)b(01')a(1'0)\}_\varepsilon \rangle \\
& + e'_A e_B e'_C e'_D {e_P}^2 \langle \{d(1'0)p(01)p(10)\}_\varepsilon | \{c(1'0)b(01)a(1'0)\}_\varepsilon \rangle \\
& + e'_A e'_B e_C e'_D {e_P}^2 \langle \{d(1'0)p(01)p(10)\}_\varepsilon | \{c(10)b(01')a(1'0)\}_\varepsilon \rangle \\
& + e'_A e'_B e'_C e'_D {e_P}^2 \langle \{d(1'0)p(01)p(10)\}_\varepsilon | \{c(1'0)b(01')a(1'0)\}_\varepsilon \rangle \\
& + e_A e'_B e_C e_D {e_P}^2 \langle \{d(10)p(01)p(10)\}_\varepsilon | \{c(10)b(01')a(10)\}_\varepsilon \rangle \\
& + e_A e_B e'_C e_D {e_P}^2 \langle \{d(10)p(01)p(10)\}_\varepsilon | \{c(1'0)b(01)a(10)\}_\varepsilon \rangle \\
& + e_A e_B e_C e'_D {e_P}^2 \langle \{d(1'0)p(01)p(10)\}_\varepsilon | \{c(10)b(01)a(10)\}_\varepsilon \rangle \\
& + e_A e'_B e'_C e_D {e_P}^2 \langle \{d(10)p(01)p(10)\}_\varepsilon | \{c(1'0)b(01')a(10)\}_\varepsilon \rangle \\
& + e_A e_B e'_C e'_D {e_P}^2 \langle \{d(1'0)p(01)p(10)\}_\varepsilon | \{c(1'0)b(01)a(10)\}_\varepsilon \rangle \\
& + e_A e'_B e_C e'_D {e_P}^2 \langle \{d(1'0)p(01)p(10)\}_\varepsilon | \{c(10)b(01')a(10)\}_\varepsilon \rangle \\
& + e_A e'_B e'_C e'_D {e_P}^2 \langle \{d(1'0)p(01)p(10)\}_\varepsilon | \{c(1'0)b(01')a(10)\}_\varepsilon \rangle \\
& + e_A e_B e_C e_D {e'_P}^2 \langle \{d(10)p(01')p(1'0)\}_\varepsilon | \{c(10)b(01)a(10)\}_\varepsilon \rangle \\
& + e'_A e_B e_C e_D {e'_P}^2 \langle \{d(10)p(01')p(1'0)\}_\varepsilon | \{c(10)b(01)a(1'0)\}_\varepsilon \rangle \\
& + e'_A e'_B e_C e_D {e'_P}^2 \langle \{d(10)p(01')p(1'0)\}_\varepsilon | \{c(10)b(01')a(1'0)\}_\varepsilon \rangle
\end{aligned}$$

$$
\begin{aligned}
&+ e'_A e_B e'_C e_D e'^{\,2}_P \langle \{d(10)p(01')p(1'0)\}_\varepsilon | \{c(1'0)b(01)a(1'0)\}_\varepsilon \rangle \\
&+ e'_A e_B e_C e'_D e'^{\,2}_P \langle \{d(1'0)p(01')p(1'0)\}_\varepsilon | \{c(10)b(01)a(1'0)\}_\varepsilon \rangle \\
&+ e'_A e'_B e'_C e_D e'^{\,2}_P \langle \{d(10)p(01')p(1'0)\}_\varepsilon | \{c(1'0)b(01')a(1'0)\}_\varepsilon \rangle \\
&+ e'_A e_B e'_C e'_D e'^{\,2}_P \langle \{d(1'0)p(01')p(1'0)\}_\varepsilon | \{c(1'0)b(01)a(1'0)\}_\varepsilon \rangle \\
&+ e'_A e'_B e_C e'_D e'^{\,2}_P \langle \{d(1'0)p(01')p(1'0)\}_\varepsilon | \{c(10)b(01')a(1'0)\}_\varepsilon \rangle \\
&+ e'_A e'_B e'_C e'_D e'^{\,2}_P \langle \{d(1'0)p(01')p(1'0)\}_\varepsilon | \{c(1'0)b(01')a(1'0)\}_\varepsilon \rangle \\
&+ e_A e'_B e_C e_D e'^{\,2}_P \langle \{d(10)p(01')p(1'0)\}_\varepsilon | \{c(10)b(01')a(10)\}_\varepsilon \rangle \\
&+ e_A e_B e'_C e_D e'^{\,2}_P \langle \{d(10)p(01')p(1'0)\}_\varepsilon | \{c(1'0)b(01)a(10)\}_\varepsilon \rangle \\
&+ e_A e_B e_C e'_D e'^{\,2}_P \langle \{d(1'0)p(01')p(1'0)\}_\varepsilon | \{c(10)b(01)a(10)\}_\varepsilon \rangle \\
&+ e_A e'_B e'_C e_D e'^{\,2}_P \langle \{d(10)p(01')p(1'0)\}_\varepsilon | \{c(1'0)b(01')a(10)\}_\varepsilon \rangle \\
&+ e_A e_B e'_C e'_D e'^{\,2}_P \langle \{d(1'0)p(01')p(1'0)\}_\varepsilon | \{c(1'0)b(01)a(10)\}_\varepsilon \rangle \\
&+ e_A e'_B e_C e'_D e'^{\,2}_P \langle \{d(1'0)p(01')p(1'0)\}_\varepsilon | \{c(10)b(01')a(10)\}_\varepsilon \rangle \\
&+ e_A e'_B e'_C e'_D e'^{\,2}_P \langle \{d(1'0)p(01')p(1'0)\}_\varepsilon | \{c(1'0)b(01')a(10)\}_\varepsilon \rangle
\end{aligned}
\tag{B.13}
$$

$$
\begin{aligned}
\langle (DABPP)_\varepsilon | (C)_\varepsilon \rangle^{++} = {} & e_A e_B e_C e_D e_P{}^2 \langle \{d(10)a(01)b(10)p(01)p(10)\}_\varepsilon | \{c(10)\}_\varepsilon \rangle \\
&+ e'_A e'_B e_C e_D e_P{}^2 \langle \{d(10)a(01')b(1'0)p(01)p(10)\}_\varepsilon | \{c(10)\}_\varepsilon \rangle \\
&+ e'_A e'_B e'_C e_D e_P{}^2 \langle \{d(10)a(01')b(1'0)p(01)p(10)\}_\varepsilon | \{c(1'0)\}_\varepsilon \rangle \\
&+ e'_A e'_B e_C e'_D e_P{}^2 \langle \{d(1'0)a(01')b(1'0)p(01)p(10)\}_\varepsilon | \{c(10)\}_\varepsilon \rangle \\
&+ e'_A e'_B e'_C e'_D e_P{}^2 \langle \{d(1'0)a(01')b(1'0)p(01)p(10)\}_\varepsilon | \{c(1'0)\}_\varepsilon \rangle \\
&+ e_A e_B e'_C e_D e_P{}^2 \langle \{d(10)a(01)b(10)p(01)p(10)\}_\varepsilon | \{c(1'0)\}_\varepsilon \rangle \\
&+ e_A e_B e_C e'_D e_P{}^2 \langle \{d(1'0)a(01)b(10)p(01)p(10)\}_\varepsilon | \{c(10)\}_\varepsilon \rangle
\end{aligned}
$$

$$
\begin{aligned}
&+ e_A e_B e'_C e'_D e_P{}^2 \langle\{d(1'0)a(01)b(10)p(01)p(10)\}_\varepsilon|\{c(1'0)\}_\varepsilon\rangle \\
&+ e_A e_B e_C e_D e'_P{}^2 \langle\{d(10)a(01)b(10)p(01')p(1'0)\}_\varepsilon|\{c(10)\}_\varepsilon\rangle \\
&+ e'_A e'_B e_C e_D e'_P{}^2 \langle\{d(10)a(01')b(1'0)p(01')p(1'0)\}_\varepsilon|\{c(10)\}_\varepsilon\rangle \\
&+ e'_A e'_B e'_C e_D e'_P{}^2 \langle\{d(10)a(01')b(1'0)p(01')p(1'0)\}_\varepsilon|\{c(1'0)\}_\varepsilon\rangle \\
&+ e'_A e'_B e_C e'_D e'_P{}^2 \langle\{d(1'0)a(01')b(1'0)p(01')p(1'0)\}_\varepsilon|\{c(10)\}_\varepsilon\rangle \\
&+ e'_A e'_B e'_C e'_D e'_P{}^2 \langle\{d(1'0)a(01')b(1'0)p(01')p(1'0)\}_\varepsilon|\{c(1'0)\}_\varepsilon\rangle \\
&+ e_A e_B e'_C e_D e'_P{}^2 \langle\{d(10)a(01)b(10)p(01')p(1'0)\}_\varepsilon|\{c(1'0)\}_\varepsilon\rangle \\
&+ e_A e_B e_C e'_D e'_P{}^2 \langle\{d(1'0)a(01)b(10)p(01')p(1'0)\}_\varepsilon|\{c(10)\}_\varepsilon\rangle \\
&+ e_A e_B e'_C e'_D e'_P{}^2 \langle\{d(1'0)a(01)b(10)p(01')p(1'0)\}_\varepsilon|\{c(1'0)\}_\varepsilon\rangle
\end{aligned}
\tag{B.14}
$$

$$
\begin{aligned}
\langle(DAB)_\varepsilon|(CPP)_\varepsilon\rangle^{++} = {} & e_A e_B e_C e_D e_P{}^2 \langle\{d(10)a(01)b(10)\}_\varepsilon|\{c(10)p(01)p(10)\}_\varepsilon\rangle \\
&+ e'_A e'_B e_C e_D e_P{}^2 \langle\{d(10)a(01')b(1'0)\}_\varepsilon|\{c(10)p(01)p(10)\}_\varepsilon\rangle \\
&+ e'_A e_B e'_C e_D e_P{}^2 \langle\{d(10)a(01')b(10)\}_\varepsilon|\{c(1'0)p(01)p(10)\}_\varepsilon\rangle \\
&+ e'_A e'_B e'_C e_D e_P{}^2 \langle\{d(10)a(01')b(1'0)\}_\varepsilon|\{c(1'0)p(01)p(10)\}_\varepsilon\rangle \\
&+ e'_A e'_B e_C e'_D e_P{}^2 \langle\{d(1'0)a(01')b(1'0)\}_\varepsilon|\{c(10)p(01)p(10)\}_\varepsilon\rangle \\
&+ e'_A e'_B e'_C e'_D e_P{}^2 \langle\{d(1'0)a(01')b(1'0)\}_\varepsilon|\{c(1'0)p(01)p(10)\}_\varepsilon\rangle \\
&+ e_A e_B e'_C e_D e_P{}^2 \langle\{d(10)a(01)b(10)\}_\varepsilon|\{c(1'0)p(01)p(10)\}_\varepsilon\rangle \\
&+ e_A e_B e_C e'_D e_P{}^2 \langle\{d(1'0)a(01)b(10)\}_\varepsilon|\{c(10)p(01)p(10)\}_\varepsilon\rangle \\
&+ e_A e_B e'_C e'_D e_P{}^2 \langle\{d(1'0)a(01)b(10)\}_\varepsilon|\{c(1'0)p(01)p(10)\}_\varepsilon\rangle \\
&+ e_A e_B e_C e_D e'_P{}^2 \langle\{d(10)a(01)b(10)\}_\varepsilon|\{c(10)p(01')p(1'0)\}_\varepsilon\rangle \\
&+ e'_A e'_B e_C e_D e'_P{}^2 \langle\{d(10)a(01')b(1'0)\}_\varepsilon|\{c(10)p(01')p(1'0)\}_\varepsilon\rangle
\end{aligned}
$$

$$
\begin{aligned}
&+ e'_A e'_B e'_C e_D {e'_P}^2 \langle \{d(10)a(01')b(1'0)\}_\varepsilon | \{c(1'0)p(01')p(1'0)\}_\varepsilon \rangle \\
&+ e'_A e'_B e_C e'_D {e'_P}^2 \langle \{d(1'0)a(01')b(1'0)\}_\varepsilon | \{c(10)p(01')p(1'0)\}_\varepsilon \rangle \\
&+ e'_A e'_B e'_C e'_D {e'_P}^2 \langle \{d(1'0)a(01')b(1'0)\}_\varepsilon | \{c(1'0)p(01')p(1'0)\}_\varepsilon \rangle \\
&+ e_A e_B e'_C e_D {e'_P}^2 \langle \{d(10)a(01)b(10)\}_\varepsilon | \{c(1'0)p(01')p(1'0)\}_\varepsilon \rangle \\
&+ e_A e_B e_C e'_D {e'_P}^2 \langle \{d(1'0)a(01)b(10)\}_\varepsilon | \{c(10)p(01')p(1'0)\}_\varepsilon \rangle \\
&+ e_A e_B e'_C e'_D {e'_P}^2 \langle \{d(1'0)a(01)b(10)\}_\varepsilon | \{c(1'0)p(01')p(1'0)\}_\varepsilon \rangle
\end{aligned}
\tag{B.15}
$$

$$
\begin{aligned}
\langle (B)_\varepsilon | (DCAPP)_\varepsilon \rangle^{+-} = {} & e_A e_B e_C e_D {e_P}^2 \langle \{b(10)\}_\varepsilon | \{d(10)c(01)a(10)p(01)p(10)\}_\varepsilon \rangle \\
&+ e'_A e_B e_C e_D {e_P}^2 \langle \{b(10)\}_\varepsilon | \{d(10)c(01)a(1'0)p(01)p(10)\}_\varepsilon \rangle \\
&+ e'_A e'_B e_C e_D {e_P}^2 \langle \{b(1'0)\}_\varepsilon | \{d(10)c(01)a(1'0)p(01)p(10)\}_\varepsilon \rangle \\
&+ e'_A e_B e'_C e_D {e_P}^2 \langle \{b(10)\}_\varepsilon | \{d(10)c(01')a(1'0)p(01)p(10)\}_\varepsilon \rangle \\
&+ e'_A e_B e_C e'_D {e_P}^2 \langle \{b(10)\}_\varepsilon | \{d(1'0)c(01)a(1'0)p(01)p(10)\}_\varepsilon \rangle \\
&+ e'_A e'_B e'_C e_D {e_P}^2 \langle \{b(1'0)\}_\varepsilon | \{d(10)c(01')a(1'0)p(01)p(10)\}_\varepsilon \rangle \\
&+ e'_A e_B e'_C e'_D {e_P}^2 \langle \{b(10)\}_\varepsilon | \{d(1'0)c(01')a(1'0)p(01)p(10)\}_\varepsilon \rangle \\
&+ e'_A e'_B e_C e'_D {e_P}^2 \langle \{b(1'0)\}_\varepsilon | \{d(1'0)c(01)a(1'0)p(01)p(10)\}_\varepsilon \rangle \\
&+ e'_A e'_B e'_C e'_D {e_P}^2 \langle \{b(1'0)\}_\varepsilon | \{d(1'0)c(01')a(1'0)p(01)p(10)\}_\varepsilon \rangle \\
&+ e_A e'_B e_C e_D {e_P}^2 \langle \{b(1'0)\}_\varepsilon | \{d(10)c(01)a(10)p(01)p(10)\}_\varepsilon \rangle \\
&+ e_A e_B e'_C e_D {e_P}^2 \langle \{b(10)\}_\varepsilon | \{d(10)c(01')a(10)p(01)p(10)\}_\varepsilon \rangle \\
&+ e_A e_B e_C e'_D {e_P}^2 \langle \{b(10)\}_\varepsilon | \{d(1'0)c(01)a(10)p(01)p(10)\}_\varepsilon \rangle \\
&+ e_A e'_B e'_C e_D {e_P}^2 \langle \{b(1'0)\}_\varepsilon | \{d(10)c(01')a(10)p(01)p(10)\}_\varepsilon \rangle \\
&+ e_A e_B e'_C e'_D {e_P}^2 \langle \{b(10)\}_\varepsilon | \{d(1'0)c(01')a(10)p(01)p(10)\}_\varepsilon \rangle
\end{aligned}
$$

$$
\begin{aligned}
&+ e_A e'_B e_C e'_D e_P{}^2 \langle \{b(1'0)\}_\varepsilon | \{d(1'0)c(01)a(10)p(01)p(10)\}_\varepsilon \rangle \\
&+ e_A e'_B e'_C e'_D e_P{}^2 \langle \{b(1'0)\}_\varepsilon | \{d(1'0)c(01')a(10)p(01)p(10)\}_\varepsilon \rangle \\
&+ e_A e_B e_C e_D e'_P{}^2 \langle \{b(10)\}_\varepsilon | \{d(10)c(01)a(10)p(01')p(1'0)\}_\varepsilon \rangle \\
&+ e'_A e_B e_C e_D e'_P{}^2 \langle \{b(10)\}_\varepsilon | \{d(10)c(01)a(1'0)p(01')p(1'0)\}_\varepsilon \rangle \\
&+ e'_A e'_B e_C e_D e'_P{}^2 \langle \{b(1'0)\}_\varepsilon | \{d(10)c(01)a(1'0)p(01')p(1'0)\}_\varepsilon \rangle \\
&+ e'_A e_B e'_C e_D e'_P{}^2 \langle \{b(10)\}_\varepsilon | \{d(10)c(01')a(1'0)p(01')p(1'0)\}_\varepsilon \rangle \\
&+ e'_A e_B e_C e'_D e'_P{}^2 \langle \{b(10)\}_\varepsilon | \{d(1'0)c(01)a(1'0)p(01')p(1'0)\}_\varepsilon \rangle \\
&+ e'_A e'_B e'_C e_D e'_P{}^2 \langle \{b(1'0)\}_\varepsilon | \{d(10)c(01')a(1'0)p(01')p(1'0)\}_\varepsilon \rangle \\
&+ e'_A e_B e'_C e'_D e'_P{}^2 \langle \{b(10)\}_\varepsilon | \{d(1'0)c(01')a(1'0)p(01')p(1'0)\}_\varepsilon \rangle \\
&+ e'_A e'_B e_C e'_D e'_P{}^2 \langle \{b(1'0)\}_\varepsilon | \{d(1'0)c(01)a(1'0)p(01')p(1'0)\}_\varepsilon \rangle \\
&+ e'_A e'_B e'_C e'_D e'_P{}^2 \langle \{b(1'0)\}_\varepsilon | \{d(1'0)c(01')a(1'0)p(01')p(1'0)\}_\varepsilon \rangle \\
&+ e_A e'_B e_C e_D e'_P{}^2 \langle \{b(1'0)\}_\varepsilon | \{d(10)c(01)a(10)p(01')p(1'0)\}_\varepsilon \rangle \\
&+ e_A e_B e'_C e_D e'_P{}^2 \langle \{b(10)\}_\varepsilon | \{d(10)c(01')a(10)p(01')p(1'0)\}_\varepsilon \rangle \\
&+ e_A e_B e_C e'_D e'_P{}^2 \langle \{b(10)\}_\varepsilon | \{d(1'0)c(01)a(10)p(01')p(1'0)\}_\varepsilon \rangle \\
&+ e_A e'_B e'_C e_D e'_P{}^2 \langle \{b(1'0)\}_\varepsilon | \{d(10)c(01')a(10)p(01')p(1'0)\}_\varepsilon \rangle \\
&+ e_A e_B e'_C e'_D e'_P{}^2 \langle \{b(10)\}_\varepsilon | \{d(1'0)c(01')a(10)p(01')p(1'0)\}_\varepsilon \rangle \\
&+ e_A e'_B e_C e'_D e'_P{}^2 \langle \{b(1'0)\}_\varepsilon | \{d(1'0)c(01)a(10)p(01')p(1'0)\}_\varepsilon \rangle \\
&+ e_A e'_B e'_C e'_D e'_P{}^2 \langle \{b(1'0)\}_\varepsilon | \{d(1'0)c(01')a(10)p(01')p(1'0)\}_\varepsilon \rangle
\end{aligned}
\tag{B.16}
$$

$$
\begin{aligned}
\langle (B)_\varepsilon | (CDAPP)_\varepsilon \rangle^{+-} = {} & e_A e_B e_C e_D e_P{}^2 \langle \{b(10)\}_\varepsilon | \{c(1'2)d(21')a(10)p(01)p(10)\}_\varepsilon \rangle \\
&+ e'_A e_B e_C e_D e_P{}^2 \langle \{b(10)\}_\varepsilon | \{c(1'2)d(21')a(1'0)p(01)p(10)\}_\varepsilon \rangle
\end{aligned}
$$

$$
\begin{aligned}
&+ e'_A e'_B e_C e_D {e_P}^2 \langle \{b(1'0)\}_\varepsilon | \{c(1'2)d(21')a(1'0)p(01)p(10)\}_\varepsilon \rangle \\
&+ e'_A e_B e'_C e_D {e_P}^2 \langle \{b(10)\}_\varepsilon | \{c(12)d(21')a(1'0)p(01)p(10)\}_\varepsilon \rangle \\
&+ e'_A e_B e_C e'_D {e_P}^2 \langle \{b(10)\}_\varepsilon | \{c(1'2)d(21)a(1'0)p(01)p(10)\}_\varepsilon \rangle \\
&+ e'_A e'_B e'_C e_D {e_P}^2 \langle \{b(1'0)\}_\varepsilon | \{c(12)d(21')a(1'0)p(01)p(10)\}_\varepsilon \rangle \\
&+ e'_A e_B e'_C e'_D {e_P}^2 \langle \{b(10)\}_\varepsilon | \{c(12)d(21)a(1'0)p(01)p(10)\}_\varepsilon \rangle \\
&+ e'_A e'_B e_C e'_D {e_P}^2 \langle \{b(1'0)\}_\varepsilon | \{c(1'2)d(21)a(1'0)p(01)p(10)\}_\varepsilon \rangle \\
&+ e'_A e'_B e'_C e'_D {e_P}^2 \langle \{b(1'0)\}_\varepsilon | \{c(12)d(21)a(1'0)p(01)p(10)\}_\varepsilon \rangle \\
&+ e_A e'_B e_C e_D {e_P}^2 \langle \{b(1'0)\}_\varepsilon | \{c(1'2)d(21')a(10)p(01)p(10)\}_\varepsilon \rangle \\
&+ e_A e_B e'_C e_D {e_P}^2 \langle \{b(10)\}_\varepsilon | \{c(12)d(21')a(10)p(01)p(10)\}_\varepsilon \rangle \\
&+ e_A e_B e_C e'_D {e_P}^2 \langle \{b(10)\}_\varepsilon | \{c(1'2)d(21)a(10)p(01)p(10)\}_\varepsilon \rangle \\
&+ e_A e'_B e'_C e_D {e_P}^2 \langle \{b(1'0)\}_\varepsilon | \{c(12)d(21')a(10)p(01)p(10)\}_\varepsilon \rangle \\
&+ e_A e_B e'_C e'_D {e_P}^2 \langle \{b(10)\}_\varepsilon | \{c(12)d(21)a(10)p(01)p(10)\}_\varepsilon \rangle \\
&+ e_A e'_B e_C e'_D {e_P}^2 \langle \{b(1'0)\}_\varepsilon | \{c(1'2)d(21)a(10)p(01)p(10)\}_\varepsilon \rangle \\
&+ e_A e'_B e'_C e'_D {e_P}^2 \langle \{b(1'0)\}_\varepsilon | \{c(12)d(21)a(10)p(01)p(10)\}_\varepsilon \rangle \\
&+ e_A e_B e_C e_D {e'_P}^2 \langle \{b(10)\}_\varepsilon | \{c(1'2)d(21')a(10)p(01')p(1'0)\}_\varepsilon \rangle \\
&+ e'_A e_B e_C e_D {e'_P}^2 \langle \{b(10)\}_\varepsilon | \{c(1'2)d(21')a(1'0)p(01')p(1'0)\}_\varepsilon \rangle \\
&+ e'_A e'_B e_C e_D {e'_P}^2 \langle \{b(1'0)\}_\varepsilon | \{c(1'2)d(21')a(1'0)p(01')p(1'0)\}_\varepsilon \rangle \\
&+ e'_A e_B e'_C e_D {e'_P}^2 \langle \{b(10)\}_\varepsilon | \{c(12)d(21')a(1'0)p(01')p(1'0)\}_\varepsilon \rangle \\
&+ e'_A e_B e_C e'_D {e'_P}^2 \langle \{b(10)\}_\varepsilon | \{c(1'2)d(21)a(1'0)p(01')p(1'0)\}_\varepsilon \rangle \\
&+ e'_A e'_B e'_C e_D {e'_P}^2 \langle \{b(1'0)\}_\varepsilon | \{c(12)d(21')a(1'0)p(01')p(1'0)\}_\varepsilon \rangle \\
&+ e'_A e_B e'_C e'_D {e'_P}^2 \langle \{b(10)\}_\varepsilon | \{c(12)d(21)a(1'0)p(01')p(1'0)\}_\varepsilon \rangle \\
&+ e'_A e'_B e_C e'_D {e'_P}^2 \langle \{b(1'0)\}_\varepsilon | \{c(1'2)d(21)a(1'0)p(01')p(1'0)\}_\varepsilon \rangle \\
&+ e'_A e'_B e'_C e'_D {e'_P}^2 \langle \{b(1'0)\}_\varepsilon | \{c(12)d(21)a(1'0)p(01')p(1'0)\}_\varepsilon \rangle
\end{aligned}
$$

$$
\begin{aligned}
&+ e_A e'_B e_C e_D {e'_P}^2 \langle \{b(1'0)\}_\varepsilon | \{c(1'2)d(21')a(10)p(01')p(1'0)\}_\varepsilon \rangle \\
&+ e_A e_B e'_C e_D {e'_P}^2 \langle \{b(10)\}_\varepsilon | \{c(12)d(21')a(10)p(01')p(1'0)\}_\varepsilon \rangle \\
&+ e_A e_B e_C e'_D {e'_P}^2 \langle \{b(10)\}_\varepsilon | \{c(1'2)d(21)a(10)p(01')p(1'0)\}_\varepsilon \rangle \\
&+ e_A e'_B e'_C e_D {e'_P}^2 \langle \{b(1'0)\}_\varepsilon | \{c(12)d(21')a(10)p(01')p(1'0)\}_\varepsilon \rangle \\
&+ e_A e_B e'_C e'_D {e'_P}^2 \langle \{b(10)\}_\varepsilon | \{c(12)d(21)a(10)p(01')p(1'0)\}_\varepsilon \rangle \\
&+ e_A e'_B e_C e'_D {e'_P}^2 \langle \{b(1'0)\}_\varepsilon | \{c(1'2)d(21)a(10)p(01')p(1'0)\}_\varepsilon \rangle \\
&+ e_A e'_B e'_C e'_D {e'_P}^2 \langle \{b(1'0)\}_\varepsilon | \{c(12)d(21)a(10)p(01')p(1'0)\}_\varepsilon \rangle
\end{aligned}
\tag{B.17}
$$

$$
\begin{aligned}
\langle (BPP)_\varepsilon | (DCA)_\varepsilon \rangle^{+-} = {} & e_A e_B e_C e_D {e_P}^2 \langle \{b(10)p(01)p(10)\}_\varepsilon | \{d(10)c(01)a(10)\}_\varepsilon \rangle \\
&+ e'_A e_B e_C e_D {e_P}^2 \langle \{b(10)p(01)p(10)\}_\varepsilon | \{d(10)c(01)a(1'0)\}_\varepsilon \rangle \\
&+ e'_A e'_B e_C e_D {e_P}^2 \langle \{b(1'0)p(01)p(10)\}_\varepsilon | \{d(10)c(01)a(1'0)\}_\varepsilon \rangle \\
&+ e'_A e_B e'_C e_D {e_P}^2 \langle \{b(10)p(01)p(10)\}_\varepsilon | \{d(10)c(01')a(1'0)\}_\varepsilon \rangle \\
&+ e'_A e_B e_C e'_D {e_P}^2 \langle \{b(10)p(01)p(10)\}_\varepsilon | \{d(1'0)c(01)a(1'0)\}_\varepsilon \rangle \\
&+ e'_A e'_B e'_C e_D {e_P}^2 \langle \{b(1'0)p(01)p(10)\}_\varepsilon | \{d(10)c(01')a(1'0)\}_\varepsilon \rangle \\
&+ e'_A e_B e'_C e'_D {e_P}^2 \langle \{b(10)p(01)p(10)\}_\varepsilon | \{d(1'0)c(01')a(1'0)\}_\varepsilon \rangle \\
&+ e'_A e'_B e_C e'_D {e_P}^2 \langle \{b(1'0)p(01)p(10)\}_\varepsilon | \{d(1'0)c(01)a(1'0)\}_\varepsilon \rangle \\
&+ e'_A e'_B e'_C e'_D {e_P}^2 \langle \{b(1'0)p(01)p(10)\}_\varepsilon | \{d(1'0)c(01')a(1'0)\}_\varepsilon \rangle \\
&+ e_A e'_B e_C e_D {e_P}^2 \langle \{b(1'0)p(01)p(10)\}_\varepsilon | \{d(10)c(01)a(10)\}_\varepsilon \rangle \\
&+ e_A e_B e'_C e_D {e_P}^2 \langle \{b(10)p(01)p(10)\}_\varepsilon | \{d(10)c(01')a(10)\}_\varepsilon \rangle \\
&+ e_A e_B e_C e'_D {e_P}^2 \langle \{b(10)p(01)p(10)\}_\varepsilon | \{d(1'0)c(01)a(10)\}_\varepsilon \rangle \\
&+ e_A e'_B e'_C e_D {e_P}^2 \langle \{b(1'0)p(01)p(10)\}_\varepsilon | \{d(10)c(01')a(10)\}_\varepsilon \rangle
\end{aligned}
$$

$$
\begin{aligned}
&+ e_A e_B e'_C e'_D {e_P}^2 \langle \{b(10)p(01)p(10)\}_\varepsilon | \{d(1'0)c(01')a(10)\}_\varepsilon \rangle \\
&+ e_A e'_B e_C e'_D {e_P}^2 \langle \{b(1'0)p(01)p(10)\}_\varepsilon | \{d(1'0)c(01)a(10)\}_\varepsilon \rangle \\
&+ e_A e'_B e'_C e'_D {e_P}^2 \langle \{b(1'0)p(01)p(10)\}_\varepsilon | \{d(1'0)c(01')a(10)\}_\varepsilon \rangle \\
&+ e_A e_B e_C e_D {e'_P}^2 \langle \{b(10)p(01')p(1'0)\}_\varepsilon | \{d(10)c(01)a(10)\}_\varepsilon \rangle \\
&+ e'_A e_B e_C e_D {e'_P}^2 \langle \{b(10)p(01')p(1'0)\}_\varepsilon | \{d(10)c(01)a(1'0)\}_\varepsilon \rangle \\
&+ e'_A e'_B e_C e_D {e'_P}^2 \langle \{b(1'0)p(01')p(1'0)\}_\varepsilon | \{d(10)c(01)a(1'0)\}_\varepsilon \rangle \\
&+ e'_A e_B e'_C e_D {e'_P}^2 \langle \{b(10)p(01')p(1'0)\}_\varepsilon | \{d(10)c(01')a(1'0)\}_\varepsilon \rangle \\
&+ e'_A e_B e_C e'_D {e'_P}^2 \langle \{b(10)p(01')p(1'0)\}_\varepsilon | \{d(1'0)c(01)a(1'0)\}_\varepsilon \rangle \\
&+ e'_A e'_B e'_C e_D {e'_P}^2 \langle \{b(1'0)p(01')p(1'0)\}_\varepsilon | \{d(10)c(01')a(1'0)\}_\varepsilon \rangle \\
&+ e'_A e_B e'_C e'_D {e'_P}^2 \langle \{b(10)p(01')p(1'0)\}_\varepsilon | \{d(1'0)c(01')a(1'0)\}_\varepsilon \rangle \\
&+ e'_A e'_B e_C e'_D {e'_P}^2 \langle \{b(1'0)p(01')p(1'0)\}_\varepsilon | \{d(1'0)c(01)a(1'0)\}_\varepsilon \rangle \\
&+ e'_A e'_B e'_C e'_D {e'_P}^2 \langle \{b(1'0)p(01')p(1'0)\}_\varepsilon | \{d(1'0)c(01')a(1'0)\}_\varepsilon \rangle \\
&+ e_A e'_B e_C e_D {e'_P}^2 \langle \{b(1'0)p(01')p(1'0)\}_\varepsilon | \{d(10)c(01)a(10)\}_\varepsilon \rangle \\
&+ e_A e_B e'_C e_D {e'_P}^2 \langle \{b(10)p(01')p(1'0)\}_\varepsilon | \{d(10)c(01')a(10)\}_\varepsilon \rangle \\
&+ e_A e_B e_C e'_D {e'_P}^2 \langle \{b(10)p(01')p(1'0)\}_\varepsilon | \{d(1'0)c(01)a(10)\}_\varepsilon \rangle \\
&+ e_A e'_B e'_C e_D {e'_P}^2 \langle \{b(1'0)p(01')p(1'0)\}_\varepsilon | \{d(10)c(01')a(10)\}_\varepsilon \rangle \\
&+ e_A e_B e'_C e'_D {e'_P}^2 \langle \{b(10)p(01')p(1'0)\}_\varepsilon | \{d(1'0)c(01')a(10)\}_\varepsilon \rangle \\
&+ e_A e'_B e_C e'_D {e'_P}^2 \langle \{b(1'0)p(01')p(1'0)\}_\varepsilon | \{d(1'0)c(01)a(10)\}_\varepsilon \rangle \\
&+ e_A e'_B e'_C e'_D {e'_P}^2 \langle \{b(1'0)p(01')p(1'0)\}_\varepsilon | \{d(1'0)c(01')a(10)\}_\varepsilon \rangle
\end{aligned}
\tag{B.18}
$$

$$
\langle (BPP)_\varepsilon | (CDA)_\varepsilon \rangle^{+-} = e_A e_B e_C e_D {e_P}^2 \langle \{b(10)p(01)p(10)\}_\varepsilon | \{c(1'2)d(21')a(10)\}_\varepsilon \rangle
$$

$$
\begin{aligned}
&+ e'_A e_B e_C e_D {e_P}^2 \langle \{b(10)p(01)p(10)\}_\varepsilon | \{c(1'2)d(21')a(1'0)\}_\varepsilon \rangle \\
&+ e'_A e'_B e_C e_D {e_P}^2 \langle \{b(1'0)p(01)p(10)\}_\varepsilon | \{c(1'2)d(21')a(1'0)\}_\varepsilon \rangle \\
&+ e'_A e_B e'_C e_D {e_P}^2 \langle \{b(10)p(01)p(10)\}_\varepsilon | \{c(12)d(21')a(1'0)\}_\varepsilon \rangle \\
&+ e'_A e_B e_C e'_D {e_P}^2 \langle \{b(10)p(01)p(10)\}_\varepsilon | \{c(1'2)d(21)a(1'0)\}_\varepsilon \rangle \\
&+ e'_A e'_B e'_C e_D {e_P}^2 \langle \{b(1'0)p(01)p(10)\}_\varepsilon | \{c(12)d(21')a(1'0)\}_\varepsilon \rangle \\
&+ e'_A e_B e'_C e'_D {e_P}^2 \langle \{b(10)p(01)p(10)\}_\varepsilon | \{c(12)d(21)a(1'0)\}_\varepsilon \rangle \\
&+ e'_A e'_B e_C e'_D {e_P}^2 \langle \{b(1'0)p(01)p(10)\}_\varepsilon | \{c(1'2)d(21)a(1'0)\}_\varepsilon \rangle \\
&+ e'_A e'_B e'_C e'_D {e_P}^2 \langle \{b(1'0)p(01)p(10)\}_\varepsilon | \{c(12)d(21)a(1'0)\}_\varepsilon \rangle \\
&+ e_A e'_B e_C e_D {e_P}^2 \langle \{b(1'0)p(01)p(10)\}_\varepsilon | \{c(1'2)d(21')a(10)\}_\varepsilon \rangle \\
&+ e_A e_B e'_C e_D {e_P}^2 \langle \{b(10)p(01)p(10)\}_\varepsilon | \{c(12)d(21')a(10)\}_\varepsilon \rangle \\
&+ e_A e_B e_C e'_D {e_P}^2 \langle \{b(10)p(01)p(10)\}_\varepsilon | \{c(1'2)d(21)a(10)\}_\varepsilon \rangle \\
&+ e_A e'_B e'_C e_D {e_P}^2 \langle \{b(1'0)p(01)p(10)\}_\varepsilon | \{c(12)d(21')a(10)\}_\varepsilon \rangle \\
&+ e_A e_B e'_C e'_D {e_P}^2 \langle \{b(10)p(01)p(10)\}_\varepsilon | \{c(12)d(21)a(10)\}_\varepsilon \rangle \\
&+ e_A e'_B e_C e'_D {e_P}^2 \langle \{b(1'0)p(01)p(10)\}_\varepsilon | \{c(1'2)d(21)a(10)\}_\varepsilon \rangle \\
&+ e_A e'_B e'_C e'_D {e_P}^2 \langle \{b(1'0)p(01)p(10)\}_\varepsilon | \{c(12)d(21)a(10)\}_\varepsilon \rangle \\
&+ e_A e_B e_C e_D {e'_P}^2 \langle \{b(10)p(01')p(1'0)\}_\varepsilon | \{c(1'2)d(21')a(10)\}_\varepsilon \rangle \\
&+ e'_A e_B e_C e_D {e'_P}^2 \langle \{b(10)p(01')p(1'0)\}_\varepsilon | \{c(1'2)d(21')a(1'0)\}_\varepsilon \rangle \\
&+ e'_A e'_B e_C e_D {e'_P}^2 \langle \{b(1'0)p(01')p(1'0)\}_\varepsilon | \{c(1'2)d(21')a(1'0)\}_\varepsilon \rangle \\
&+ e'_A e_B e'_C e_D {e'_P}^2 \langle \{b(10)p(01')p(1'0)\}_\varepsilon | \{c(12)d(21')a(1'0)\}_\varepsilon \rangle \\
&+ e'_A e_B e_C e'_D {e'_P}^2 \langle \{b(10)p(01')p(1'0)\}_\varepsilon | \{c(1'2)d(21)a(1'0)\}_\varepsilon \rangle \\
&+ e'_A e'_B e'_C e_D {e'_P}^2 \langle \{b(1'0)p(01')p(1'0)\}_\varepsilon | \{c(12)d(21')a(1'0)\}_\varepsilon \rangle \\
&+ e'_A e_B e'_C e'_D {e'_P}^2 \langle \{b(10)p(01')p(1'0)\}_\varepsilon | \{c(12)d(21)a(1'0)\}_\varepsilon \rangle \\
&+ e'_A e'_B e_C e'_D {e'_P}^2 \langle \{b(1'0)p(01')p(1'0)\}_\varepsilon | \{c(1'2)d(21)a(1'0)\}_\varepsilon \rangle
\end{aligned}
$$

$$
\begin{aligned}
&+ e'_A e'_B e'_C e'_D {e'_P}^2 \langle \{b(1'0)p(01')p(1'0)\}_\varepsilon | \{c(12)d(21)a(1'0)\}_\varepsilon \rangle \\
&+ e_A e'_B e_C e_D {e'_P}^2 \langle \{b(1'0)p(01')p(1'0)\}_\varepsilon | \{c(1'2)d(21')a(10)\}_\varepsilon \rangle \\
&+ e_A e_B e'_C e_D {e'_P}^2 \langle \{b(10)p(01')p(1'0)\}_\varepsilon | \{c(12)d(21')a(10)\}_\varepsilon \rangle \\
&+ e_A e_B e_C e'_D {e'_P}^2 \langle \{b(10)p(01')p(1'0)\}_\varepsilon | \{c(1'2)d(21)a(10)\}_\varepsilon \rangle \\
&+ e_A e'_B e'_C e_D {e'_P}^2 \langle \{b(1'0)p(01')p(1'0)\}_\varepsilon | \{c(12)d(21')a(10)\}_\varepsilon \rangle \\
&+ e_A e_B e'_C e'_D {e'_P}^2 \langle \{b(10)p(01')p(1'0)\}_\varepsilon | \{c(12)d(21)a(10)\}_\varepsilon \rangle \\
&+ e_A e'_B e_C e'_D {e'_P}^2 \langle \{b(1'0)p(01')p(1'0)\}_\varepsilon | \{c(1'2)d(21)a(10)\}_\varepsilon \rangle \\
&+ e_A e'_B e'_C e'_D {e'_P}^2 \langle \{b(1'0)p(01')p(1'0)\}_\varepsilon | \{c(12)d(21)a(10)\}_\varepsilon \rangle
\end{aligned}
\tag{B.19}
$$

$$
\begin{aligned}
\langle (DCBPP)_\varepsilon | (A)_\varepsilon \rangle^{+-} = {} & e_A e_B e_C e_D {e_P}^2 \langle \{d(1'2)c(21')b(10)p(01)p(10)\}_\varepsilon | \{a(10)\}_\varepsilon \rangle \\
&+ e'_A e_B e_C e_D {e_P}^2 \langle \{d(1'2)c(21')b(10)p(01)p(10)\}_\varepsilon | \{a(1'0)\}_\varepsilon \rangle \\
&+ e'_A e'_B e_C e_D {e_P}^2 \langle \{d(1'2)c(21')b(1'0)p(01)p(10)\}_\varepsilon | \{a(1'0)\}_\varepsilon \rangle \\
&+ e'_A e_B e'_C e_D {e_P}^2 \langle \{d(1'2)c(21)b(10)p(01)p(10)\}_\varepsilon | \{a(1'0)\}_\varepsilon \rangle \\
&+ e'_A e_B e_C e'_D {e_P}^2 \langle \{d(12)c(21')b(10)p(01)p(10)\}_\varepsilon | \{a(1'0)\}_\varepsilon \rangle \\
&+ e'_A e'_B e'_C e_D {e_P}^2 \langle \{d(1'2)c(21)b(1'0)p(01)p(10)\}_\varepsilon | \{a(1'0)\}_\varepsilon \rangle \\
&+ e'_A e_B e'_C e'_D {e_P}^2 \langle \{d(12)c(21)b(10)p(01)p(10)\}_\varepsilon | \{a(1'0)\}_\varepsilon \rangle \\
&+ e'_A e'_B e_C e'_D {e_P}^2 \langle \{d(12)c(21')b(1'0)p(01)p(10)\}_\varepsilon | \{a(1'0)\}_\varepsilon \rangle \\
&+ e'_A e'_B e'_C e'_D {e_P}^2 \langle \{d(12)c(21)b(1'0)p(01)p(10)\}_\varepsilon | \{a(1'0)\}_\varepsilon \rangle \\
&+ e_A e'_B e_C e_D {e_P}^2 \langle \{d(1'2)c(21')b(1'0)p(01)p(10)\}_\varepsilon | \{a(10)\}_\varepsilon \rangle \\
&+ e_A e_B e'_C e_D {e_P}^2 \langle \{d(1'2)c(21)b(10)p(01)p(10)\}_\varepsilon | \{a(10)\}_\varepsilon \rangle \\
&+ e_A e_B e_C e'_D {e_P}^2 \langle \{d(12)c(21')b(10)p(01)p(10)\}_\varepsilon | \{a(10)\}_\varepsilon \rangle
\end{aligned}
$$

$$
\begin{aligned}
&+ e_A e'_B e'_C e_D e_P{}^2 \langle \{d(1'2)c(21)b(1'0)p(01)p(10)\}_\varepsilon | \{a(10)\}_\varepsilon \rangle \\
&+ e_A e_B e'_C e'_D e_P{}^2 \langle \{d(12)c(21)b(10)p(01)p(10)\}_\varepsilon | \{a(10)\}_\varepsilon \rangle \\
&+ e_A e'_B e_C e'_D e_P{}^2 \langle \{d(12)c(21')b(1'0)p(01)p(10)\}_\varepsilon | \{a(10)\}_\varepsilon \rangle \\
&+ e_A e'_B e'_C e'_D e_P{}^2 \langle \{d(12)c(21)b(1'0)p(01)p(10)\}_\varepsilon | \{a(10)\}_\varepsilon \rangle \\
&+ e_A e_B e_C e_D e'_P{}^2 \langle \{d(1'2)c(21')b(10)p(01')p(1'0)\}_\varepsilon | \{a(10)\}_\varepsilon \rangle \\
&+ e'_A e_B e_C e_D e'_P{}^2 \langle \{d(1'2)c(21')b(10)p(01')p(1'0)\}_\varepsilon | \{a(1'0)\}_\varepsilon \rangle \\
&+ e'_A e'_B e_C e_D e'_P{}^2 \langle \{d(1'2)c(21')b(1'0)p(01')p(1'0)\}_\varepsilon | \{a(1'0)\}_\varepsilon \rangle \\
&+ e'_A e_B e'_C e_D e'_P{}^2 \langle \{d(1'2)c(21)b(10)p(01')p(1'0)\}_\varepsilon | \{a(1'0)\}_\varepsilon \rangle \\
&+ e'_A e_B e_C e'_D e'_P{}^2 \langle \{d(12)c(21')b(10)p(01')p(1'0)\}_\varepsilon | \{a(1'0)\}_\varepsilon \rangle \\
&+ e'_A e'_B e'_C e_D e'_P{}^2 \langle \{d(1'2)c(21)b(1'0)p(01')p(1'0)\}_\varepsilon | \{a(1'0)\}_\varepsilon \rangle \\
&+ e'_A e_B e'_C e'_D e'_P{}^2 \langle \{d(12)c(21)b(10)p(01')p(1'0)\}_\varepsilon | \{a(1'0)\}_\varepsilon \rangle \\
&+ e'_A e'_B e_C e'_D e'_P{}^2 \langle \{d(12)c(21')b(1'0)p(01')p(1'0)\}_\varepsilon | \{a(1'0)\}_\varepsilon \rangle \\
&+ e'_A e'_B e'_C e'_D e'_P{}^2 \langle \{d(12)c(21)b(1'0)p(01')p(1'0)\}_\varepsilon | \{a(1'0)\}_\varepsilon \rangle \\
&+ e_A e'_B e_C e_D e'_P{}^2 \langle \{d(1'2)c(21')b(1'0)p(01')p(1'0)\}_\varepsilon | \{a(10)\}_\varepsilon \rangle \\
&+ e_A e_B e'_C e_D e'_P{}^2 \langle \{d(1'2)c(21)b(10)p(01')p(1'0)\}_\varepsilon | \{a(10)\}_\varepsilon \rangle \\
&+ e_A e_B e_C e'_D e'_P{}^2 \langle \{d(12)c(21')b(10)p(01')p(1'0)\}_\varepsilon | \{a(10)\}_\varepsilon \rangle \\
&+ e_A e'_B e'_C e_D e'_P{}^2 \langle \{d(1'2)c(21)b(1'0)p(01')p(1'0)\}_\varepsilon | \{a(10)\}_\varepsilon \rangle \\
&+ e_A e_B e'_C e'_D e'_P{}^2 \langle \{d(12)c(21)b(10)p(01')p(1'0)\}_\varepsilon | \{a(10)\}_\varepsilon \rangle \\
&+ e_A e'_B e_C e'_D e'_P{}^2 \langle \{d(12)c(21')b(1'0)p(01')p(1'0)\}_\varepsilon | \{a(10)\}_\varepsilon \rangle \\
&+ e_A e'_B e'_C e'_D e'_P{}^2 \langle \{d(12)c(21)b(1'0)p(01')p(1'0)\}_\varepsilon | \{a(10)\}_\varepsilon \rangle
\end{aligned}
\tag{B.20}
$$

$$
\begin{aligned}
\langle (CDBPP)_\varepsilon | (A)_\varepsilon \rangle^{+-} = {} & e_A e_B e_C e_D {e_P}^2 \langle \{c(10)d(01)b(10)p(01)p(10)\}_\varepsilon | \{a(10)\}_\varepsilon \rangle \\
& + e'_A e_B e_C e_D {e_P}^2 \langle \{c(10)d(01)b(10)p(01)p(10)\}_\varepsilon | \{a(1'0)\}_\varepsilon \rangle \\
& + e'_A e'_B e_C e_D {e_P}^2 \langle \{c(10)d(01)b(1'0)p(01)p(10)\}_\varepsilon | \{a(1'0)\}_\varepsilon \rangle \\
& + e'_A e_B e'_C e_D {e_P}^2 \langle \{c(1'0)d(01)b(10)p(01)p(10)\}_\varepsilon | \{a(1'0)\}_\varepsilon \rangle \\
& + e'_A e_B e_C e'_D {e_P}^2 \langle \{c(10)d(01')b(10)p(01)p(10)\}_\varepsilon | \{a(1'0)\}_\varepsilon \rangle \\
& + e'_A e'_B e'_C e_D {e_P}^2 \langle \{c(1'0)d(01)b(1'0)p(01)p(10)\}_\varepsilon | \{a(1'0)\}_\varepsilon \rangle \\
& + e'_A e_B e'_C e'_D {e_P}^2 \langle \{c(1'0)d(01')b(10)p(01)p(10)\}_\varepsilon | \{a(1'0)\}_\varepsilon \rangle \\
& + e'_A e'_B e_C e'_D {e_P}^2 \langle \{c(10)d(01')b(1'0)p(01)p(10)\}_\varepsilon | \{a(1'0)\}_\varepsilon \rangle \\
& + e'_A e'_B e'_C e'_D {e_P}^2 \langle \{c(1'0)d(01')b(1'0)p(01)p(10)\}_\varepsilon | \{a(1'0)\}_\varepsilon \rangle \\
& + e_A e'_B e_C e_D {e_P}^2 \langle \{c(10)d(01)b(1'0)p(01)p(10)\}_\varepsilon | \{a(10)\}_\varepsilon \rangle \\
& + e_A e_B e'_C e_D {e_P}^2 \langle \{c(1'0)d(01)b(10)p(01)p(10)\}_\varepsilon | \{a(10)\}_\varepsilon \rangle \\
& + e_A e_B e_C e'_D {e_P}^2 \langle \{c(10)d(01')b(10)p(01)p(10)\}_\varepsilon | \{a(10)\}_\varepsilon \rangle \\
& + e_A e'_B e'_C e_D {e_P}^2 \langle \{c(1'0)d(01)b(1'0)p(01)p(10)\}_\varepsilon | \{a(10)\}_\varepsilon \rangle \\
& + e_A e_B e'_C e'_D {e_P}^2 \langle \{c(1'0)d(01')b(10)p(01)p(10)\}_\varepsilon | \{a(10)\}_\varepsilon \rangle \\
& + e_A e'_B e_C e'_D {e_P}^2 \langle \{c(10)d(01')b(1'0)p(01)p(10)\}_\varepsilon | \{a(10)\}_\varepsilon \rangle \\
& + e_A e'_B e'_C e'_D {e_P}^2 \langle \{c(1'0)d(01')b(1'0)p(01)p(10)\}_\varepsilon | \{a(10)\}_\varepsilon \rangle \\
& + e_A e_B e_C e_D {e'_P}^2 \langle \{c(10)d(01)b(10)p(01')p(1'0)\}_\varepsilon | \{a(10)\}_\varepsilon \rangle \\
& + e'_A e_B e_C e_D {e'_P}^2 \langle \{c(10)d(01)b(10)p(01')p(1'0)\}_\varepsilon | \{a(1'0)\}_\varepsilon \rangle \\
& + e'_A e'_B e_C e_D {e'_P}^2 \langle \{c(10)d(01)b(1'0)p(01')p(1'0)\}_\varepsilon | \{a(1'0)\}_\varepsilon \rangle \\
& + e'_A e_B e'_C e_D {e'_P}^2 \langle \{c(1'0)d(01)b(10)p(01')p(1'0)\}_\varepsilon | \{a(1'0)\}_\varepsilon \rangle \\
& + e'_A e_B e_C e'_D {e'_P}^2 \langle \{c(10)d(01')b(10)p(01')p(1'0)\}_\varepsilon | \{a(1'0)\}_\varepsilon \rangle
\end{aligned}
$$

$$
\begin{aligned}
&+ e'_A e'_B e'_C e_D {e'_P}^2 \langle\{c(1'0)d(01)b(1'0)p(01')p(1'0)\}_\varepsilon|\{a(1'0)\}_\varepsilon\rangle \\
&+ e'_A e_B e'_C e'_D {e'_P}^2 \langle\{c(1'0)d(01')b(10)p(01')p(1'0)\}_\varepsilon|\{a(1'0)\}_\varepsilon\rangle \\
&+ e'_A e'_B e_C e'_D {e'_P}^2 \langle\{c(10)d(01')b(1'0)p(01')p(1'0)\}_\varepsilon|\{a(1'0)\}_\varepsilon\rangle \\
&+ e'_A e'_B e'_C e'_D {e'_P}^2 \langle\{c(1'0)d(01')b(1'0)p(01')p(1'0)\}_\varepsilon|\{a(1'0)\}_\varepsilon\rangle \\
&+ e_A e'_B e_C e_D {e'_P}^2 \langle\{c(10)d(01)b(1'0)p(01')p(1'0)\}_\varepsilon|\{a(10)\}_\varepsilon\rangle \\
&+ e_A e_B e'_C e_D {e'_P}^2 \langle\{c(1'0)d(01)b(10)p(01')p(1'0)\}_\varepsilon|\{a(10)\}_\varepsilon\rangle \\
&+ e_A e_B e_C e'_D {e'_P}^2 \langle\{c(10)d(01')b(10)p(01')p(1'0)\}_\varepsilon|\{a(10)\}_\varepsilon\rangle \\
&+ e_A e'_B e'_C e_D {e'_P}^2 \langle\{c(1'0)d(01)b(1'0)p(01')p(1'0)\}_\varepsilon|\{a(10)\}_\varepsilon\rangle \\
&+ e_A e_B e'_C e'_D {e'_P}^2 \langle\{c(1'0)d(01')b(10)p(01')p(1'0)\}_\varepsilon|\{a(10)\}_\varepsilon\rangle \\
&+ e_A e'_B e_C e'_D {e'_P}^2 \langle\{c(10)d(01')b(1'0)p(01')p(1'0)\}_\varepsilon|\{a(10)\}_\varepsilon\rangle \\
&+ e_A e'_B e'_C e'_D {e'_P}^2 \langle\{c(1'0)d(01')b(1'0)p(01')p(1'0)\}_\varepsilon|\{a(10)\}_\varepsilon\rangle
\end{aligned}
\tag{B.21}
$$

$$
\begin{aligned}
\langle(DCB)_\varepsilon|(APP)_\varepsilon\rangle^{+-} = {} & e_A e_B e_C e_D {e_P}^2 \langle\{d(1'2)c(21')b(10)\}_\varepsilon|\{a(10)p(01)p(10)\}_\varepsilon\rangle \\
&+ e'_A e_B e_C e_D {e_P}^2 \langle\{d(1'2)c(21')b(10)\}_\varepsilon|\{a(1'0)p(01)p(10)\}_\varepsilon\rangle \\
&+ e'_A e'_B e_C e_D {e_P}^2 \langle\{d(1'2)c(21')b(1'0)\}_\varepsilon|\{a(1'0)p(01)p(10)\}_\varepsilon\rangle \\
&+ e'_A e_B e'_C e_D {e_P}^2 \langle\{d(1'2)c(21)b(10)\}_\varepsilon|\{a(1'0)p(01)p(10)\}_\varepsilon\rangle \\
&+ e'_A e_B e_C e'_D {e_P}^2 \langle\{d(12)c(21')b(10)\}_\varepsilon|\{a(1'0)p(01)p(10)\}_\varepsilon\rangle \\
&+ e'_A e'_B e'_C e_D {e_P}^2 \langle\{d(1'2)c(21)b(1'0)\}_\varepsilon|\{a(1'0)p(01)p(10)\}_\varepsilon\rangle \\
&+ e'_A e_B e'_C e'_D {e_P}^2 \langle\{d(12)c(21)b(10)\}_\varepsilon|\{a(1'0)p(01)p(10)\}_\varepsilon\rangle \\
&+ e'_A e'_B e_C e'_D {e_P}^2 \langle\{d(12)c(21')b(1'0)\}_\varepsilon|\{a(1'0)p(01)p(10)\}_\varepsilon\rangle \\
&+ e'_A e'_B e'_C e'_D {e_P}^2 \langle\{d(12)c(21)b(1'0)\}_\varepsilon|\{a(1'0)p(01)p(10)\}_\varepsilon\rangle
\end{aligned}
$$

$$
\begin{aligned}
&+ e_A e'_B e_C e_D {e_P}^2 \langle \{d(1'2)c(21')b(1'0)\}_\varepsilon | \{a(10)p(01)p(10)\}_\varepsilon \rangle \\
&+ e_A e_B e'_C e_D {e_P}^2 \langle \{d(1'2)c(21)b(10)\}_\varepsilon | \{a(10)p(01)p(10)\}_\varepsilon \rangle \\
&+ e_A e_B e_C e'_D {e_P}^2 \langle \{d(12)c(21')b(10)\}_\varepsilon | \{a(10)p(01)p(10)\}_\varepsilon \rangle \\
&+ e_A e'_B e'_C e_D {e_P}^2 \langle \{d(1'2)c(21)b(1'0)\}_\varepsilon | \{a(10)p(01)p(10)\}_\varepsilon \rangle \\
&+ e_A e_B e'_C e'_D {e_P}^2 \langle \{d(12)c(21)b(10)\}_\varepsilon | \{a(10)p(01)p(10)\}_\varepsilon \rangle \\
&+ e_A e'_B e_C e'_D {e_P}^2 \langle \{d(12)c(21')b(1'0)\}_\varepsilon | \{a(10)p(01)p(10)\}_\varepsilon \rangle \\
&+ e_A e'_B e'_C e'_D {e_P}^2 \langle \{d(12)c(21)b(1'0)\}_\varepsilon | \{a(10)p(01)p(10)\}_\varepsilon \rangle \\
&+ e_A e_B e_C e_D {e'_P}^2 \langle \{d(1'2)c(21')b(10)\}_\varepsilon | \{a(10)p(01')p(1'0)\}_\varepsilon \rangle \\
&+ e'_A e_B e_C e_D {e'_P}^2 \langle \{d(1'2)c(21')b(10)\}_\varepsilon | \{a(1'0)p(01')p(1'0)\}_\varepsilon \rangle \\
&+ e'_A e'_B e_C e_D {e'_P}^2 \langle \{d(1'2)c(21')b(1'0)\}_\varepsilon | \{a(1'0)p(01')p(1'0)\}_\varepsilon \rangle \\
&+ e'_A e_B e'_C e_D {e'_P}^2 \langle \{d(1'2)c(21)b(10)\}_\varepsilon | \{a(1'0)p(01')p(1'0)\}_\varepsilon \rangle \\
&+ e'_A e_B e_C e'_D {e'_P}^2 \langle \{d(12)c(21')b(10)\}_\varepsilon | \{a(1'0)p(01')p(1'0)\}_\varepsilon \rangle \\
&+ e'_A e'_B e'_C e_D {e'_P}^2 \langle \{d(1'2)c(21)b(1'0)\}_\varepsilon | \{a(1'0)p(01')p(1'0)\}_\varepsilon \rangle \\
&+ e'_A e_B e'_C e'_D {e'_P}^2 \langle \{d(12)c(21)b(10)\}_\varepsilon | \{a(1'0)p(01')p(1'0)\}_\varepsilon \rangle \\
&+ e'_A e'_B e_C e'_D {e'_P}^2 \langle \{d(12)c(21')b(1'0)\}_\varepsilon | \{a(1'0)p(01')p(1'0)\}_\varepsilon \rangle \\
&+ e'_A e'_B e'_C e'_D {e'_P}^2 \langle \{d(12)c(21)b(1'0)\}_\varepsilon | \{a(1'0)p(01')p(1'0)\}_\varepsilon \rangle \\
&+ e_A e'_B e_C e_D {e'_P}^2 \langle \{d(1'2)c(21')b(1'0)\}_\varepsilon | \{a(10)p(01')p(1'0)\}_\varepsilon \rangle \\
&+ e_A e_B e'_C e_D {e'_P}^2 \langle \{d(1'2)c(21)b(10)\}_\varepsilon | \{a(10)p(01')p(1'0)\}_\varepsilon \rangle \\
&+ e_A e_B e_C e'_D {e'_P}^2 \langle \{d(12)c(21')b(10)\}_\varepsilon | \{a(10)p(01')p(1'0)\}_\varepsilon \rangle \\
&+ e_A e'_B e'_C e_D {e'_P}^2 \langle \{d(1'2)c(21)b(1'0)\}_\varepsilon | \{a(10)p(01')p(1'0)\}_\varepsilon \rangle \\
&+ e_A e_B e'_C e'_D {e'_P}^2 \langle \{d(12)c(21)b(10)\}_\varepsilon | \{a(10)p(01')p(1'0)\}_\varepsilon \rangle \\
&+ e_A e'_B e_C e'_D {e'_P}^2 \langle \{d(12)c(21')b(1'0)\}_\varepsilon | \{a(10)p(01')p(1'0)\}_\varepsilon \rangle
\end{aligned}
$$

$$+ e_A e'_B e'_C e'_D {e'_P}^2 \langle\{d(12)c(21)b(1'0)\}_\varepsilon|\{a(10)p(01')p(1'0)\}_\varepsilon\rangle \tag{B.22}$$

$$\begin{aligned}
\langle(CDB)_\varepsilon|(APP)_\varepsilon\rangle^{+-} &= e_A e_B e_C e_D {e_P}^2 \langle\{c(10)d(01)b(10)\}_\varepsilon|\{a(10)p(01)p(10)\}_\varepsilon\rangle \\
&+ e'_A e_B e_C e_D {e_P}^2 \langle\{c(10)d(01)b(10)\}_\varepsilon|\{a(1'0)p(01)p(10)\}_\varepsilon\rangle \\
&+ e'_A e'_B e_C e_D {e_P}^2 \langle\{c(10)d(01)b(1'0)\}_\varepsilon|\{a(1'0)p(01)p(10)\}_\varepsilon\rangle \\
&+ e'_A e_B e'_C e_D {e_P}^2 \langle\{c(1'0)d(01)b(10)\}_\varepsilon|\{a(1'0)p(01)p(10)\}_\varepsilon\rangle \\
&+ e'_A e_B e_C e'_D {e_P}^2 \langle\{c(10)d(01')b(10)\}_\varepsilon|\{a(1'0)p(01)p(10)\}_\varepsilon\rangle \\
&+ e'_A e'_B e'_C e_D {e_P}^2 \langle\{c(1'0)d(01)b(1'0)\}_\varepsilon|\{a(1'0)p(01)p(10)\}_\varepsilon\rangle \\
&+ e'_A e_B e'_C e'_D {e_P}^2 \langle\{c(1'0)d(01')b(10)\}_\varepsilon|\{a(1'0)p(01)p(10)\}_\varepsilon\rangle \\
&+ e'_A e'_B e_C e'_D {e_P}^2 \langle\{c(10)d(01')b(1'0)\}_\varepsilon|\{a(1'0)p(01)p(10)\}_\varepsilon\rangle \\
&+ e'_A e'_B e'_C e'_D {e_P}^2 \langle\{c(1'0)d(01')b(1'0)\}_\varepsilon|\{a(1'0)p(01)p(10)\}_\varepsilon\rangle \\
&+ e_A e'_B e_C e_D {e_P}^2 \langle\{c(10)d(01)b(1'0)\}_\varepsilon|\{a(10)p(01)p(10)\}_\varepsilon\rangle \\
&+ e_A e_B e'_C e_D {e_P}^2 \langle\{c(1'0)d(01)b(10)\}_\varepsilon|\{a(10)p(01)p(10)\}_\varepsilon\rangle \\
&+ e_A e_B e_C e'_D {e_P}^2 \langle\{c(10)d(01')b(10)\}_\varepsilon|\{a(10)p(01)p(10)\}_\varepsilon\rangle \\
&+ e_A e'_B e'_C e_D {e_P}^2 \langle\{c(1'0)d(01)b(1'0)\}_\varepsilon|\{a(10)p(01)p(10)\}_\varepsilon\rangle \\
&+ e_A e_B e'_C e'_D {e_P}^2 \langle\{c(1'0)d(01')b(10)\}_\varepsilon|\{a(10)p(01)p(10)\}_\varepsilon\rangle \\
&+ e_A e'_B e_C e'_D {e_P}^2 \langle\{c(10)d(01')b(1'0)\}_\varepsilon|\{a(10)p(01)p(10)\}_\varepsilon\rangle \\
&+ e_A e'_B e'_C e'_D {e_P}^2 \langle\{c(1'0)d(01')b(1'0)\}_\varepsilon|\{a(10)p(01)p(10)\}_\varepsilon\rangle \\
&+ e_A e_B e_C e_D {e'_P}^2 \langle\{c(10)d(01)b(10)\}_\varepsilon|\{a(10)p(01')p(1'0)\}_\varepsilon\rangle \\
&+ e'_A e_B e_C e_D {e'_P}^2 \langle\{c(10)d(01)b(10)\}_\varepsilon|\{a(1'0)p(01')p(1'0)\}_\varepsilon\rangle \\
&+ e'_A e'_B e_C e_D {e'_P}^2 \langle\{c(10)d(01)b(1'0)\}_\varepsilon|\{a(1'0)p(01')p(1'0)\}_\varepsilon\rangle
\end{aligned}$$

$$
\begin{aligned}
&+ e'_A e_B e'_C e_D {e'_P}^2 \langle\{c(1'0)d(01)b(10)\}_\varepsilon|\{a(1'0)p(01')p(1'0)\}_\varepsilon\rangle \\
&+ e'_A e_B e_C e'_D {e'_P}^2 \langle\{c(10)d(01')b(10)\}_\varepsilon|\{a(1'0)p(01')p(1'0)\}_\varepsilon\rangle \\
&+ e'_A e'_B e'_C e_D {e'_P}^2 \langle\{c(1'0)d(01)b(1'0)\}_\varepsilon|\{a(1'0)p(01')p(1'0)\}_\varepsilon\rangle \\
&+ e'_A e_B e'_C e'_D {e'_P}^2 \langle\{c(1'0)d(01')b(10)\}_\varepsilon|\{a(1'0)p(01')p(1'0)\}_\varepsilon\rangle \\
&+ e'_A e'_B e_C e'_D {e'_P}^2 \langle\{c(10)d(01')b(1'0)\}_\varepsilon|\{a(1'0)p(01')p(1'0)\}_\varepsilon\rangle \\
&+ e'_A e'_B e'_C e'_D {e'_P}^2 \langle\{c(1'0)d(01')b(1'0)\}_\varepsilon|\{a(1'0)p(01')p(1'0)\}_\varepsilon\rangle \\
&+ e_A e'_B e_C e_D {e'_P}^2 \langle\{c(10)d(01)b(1'0)\}_\varepsilon|\{a(10)p(01')p(1'0)\}_\varepsilon\rangle \\
&+ e_A e_B e'_C e_D {e'_P}^2 \langle\{c(1'0)d(01)b(10)\}_\varepsilon|\{a(10)p(01')p(1'0)\}_\varepsilon\rangle \\
&+ e_A e_B e_C e'_D {e'_P}^2 \langle\{c(10)d(01')b(10)\}_\varepsilon|\{a(10)p(01')p(1'0)\}_\varepsilon\rangle \\
&+ e_A e'_B e'_C e_D {e'_P}^2 \langle\{c(1'0)d(01)b(1'0)\}_\varepsilon|\{a(10)p(01')p(1'0)\}_\varepsilon\rangle \\
&+ e_A e_B e'_C e'_D {e'_P}^2 \langle\{c(1'0)d(01')b(10)\}_\varepsilon|\{a(10)p(01')p(1'0)\}_\varepsilon\rangle \\
&+ e_A e'_B e_C e'_D {e'_P}^2 \langle\{c(10)d(01')b(1'0)\}_\varepsilon|\{a(10)p(01')p(1'0)\}_\varepsilon\rangle \\
&+ e_A e'_B e'_C e'_D {e'_P}^2 \langle\{c(1'0)d(01')b(1'0)\}_\varepsilon|\{a(10)p(01')p(1'0)\}_\varepsilon\rangle
\end{aligned}
\tag{B.23}
$$

$$
\begin{aligned}
\langle(C)_\varepsilon|(DBAPP)_\varepsilon\rangle^{+-} &= e_A e_B e_C e_D {e_P}^2 \langle\{c(10)\}_\varepsilon|\{d(10)b(01)a(10)p(01)p(10)\}_\varepsilon\rangle \\
&+ e'_A e_B e_C e_D {e_P}^2 \langle\{c(10)\}_\varepsilon|\{d(10)b(01)a(1'0)p(01)p(10)\}_\varepsilon\rangle \\
&+ e'_A e'_B e_C e_D {e_P}^2 \langle\{c(10)\}_\varepsilon|\{d(10)b(01')a(1'0)p(01)p(10)\}_\varepsilon\rangle \\
&+ e'_A e_B e'_C e_D {e_P}^2 \langle\{c(1'0)\}_\varepsilon|\{d(10)b(01)a(1'0)p(01)p(10)\}_\varepsilon\rangle \\
&+ e'_A e_B e_C e'_D {e_P}^2 \langle\{c(10)\}_\varepsilon|\{d(1'0)b(01)a(1'0)p(01)p(10)\}_\varepsilon\rangle \\
&+ e'_A e'_B e'_C e_D {e_P}^2 \langle\{c(1'0)\}_\varepsilon|\{d(10)b(01')a(1'0)p(01)p(10)\}_\varepsilon\rangle \\
&+ e'_A e_B e'_C e'_D {e_P}^2 \langle\{c(1'0)\}_\varepsilon|\{d(1'0)b(01)a(1'0)p(01)p(10)\}_\varepsilon\rangle
\end{aligned}
$$

$$
\begin{aligned}
&+ e'_A e'_B e_C e'_D e_P{}^2 \langle \{c(10)\}_\varepsilon | \{d(1'0)b(01')a(1'0)p(01)p(10)\}_\varepsilon \rangle \\
&+ e'_A e'_B e'_C e'_D e_P{}^2 \langle \{c(1'0)\}_\varepsilon | \{d(1'0)b(01')a(1'0)p(01)p(10)\}_\varepsilon \rangle \\
&+ e_A e'_B e_C e_D e_P{}^2 \langle \{c(10)\}_\varepsilon | \{d(10)b(01')a(10)p(01)p(10)\}_\varepsilon \rangle \\
&+ e_A e_B e'_C e_D e_P{}^2 \langle \{c(1'0)\}_\varepsilon | \{d(10)b(01)a(10)p(01)p(10)\}_\varepsilon \rangle \\
&+ e_A e_B e_C e'_D e_P{}^2 \langle \{c(10)\}_\varepsilon | \{d(1'0)b(01)a(10)p(01)p(10)\}_\varepsilon \rangle \\
&+ e_A e'_B e'_C e_D e_P{}^2 \langle \{c(1'0)\}_\varepsilon | \{d(10)b(01')a(10)p(01)p(10)\}_\varepsilon \rangle \\
&+ e_A e_B e'_C e'_D e_P{}^2 \langle \{c(1'0)\}_\varepsilon | \{d(1'0)b(01)a(10)p(01)p(10)\}_\varepsilon \rangle \\
&+ e_A e'_B e_C e'_D e_P{}^2 \langle \{c(10)\}_\varepsilon | \{d(1'0)b(01')a(10)p(01)p(10)\}_\varepsilon \rangle \\
&+ e_A e'_B e'_C e'_D e_P{}^2 \langle \{c(1'0)\}_\varepsilon | \{d(1'0)b(01')a(10)p(01)p(10)\}_\varepsilon \rangle \\
&+ e_A e_B e_C e_D e'_P{}^2 \langle \{c(10)\}_\varepsilon | \{d(10)b(01)a(10)p(01')p(1'0)\}_\varepsilon \rangle \\
&+ e'_A e_B e_C e_D e'_P{}^2 \langle \{c(10)\}_\varepsilon | \{d(10)b(01)a(1'0)p(01')p(1'0)\}_\varepsilon \rangle \\
&+ e'_A e'_B e_C e_D e'_P{}^2 \langle \{c(10)\}_\varepsilon | \{d(10)b(01')a(1'0)p(01')p(1'0)\}_\varepsilon \rangle \\
&+ e'_A e_B e'_C e_D e'_P{}^2 \langle \{c(1'0)\}_\varepsilon | \{d(10)b(01)a(1'0)p(01')p(1'0)\}_\varepsilon \rangle \\
&+ e'_A e_B e_C e'_D e'_P{}^2 \langle \{c(10)\}_\varepsilon | \{d(1'0)b(01)a(1'0)p(01')p(1'0)\}_\varepsilon \rangle \\
&+ e'_A e'_B e'_C e_D e'_P{}^2 \langle \{c(1'0)\}_\varepsilon | \{d(10)b(01')a(1'0)p(01')p(1'0)\}_\varepsilon \rangle \\
&+ e'_A e_B e'_C e'_D e'_P{}^2 \langle \{c(1'0)\}_\varepsilon | \{d(1'0)b(01)a(1'0)p(01')p(1'0)\}_\varepsilon \rangle \\
&+ e'_A e'_B e_C e'_D e'_P{}^2 \langle \{c(10)\}_\varepsilon | \{d(1'0)b(01')a(1'0)p(01')p(1'0)\}_\varepsilon \rangle \\
&+ e'_A e'_B e'_C e'_D e'_P{}^2 \langle \{c(1'0)\}_\varepsilon | \{d(1'0)b(01')a(1'0)p(01')p(1'0)\}_\varepsilon \rangle \\
&+ e_A e'_B e_C e_D e'_P{}^2 \langle \{c(10)\}_\varepsilon | \{d(10)b(01')a(10)p(01')p(1'0)\}_\varepsilon \rangle \\
&+ e_A e_B e'_C e_D e'_P{}^2 \langle \{c(1'0)\}_\varepsilon | \{d(10)b(01)a(10)p(01')p(1'0)\}_\varepsilon \rangle \\
&+ e_A e_B e_C e'_D e'_P{}^2 \langle \{c(10)\}_\varepsilon | \{d(1'0)b(01)a(10)p(01')p(1'0)\}_\varepsilon \rangle \\
&+ e_A e'_B e'_C e_D e'_P{}^2 \langle \{c(1'0)\}_\varepsilon | \{d(10)b(01')a(10)p(01')p(1'0)\}_\varepsilon \rangle \\
&+ e_A e_B e'_C e'_D e'_P{}^2 \langle \{c(1'0)\}_\varepsilon | \{d(1'0)b(01)a(10)p(01')p(1'0)\}_\varepsilon \rangle
\end{aligned}
$$

$$
\begin{aligned}
&+ e_A e'_B e_C e'_D {e'_P}^2 \langle \{c(10)\}_\varepsilon | \{d(1'0)b(01')a(10)p(01')p(1'0)\}_\varepsilon \rangle \\
&+ e_A e'_B e'_C e'_D {e'_P}^2 \langle \{c(1'0)\}_\varepsilon | \{d(1'0)b(01')a(10)p(01')p(1'0)\}_\varepsilon \rangle
\end{aligned} \tag{B.24}
$$

$$
\begin{aligned}
\langle (CPP)_\varepsilon | (DBA)_\varepsilon \rangle^{+-} = {} & e_A e_B e_C e_D {e_P}^2 \langle \{c(10)p(01)p(10)\}_\varepsilon | \{d(10)b(01)a(10)\}_\varepsilon \rangle \\
&+ e'_A e_B e_C e_D {e_P}^2 \langle \{c(10)p(01)p(10)\}_\varepsilon | \{d(10)b(01)a(1'0)\}_\varepsilon \rangle \\
&+ e'_A e'_B e_C e_D {e_P}^2 \langle \{c(10)p(01)p(10)\}_\varepsilon | \{d(10)b(01')a(1'0)\}_\varepsilon \rangle \\
&+ e'_A e_B e'_C e_D {e_P}^2 \langle \{c(1'0)p(01)p(10)\}_\varepsilon | \{d(10)b(01)a(1'0)\}_\varepsilon \rangle \\
&+ e'_A e_B e_C e'_D {e_P}^2 \langle \{c(10)p(01)p(10)\}_\varepsilon | \{d(1'0)b(01)a(1'0)\}_\varepsilon \rangle \\
&+ e'_A e'_B e'_C e_D {e_P}^2 \langle \{c(1'0)p(01)p(10)\}_\varepsilon | \{d(10)b(01')a(1'0)\}_\varepsilon \rangle \\
&+ e'_A e_B e'_C e'_D {e_P}^2 \langle \{c(1'0)p(01)p(10)\}_\varepsilon | \{d(1'0)b(01)a(1'0)\}_\varepsilon \rangle \\
&+ e'_A e'_B e_C e'_D {e_P}^2 \langle \{c(10)p(01)p(10)\}_\varepsilon | \{d(1'0)b(01')a(1'0)\}_\varepsilon \rangle \\
&+ e'_A e'_B e'_C e'_D {e_P}^2 \langle \{c(1'0)p(01)p(10)\}_\varepsilon | \{d(1'0)b(01')a(1'0)\}_\varepsilon \rangle \\
&+ e_A e'_B e_C e_D {e_P}^2 \langle \{c(10)p(01)p(10)\}_\varepsilon | \{d(10)b(01')a(10)\}_\varepsilon \rangle \\
&+ e_A e_B e'_C e_D {e_P}^2 \langle \{c(1'0)p(01)p(10)\}_\varepsilon | \{d(10)b(01)a(10)\}_\varepsilon \rangle \\
&+ e_A e_B e_C e'_D {e_P}^2 \langle \{c(10)p(01)p(10)\}_\varepsilon | \{d(1'0)b(01)a(10)\}_\varepsilon \rangle \\
&+ e_A e'_B e'_C e_D {e_P}^2 \langle \{c(1'0)p(01)p(10)\}_\varepsilon | \{d(10)b(01')a(10)\}_\varepsilon \rangle \\
&+ e_A e_B e'_C e'_D {e_P}^2 \langle \{c(1'0)p(01)p(10)\}_\varepsilon | \{d(1'0)b(01)a(10)\}_\varepsilon \rangle \\
&+ e_A e'_B e_C e'_D {e_P}^2 \langle \{c(10)p(01)p(10)\}_\varepsilon | \{d(1'0)b(01')a(10)\}_\varepsilon \rangle \\
&+ e_A e'_B e'_C e'_D {e_P}^2 \langle \{c(1'0)p(01)p(10)\}_\varepsilon | \{d(1'0)b(01')a(10)\}_\varepsilon \rangle \\
&+ e_A e_B e_C e_D {e'_P}^2 \langle \{c(10)p(01')p(1'0)\}_\varepsilon | \{d(10)b(01)a(10)\}_\varepsilon \rangle \\
&+ e'_A e_B e_C e_D {e'_P}^2 \langle \{c(10)p(01')p(1'0)\}_\varepsilon | \{d(10)b(01)a(1'0)\}_\varepsilon \rangle
\end{aligned}
$$

$$
\begin{aligned}
&+ e'_A e'_B e_C e_D {e'_P}^2 \langle\{c(10)p(01')p(1'0)\}_\varepsilon|\{d(10)b(01')a(1'0)\}_\varepsilon\rangle \\
&+ e'_A e_B e'_C e_D {e'_P}^2 \langle\{c(1'0)p(01')p(1'0)\}_\varepsilon|\{d(10)b(01)a(1'0)\}_\varepsilon\rangle \\
&+ e'_A e_B e_C e'_D {e'_P}^2 \langle\{c(10)p(01')p(1'0)\}_\varepsilon|\{d(1'0)b(01)a(1'0)\}_\varepsilon\rangle \\
&+ e'_A e'_B e'_C e_D {e'_P}^2 \langle\{c(1'0)p(01')p(1'0)\}_\varepsilon|\{d(10)b(01')a(1'0)\}_\varepsilon\rangle \\
&+ e'_A e_B e'_C e'_D {e'_P}^2 \langle\{c(1'0)p(01')p(1'0)\}_\varepsilon|\{d(1'0)b(01)a(1'0)\}_\varepsilon\rangle \\
&+ e'_A e'_B e_C e'_D {e'_P}^2 \langle\{c(10)p(01')p(1'0)\}_\varepsilon|\{d(1'0)b(01')a(1'0)\}_\varepsilon\rangle \\
&+ e'_A e'_B e'_C e'_D {e'_P}^2 \langle\{c(1'0)p(01')p(1'0)\}_\varepsilon|\{d(1'0)b(01')a(1'0)\}_\varepsilon\rangle \\
&+ e_A e'_B e_C e_D {e'_P}^2 \langle\{c(10)p(01')p(1'0)\}_\varepsilon|\{d(10)b(01')a(10)\}_\varepsilon\rangle \\
&+ e_A e_B e'_C e_D {e'_P}^2 \langle\{c(1'0)p(01')p(1'0)\}_\varepsilon|\{d(10)b(01)a(10)\}_\varepsilon\rangle \\
&+ e_A e_B e_C e'_D {e'_P}^2 \langle\{c(10)p(01')p(1'0)\}_\varepsilon|\{d(1'0)b(01)a(10)\}_\varepsilon\rangle \\
&+ e_A e'_B e'_C e_D {e'_P}^2 \langle\{c(1'0)p(01')p(1'0)\}_\varepsilon|\{d(10)b(01')a(10)\}_\varepsilon\rangle \\
&+ e_A e_B e'_C e'_D {e'_P}^2 \langle\{c(1'0)p(01')p(1'0)\}_\varepsilon|\{d(1'0)b(01)a(10)\}_\varepsilon\rangle \\
&+ e_A e'_B e_C e'_D {e'_P}^2 \langle\{c(10)p(01')p(1'0)\}_\varepsilon|\{d(1'0)b(01')a(10)\}_\varepsilon\rangle \\
&+ e_A e'_B e'_C e'_D {e'_P}^2 \langle\{c(1'0)p(01')p(1'0)\}_\varepsilon|\{d(1'0)b(01')a(10)\}_\varepsilon\rangle
\end{aligned}
\tag{B.25}
$$

$$
\begin{aligned}
\langle(CABPP)_\varepsilon|(D)_\varepsilon\rangle^{+-} = {} & e_A e_B e_C e_D {e_P}^2 \langle\{c(10)a(01)b(10)p(01)p(10)\}_\varepsilon|\{d(10)\}_\varepsilon\rangle \\
&+ e'_A e'_B e_C e_D {e_P}^2 \langle\{c(10)a(01')b(1'0)p(01)p(10)\}_\varepsilon|\{d(10)\}_\varepsilon\rangle \\
&+ e'_A e'_B e'_C e_D {e_P}^2 \langle\{c(1'0)a(01')b(1'0)p(01)p(10)\}_\varepsilon|\{d(10)\}_\varepsilon\rangle \\
&+ e'_A e'_B e_C e'_D {e_P}^2 \langle\{c(10)a(01')b(1'0)p(01)p(10)\}_\varepsilon|\{d(1'0)\}_\varepsilon\rangle \\
&+ e'_A e'_B e'_C e'_D {e_P}^2 \langle\{c(1'0)a(01')b(1'0)p(01)p(10)\}_\varepsilon|\{d(1'0)\}_\varepsilon\rangle \\
&+ e_A e_B e'_C e_D {e_P}^2 \langle\{c(1'0)a(01)b(10)p(01)p(10)\}_\varepsilon|\{d(10)\}_\varepsilon\rangle
\end{aligned}
$$

$$
\begin{aligned}
&+ e_A e_B e_C e'_D {e_P}^2 \langle \{c(10)a(01)b(10)p(01)p(10)\}_\varepsilon | \{d(1'0)\}_\varepsilon \rangle \\
&+ e_A e_B e'_C e'_D {e_P}^2 \langle \{c(1'0)a(01)b(10)p(01)p(10)\}_\varepsilon | \{d(1'0)\}_\varepsilon \rangle \\
&+ e_A e_B e_C e_D {e'_P}^2 \langle \{c(10)a(01)b(10)p(01')p(1'0)\}_\varepsilon | \{d(10)\}_\varepsilon \rangle \\
&+ e'_A e'_B e_C e_D {e'_P}^2 \langle \{c(10)a(01')b(1'0)p(01')p(1'0)\}_\varepsilon | \{d(10)\}_\varepsilon \rangle \\
&+ e'_A e'_B e'_C e_D {e'_P}^2 \langle \{c(1'0)a(01')b(1'0)p(01')p(1'0)\}_\varepsilon | \{d(10)\}_\varepsilon \rangle \\
&+ e'_A e'_B e_C e'_D {e'_P}^2 \langle \{c(10)a(01')b(1'0)p(01')p(1'0)\}_\varepsilon | \{d(1'0)\}_\varepsilon \rangle \\
&+ e'_A e'_B e'_C e'_D {e'_P}^2 \langle \{c(1'0)a(01')b(1'0)p(01')p(1'0)\}_\varepsilon | \{d(1'0)\}_\varepsilon \rangle \\
&+ e_A e_B e'_C e_D {e'_P}^2 \langle \{c(1'0)a(01)b(10)p(01')p(1'0)\}_\varepsilon | \{d(10)\}_\varepsilon \rangle \\
&+ e_A e_B e_C e'_D {e'_P}^2 \langle \{c(10)a(01)b(10)p(01')p(1'0)\}_\varepsilon | \{d(1'0)\}_\varepsilon \rangle \\
&+ e_A e_B e'_C e'_D {e'_P}^2 \langle \{c(1'0)a(01)b(10)p(01')p(1'0)\}_\varepsilon | \{d(1'0)\}_\varepsilon \rangle
\end{aligned}
\tag{B.26}
$$

$$
\begin{aligned}
\langle (CAB)_\varepsilon | (DPP)_\varepsilon \rangle^{+-} = {} & e_A e_B e_C e_D {e_P}^2 \langle \{c(10)a(01)b(10)\}_\varepsilon | \{d(10)p(01)p(10)\}_\varepsilon \rangle \\
&+ e'_A e'_B e_C e_D {e_P}^2 \langle \{c(10)a(01')b(1'0)\}_\varepsilon | \{d(10)p(01)p(10)\}_\varepsilon \rangle \\
&+ e'_A e'_B e'_C e_D {e_P}^2 \langle \{c(1'0)a(01')b(1'0)\}_\varepsilon | \{d(10)p(01)p(10)\}_\varepsilon \rangle \\
&+ e'_A e'_B e_C e'_D {e_P}^2 \langle \{c(10)a(01')b(1'0)\}_\varepsilon | \{d(1'0)p(01)p(10)\}_\varepsilon \rangle \\
&+ e'_A e'_B e'_C e'_D {e_P}^2 \langle \{c(1'0)a(01')b(1'0)\}_\varepsilon | \{d(1'0)p(01)p(10)\}_\varepsilon \rangle \\
&+ e_A e_B e'_C e_D {e_P}^2 \langle \{c(1'0)a(01)b(10)\}_\varepsilon | \{d(10)p(01)p(10)\}_\varepsilon \rangle \\
&+ e_A e_B e_C e'_D {e_P}^2 \langle \{c(10)a(01)b(10)\}_\varepsilon | \{d(1'0)p(01)p(10)\}_\varepsilon \rangle \\
&+ e_A e_B e'_C e'_D {e_P}^2 \langle \{c(1'0)a(01)b(10)\}_\varepsilon | \{d(1'0)p(01)p(10)\}_\varepsilon \rangle \\
&+ e_A e_B e_C e_D {e'_P}^2 \langle \{c(10)a(01)b(10)\}_\varepsilon | \{d(10)p(01')p(1'0)\}_\varepsilon \rangle \\
&+ e'_A e'_B e_C e_D {e'_P}^2 \langle \{c(10)a(01')b(1'0)\}_\varepsilon | \{d(10)p(01')p(1'0)\}_\varepsilon \rangle
\end{aligned}
$$

$$
\begin{aligned}
&+ e'_A e'_B e'_C e_D {e'_P}^2 \langle \{c(1'0)a(01')b(1'0)\}_\varepsilon | \{d(10)p(01')p(1'0)\}_\varepsilon \rangle \\
&+ e'_A e'_B e_C e'_D {e'_P}^2 \langle \{c(10)a(01')b(1'0)\}_\varepsilon | \{d(1'0)p(01')p(1'0)\}_\varepsilon \rangle \\
&+ e'_A e'_B e'_C e'_D {e'_P}^2 \langle \{c(1'0)a(01')b(1'0)\}_\varepsilon | \{d(1'0)p(01')p(1'0)\}_\varepsilon \rangle \\
&+ e_A e_B e'_C e_D {e'_P}^2 \langle \{c(1'0)a(01)b(10)\}_\varepsilon | \{d(10)p(01')p(1'0)\}_\varepsilon \rangle \\
&+ e_A e_B e_C e'_D {e'_P}^2 \langle \{c(10)a(01)b(10)\}_\varepsilon | \{d(1'0)p(01')p(1'0)\}_\varepsilon \rangle \\
&+ e_A e_B e'_C e'_D {e'_P}^2 \langle \{c(1'0)a(01)b(10)\}_\varepsilon | \{d(1'0)p(01')p(1'0)\}_\varepsilon \rangle
\end{aligned}
\tag{B.27}
$$

APPENDIX C

PUMP-PROBE LIMIT OF MD-WPI SIGNAL FOLLOWING CONTROL PULSE

Here we provide detailed expressions for the pump-probe limit to the multidimensional wave-packet interferometry signal from an energy transfer complex subjected to a pre-resonant control pulse (derived in Section D of Chapter II). The signal is composed of three components

$$\Theta_\varepsilon = \Theta_\varepsilon^{GSB} + \Theta_\varepsilon^{ESA} + \Theta_\varepsilon^{SE} \,. \tag{C.1}$$

$$\Theta_\varepsilon^{GSB} = 8\mathrm{Re}\left(\langle (C)_\varepsilon | (DBAPP)_\varepsilon \rangle^{+-} + \langle (CPP)_\varepsilon | (DBA)_\varepsilon \rangle^{+-}\right) \tag{C.2}$$

$$\Theta_\varepsilon^{ESA} = 8\mathrm{Re}\left(\langle (B)_\varepsilon | (CDAPP)_\varepsilon \rangle^{+-} + \langle (BPP)_\varepsilon | (CDA)_\varepsilon \rangle^{+-}\right) \tag{C.3}$$

$$\Theta_\varepsilon^{SE} = 8\mathrm{Re}\left(\langle (B)_\varepsilon | (DCAPP)_\varepsilon \rangle^{+-} + \langle (BPP)_\varepsilon | (DCA)_\varepsilon \rangle^{+-}\right) \tag{C.4}$$

In the ground-state bleach terms, the *A-B* pulse acts twice to return amplitude to the ground electronic state. In the remaining terms, the *C-D* pulse acts twice on a wave packet already prepared in an excited electronic state by the *A-B* pulse ($\varepsilon \leftarrow 2 \leftarrow \varepsilon$ for excited-state absorption and $\varepsilon \leftarrow 0 \leftarrow \varepsilon$ for stimulated emission).

In the GSB terms the contributing amplitudes are in the electronic-ground state during the inter-pulse delay t_{CA}. Since we ignore energy transfer on the short timescale of interaction with the pulse, these contributions are therefore insensitive to EET (i.e. they do not change in going to the $J \rightarrow 0$ limit). In the SE and ESA terms, however, both the bra and

ket evolve in the one-exciton manifold during t_{CA}. Accounting for the possibility of energy transfer during this interval, these terms therefore contain four times as many contributions as the GSB terms.

$$\begin{aligned}
\langle (C)_\varepsilon | (DBAPP)_\varepsilon \rangle^{+-} = {} & e_A e_B e_C e_D {e_P}^2 \langle \{c(10)\}_\varepsilon | \{c(10)a(01)a(10)p(01)p(10)\}_\varepsilon \rangle \\
& + e'_A e'_B e_C e_D e_P{}^2 \langle \{c(10)\}_\varepsilon | \{c(10)a(01')a(1'0)p(01)p(10)\}_\varepsilon \rangle \\
& + e'_A e'_B e'_C e'_D e_P{}^2 \langle \{c(1'0)\}_\varepsilon | \{c(1'0)a(01')a(1'0)p(01)p(10)\}_\varepsilon \rangle \\
& + e_A e_B e'_C e'_D e_P{}^2 \langle \{c(1'0)\}_\varepsilon | \{c(1'0)a(01)a(10)p(01)p(10)\}_\varepsilon \rangle \\
& + e_A e_B e_C e_D e'_P{}^2 \langle \{c(10)\}_\varepsilon | \{c(10)a(01)a(10)p(01')p(1'0)\}_\varepsilon \rangle \\
& + e'_A e'_B e_C e_D e'_P{}^2 \langle \{c(10)\}_\varepsilon | \{c(10)a(01')a(1'0)p(01')p(1'0)\}_\varepsilon \rangle \\
& + e'_A e'_B e'_C e'_D e'_P{}^2 \langle \{c(1'0)\}_\varepsilon | \{c(1'0)a(01')a(1'0)p(01')p(1'0)\}_\varepsilon \rangle \\
& + e_A e_B e'_C e'_D e'_P{}^2 \langle \{c(1'0)\}_\varepsilon | \{c(1'0)a(01)a(10)p(01')p(1'0)\}_\varepsilon \rangle
\end{aligned} \tag{C.5}$$

$$\begin{aligned}
\langle (CPP)_\varepsilon | (DBA)_\varepsilon \rangle^{+-} = {} & e_A e_B e_C e_D {e_P}^2 \langle \{c(10)p(01)p(10)\}_\varepsilon | \{c(10)a(01)a(10)\}_\varepsilon \rangle \\
& + e'_A e'_B e_C e_D e_P{}^2 \langle \{c(10)p(01)p(10)\}_\varepsilon | \{c(10)a(01')a(1'0)\}_\varepsilon \rangle \\
& + e'_A e'_B e'_C e'_D e_P{}^2 \langle \{c(1'0)p(01)p(10)\}_\varepsilon | \{c(1'0)a(01')a(1'0)\}_\varepsilon \rangle \\
& + e_A e_B e'_C e'_D e_P{}^2 \langle \{c(1'0)p(01)p(10)\}_\varepsilon | \{c(1'0)a(01)a(10)\}_\varepsilon \rangle \\
& + e_A e_B e_C e_D e'_P{}^2 \langle \{c(10)p(01')p(1'0)\}_\varepsilon | \{c(10)a(01)a(10)\}_\varepsilon \rangle \\
& + e'_A e'_B e_C e_D e'_P{}^2 \langle \{c(10)p(01')p(1'0)\}_\varepsilon | \{c(10)a(01')a(1'0)\}_\varepsilon \rangle \\
& + e'_A e'_B e'_C e'_D e'_P{}^2 \langle \{c(1'0)p(01')p(1'0)\}_\varepsilon | \{c(1'0)a(01')a(1'0)\}_\varepsilon \rangle
\end{aligned}$$

$$+ e_A e_B e'_C e'_D {e'_P}^2 \langle\{c(1'0)p(01')p(1'0)\}_\varepsilon|\{c(1'0)a(01)a(10)\}_\varepsilon\rangle \tag{C.6}$$

$$\begin{aligned}
\langle(B)_\varepsilon|(CDAPP)_\varepsilon\rangle^{+-} &= e_A e_B e_C e_D {e_P}^2 \langle\{a(10)\}_\varepsilon|\{c(1'2)c(21')a(10)p(01)p(10)\}_\varepsilon\rangle \\
&+ e'_A e_B e_C e_D {e_P}^2 \langle\{a(10)\}_\varepsilon|\{c(1'2)c(21')a(1'0)p(01)p(10)\}_\varepsilon\rangle \\
&+ e'_A e'_B e_C e_D {e_P}^2 \langle\{a(1'0)\}_\varepsilon|\{c(1'2)c(21')a(1'0)p(01)p(10)\}_\varepsilon\rangle \\
&+ e'_A e_B e'_C e_D {e_P}^2 \langle\{a(10)\}_\varepsilon|\{c(12)c(21')a(1'0)p(01)p(10)\}_\varepsilon\rangle \\
&+ e'_A e_B e_C e'_D {e_P}^2 \langle\{a(10)\}_\varepsilon|\{c(1'2)c(21)a(1'0)p(01)p(10)\}_\varepsilon\rangle \\
&+ e'_A e'_B e'_C e_D {e_P}^2 \langle\{a(1'0)\}_\varepsilon|\{c(12)c(21')a(1'0)p(01)p(10)\}_\varepsilon\rangle \\
&+ e'_A e_B e'_C e'_D {e_P}^2 \langle\{a(10)\}_\varepsilon|\{c(12)c(21)a(1'0)p(01)p(10)\}_\varepsilon\rangle \\
&+ e'_A e'_B e_C e'_D {e_P}^2 \langle\{a(1'0)\}_\varepsilon|\{c(1'2)c(21)a(1'0)p(01)p(10)\}_\varepsilon\rangle \\
&+ e'_A e'_B e'_C e'_D {e_P}^2 \langle\{a(1'0)\}_\varepsilon|\{c(12)c(21)a(1'0)p(01)p(10)\}_\varepsilon\rangle \\
&+ e_A e'_B e_C e_D {e_P}^2 \langle\{a(1'0)\}_\varepsilon|\{c(1'2)c(21')a(10)p(01)p(10)\}_\varepsilon\rangle \\
&+ e_A e_B e'_C e_D {e_P}^2 \langle\{a(10)\}_\varepsilon|\{c(12)c(21')a(10)p(01)p(10)\}_\varepsilon\rangle \\
&+ e_A e_B e_C e'_D {e_P}^2 \langle\{a(10)\}_\varepsilon|\{c(1'2)c(21)a(10)p(01)p(10)\}_\varepsilon\rangle \\
&+ e_A e'_B e'_C e_D {e_P}^2 \langle\{a(1'0)\}_\varepsilon|\{c(12)c(21')a(10)p(01)p(10)\}_\varepsilon\rangle \\
&+ e_A e_B e'_C e'_D {e_P}^2 \langle\{a(10)\}_\varepsilon|\{c(12)c(21)a(10)p(01)p(10)\}_\varepsilon\rangle \\
&+ e_A e'_B e_C e'_D {e_P}^2 \langle\{a(1'0)\}_\varepsilon|\{c(1'2)c(21)a(10)p(01)p(10)\}_\varepsilon\rangle \\
&+ e_A e'_B e'_C e'_D {e_P}^2 \langle\{a(1'0)\}_\varepsilon|\{c(12)c(21)a(10)p(01)p(10)\}_\varepsilon\rangle \\
&+ e_A e_B e_C e_D {e'_P}^2 \langle\{a(10)\}_\varepsilon|\{c(1'2)c(21')a(10)p(01')p(1'0)\}_\varepsilon\rangle \\
&+ e'_A e_B e_C e_D {e'_P}^2 \langle\{a(10)\}_\varepsilon|\{c(1'2)c(21')a(1'0)p(01')p(1'0)\}_\varepsilon\rangle \\
&+ e'_A e'_B e_C e_D {e'_P}^2 \langle\{a(1'0)\}_\varepsilon|\{c(1'2)c(21')a(1'0)p(01')p(1'0)\}_\varepsilon\rangle
\end{aligned}$$

$$
\begin{aligned}
&+ e'_A e_B e'_C e_D {e'_P}^2 \langle \{a(10)\}_\varepsilon | \{c(12)c(21')a(1'0)p(01')p(1'0)\}_\varepsilon \rangle \\
&+ e'_A e_B e_C e'_D {e'_P}^2 \langle \{a(10)\}_\varepsilon | \{c(1'2)c(21)a(1'0)p(01')p(1'0)\}_\varepsilon \rangle \\
&+ e'_A e'_B e'_C e_D {e'_P}^2 \langle \{a(1'0)\}_\varepsilon | \{c(12)c(21')a(1'0)p(01')p(1'0)\}_\varepsilon \rangle \\
&+ e'_A e_B e'_C e'_D {e'_P}^2 \langle \{a(10)\}_\varepsilon | \{c(12)c(21)a(1'0)p(01')p(1'0)\}_\varepsilon \rangle \\
&+ e'_A e'_B e_C e'_D {e'_P}^2 \langle \{a(1'0)\}_\varepsilon | \{c(1'2)c(21)a(1'0)p(01')p(1'0)\}_\varepsilon \rangle \\
&+ e'_A e'_B e'_C e'_D {e'_P}^2 \langle \{a(1'0)\}_\varepsilon | \{c(12)c(21)a(1'0)p(01')p(1'0)\}_\varepsilon \rangle \\
&+ e_A e'_B e_C e_D {e'_P}^2 \langle \{a(1'0)\}_\varepsilon | \{c(1'2)c(21')a(10)p(01')p(1'0)\}_\varepsilon \rangle \\
&+ e_A e_B e'_C e_D {e'_P}^2 \langle \{a(10)\}_\varepsilon | \{c(12)c(21')a(10)p(01')p(1'0)\}_\varepsilon \rangle \\
&+ e_A e_B e_C e'_D {e'_P}^2 \langle \{a(10)\}_\varepsilon | \{c(1'2)c(21)a(10)p(01')p(1'0)\}_\varepsilon \rangle \\
&+ e_A e'_B e'_C e_D {e'_P}^2 \langle \{a(1'0)\}_\varepsilon | \{c(12)c(21')a(10)p(01')p(1'0)\}_\varepsilon \rangle \\
&+ e_A e_B e'_C e'_D {e'_P}^2 \langle \{a(10)\}_\varepsilon | \{c(12)c(21)a(10)p(01')p(1'0)\}_\varepsilon \rangle \\
&+ e_A e'_B e_C e'_D {e'_P}^2 \langle \{a(1'0)\}_\varepsilon | \{c(1'2)c(21)a(10)p(01')p(1'0)\}_\varepsilon \rangle \\
&+ e_A e'_B e'_C e'_D {e'_P}^2 \langle \{a(1'0)\}_\varepsilon | \{c(12)c(21)a(10)p(01')p(1'0)\}_\varepsilon \rangle
\end{aligned}
\tag{C.7}
$$

$$
\begin{aligned}
\langle (BPP)_\varepsilon | (CDA)_\varepsilon \rangle^{+-} = {} & e_A e_B e_C e_D {e_P}^2 \langle \{a(10)p(01)p(10)\}_\varepsilon | \{c(1'2)c(21')a(10)\}_\varepsilon \rangle \\
&+ e'_A e_B e_C e_D {e_P}^2 \langle \{a(10)p(01)p(10)\}_\varepsilon | \{c(1'2)c(21')a(1'0)\}_\varepsilon \rangle \\
&+ e'_A e'_B e_C e_D {e_P}^2 \langle \{a(1'0)p(01)p(10)\}_\varepsilon | \{c(1'2)c(21')a(1'0)\}_\varepsilon \rangle \\
&+ e'_A e_B e'_C e_D {e_P}^2 \langle \{a(10)p(01)p(10)\}_\varepsilon | \{c(12)c(21')a(1'0)\}_\varepsilon \rangle \\
&+ e'_A e_B e_C e'_D {e_P}^2 \langle \{a(10)p(01)p(10)\}_\varepsilon | \{c(1'2)c(21)a(1'0)\}_\varepsilon \rangle \\
&+ e'_A e'_B e'_C e_D {e_P}^2 \langle \{a(1'0)p(01)p(10)\}_\varepsilon | \{c(12)c(21')a(1'0)\}_\varepsilon \rangle \\
&+ e'_A e_B e'_C e'_D {e_P}^2 \langle \{a(10)p(01)p(10)\}_\varepsilon | \{c(12)c(21)a(1'0)\}_\varepsilon \rangle
\end{aligned}
$$

$$
\begin{aligned}
&+ e'_A e'_B e_C e'_D e_P{}^2 \langle \{a(1'0)p(01)p(10)\}_\varepsilon | \{c(1'2)c(21)a(1'0)\}_\varepsilon \rangle \\
&+ e'_A e'_B e'_C e'_D e_P{}^2 \langle \{a(1'0)p(01)p(10)\}_\varepsilon | \{c(12)c(21)a(1'0)\}_\varepsilon \rangle \\
&+ e_A e'_B e_C e_D e_P{}^2 \langle \{a(1'0)p(01)p(10)\}_\varepsilon | \{c(1'2)c(21')a(10)\}_\varepsilon \rangle \\
&+ e_A e_B e'_C e_D e_P{}^2 \langle \{a(10)p(01)p(10)\}_\varepsilon | \{c(12)c(21')a(10)\}_\varepsilon \rangle \\
&+ e_A e_B e_C e'_D e_P{}^2 \langle \{a(10)p(01)p(10)\}_\varepsilon | \{c(1'2)c(21)a(10)\}_\varepsilon \rangle \\
&+ e_A e'_B e'_C e_D e_P{}^2 \langle \{a(1'0)p(01)p(10)\}_\varepsilon | \{c(12)c(21')a(10)\}_\varepsilon \rangle \\
&+ e_A e_B e'_C e'_D e_P{}^2 \langle \{a(10)p(01)p(10)\}_\varepsilon | \{c(12)c(21)a(10)\}_\varepsilon \rangle \\
&+ e_A e'_B e_C e'_D e_P{}^2 \langle \{a(1'0)p(01)p(10)\}_\varepsilon | \{c(1'2)c(21)a(10)\}_\varepsilon \rangle \\
&+ e_A e'_B e'_C e'_D e_P{}^2 \langle \{a(1'0)p(01)p(10)\}_\varepsilon | \{c(12)c(21)a(10)\}_\varepsilon \rangle \\
&+ e_A e_B e_C e_D e'_P{}^2 \langle \{a(10)p(01')p(1'0)\}_\varepsilon | \{c(1'2)c(21')a(10)\}_\varepsilon \rangle \\
&+ e'_A e_B e_C e_D e'_P{}^2 \langle \{a(10)p(01')p(1'0)\}_\varepsilon | \{c(1'2)c(21')a(1'0)\}_\varepsilon \rangle \\
&+ e'_A e'_B e_C e_D e'_P{}^2 \langle \{a(1'0)p(01')p(1'0)\}_\varepsilon | \{c(1'2)c(21')a(1'0)\}_\varepsilon \rangle \\
&+ e'_A e_B e'_C e_D e'_P{}^2 \langle \{a(10)p(01')p(1'0)\}_\varepsilon | \{c(12)c(21')a(1'0)\}_\varepsilon \rangle \\
&+ e'_A e_B e_C e'_D e'_P{}^2 \langle \{a(10)p(01')p(1'0)\}_\varepsilon | \{c(1'2)c(21)a(1'0)\}_\varepsilon \rangle \\
&+ e'_A e'_B e'_C e_D e'_P{}^2 \langle \{a(1'0)p(01')p(1'0)\}_\varepsilon | \{c(12)c(21')a(1'0)\}_\varepsilon \rangle \\
&+ e'_A e_B e'_C e'_D e'_P{}^2 \langle \{a(10)p(01')p(1'0)\}_\varepsilon | \{c(12)c(21)a(1'0)\}_\varepsilon \rangle \\
&+ e'_A e'_B e_C e'_D e'_P{}^2 \langle \{a(1'0)p(01')p(1'0)\}_\varepsilon | \{c(1'2)c(21)a(1'0)\}_\varepsilon \rangle \\
&+ e'_A e'_B e'_C e'_D e'_P{}^2 \langle \{a(1'0)p(01')p(1'0)\}_\varepsilon | \{c(12)c(21)a(1'0)\}_\varepsilon \rangle \\
&+ e_A e'_B e_C e_D e'_P{}^2 \langle \{a(1'0)p(01')p(1'0)\}_\varepsilon | \{c(1'2)c(21')a(10)\}_\varepsilon \rangle \\
&+ e_A e_B e'_C e_D e'_P{}^2 \langle \{a(10)p(01')p(1'0)\}_\varepsilon | \{c(12)c(21')a(10)\}_\varepsilon \rangle \\
&+ e_A e_B e_C e'_D e'_P{}^2 \langle \{a(10)p(01')p(1'0)\}_\varepsilon | \{c(1'2)c(21)a(10)\}_\varepsilon \rangle \\
&+ e_A e'_B e'_C e_D e'_P{}^2 \langle \{a(1'0)p(01')p(1'0)\}_\varepsilon | \{c(12)c(21')a(10)\}_\varepsilon \rangle \\
&+ e_A e_B e'_C e'_D e'_P{}^2 \langle \{a(10)p(01')p(1'0)\}_\varepsilon | \{c(12)c(21)a(10)\}_\varepsilon \rangle
\end{aligned}
$$

$$
\begin{aligned}
&+ e_A e'_B e_C e'_D {e'_P}^2 \langle\{a(1'0)p(01')p(1'0)\}_\varepsilon|\{c(1'2)c(21)a(10)\}_\varepsilon\rangle \\
&+ e_A e'_B e'_C e'_D {e'_P}^2 \langle\{a(1'0)p(01')p(1'0)\}_\varepsilon|\{c(12)c(21)a(10)\}_\varepsilon\rangle
\end{aligned} \tag{C.8}
$$

$$
\begin{aligned}
\langle(B)_\varepsilon|(DCAPP)_\varepsilon\rangle^{+-} = {} & e_A e_B e_C e_D {e_P}^2 \langle\{a(10)\}_\varepsilon|\{c(10)c(01)a(10)p(01)p(10)\}_\varepsilon\rangle \\
&+ e'_A e_B e_C e_D {e_P}^2 \langle\{a(10)\}_\varepsilon|\{c(10)c(01)a(1'0)p(01)p(10)\}_\varepsilon\rangle \\
&+ e'_A e'_B e_C e_D {e_P}^2 \langle\{a(1'0)\}_\varepsilon|\{c(10)c(01)a(1'0)p(01)p(10)\}_\varepsilon\rangle \\
&+ e'_A e_B e'_C e_D {e_P}^2 \langle\{a(10)\}_\varepsilon|\{c(10)c(01')a(1'0)p(01)p(10)\}_\varepsilon\rangle \\
&+ e'_A e_B e_C e'_D {e_P}^2 \langle\{a(10)\}_\varepsilon|\{c(1'0)c(01)a(1'0)p(01)p(10)\}_\varepsilon\rangle \\
&+ e'_A e'_B e'_C e_D {e_P}^2 \langle\{a(1'0)\}_\varepsilon|\{c(10)c(01')a(1'0)p(01)p(10)\}_\varepsilon\rangle \\
&+ e'_A e_B e'_C e'_D {e_P}^2 \langle\{a(10)\}_\varepsilon|\{c(1'0)c(01')a(1'0)p(01)p(10)\}_\varepsilon\rangle \\
&+ e'_A e'_B e_C e'_D {e_P}^2 \langle\{a(1'0)\}_\varepsilon|\{c(1'0)c(01)a(1'0)p(01)p(10)\}_\varepsilon\rangle \\
&+ e'_A e'_B e'_C e'_D {e_P}^2 \langle\{a(1'0)\}_\varepsilon|\{c(1'0)c(01')a(1'0)p(01)p(10)\}_\varepsilon\rangle \\
&+ e_A e'_B e_C e_D {e_P}^2 \langle\{a(1'0)\}_\varepsilon|\{c(10)c(01)a(10)p(01)p(10)\}_\varepsilon\rangle \\
&+ e_A e_B e'_C e_D {e_P}^2 \langle\{a(10)\}_\varepsilon|\{c(10)c(01')a(10)p(01)p(10)\}_\varepsilon\rangle \\
&+ e_A e_B e_C e'_D {e_P}^2 \langle\{a(10)\}_\varepsilon|\{c(1'0)c(01)a(10)p(01)p(10)\}_\varepsilon\rangle \\
&+ e_A e'_B e'_C e_D {e_P}^2 \langle\{a(1'0)\}_\varepsilon|\{c(10)c(01')a(10)p(01)p(10)\}_\varepsilon\rangle \\
&+ e_A e_B e'_C e'_D {e_P}^2 \langle\{a(10)\}_\varepsilon|\{c(1'0)c(01')a(10)p(01)p(10)\}_\varepsilon\rangle \\
&+ e_A e'_B e_C e'_D {e_P}^2 \langle\{a(1'0)\}_\varepsilon|\{c(1'0)c(01)a(10)p(01)p(10)\}_\varepsilon\rangle \\
&+ e_A e'_B e'_C e'_D {e_P}^2 \langle\{a(1'0)\}_\varepsilon|\{c(1'0)c(01')a(10)p(01)p(10)\}_\varepsilon\rangle \\
&+ e_A e_B e_C e_D {e'_P}^2 \langle\{a(10)\}_\varepsilon|\{c(10)c(01)a(10)p(01')p(1'0)\}_\varepsilon\rangle \\
&+ e'_A e_B e_C e_D {e'_P}^2 \langle\{a(10)\}_\varepsilon|\{c(10)c(01)a(1'0)p(01')p(1'0)\}_\varepsilon\rangle
\end{aligned}
$$

$$
\begin{aligned}
&+ e'_A e'_B e_C e_D {e'_P}^2 \langle \{a(1'0)\}_\varepsilon | \{c(10)c(01)a(1'0)p(01')p(1'0)\}_\varepsilon \rangle \\
&+ e'_A e_B e'_C e_D {e'_P}^2 \langle \{a(10)\}_\varepsilon | \{c(10)c(01')a(1'0)p(01')p(1'0)\}_\varepsilon \rangle \\
&+ e'_A e_B e_C e'_D {e'_P}^2 \langle \{a(10)\}_\varepsilon | \{c(1'0)c(01)a(1'0)p(01')p(1'0)\}_\varepsilon \rangle \\
&+ e'_A e'_B e'_C e_D {e'_P}^2 \langle \{a(1'0)\}_\varepsilon | \{c(10)c(01')a(1'0)p(01')p(1'0)\}_\varepsilon \rangle \\
&+ e'_A e_B e'_C e'_D {e'_P}^2 \langle \{a(10)\}_\varepsilon | \{c(1'0)c(01')a(1'0)p(01')p(1'0)\}_\varepsilon \rangle \\
&+ e'_A e'_B e_C e'_D {e'_P}^2 \langle \{a(1'0)\}_\varepsilon | \{c(1'0)c(01)a(1'0)p(01')p(1'0)\}_\varepsilon \rangle \\
&+ e'_A e'_B e'_C e'_D {e'_P}^2 \langle \{a(1'0)\}_\varepsilon | \{c(1'0)c(01')a(1'0)p(01')p(1'0)\}_\varepsilon \rangle \\
&+ e_A e'_B e_C e_D {e'_P}^2 \langle \{a(1'0)\}_\varepsilon | \{c(10)c(01)a(10)p(01')p(1'0)\}_\varepsilon \rangle \\
&+ e_A e_B e'_C e_D {e'_P}^2 \langle \{a(10)\}_\varepsilon | \{c(10)c(01')a(10)p(01')p(1'0)\}_\varepsilon \rangle \\
&+ e_A e_B e_C e'_D {e'_P}^2 \langle \{a(10)\}_\varepsilon | \{c(1'0)c(01)a(10)p(01')p(1'0)\}_\varepsilon \rangle \\
&+ e_A e'_B e'_C e_D {e'_P}^2 \langle \{a(1'0)\}_\varepsilon | \{c(10)c(01')a(10)p(01')p(1'0)\}_\varepsilon \rangle \\
&+ e_A e_B e'_C e'_D {e'_P}^2 \langle \{a(10)\}_\varepsilon | \{c(1'0)c(01')a(10)p(01')p(1'0)\}_\varepsilon \rangle \\
&+ e_A e'_B e_C e'_D {e'_P}^2 \langle \{a(1'0)\}_\varepsilon | \{c(1'0)c(01)a(10)p(01')p(1'0)\}_\varepsilon \rangle \\
&+ e_A e'_B e'_C e'_D {e'_P}^2 \langle \{a(1'0)\}_\varepsilon | \{c(1'0)c(01')a(10)p(01')p(1'0)\}_\varepsilon \rangle
\end{aligned}
\tag{C.9}
$$

$$
\begin{aligned}
\langle (BPP)_\varepsilon | (DCA)_\varepsilon \rangle^{+-} = {} & e_A e_B e_C e_D {e_P}^2 \langle \{a(10)p(01)p(10)\}_\varepsilon | \{c(10)c(01)a(10)\}_\varepsilon \rangle \\
&+ e'_A e_B e_C e_D {e_P}^2 \langle \{a(10)p(01)p(10)\}_\varepsilon | \{c(10)c(01)a(1'0)\}_\varepsilon \rangle \\
&+ e'_A e'_B e_C e_D {e_P}^2 \langle \{a(1'0)p(01)p(10)\}_\varepsilon | \{c(10)c(01)a(1'0)\}_\varepsilon \rangle \\
&+ e'_A e_B e'_C e_D {e_P}^2 \langle \{a(10)p(01)p(10)\}_\varepsilon | \{c(10)c(01')a(1'0)\}_\varepsilon \rangle \\
&+ e'_A e_B e_C e'_D {e_P}^2 \langle \{a(10)p(01)p(10)\}_\varepsilon | \{c(1'0)c(01)a(1'0)\}_\varepsilon \rangle \\
&+ e'_A e'_B e'_C e_D {e_P}^2 \langle \{a(1'0)p(01)p(10)\}_\varepsilon | \{c(10)c(01')a(1'0)\}_\varepsilon \rangle
\end{aligned}
$$

$$
\begin{aligned}
&+ e'_A e_B e'_C e'_D e_P{}^2 \langle \{a(10)p(01)p(10)\}_\varepsilon | \{c(1'0)c(01')a(1'0)\}_\varepsilon \rangle \\
&+ e'_A e'_B e_C e'_D e_P{}^2 \langle \{a(1'0)p(01)p(10)\}_\varepsilon | \{c(1'0)c(01)a(1'0)\}_\varepsilon \rangle \\
&+ e'_A e'_B e'_C e'_D e_P{}^2 \langle \{a(1'0)p(01)p(10)\}_\varepsilon | \{c(1'0)c(01')a(1'0)\}_\varepsilon \rangle \\
&+ e_A e'_B e_C e_D e_P{}^2 \langle \{a(1'0)p(01)p(10)\}_\varepsilon | \{c(10)c(01)a(10)\}_\varepsilon \rangle \\
&+ e_A e_B e'_C e_D e_P{}^2 \langle \{a(10)p(01)p(10)\}_\varepsilon | \{c(10)c(01')a(10)\}_\varepsilon \rangle \\
&+ e_A e_B e_C e'_D e_P{}^2 \langle \{a(10)p(01)p(10)\}_\varepsilon | \{c(1'0)c(01)a(10)\}_\varepsilon \rangle \\
&+ e_A e'_B e'_C e_D e_P{}^2 \langle \{a(1'0)p(01)p(10)\}_\varepsilon | \{c(10)c(01')a(10)\}_\varepsilon \rangle \\
&+ e_A e_B e'_C e'_D e_P{}^2 \langle \{a(10)p(01)p(10)\}_\varepsilon | \{c(1'0)c(01')a(10)\}_\varepsilon \rangle \\
&+ e_A e'_B e_C e'_D e_P{}^2 \langle \{a(1'0)p(01)p(10)\}_\varepsilon | \{c(1'0)c(01)a(10)\}_\varepsilon \rangle \\
&+ e_A e'_B e'_C e'_D e_P{}^2 \langle \{a(1'0)p(01)p(10)\}_\varepsilon | \{c(1'0)c(01')a(10)\}_\varepsilon \rangle \\
&+ e_A e_B e_C e_D e'_P{}^2 \langle \{a(10)p(01')p(1'0)\}_\varepsilon | \{c(10)c(01)a(10)\}_\varepsilon \rangle \\
&+ e'_A e_B e_C e_D e'_P{}^2 \langle \{a(10)p(01')p(1'0)\}_\varepsilon | \{c(10)c(01)a(1'0)\}_\varepsilon \rangle \\
&+ e'_A e'_B e_C e_D e'_P{}^2 \langle \{a(1'0)p(01')p(1'0)\}_\varepsilon | \{c(10)c(01)a(1'0)\}_\varepsilon \rangle \\
&+ e'_A e_B e'_C e_D e'_P{}^2 \langle \{a(10)p(01')p(1'0)\}_\varepsilon | \{c(10)c(01')a(1'0)\}_\varepsilon \rangle \\
&+ e'_A e_B e_C e'_D e'_P{}^2 \langle \{a(10)p(01')p(1'0)\}_\varepsilon | \{c(1'0)c(01)a(1'0)\}_\varepsilon \rangle \\
&+ e'_A e'_B e'_C e_D e'_P{}^2 \langle \{a(1'0)p(01')p(1'0)\}_\varepsilon | \{c(10)c(01')a(1'0)\}_\varepsilon \rangle \\
&+ e'_A e_B e'_C e'_D e'_P{}^2 \langle \{a(10)p(01')p(1'0)\}_\varepsilon | \{c(1'0)c(01')a(1'0)\}_\varepsilon \rangle \\
&+ e'_A e'_B e_C e'_D e'_P{}^2 \langle \{a(1'0)p(01')p(1'0)\}_\varepsilon | \{c(1'0)c(01)a(1'0)\}_\varepsilon \rangle \\
&+ e'_A e'_B e'_C e'_D e'_P{}^2 \langle \{a(1'0)p(01')p(1'0)\}_\varepsilon | \{c(1'0)c(01')a(1'0)\}_\varepsilon \rangle \\
&+ e_A e'_B e_C e_D e'_P{}^2 \langle \{a(1'0)p(01')p(1'0)\}_\varepsilon | \{c(10)c(01)a(10)\}_\varepsilon \rangle \\
&+ e_A e_B e'_C e_D e'_P{}^2 \langle \{a(10)p(01')p(1'0)\}_\varepsilon | \{c(10)c(01')a(10)\}_\varepsilon \rangle \\
&+ e_A e_B e_C e'_D e'_P{}^2 \langle \{a(10)p(01')p(1'0)\}_\varepsilon | \{c(1'0)c(01)a(10)\}_\varepsilon \rangle \\
&+ e_A e'_B e'_C e_D e'_P{}^2 \langle \{a(1'0)p(01')p(1'0)\}_\varepsilon | \{c(10)c(01')a(10)\}_\varepsilon \rangle
\end{aligned}
$$

$$+ e_A e_B e'_C e'_D {e'_P}^2 \langle \{a(10)p(01')p(1'0)\}_\varepsilon | \{c(1'0)c(01')a(10)\}_\varepsilon \rangle$$
$$+ e_A e'_B e_C e'_D {e'_P}^2 \langle \{a(1'0)p(01')p(1'0)\}_\varepsilon | \{c(1'0)c(01)a(10)\}_\varepsilon \rangle$$
$$+ e_A e'_B e'_C e'_D {e'_P}^2 \langle \{a(1'0)p(01')p(1'0)\}_\varepsilon | \{c(1'0)c(01')a(10)\}_\varepsilon \rangle \quad \text{(C.10)}$$

APPENDIX D

POPULATION TRANSFER FOR $J \ll \omega$

Oscillations at the vibrational frequency are generally less prominent in the survival probability traces of Figs. 3.1, 3.6, and 3.8 than they are in the corresponding pump-probe and pump-probe difference signals of Figs. 3.2, 3.5, and 3.9, respectively. While the latter signals are sensitive to the nuclear probability density in localized spatial windows, the former depend on the nuclear dynamics only through its effect on the detailed time-course of population transfer between the site-excited electronic states. When the EET coupling constant J is small compared to the vibrational energy spacing, energy transfer occurs predominantly between vibronic states of nearly equal energy in the two site-state manifolds, if such energy matches exist. In the absence of interfering transition amplitudes from multiple vibronic levels of the donor, for instance, vibrational coherences do not impress themselves on the population evolution of a given vibronic level in the acceptor. The total acceptor population and the survival probability of the donor excitation are then largely devoid of vibrational-frequency oscillations.

Let us consider the electronic population dynamics in the one-exciton manifold of a system governed by

$$H_{one} = |1\rangle\, H_1\, \langle 1| + |1'\rangle\, H_{1'}\, \langle 1'| + V, \tag{D.1}$$

in which H_1 and $H_{1'}$ are given by Eq. (3.1), with $\varepsilon_{1'} \leq \varepsilon_1$, and

$$V = J\left(|1'\rangle\langle 1| + |1\rangle\langle 1'|\right). \tag{D.2}$$

The population evolution can be efficiently described by switching to symmetric and antisymmetric combinations of the donor and acceptor nuclear coordinates and momenta: $Q_S = (q_b + q_a)/\sqrt{2}$, $P_S = (p_b + p_a)/\sqrt{2}$, $Q_A = (q_b - q_a)/\sqrt{2}$, and $P_A = (p_b - p_a)/\sqrt{2}$ (see Figure D.1). In terms of these operators,

$$H_1 = \frac{P_S^2 + P_A^2}{2m} + \frac{m\omega^2}{2}\left[\left(Q_S - \frac{d}{\sqrt{2}}\right)^2 + \left(Q_A + \frac{d}{\sqrt{2}}\right)^2\right] + \varepsilon_1 \tag{D.3}$$

and

$$H_{1'} = \frac{P_S^2 + P_A^2}{2m} + \frac{m\omega^2}{2}\left[\left(Q_S - \frac{d}{\sqrt{2}}\right)^2 + \left(Q_A - \frac{d}{\sqrt{2}}\right)^2\right] + \varepsilon_{1'}. \tag{D.4}$$

We denote by $|(\nu_S\nu_A)_1\rangle$ (or $|(\nu_S\nu_A)_{1'}\rangle$) an eigenket of H_1 (or $H_{1'}$) with energy $\omega(\nu_S + \nu_A + 1) + \varepsilon_1$ (or $\omega(\nu_S + \nu_A + 1) + \varepsilon_{1'}$). Note that the equilibrium values of (Q_S, Q_A) are $(d/\sqrt{2}, -d/\sqrt{2})$ and $(d/\sqrt{2}, d/\sqrt{2})$ in state-1 and state-1′ , respectively; only the equilibrium value of the antisymmetric coordinate differs in the two states.

We wish to determine the survival probability

$$P_1(t) = \langle\psi_1|\langle 1|e^{iH_{one}t}|1\rangle\langle 1|e^{-iH_{one}t}|1\rangle|\psi_1\rangle \tag{D.5}$$

for an initial state in the donor-excited manifold (with $\langle\psi_1|\psi_1\rangle = 1$). This can be accomplished by solving the equation of motion

$$\frac{d}{dt}e^{i(H_{one}-V)t}e^{-iH_{one}t} = -i\tilde{V}(t)e^{i(H_{one}-V)t}e^{-iH_{one}t} \tag{D.6}$$

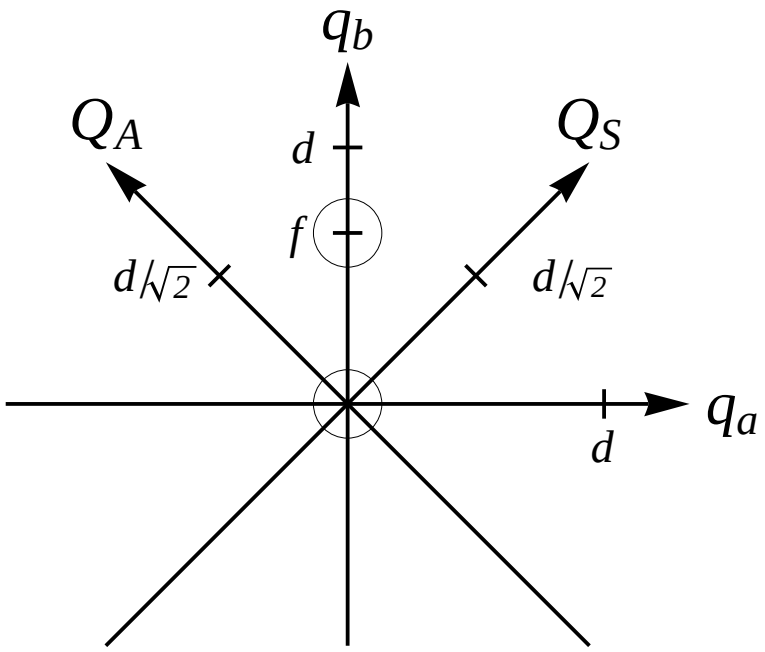

Figure D.1: Symmetric and antisymmetric vibrational coordinates plotted on donor and acceptor coordinate axes. The lowest-energy vibrational state in the donor-excited (acceptor-excited) electronic state is centered at $(q_a, q_b) = (d, 0)$ $[(q_a, q_b) = (0, d)]$. Also shown are the location (at the origin) of the lowest vibrational state in the electronic ground state and the location of a ground-state wave packet displaced by f along the q_b axis.

for the one-exciton time-evolution operator in the interaction picture, where

$$\tilde{V}(t) = e^{i(H_{one}-V)t} V e^{-i(H_{one}-V)t}. \tag{D.7}$$

The interaction-picture "Hamiltonian" (D.7) has matrix elements

$$\langle (\nu'_S \nu'_A)_{1'}| \langle 1'| \tilde{V}(t) |1\rangle |(\nu_S \nu_A)_1\rangle = J e^{i(\varepsilon_{1'}-\varepsilon_1)t + i\omega(\nu'_A - \nu_A)t} \langle (\nu'_A)_{1'}| (\nu_A)_1\rangle \delta_{\nu'_S,\nu_S} \tag{D.8}$$

and

$$\langle (\nu_S \nu_A)_1| \langle 1| \tilde{V}(t) |1'\rangle |(\nu'_S \nu'_A)_{1'}\rangle = J e^{i(\varepsilon_1-\varepsilon_{1'})t + i\omega(\nu_A - \nu'_A)t} \langle (\nu_A)_1| (\nu'_A)_{1'}\rangle \delta_{\nu_S,\nu'_S}. \tag{D.9}$$

Elements (D.8) and (D.9) both oscillate at frequency $(\varepsilon_{1'} - \varepsilon_1) + \omega(\nu'_A - \nu_A)$; in the weak-coupling case ($J << \omega$), they are therefore ineffectual unless $\varepsilon_{1'} + \nu'_A\omega \approx \varepsilon_1 + \nu_A\omega$.

In order to investigate the simplification that becomes possible when the site energies are equal or differ by multiple vibrational quanta, we assume $\varepsilon_1 - \varepsilon_{1'} = N\omega$. In this situation, it is reasonable to omit the time-dependent elements of $\tilde{V}$, and replace it by

$$\tilde{v} = J \sum_{\nu_S,\nu_A} |1'\rangle |(\nu_S, \nu_A + N)_{1'}\rangle \langle (\nu_A + N)_{1'} \mid (\nu_A)_1\rangle \langle (\nu_S, \nu_A)_1| \langle 1| + H.c.\,, \tag{D.10}$$

which is time-independent. Substitution in Eq. (D.6), integration, and return to the Schrödinger picture then yield

$$e^{-iH_{one}t} \cong e^{-i(H_{one}-V)t} e^{-i\tilde{v}t}. \tag{D.11}$$

Under this approximation, the survival probability (D.5) becomes

$$\begin{aligned} P_1(t) \cong & \langle\psi_1| \langle 1| e^{i\tilde{v}t} |1\rangle e^{iH_1 t} e^{-iH_1 t} \langle 1| e^{-i\tilde{v}t} |1\rangle |\psi_1\rangle \\ = & \langle\psi_1| \langle 1| \cos\tilde{v}t |1\rangle \langle 1| \cos\tilde{v}t |1\rangle |\psi_1\rangle \\ = & \langle\psi_1| \langle 1| \cos^2\tilde{v}t |1\rangle |\psi_1\rangle \\ = & \frac{1}{2} + \frac{1}{2} \sum_{\nu_S,\nu_A} |\langle(\nu_S\nu_A)_1| \psi_1\rangle|^2 \cos\left[2tJ \langle(\nu_A+N)_{1'} \mid (\nu_A)_1\rangle\right]. \end{aligned} \tag{D.12}$$

We want to evaluate Eq. (D.12) in situations where, as a result of impulsive control-pulse excitation, the initial wave packet takes the approximate form of the lowest state-0 vibrational eigenket displaced a distance f along the acceptor mode (as illustrated in Fig. 13):

$$\begin{aligned} |\psi_1\rangle &= e^{-ip_b f} |(0_a 0_b)_0\rangle \\ &= e^{-iP_S f/\sqrt{2}} e^{-iP_A f/\sqrt{2}} |(0_S 0_A)_0\rangle . \end{aligned} \tag{D.13}$$

We also have

$$\begin{aligned} |(\nu_S\nu_A)_1\rangle &= e^{-ip_a d} |(\nu_S\nu_A)_0\rangle \\ &= e^{-iP_S d/\sqrt{2}} e^{iP_A d/\sqrt{2}} |(\nu_S\nu_A)_0\rangle , \end{aligned} \tag{D.14}$$

so the two-dimensional overlap in Eq. (D.12) becomes

$$\langle(\nu_S\nu_A)_1 |\psi_1\rangle = \frac{e^{-\frac{m\omega}{4}(f^2+d^2)}}{\sqrt{\nu_S!\nu_A!}} \left[\frac{\sqrt{m\omega}}{2}(f-d)\right]^{\nu_S} \left[\frac{\sqrt{m\omega}}{2}(f+d)\right]^{\nu_A}. \tag{D.15}$$

The survival probability is thereby obtained in the form

$$P_1(t) = \frac{1}{2} + \frac{1}{2} e^{-\frac{m\omega}{4}(f+d)^2} \sum_{\nu_A=0}^{\infty} \frac{1}{\nu_A!} \left[\frac{m\omega}{4}(f+d)^2\right]^{\nu_A} \cos\left[2tJ \langle(\nu_A+N)_{1'} \mid (\nu_A)_1\rangle\right]. \tag{D.16}$$

The requisite one-dimensional Franck-Condon overlaps are straightforwardly evaluated using the relation

$$\langle (\nu_A + N)_{1'} \mid (\nu_A)_1 \rangle = (-\sqrt{2}\,\delta)^N e^{-\delta^2} \sum_{k=0}^{\nu_A} (-2\delta^2)^k \frac{\sqrt{(\nu_A + N)!\nu_A!}}{k!(k+N)!(\nu_A - k)!}. \qquad \text{(D.17)}$$

In the case of "ideal" displacement $f = -d$, the approximate survival probability (D.16) reduces to

$$P_1(t) = \frac{1}{2} + \frac{1}{2}\cos\left[2tJ\,\langle (N_A)_{1'} \mid (0_A)_1 \rangle\right], \qquad \text{(D.18)}$$

and population transfer proceeds as if the state-1 wave packet were the lowest vibrational level of the donor-excited electronic state. This behavior is to be compared with the survival probability following direct Franck-Condon excitation ($f = 0$),

$$P_1(t) = \frac{1}{2} + \frac{1}{2}e^{-\delta^2/2} \sum_{\nu_A=0}^{\infty} \frac{(\delta^2/2)^{\nu_A}}{\nu_A!} \cos\left[2tJ\,\langle (\nu_A + N)_{1'} \mid (\nu_A)_1 \rangle\right], \qquad \text{(D.19)}$$

in which non-zero populations in higher donor-excited levels also contribute. The relative speed of short-time EET evidently hinges on the size of the overlaps (D.17) for contributing donor-excited vibronic states.

The weak electronic-vibrational coupling limit ($\delta^2 << 1$) is exemplified for the case of equal site energies by the DTA-12 calculations of subsection B.2 of Chapter III. In this system, the vibrationally excited antisymmetric-mode overlaps are all smaller in size than $\langle (0_A)_{1'} \mid (0_A)_1 \rangle$, so the short-time donor-population falls off more rapidly following acceptor-mode displacement (Eq. (D.16) with $f = -0.54d$) than it does under Franck-Condon excitation (Eq. (D.19)). These predictions of the weak EET-coupling approximation are consistent with the rigorously calculated population dynamics shown in Fig. 3.6. In addition, they differ only slightly from the survival probability calculated by means of Eq. (D.12) using the $|\psi_1\rangle$ actually generated by the sequential action of the control and pump

pulses, rather than the approximate form (D.13) (results not shown).

The model system studied in subsection B.1 of Chapter III features equal site energies, moderate electronic-vibrational coupling ($\delta^2 = 2.5$), and moderate energy-transfer coupling ($J = 0.2\omega$). For this system under "ideal" impulsive displacement of the acceptor mode ($f = -d$), Eq. (D.18) with $N_A = 0$ predicts

$$P_1(t) = \frac{1}{2} + \frac{1}{2}\cos\left(\frac{2Jt}{e^{5/2}}\right). \tag{D.20}$$

According to Eq. (D.19), vertical donor excitation without prior vibrational displacement leads to

$$\begin{aligned} P_1(t) \cong & \frac{1}{2} + \frac{1}{2e^{5/4}}\left[\cos\left(\frac{2Jt}{e^{5/2}}\right) + \frac{5}{4}\cos\left(\frac{8Jt}{e^{5/2}}\right) + \frac{25}{32}\cos\left(\frac{7Jt}{e^{5/2}}\right)\right. \\ & \left. + \frac{125}{384}\cos\left(\frac{16Jt}{3e^{5/2}}\right) + \frac{625}{6144}\cos\left(\frac{31Jt}{12e^{5/2}}\right) + \cdots\right]. \end{aligned} \tag{D.21}$$

Here $\nu_A = 1$–4 all have larger overlaps than $\nu_A = 0$, so the donor-state population falls off more rapidly after direct Franck-Condon excitation than it does following prior acceptor-mode displacement. For the displacement, $f = -0.338d$, achieved by the impulsive Raman process described in subsection B.1 of Chapter III, Eq. (D.16) predicts

$$\begin{aligned} P_1(t) \cong & \frac{1}{2} + \frac{1}{2e^{0.5478}}\left[\cos\left(\frac{2Jt}{e^{5/2}}\right) + 0.5478\cos\left(\frac{8Jt}{e^{5/2}}\right) + 0.1500\cos\left(\frac{7Jt}{e^{5/2}}\right)\right. \\ & \left. + 0.0274\cos\left(\frac{16Jt}{3e^{5/2}}\right) + 0.0038\cos\left(\frac{31Jt}{12e^{5/2}}\right) + \cdots\right]. \end{aligned} \tag{D.22}$$

This function is plotted along with the rigorously calculated population in Fig. 3.1; a similar form that agrees slightly better with the rigorous result (not shown) is obtained from Eq. (D.12) evaluated with the numerically calculated components $\langle(\nu_S\nu_A)_1|\ \psi_1\rangle$ generated by the actual impulsive Raman process and subsequent pump-pulse excitation.

In the intermediate electronic-vibrational coupling case $\delta = 1$, the Franck-Condon overlaps for $N = 0$ given by Eq. (D.17) depend only weakly (in magnitude) on the anti-symmetric mode quantum number, taking values $1/e$, $-1/e$, $-1/e$, $-1/3e$, and $1/3e$ for $\nu_A = 0$–4, respectively. These overlaps give rise to survival probabilities

$$P_1(t) = \frac{1}{2} + \frac{1}{2}\cos\left(\frac{2Jt}{e}\right) \tag{D.23}$$

for $f = -d$ and

$$\begin{aligned} P_1(t) \cong & \frac{1}{2} + \frac{13}{16e^{1/2}}\cos\left(\frac{2Jt}{e}\right) + \frac{3}{256e^{1/2}}\cos\left(\frac{2Jt}{3e}\right) \\ = & \frac{1}{2} + 0.493\cos\left(\frac{2Jt}{e}\right) + 0.007\cos\left(\frac{2Jt}{3e}\right) \end{aligned} \tag{D.24}$$

for $f = 0$, so the acceptor-mode displacement has only a small effect in this case. This pattern suggests that simple displacement of a moderately Franck-Condon active acceptor vibration, such as mode-6 of anthracene (with $\delta_6 \cong 1.05\omega_6 \cong 1400\,\mathrm{cm}^{-1}$) in DTA, would be largely ineffective as a means of controlling electronic excitation transfer. We have verified this prediction with numerical calculations (not shown) of the donor-state survival probability and pump-probe signal for a DTA-6 model analogous to the DTA-12 results of subsection B.2 of Chapter III.

In the downhill model considered in subsection B.3 of Chapter III, the relevant overlaps are $\langle (\nu_A + 5)_{1'} | (\nu_A)_1 \rangle$ = -0.4189, -0.1710, 0.1371, 0.2706, and 0.2037 for $\nu_A = 0$–4, respectively. The corresponding population-weights to be used in Eq. (D.16) with $f = 0$ and $f = -0.338d$ are the same as those appearing in Eqs. (D.21) and (D.22), respectively. The resulting, approximate predictions for $P_1(t)$ are plotted in Fig. 3.8 along with the rigorously calculated traces.

APPENDIX E

VIBRONIC MATRIX ELEMENTS FOR SECOND-ORDER PULSE PROPAGATORS

In going to the pump-probe limit of a md-WPI experiment, the interpulse delays for pulses within a phase-related pair are set to zero. The treatment described in Paper 1 (see Eq. (13)) properly accounts for the non-negligible effects of pulse overlap that enter in this limit. We construct second-order pulse propagators for ground-state bleach (GSB), stimulated emission (SE), or excited-state absorption (ESA) depending on the particular action of the pulse ($0 \rightarrow \varepsilon \rightarrow 0$, $\varepsilon \rightarrow 0 \rightarrow \varepsilon$, or $\varepsilon \rightarrow 2 \rightarrow \varepsilon$ respectively).

Propagators for GSB take the form

$$p_I^{(01)}(\infty;\, t_2)p_I^{(10)}(t_2;\, t_1) = \left(\tfrac{iE_I m}{2}\right)^2 \int_{-\infty}^{\infty} dt_2 \int_{-\infty}^{t_2} dt_1\, f_I(t_2) f_I(t_1) e^{i\Phi_I(t_2) - i\Phi_I(t_1)} \times e^{-iH_0(t_I - t_2)} e^{-iH_1(t_2 - t_I)} e^{-iH_1(t_I - t_1)} e^{-iH_0(t_1 - t_I)} \quad . \tag{E.1}$$

To calculate the matrix elements for this operator in the eigenbasis of H_0, we introduce com-

pleteness relations in the eigenbasis of H_1,

$$\begin{aligned}
&\left\langle (\nu_a,\nu_b)_0 \left| p_I^{(01)}(\infty;\, t_2) p_I^{(10)}(t_2;\, t_1) \right| (\bar\nu_a,\bar\nu_b)_0 \right\rangle \\
&\quad = \left(\tfrac{iE_I m}{2}\right)^2 \int_{-\infty}^{\infty} dt_2 \int_{-\infty}^{t_2} dt_1\, e^{-(t_1-t_I)^2/2\sigma_I^2} e^{-(t_2-t_I)^2/2\sigma_I^2} e^{i\Omega_I(t_2-t_I)-i\Omega_I(t_1-t_I)} \\
&\qquad \times \left\langle (\nu_a,\nu_b)_0 \left| e^{-iH_0(t_I-t_2)} e^{-iH_1(t_2-t_I)} e^{-iH_1(t_I-t_1)} e^{-iH_0(t_1-t_I)} \right| (\bar\nu_a,\bar\nu_b)_0 \right\rangle \\
&\quad = \delta_{\nu_b\bar\nu_b} \left(\tfrac{iE_I m}{2}\right)^2 \sum_{\bar{\bar\nu}_a} \langle (\nu_a)_g |\, (\,\bar{\bar\nu}_a)_e\rangle \langle (\,\bar{\bar\nu}_a)_e |\, (\,\bar\nu_a)_g\rangle \\
&\qquad \times \int_{-\infty}^{\infty} d\tau_2 \int_{-\infty}^{\tau_2} d\tau_1\, \exp\left\{ -\tfrac{\tau_1^2}{2\sigma_I^2} + i\left(\omega(\bar{\bar\nu}_a - \bar\nu_a) + \varepsilon_1 - \Omega_I\right)\tau_1 \right\} \\
&\qquad \times \exp\left\{ -\tfrac{\tau_2^2}{2\sigma_I^2} - i\left(\omega(\bar{\bar\nu}_a - \nu_a) + \varepsilon_1 - \Omega_I\right)\tau_2 \right\} \ .
\end{aligned} \tag{E.2}$$

A closed-form expression can be derived for nested time integrals of the form appearing in Eq. (E.2), due to the Gaussian nature of the integrand. The first step is to change the order of integration,

$$\begin{aligned}
I(\alpha,\beta) &\equiv \int_{-\infty}^{\infty} d\tau_2 \int_{-\infty}^{\tau_2} d\tau_1\, \exp\left\{ -\frac{\tau_1^2}{2\sigma_I^2} + i\,\alpha\,\tau_1 - \frac{\tau_2^2}{2\sigma_I^2} - i\,\beta\,\tau_2 \right\} \\
&= \int_{-\infty}^{\infty} d\tau_1 \int_{\tau_1}^{\infty} d\tau_2\, \exp\left\{ -\frac{\tau_1^2}{2\sigma_I^2} + i\,\alpha\,\tau_1 - \frac{\tau_2^2}{2\sigma_I^2} - i\,\beta\,\tau_2 \right\} \ .
\end{aligned} \tag{E.3}$$

We now make a change of variables, letting $\tau = \tau_2 - \tau_1$

$$I(\alpha,\beta) = \int_{-\infty}^{\infty} d\tau_1 \int_{0}^{\infty} d\tau\ \exp\left\{ -\frac{\tau_1^2}{2\sigma_I^2} + i\,\alpha\,\tau_1 - \frac{\tau_1^2 + \tau^2 + 2\,\tau\,\tau_1}{2\sigma_I^2} - i\,\beta\,(\tau+\tau_1) \right\}, \tag{E.4}$$

and then change integration order again to obtain

$$I(\alpha,\beta) = \int_{0}^{\infty} d\tau \exp\left\{ -\frac{\tau^2}{2\sigma_I^2} - i\,\beta\,\tau \right\} \int_{-\infty}^{\infty} d\tau_1\, \exp\left\{ -\frac{\tau_2^2}{\sigma_I^2} + i\,(\alpha-\beta)\tau_1 - \frac{\tau\,\tau_1}{\sigma_I^2} \right\} . \tag{E.5}$$

The inner integral is solved in the usual way, giving

$$I(\alpha,\beta) = \sqrt{\pi}\sigma \exp\left\{-\frac{(\alpha-\beta)^2}{4\sigma_I^2}\right\} \int_0^\infty d\tau \exp\left\{-\frac{\tau^2}{4\sigma_I^2} - i\,\tau\left(\frac{\alpha+\beta}{2}\right)\right\}, \tag{E.6}$$

which can be written in terms of the error function,

$$I(\alpha,\beta) = \pi\,\sigma_I^2 \exp\left\{-\frac{\sigma_I^2}{2}(\alpha^2+\beta^2)\right\}\left(1 - \mathrm{erf}\left\{\frac{i\sigma_I}{2}(\alpha+\beta)\right\}\right). \tag{E.7}$$

We can now return to the vibronic matrix element for the GSB propagator, which by Eq. (E.7) can be written as

$$\begin{aligned}\langle(\nu_a,\nu_b)_0|\, p_I^{(01)}(\infty;\,t_2)p_I^{(10)}(t_2;\,t_1)\,|(\bar{\nu}_a,\bar{\nu}_b)_0\rangle& \\ = \delta_{\nu_b,\bar{\nu}_b}\left(\frac{iE_Im}{2}\right)^2 \sum_{\bar{\bar{\nu}}_a} \langle(\nu_a)_g|\,(\bar{\bar{\nu}}_a)_e\rangle\,\langle(\bar{\bar{\nu}}_a)_e|\,(\bar{\nu}_a)_g\rangle& \\ \times\; I\left(\omega(\bar{\bar{\nu}}_a-\bar{\nu}_a)+\varepsilon_1-\Omega_I, \omega(\bar{\bar{\nu}}_a-\nu_a)+\varepsilon_1-\Omega_I\right)\quad.&\end{aligned} \tag{E.8}$$

Matrix elements of the operator $p_I^{(01')}(\infty;\,t_2)p_I^{(1'0)}(t_2;\,t_1)$ follow analogously. A GSB propagator also describes the action of the pre-resonant control pulse, whose effect on the system is primarily the creation of a ground-state wave packet, and Eq. (2.15) of the main text is equivalent to Eq. (E.8).

The ESA propagators are obtained in a similar fashion,

$$\begin{aligned}
&\left\langle (\nu_a,\nu_b)_1 \left| p_I^{(12)}(\infty;\, t_2) p_I^{(21)}(t_2;\, t_1) \right| (\bar{\nu}_a,\bar{\nu}_b)_1 \right\rangle \\
&\quad = \left(\tfrac{iE_I m}{2}\right)^2 \int_{-\infty}^{\infty} dt_2 \int_{-\infty}^{t_2} dt_1\, e^{-(t_1-t_I)^2/2\sigma_1^2} e^{-(t_2-t_I)^2/2\sigma_1^2} e^{i\Omega_I(t_2-t_I)-i\Omega_I(t_1-t_I)} \\
&\qquad \times \left\langle (\nu_a,\nu_b)_1 \left| e^{-iH_1(t_I-t_2)} e^{-iH_2(t_2-t_I)} e^{-iH_2(t_I-t_1)} e^{-iH_1(t_1-t_I)} \right| (\bar{\nu}_a,\bar{\nu}_b)_1 \right\rangle \\
&\quad = \delta_{\nu_a\bar{\nu}_a} \left(\tfrac{iE_I m}{2}\right)^2 \sum_{\bar{\bar{\nu}}_b} \langle (\nu_b)_g |\, (\,\bar{\bar{\nu}}_b)_e \rangle \langle (\,\bar{\bar{\nu}}_b)_e |\, (\,\bar{\nu}_b)_g \rangle \\
&\qquad \times I\left(\omega(\bar{\bar{\nu}}_b - \bar{\nu}_b) + (\varepsilon_2 - \varepsilon_1) - \Omega_I, \omega(\bar{\bar{\nu}}_b - \nu_b) + (\varepsilon_2 - \varepsilon_1) - \Omega_I\right) \ .
\end{aligned} \tag{E.9}$$

and the corresponding elements of $p_I^{(1'2)}(\infty;\, t_2) p_I^{(21')}(t_2;\, t_1)$ follow by direct analogy. Unlike in the case of GSB, we now have the possibility that the final and initial electronic states will be different. We then need matrix elements of the form

$$\begin{aligned}
&\left\langle (\nu_a,\nu_b)_{1'} \left| p_I^{(1'2)}(\infty;\, t_2) p_I^{(21)}(t_2;\, t_1) \right| (\bar{\nu}_a,\bar{\nu}_b)_1 \right\rangle \\
&\quad = \left(\tfrac{iE_I m}{2}\right)^2 \int_{-\infty}^{\infty} dt_2 \int_{-\infty}^{t_2} dt_1\, e^{-(t_1-t_I)^2/2\sigma_1^2} e^{-(t_2-t_I)^2/2\sigma_1^2} e^{i\Omega_I(t_2-t_I)-i\Omega_I(t_1-t_I)} \\
&\qquad \times \left\langle (\nu_a,\nu_b)_1 \left| e^{-iH_{1'}(t_I-t_2)} e^{-iH_2(t_2-t_I)} e^{-iH_2(t_I-t_1)} e^{-iH_1(t_1-t_I)} \right| (\bar{\nu}_a,\bar{\nu}_b)_1 \right\rangle \\
&\quad = \left(\tfrac{iE_I m}{2}\right)^2 \langle (\nu_a)_g \mid (\,\bar{\nu}_a)_e \rangle \langle (\,\nu_b)_e |\, (\,\bar{\nu}_b)_g \rangle \\
&\qquad \times I\left(\omega(\nu_b - \bar{\nu}_b) + (\varepsilon_2 - \varepsilon_1) - \Omega_I, \omega(\bar{\nu}_a - \nu_a) + (\varepsilon_2 - \varepsilon_{1'}) - \Omega_I\right) \ .
\end{aligned} \tag{E.10}$$

Finally, the SE propagators are written

$$\begin{aligned}
&\left\langle (\nu_a,\nu_b)_1 \left| p_I^{(10)}(\infty;\, t_2) p_I^{(01)}(t_2;\, t_1) \right| (\bar{\nu}_a,\bar{\nu}_b)_1 \right\rangle \\
&\quad = \left(\tfrac{iE_I m}{2}\right)^2 \int_{-\infty}^{\infty} dt_2 \int_{-\infty}^{t_2} dt_1\, e^{-(t_1-t_I)^2/2\sigma_1^2} e^{-(t_2-t_I)^2/2\sigma_1^2} e^{-i\Omega_I(t_2-t_I)+i\Omega_I(t_1-t_I)} \\
&\qquad \times \left\langle (\nu_a,\nu_b)_1 \left| e^{-iH_1(t_I-t_2)} e^{-iH_0(t_2-t_I)} e^{-iH_0(t_I-t_1)} e^{-iH_1(t_1-t_I)} \right| (\bar{\nu}_a,\bar{\nu}_b)_1 \right\rangle \\
&\quad = \delta_{\nu_b\bar{\nu}_b} \left(\tfrac{iE_I m}{2}\right)^2 \sum_{\bar{\bar{\nu}}_a} \langle (\nu_a)_e |\, (\,\bar{\bar{\nu}}_a)_g \rangle \langle (\,\bar{\bar{\nu}}_a)_g |\, (\,\bar{\nu}_a)_e \rangle \\
&\qquad \times I\left(\Omega_I - \omega(\bar{\bar{\nu}}_a - \bar{\nu}_a) - \varepsilon_1, \Omega_I - \omega(\bar{\bar{\nu}}_a - \nu_a) - \varepsilon_1\right) \ ,
\end{aligned} \tag{E.11}$$

and

$$\begin{aligned}
&\left\langle (\nu_a,\nu_b)_{1'} \left| p_I^{(1'0)}(\infty;\, t_2) p_I^{(01)}(t_2;\, t_1) \right| (\bar{\nu}_a,\bar{\nu}_b)_1 \right\rangle \\
&\quad = \left(\tfrac{iE_I m}{2}\right)^2 \int_{-\infty}^{\infty} dt_2 \int_{-\infty}^{t_2} dt_1\, e^{-(t_1-t_I)^2/2\sigma_1^2} e^{-(t_2-t_I)^2/2\sigma_1^2} e^{-i\Omega_I(t_2-t_I)+i\Omega_I(t_1-t_I)} \\
&\qquad \times \left\langle (\nu_a,\nu_b)_1 \left| e^{-iH_{1'}(t_I-t_2)} e^{-iH_0(t_2-t_I)} e^{-iH_0(t_I-t_1)} e^{-iH_1(t_1-t_I)} \right| (\bar{\nu}_a,\bar{\nu}_b)_1 \right\rangle \\
&\quad = \left(\tfrac{iE_I m}{2}\right)^2 \langle (\,\nu_b)_e |\, (\,\bar{\nu}_b)_g \rangle \, \langle (\nu_a)_g \mid (\,\bar{\nu}_a)_e \rangle \\
&\qquad \times I\left(\Omega_I - \omega(\nu_a - \bar{\nu}_a) - \varepsilon_1, \Omega_I - \omega(\bar{\nu}_b - \nu_b) - \varepsilon_{1'}\right) \ .
\end{aligned} \tag{E.12}$$

APPENDIX F

INITIAL ANISOTROPY VALUES FOR PUMP-PROBE AND PUMP-PROBE DIFFERENCE SIGNALS

For the pump-probe signal, the anisotropy is defined by

$$r_{\mathrm{PP}}(t_{CA}) = \frac{\text{HH - HV}}{\text{HH + 2HV}} \ . \tag{F.1}$$

Using well-known orientational factors, we can write the stimulated emission component to the numerator above (assuming the monomers have orthogonal transition dipole moments) as

$$\begin{aligned}
\mathrm{HH} - \mathrm{HV} = & \frac{1}{30}\mathrm{Re}\,(4\,\langle\{a(10)\}_1 \mid \{c(10)c(01)a(10)\}_1\rangle \\
& + 4\,\langle\{a(1'0)\}_{1'} \mid \{c(1'0)c(01')a(1'0)\}_{1'}\rangle \\
& - 2\,\langle\{a(1'0)\}_1 \mid \{c(10)c(01)a(1'0)\}_1\rangle \\
& + 3\,\langle\{a(1'0)\}_{1'} \mid \{c(1'0)c(01)a(10)\}_{1'}\rangle \\
& + 3\,\langle\{a(1'0)\}_1 \mid \{c(10)c(01')a(10)\}_1\rangle \\
& + 3\,\langle\{a(10)\}_{1'} \mid \{c(1'0)c(01)a(1'0)\}_{1'}\rangle \\
& + 3\,\langle\{a(10)\}_1 \mid \{c(10)c(01')a(1'0)\}_1\rangle \\
& - 2\,\langle\{a(10)\}_{1'} \mid \{c(1'0)c(01')a(10)\}_{1'}\rangle)\,.
\end{aligned} \tag{F.2}$$

We can make use of the fact that for equal-energy homodimers the overlaps retain their value

when the labels 1 and $1'$ are interchanged, simplifying the above expression as

$$\begin{aligned}\mathrm{HH}-\mathrm{HV}=&\frac{2}{30}\mathrm{Re}\,(4\,\langle\{a(10)\}_1\mid\{c(10)c(01)a(10)\}_1\rangle\\&-2\,\langle\{a(1'0)\}_1\mid\{c(10)c(01)a(1'0)\}_1\rangle\\&+3\,\langle\{a(1'0)\}_{1'}\mid\{c(1'0)c(01)a(10)\}_{1'}\rangle\\&+3\,\langle\{a(1'0)\}_1\mid\{c(10)c(01')a(10)\}_1\rangle)\,.\end{aligned}\tag{F.3}$$

The denominator is

$$\begin{aligned}\mathrm{HH}+2\mathrm{HV}=&\frac{1}{3}\mathrm{Re}\,(\langle\{a(10)\}_1\mid\{c(10)c(01)a(10)\}_1\rangle\\&+\langle\{a(1'0)\}_1\mid\{c(10)c(01)a(1'0)\}_1\rangle\\&+\langle\{a(10)\}_{1'}\mid\{c(1'0)c(01')a(10)\}_{1'}\rangle\\&+\langle\{a(1'0)\}_{1'}\mid\{c(1'0)c(01')a(1'0)\}_{1'}\rangle)\\=&\frac{2}{3}\mathrm{Re}\,(\langle\{a(10)\}_1\mid\{c(10)c(01)a(10)\}_1\rangle\\&+\langle\{a(1'0)\}_1\mid\{c(10)c(01)a(1'0)\}_1\rangle)\quad.\end{aligned}\tag{F.4}$$

When the interpulse delay t_{CA} is zero, overlaps like $\langle\{a(1'0)\}_1|\{c(10)c(01)a(1'0)\}_1\rangle$ vanish, as there is no interval of free evolution during which energy transfer can take place. This simplification gives a compact expression for the initial anisotropy

$$r_{\mathrm{PP}}(0)=0.4+0.3\frac{\mathrm{Re}\,\langle\{a(1'0)\}_{1'}|\{c(1'0)c(01)a(10)\}_{1'}\rangle}{\mathrm{Re}\,\langle\{a(10)\}_1|\{c(10)c(01)a(10)\}_1\rangle}\quad,\tag{F.5}$$

which reduces to 0.4 or 0.7 when the ratio of wave-packet overlaps in the second term is 0 or 1, respectively. This ratio is essentially zero under the conditions of our simulations (which use a red-shifted probe pulse) due to the fact that the spatial region in which the probe pulse is resonant with the $1\rightarrow 0$ transition (near $q_a=2d$) overlaps the region in which it is resonant

with the $1' \leftarrow 0$ transition ($q_b = 2d$) far from the location of the wave packet created by the pump pulse. Were the pump and probe to have the same center frequency, or were the probe pulse sufficiently short that its center frequency became irrelevant, the value of $r_{PP}(0) = 0.7$ would be obtained (see Figure D panel A).

The anisotropy for the pump-probe difference signal, in which the system first interacts with a vertically polarized control pulse, is given by

$$r_{\mathrm{PPD}}(t_{CA}) = \frac{\text{VHH - VHV}}{\text{VHH + 2VHV}} \ . \tag{F.6}$$

Omitting those overlaps that depend on energy transfer between pulses, and again making use of the symmetry with respect to interchange of 1 and $1'$, we find

$$\begin{aligned}
\text{VHH} - \text{VHV} = \frac{2}{30}\mathrm{Re}\,(2\,\langle\{a(10)\}_1 \mid \{c(10)c(01)a(10)p(01')p(1'0)\}_1\rangle \\
+ \langle\{a(1'0)\}_{1'} \mid \{c(1'0)c(01)a(10)p(01)p(10)\}_{1'}\rangle \\
+ \langle\{a(1'0)\}_{1'} \mid \{c(1'0)c(01)a(10)p(01')p(1'0)\}_{1'}\rangle \\
+ 2\,\langle\{a(10)p(01')p(1'0)\}_1 \mid \{c(10)c(01)a(10)\}_1\rangle \\
+ \langle\{a(1'0)p(01)p(10)\}_{1'} \mid \{c(1'0)c(01)a(10)\}_{1'}\rangle \\
+ \langle\{a(1'0)p(01')p(1'0)\}_{1'} \mid \{c(1'0)c(01)a(10)\}_{1'}\rangle)
\end{aligned} \tag{F.7}$$

and

$$\begin{aligned}\mathrm{VHH} + 2\mathrm{VHV} = &\frac{2}{105}\mathrm{Re}\,(9\,\langle\{a(10)\}_1 \mid \{c(10)c(01)a(10)p(01)p(10)\}_1\rangle \\ &- \langle\{a(1'0)\}_{1'} \mid \{c(1'0)c(01)a(10)p(01)p(10)\}_{1'}\rangle \\ &- \langle\{a(1'0)\}_{1'} \mid \{c(1'0)c(01)a(10)p(01')p(1'0)\}_1\rangle \\ &+ 13\,\langle\{a(10)\}_1 \mid \{c(10)c(01)a(10)p(01')p(1'0)\}_1\rangle \\ &+ 9\,\langle\{a(10)p(01)p(10)\}_1 \mid \{c(10)c(01)a(10)\}_1\rangle \\ &- \langle\{a(1'0)p(01)p(10)\}_{1'} \mid \{c(1'0)c(01)a(10)\}_{1'}\rangle \\ &- \langle\{a(1'0)p(01')p(1'0)\}_{1'} \mid \{c(1'0)c(01)a(10)\}_1\rangle \\ &+ 13\,\langle\{a(10)p(01')p(1'0)\}_1 \mid \{c(10)c(01)a(10)\}_1\rangle)\end{aligned} \tag{F.8}$$

In the case that all of the overlaps listed in Eqs. (F.7) and (F.8) are equal in value (which happens when the pump and probe are arbitrarily short), the initial anisotropy is 0.7. Numerically, we find an initial anisotropy of 0.69 when σ_A and σ_C are set equal to one hundredth of the vibrational period for the equal-energy dimer used in Section B.1 of the main text (see Figure D panels B and C).

When the overlaps containing $c(1'0)c(01)$ do not contribute, for the same reason as described above, we have

$$r_{\mathrm{PPD}}(0) = \frac{7}{13 + 9\frac{\mathrm{Re}\left(\left\langle\{a(10)\}_1\middle|\{c(10)c(01)a(10)p(01)p(10)\}_1\right\rangle + \left\langle\{a(10)p(01)p(10)\}_1\middle|\{c(10)c(01)a(10)\}_1\right\rangle\right)}{\mathrm{Re}\left(\left\langle\{a(10)\}_1\middle|\{c(10)c(01)a(10)p(01')p(1'0)\}_1\right\rangle + \left\langle\{a(10)p(01')p(1'0)\}_1\middle|\{c(10)c(01)a(10)\}_1\right\rangle\right)}}. \tag{F.9}$$

In general, this expression gives an initial anisotropy that changes with pulse and molecular parameters, in contrast with the initial value of 0.4 often found in pump-probe experiments. Were the control pulse arbitrarily short, it would be ineffective in driving nu-

clear motion in the electronic ground state, and $|\{a(10)p(01)p(10)\}_1\rangle$ would be identical to$|\{a(10)p(01')p(1'0)\}_1\rangle$. In this limit, Eq. (F.9) reduces to a value of $7/22 \approx 0.32$ for non-impulsive pump and probe pulses (see Figure D panel B). That this value for an impulsive control pulse is different from 0.4 is not unexpected. The control pulse creates a copy of the ground-state nuclear wave packet only in those molecules in which one of the monomers has a nonzero transition dipole component along the V axis. It is this subset of the total isotropic population upon which a pump-probe experiment is conducted. In the situation of interest - where the control pulse does generate motion on the electronic ground state - we find no single limiting value for Eq. (F.9) (see Figure D panel C).

It should be recalled that our numerical simulations explicitly ignore overlap between the pump and probe pulses, and our results are therefore only strictly valid for interpulse delays longer than the pulse lengths. Numerical calculations that rigorously include overlap between the pump and probe (not included here) show that neglecting this overlap tends to result in an overestimation of the initial anisotropy for the pump-probe difference. For example, using the same pulse and molecular parameters as in Fig. 4 of the main body of the paper and neglecting pulse overlap gives an initial anisotropy of 0.25 (which is largely unaffected by inhomogeneous broadening), whereas properly treating the effects of pulse overlap reduces this value to 0.14. Thus the "initial anisotropies" plotted as a function of pump and probe pulse duration do not strictly depict the true initial anisotropy. Nonetheless, due to the presence of a single vibrational period in our two-mode model system, they do hold significance as the anisotropy when the interpulse delay is equal to the vibrational period, if energy transfer is neglected on this time scale.

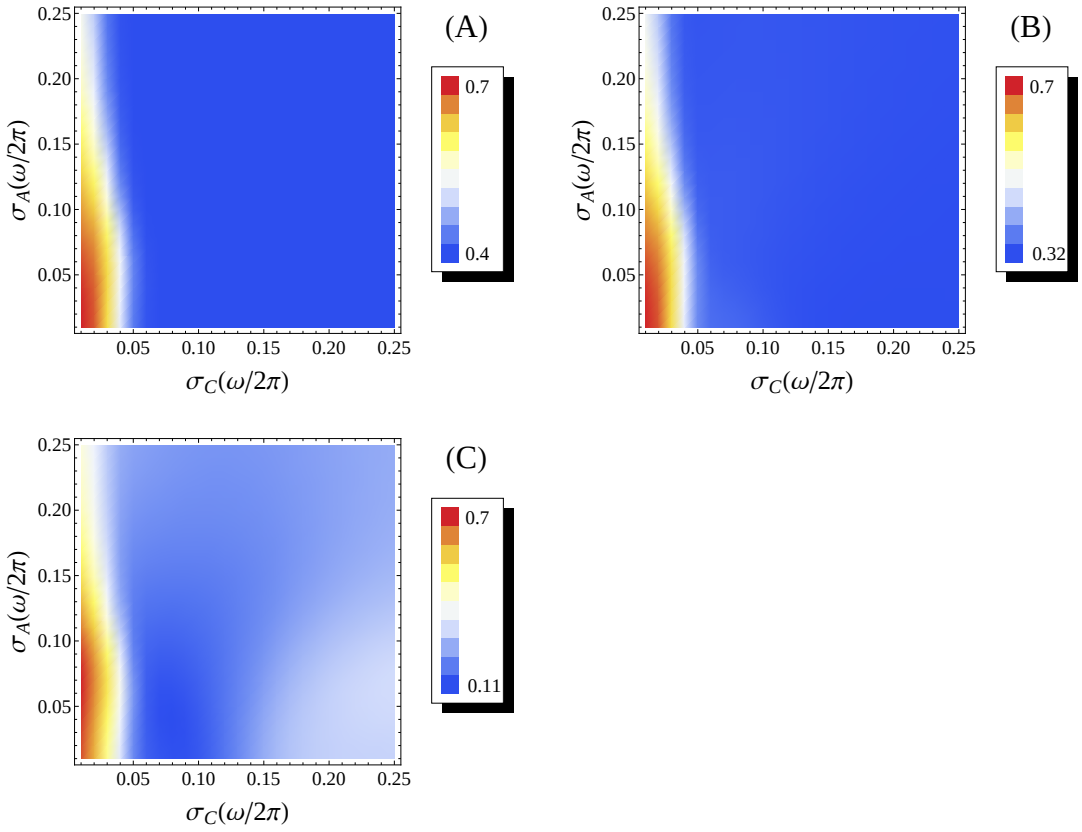

Figure F.1: Initial anisotropy neglecting pulse overlap (or the anisotropy one vibrational period after the pump pulse arrives, neglecting energy transfer) as a function of pump and probe pulse duration for the equal-energy model system with moderate electron-vibrational coupling ($\delta^2 = 2.5$). The pump pulse is vertically resonant at the ground-state equilibrium geometry, while the probe is resonant at the outer turning point for nuclear motion in the excited electronic state ($\Omega_A = \varepsilon_1 + \delta^2\omega$ and $\Omega_C = \varepsilon_1 - 3\delta^2\omega$). A) The pump-probe anisotropy takes a value of 0.7 for an impulsive probe, and 0.4 otherwise. B) The pump-probe difference anisotropy using an impulsive control pulse, showing the same behavior as (A) but with a lower limit of 7/22 rather than 0.4. C) The pump-probe difference anisotropy using a control pulse optimized to generate coherent ground-state nuclear motion (as described in the main text) shows more complicated behavior than (A) or (B). The anisotropy is high for an impulsive probe, however as the probe pulse becomes longer the initial anisotropy does not decrease monotonically.

APPENDIX G

SEMICLASSICAL PREDICTIONS FOR CONTROL-PULSE INDUCED TRAJECTORIES

In Appendix D we investigate the effect on short-time EET of prior displacement of the acceptor nuclear mode, using an approximate quantum theory valid in the limit $J \ll \omega$. In that theory, only coupling between iso-energetic vibronic states is considered. There we show that for a wave packet which is initially located at $(q_a, q_b) = (0, -d)$, and therefore follows the trajectory indicated by the dashed line in 2.1 and the blue line in 5.1, energy transfer is diminished relative to vertical excitation when the excited state displacement, d, is larger than twice the RMS width of the minimum-uncertainty wave packet (i.e. when δ is greater than one). When δ is less than one, energy transfer is enhanced by this displacement, rather than diminished.

This change in the directionality of our control strategy is due to the fact that, when $\delta < 1$, the nuclear overlap between the antisymmetric ground vibrational states in the 1 and $1'$ electronic states is greater than the overlap between higher-excited vibrational states. That is,

$$\langle (0_A)_{1'} \mid (0_A)_1 \rangle > \langle (n_A)_{1'} \mid (n_A)_1 \rangle \tag{G.1}$$

for all n_A when $\delta < 1$. When $\delta > 1$ the relation (G.1) is reversed for n_A between one and four. In the low-J limit in which that approximate theory is valid, these nuclear overlaps are proportional to the oscillation frequency between antisymmetric nuclear states in the 1 and $1'$ electronic states. Therefore, for small (large) δ, the antisymmetric ground-vibrational state

will transfer amplitude faster (slower) than the coherent state created by vertical excitation of the ground state. We further showed that when $\delta = 1$ the type of intramolecular nuclear motion considered here has no effect on electronic population dynamics.

Here we show that this is consistent with the semiclassical picture that a wave packet that spends more time on, or near, the intersection of the potential energy surfaces will be experience greater EET. As a relative measure of the initial energy transfer, we take the amplitude of the wave packet in a region around the potential intersection, averaged over a single period of motion along the classical trajectory associated with the initial displacement. Just as in Appendix D, it is useful to switch symmetric and antisymmetric coordinates defined by $Q_S = (q_b + q_a)/\sqrt{2}$, and $Q_A = (q_b - q_a)/\sqrt{2}$, (see Fig. D.1). We define the semiclassical energy transfer parameter as

$$\zeta = \frac{1}{\tau_{\text{vib}}} \int_0^{\tau_{\text{vib}}} dt \int_{-\infty}^{\infty} dQ_A \int_{-\infty}^{\infty} dQ_S \left|\psi\left(Q_A, Q_S, t\right)\right| W\left(Q_A, Q_S\right), \tag{G.2}$$

where W is a window function that selects for amplitude near the potential intersection located at $Q_A = 0$.

We take $\psi\left(Q_A, Q_S, t\right)$ to be a minimum-uncertainty wave packet following the classical trajectory following from a given initial position on the 1-state potential. For times small compared with the time-scale for back-and-forth excitation transfer, $t \ll 2\pi/J$, this is a good approximation to the actual 1-state nuclear wave packet. We can write the amplitude for this wave packet, setting $\Delta q_{\text{rms}} \equiv \sqrt{\hbar/2m\omega} = 1$, as

$$\left|\psi\left(Q_A, Q_S, t\right)\right| = (2\pi)^{-1/2} \exp\left(-\frac{1}{4}\left((Q_S - \overline{Q}_S(t))^2 + (Q_A - \overline{Q}_S(t))^2\right)\right). \tag{G.3}$$

For simplicity we set $W\left(Q_A, Q_S\right) = \delta\left(Q_A\right)$,* which allows us to perform the spatial inte-

*One could just as easily choose a rectangular window function with a width ξ, by $W\left(Q_A, Q_S\right) = u\left(Q_A + \xi/2\right) - u\left(Q_A - \xi/2\right)$, where $u(x)$ is the Heavyside step function. The results are not qualitatively

gration in Eq.(G.2) and arrive at

$$\zeta = \sqrt{2} \int_0^{\tau_{\text{vib}}} dt e^{-\overline{Q}_A(t)^2/4}. \tag{G.4}$$

Just as we saw in Appendix D, only nuclear motion in the antisymmetric mode can affect EET.

We numerically evaluate Eq. (G.4) for the trajectories shown in Fig. 5.1, for values of δ between zero and two, and plot the results in Fig. G.1. This range of δ covers both DTA-12, where $\delta = 0.56$, and the model system treated in Subsection B.1 of Chapter III, where $\delta = 1.6$. We can see from the blue and purple traces in Fig. G.1 that when δ is small, negative acceptor-displacement results in a higher value for ζ than is found for vertical excitation while the reverse is true for larger δ. We see from the red trace that positive acceptor displacement results in a lower ζ value than vertical excitation for all δ in this range. This is in agreement with the results given in Chapters III and V for DTA-12, where short-time EET is enhanced by negative acceptor displacement and diminished by positive acceptor displacement. The value of δ at which negative acceptor displacement causes no change in ζ, located at $\delta \approx 1.07$, is in qualitative agreement with the results of Appendix D, where we find that a value of $\delta = 1$ leads to minimal change in the calculated survival probabilities.

The trajectories shown in Fig. 5.3 correspond exactly and oppositely to those in the in Fig. 5.1 when symmetric-mode motion is ignored. When the donor is negatively displaced, the antisymmetric coordinate oscillates between $d/\sqrt{2}$ and $-3d/\sqrt{2}$, the same range for positive acceptor displacement. When the donor is positively displaced, the antisymmetric coordinate is constant, just as it is when the acceptor is negatively displaced. This explains the mirror symmetry seen in the survival probabilities of Fig. 5.5, which include the effect of an actual control pulse on an oriented DTA-12 complex.

---

different in this case, but do depend on the choice of ξ.

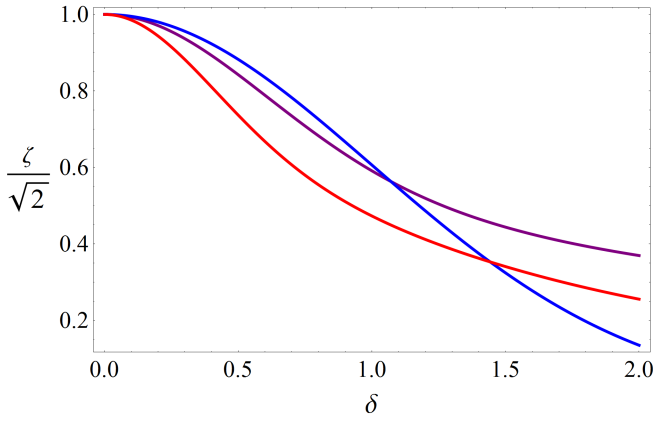

Figure G.1: Semiclassical EET parameter as a function of δ for three different wave-packet trajectories. The colors match the trajectories shown in Fig. 5.1, and are opposite to those shown in Fig. 5.3. The purple trace corresponds to vertical excitation, the red trace to positive acceptor displacement (or negative donor displacement), and the blue trace to negative acceptor displacement (or positive donor displacement).

Fig. G.1 also makes clear that ζ is a decreasing function of δ for all trajectories. This is consistent with the fact that the model systems of Subsections B.1 and B.2 of Chapter III feature similar timescales for energy transfer, as is seen in the survival probabilities of Figs. 3.1 and 3.6, even though the ratio J/ω is four times lower in DTA-12. Furthermore this fact is exemplified in the calculations on $(\mathrm{TFMA})_2$ in Chapter VI ($\delta \approx 6$), where back-and-forth electronic population oscillation of the sort seen in DTA-12 is suppressed even in the absence of a control pulse.

REFERENCES

Abe, M., Ohtsuki, Y., Fujimura, Y., and Domcke, W. (2005). Optimal control of ultrafast cis-trans photoisomerization of retinal in rhodopsin via a conical intersection. *Journal of Chemical Physics*, 123(14):144508.

Abramavicius, D. and Mukamel, S. (2010). Energy-transfer and charge-separation pathways in the reaction center of photosystem ii revealed by coherent two-dimensional optical spectroscopy. *The Journal of Chemical Physics*, 133(18):184501.

Amstrup, B. and Henriksen, N. E. (1992). Control of HOD photodissociation dynamics via bond-selective infrared multiphoton excitation and a femtosecond ultraviolet laser pulse. *Journal of Chemical Physics*, 97(11):8285–8295.

Anderson, P. (1958). Absence of diffusion in certain random lattices, phys. rev. 109, 1492 (1958). *Physical Review*, 109:1492.

Andrews, D. L. and Demidov, A. A. (1999). *Resonance Energy Transfer*. Wiley, Chichester, UK.

Asadian, A., Tiersch, M., Guerreschi, G. G., Cai, J. M., Popescu, S., and Briegel, H. J. (2010). Motional effects on the efficiency of excitation transfer. *New Journal of Physics*, 12:075019.

Ballard, J. B., Stauffer, H. U., Amitay, Z., and Leone, S. R. (2002). Optimization of wave packet coefficients in Li_2 using an evolutionary algorithm: The role of resonant and nonresonant wavelengths. *Journal of Chemical Physics*, 116(4):1350–1360.

Banin, U., Bartana, A., Ruhman, S., and Kosloff, R. (1994). Impulsive excitation of coherent vibrational motion ground surface dynamics induced by intense short pulses. *Journal of Chemical Physics*, 101(10):8461–8481.

Bardeen, C. J., Wang, Q., and Shank, C. V. (1998). Femtosecond chirped pulse excitation of vibrational wave packets in LD690 and bacteriorhodopsin. *Journal of Physical Chemistry A*, 102(17):2759–2766.

Becke, A. D. (1993). Density-functional thermochemistry 3. the role of exact exchange. *Journal of Chemical Physics*, 98(7):5648–5652.

Beljonne, D., Curutchet, C., Scholes, G. D., and Silbey, R. J. (2009). Beyond Förster resonance energy transfer in biological and nanoscale systems. *Journal Of Physical Chemistry B*, 113(19):6583–6599.

Biggs, J. D. and Cina, J. A. (2009a). Calculations of nonlinear wave-packet interferometry signals in the pump-probe limit as tests for vibrational control over electronic excitation transfer. *Journal of Chemical Physics*, 131(22):224101.

Biggs, J. D. and Cina, J. A. (2009b). Using wave-packet interferometry to monitor the external vibrational control of electronic excitation transfer. *Journal of Chemical Physics*, 131(22):224302.

Blankenship, R. E. (2001). *Molecular Mechanisms of Photosynthesis*. Wiley-Blackwell.

Bouchene, M. A., Nicole, C., and Girard, B. (1999). Wavepacket interferometry with chirped pulses. *Journal of Physics B-Atomic Molecular and Optical Physics*, 32(21):5167–5177.

Bradforth, S. E., Jimenez, R., Vanmourik, F., van Grondelle, R., and Fleming, G. R. (1995). Excitation transfer in the core light-harvesting complex (LH-1) of *rhodobacter sphaeroides*: An ultrafast fluorescence depolarization and annihilation study. *Journal of Physical Chemistry*, 99(43):16179–16191.

Brinks, D., Stefani, F. D., Kulzer, F., Hildner, R., Taminiau, T. H., Avlasevich, Y., Muellen, K., and Van Hulst, N. F. (2010). Visualizing and controlling vibrational wave packets of single molecules. *Nature*, 465(7300):905.

Brixner, T., Mančal, T., Stiopkin, I. V., and Fleming, G. R. (2004). Phase-stabilized two-dimensional electronic spectroscopy. *Journal of Chemical Physics*, 121(9):4221–4236.

Brixner, T., Stenger, J., Vaswani, H. M., Cho, M., Blankenship, R. E., and Fleming, G. R. (2005). Two-dimensional spectroscopy of electronic couplings in photosynthesis. *Nature*, 434(7033):625–628.

Buckup, T., Hauer, J., Mohring, J., and Motzkus, M. (2009). Multidimensional spectroscopy of beta-carotene: Vibrational cooling in the excited state. *Archives of Biochemistry and Biophysics*, 483(2):219–223.

Butcher, P. N. and Cotter, D. (1991). *The Elements of Nonlinear Optics*. Cambridge University Press, Cambridge.

Cangelosi, V. M., Sather, A. C., Zakharov, L. N., Berryman, O. B., and Johnson, D. W. (2007). Diastereoselectivity in the self-assembly of $As_2L_2Cl_2$ macrocycles is directed by the as-π interaction. *Inorganic Chemistry*, 46(22):9278–9284.

Cao, Y., Zhang, L., Yang, Y., Sun, Z. R., and Wang, Z. G. (2007). Molecular rovibrational dynamics investigated by two-photon wavepacket interferometry with phase-locked pulse pairs. *Chemical Physics Letters*, 442(1-3):53–57.

Caruso, F., Chin, A. W., Datta, A., Huelga, S. F., and Plenio, M. B. (2009). Highly efficient energy excitation transfer in light-harvesting complexes: The fundamental role of noise-assisted transport. *Journal of Chemical Physics*, 131(10):105106.

Chapman, C. T. and Cina, J. A. (2007). Semiclassical treatments for small-molecule dynamics in low-temperature crystals using fixed and adiabatic vibrational bases. *Journal of Chemical Physics*, 127(11):10.

Cheng, Y.-C., Engel, G. S., and Fleming, G. R. (2007). Elucidation of population and coherence dynamics using cross-peaks in two-dimensional electronic spectroscopy. *Chemical Physics*, 341(1-3):285–295.

Cheng, Y.-C. and Fleming, G. R. (2009). Dynamics of light harvesting in photosynthesis. *Annual Review of Physical Chemistry*, 60(1):241–262.

Cho, M. (2006). Coherent two-dimensional optical spectroscopy. *Bulletin of the Korean Chemical Society*, 27(12):1940–1960.

Cho, M. (2009). *Two-Dimensional Optical Spectroscopy*. CRC press, Boca Raton.

Christensson, N., Milota, F., Nemeth, A., Sperling, J., Kauffmann, H. F., Pullerits, T., and Hauer, J. (2009). Two-dimensional electronic spectroscopy of beta-carotene. *Journal of Physical Chemistry B*, 113(51):16409–16419.

Christopher, P. S., Shapiro, M., and Brumer, P. (2006). Quantum control of internal conversion in 24-vibrational-mode pyrazine. *Journal of Chemical Physics*, 125(12):124310.

Cina, J. A. (2000). Nonlinear wavepacket interferometry for polyatomic molecules. *Journal of Chemical Physics*, 113(21):9488–9496.

Cina, J. A. (2008). Wave-packet interferometry and molecular state reconstruction: Spectroscopic adventures on the left-hand side of the schrodinger equation. *Annual Review of Physical Chemistry*, 59:319–342.

Cina, J. A. and Fleming, G. R. (2004). Vibrational coherence transfer and trapping as sources for long-lived quantum beats in polarized emission from energy transfer complexes. *Journal of Physical Chemistry A*, 108(51):11196–11208.

Cina, J. A., Kilin, D. S., and Humble, T. S. (2003). Wave packet interferometry for short-time electronic energy transfer: Multidimensional optical spectroscopy in the time domain. *Journal of Chemical Physics*, 118(1):46–61.

Cohen-Tannoudji, C., Diu, B., and Laloë, F. (1977). *complement G_V*, volume 1, page 559. John Wiley & Sons, New York.

Collini, E. and Scholes, G. D. (2009). Electronic and vibrational coherences in resonance energy transfer along MEH-PPV chains at room temperature. *Journal of Physical Chemistry A*, 113(16):4223–4241.

Collini, E., Wong, C. Y., Wilk, K. E., Curmi, P. M. G., Brumer, P., and Scholes, G. D. (2010). Coherently wired light-harvesting in photosynthetic marine algae at ambient temperature. *Nature*, 463(7281):644–U69.

Cowan, M. L., Ogilvie, J. P., and Miller, R. J. D. (2004). Two-dimensional spectroscopy using diffractive optics based phased-locked photon echoes. *Chemical Physics Letters*, 386(1-3):184–189.

Dhar, L., Rogers, J. A., and Nelson, K. A. (1994). Time-resolved vibrational spectroscopy in the impulsive limit. *Chemical Reviews*, 94(1):157–193.

Ding, F. Fulmer, E. C. and Zanni, M. T. (2005). Heterodyned fifth-order two-dimensional IR spectroscopy: Third-quantum states and polarization selectivity. *Journal of Chemical Physics*, 123:094502.

Donoso, A., Kohen, D., and Martens, C. C. (2000). Simulation of nonadiabatic wave packet interferometry using classical trajectories. *Journal of Chemical Physics*, 112(17):7345–7354.

Egorova, D. and Domcke, W. (2004). Coherent vibrational dynamics during ultrafast photoinduced electron-transfer reactions: quantum dynamical simulations within multilevel Redfield theory. *Chemical Physics Letters*, 384(1-3):157–164.

Egorova, D., Gelin, M. F., and Domcke, W. (2005). Time- and frequency-resolved fluorescence spectra of nonadiabatic dissipative systems: What photons can tell us. *Journal of Chemical Physics*, 122(13):9793.

Egorova, D., Gelin, M. F., and Domcke, W. (2007). Analysis of cross peaks in two-dimensional electronic photon-echo spectroscopy for simple models with vibrations and dissipation. *Journal of Chemical Physics*, 126(7):11.

Elghobashi, N., Krause, P., Manz, J., and Oppel, M. (2003). IR+UV laser pulse control of momenta directed to specific products: Quantum model simulations for HOD*-> H+OD versus HO+D. *Physical Chemistry Chemical Physics*, 5(21):4806–4813.

Engel, G. S., Calhoun, T. R., Read, E. L., Ahn, T. K., Manŏcal, T., Cheng, Y. C., Blankenship, R. E., and Fleming, G. R. (2007). Evidence for wavelike energy transfer through quantum coherence in photosynthetic systems. *Nature*, 446(7137):782–786.

Farrow, D. A., Qian, W., Smith, E. R., Ferro, A. A., and Jonas, D. M. (2008). Polarized pump-probe measurements of electronic motion via a conical intersection. *Journal of Chemical Physics*, 128(14):144510.

Förster, T. (1965). *Delocalized excitation and excitation transfer*, volume 3, pages 93–137. Academic Press, New York.

Frisch, M. J., Trucks, G. W., Schlegel, H. B., Scuseria, G. E., Robb, M. A., Cheeseman, J. R., Scalmani, G., Barone, V., Mennucci, B., Petersson, G. A., Nakatsuji, H., Caricato, M., Li, X., Hratchian, H. P., Izmaylov, A. F., Bloino, J., Zheng, G., Sonnenberg, J. L., Hada, M., Ehara, M., Toyota, K., Fukuda, R., Hasegawa, J., Ishida, M., Nakajima, T., Honda, Y., Kitao, O., Nakai, H., Vreven, T., Montgomery, Jr., J. A., Peralta, J. E., Ogliaro, F., Bearpark, M., Heyd, J. J., Brothers, E., Kudin, K. N., Staroverov, V. N., Kobayashi, R., Normand, J., Raghavachari, K., Rendell, A., Burant, J. C., Iyengar, S. S., Tomasi, J., Cossi, M., Rega, N., Millam, N. J., Klene, M., Knox, J. E., Cross, J. B., Bakken, V., Adamo, C., Jaramillo, J., Gomperts, R., Stratmann, R. E., Yazyev, O., Austin, A. J., Cammi, R., Pomelli, C., Ochterski, J. W., Martin, R. L., Morokuma, K., Zakrzewski, V. G., Voth, G. A., Salvador, P., Dannenberg, J. J., Dapprich, S., Daniels, A. D., Farkas, O., Foresman, J. B., Ortiz, J. V., Cioslowski, J., and Fox, D. J. Gaussian 09 Revision A.2. Gaussian Inc. Wallingford CT 2009.

Fujiyoshi, S., Takeuchi, S., and Tahara, T. (2003). Time-resolved impulsive stimulated Raman scattering from excited-state polyatomic molecules in solution. *Journal of Physical Chemistry A*, 107(4):494–500.

Fujiyoshi, S., Takeuchi, S., and Tahara, T. (2004). Time-resolved impulsive stimulated raman studies of $1,1'$-binaphthyl in the excited state: Low-frequency vibrations and conformational relaxation. *Journal of Physical Chemistry A*, 108(28):5938–5943.

Fushitani, M., Bargheer, M., Guhr, M., Ibrahim, H., and Schwentner, N. (2008). Control of chromophore-to-bath coupling by interferometry: Cl_2 vibrational wave packets in solid ar. *Journal of Physics B-Atomic Molecular and Optical Physics*, 41(7):074013.

Gelman, D. and Kosloff, R. (2005). Minimizing broadband excitation under dissipative conditions. *Journal of Chemical Physics*, 123(23):11.

Harris, R. A. and Silbey, R. (1983). On the stabilization of optical isomers through tunneling friction. *Journal of Chemical Physics*, 78(12):7330–7333.

Hasegawa, H. and Ohshima, Y. (2008). Quantum state reconstruction of a rotational wave packet created by a nonresonant intense femtosecond laser field. *Physical Review Letters*, 101(5):4.

Hauer, J., Skenderovic, H., Kompa, K. L., and Motzkus, M. (2006). Enhancement of Raman modes by coherent control in beta-carotene. *Chemical Physics Letters*, 421(4-6):523–528.

Heller, E. J. (1981). The semiclassical way to molecular spectroscopy. *Accounts of Chemical Research*, 14(12):368–375.

Herek, J. L., Wohlleben, W., Cogdell, R. J., Zeidler, D., and Motzkus, M. (2002). Quantum control of energy flow in light harvesting. *Nature*, 417(6888):533–535.

Hernando, J., van Dijk, E., Hoogenboom, J. P., Garcia-Lopez, J. J., Reinhoudt, D. N., Crego-Calama, M., Garcia-Parajo, M. F., and van Hulst, N. F. (2006). Effect of disorder on ultrafast exciton dynamics probed by single molecule spectroscopy. *Physical Review Letters*, 97(21):216403.

Hiller, E. M. and Cina, J. A. (1996a). Can chirp enhance cumulative pre-resonant impulsive stimulated Raman excitation? *Journal of Chemical Physics*, 105(9):3419–3430.

Hiller, E. M. and Cina, J. A. (1996b). Can chirp enhance cumulative pre-resonant impulsive stimulated Raman excitation? *Journal of Chemical Physics*, 105(9):3419–3430.

Hoffmann, M. and Soos, Z. G. (2002). Optical absorption spectra of the Holstein molecular crystal for weak and intermediate electronic coupling. *Physical Review B*, 66(2):024305.

Humble, T. S. and Cina, J. A. (2004). Molecular state reconstruction by nonlinear wave packet interferometry. *Physical Review Letters*, 93(6):060402.

Humble, T. S. and Cina, J. A. (2006). Nonlinear wave-packet interferometry and molecular state reconstruction in a vibrating and rotating diatomic molecule. *Journal of Physical Chemistry B*, 110(38):18879–18892.

Ishizaki, A., Calhoun, T. R., Schlau-Cohen, G. S., and Fleming, G. R. (2010). Quantum coherence and its interplay with protein environments in photosynthetic electronic energy transfer. *Physical Chemistry Chemical Physics*, 12(27):7319–7337.

Ishizaki, A. and Fleming, G. R. (2009). Theoretical examination of quantum coherence in a photosynthetic system at physiological temperature. *Proceedings of the National Academy of Sciences of the United States of America*, 106(41):17255–17260.

Jang, S. (2007). Generalization of the Förster resonance energy transfer theory for quantum mechanical modulation of the donor-acceptor coupling. *Journal of Chemical Physics*, 127(17):174710.

Jang, S. (2009). Theory of coherent resonance energy transfer for coherent initial condition. *Journal Of Chemical Physics*, 131(16):164101.

Jang, S., Cheng, Y. C., Reichman, D. R., and Eaves, J. D. (2008). Theory of coherent resonance energy transfer. *Journal of Chemical Physics*, 129(10):101104.

Jang, S., Jung, Y. J., and Silbey, R. J. (2002). Nonequilibrium generalization of Förster-dexter theory for excitation energy transfer. *Chemical Physics*, 275(1-3):319–332.

Jang, S. J., Newton, M. D., and Silbey, R. J. (2004). Multichromophoric Förster resonance energy transfer. *Physical Review Letters*, 92(21):218301.

Jonas, D. M. (2003). Two-dimensional femtosecond spectroscopy. *Annual Review of Physical Chemistry*, 54:425–463.

Kahan, A., Nahmias, O., Friedman, N., Sheves, M., and Ruhman, S. (2007). Following photoinduced dynamics in bacteriorhodopsin with 7-fs impulsive vibrational spectroscopy. *Journal of the American Chemical Society*, 129(3):537–546.

Katsuki, H., Chiba, H., Meier, C., Girard, B., and Ohmori, K. (2009). Actively tailored spatiotemporal images of quantum interference on the picometer and femtosecond scales. *Physical Review Letters*, 102(10):103602.

Keusters, D., Tan, H. S., and Warren, W. S. (1999). Role of pulse phase and direction in two-dimensional optical spectroscopy. *Journal of Physical Chemistry A*, 103(49):10369–10380.

Kilin, D. S., Prezhdo, O. V., and Schreiber, M. (2007). Photoinduced vibrational coherence transfer in molecular dimers. *Journal of Physical Chemistry A*, 111(41):10212–10219.

Kishi, R., Nakano, M., Minami, T., Fukui, H., Nagai, H., Yoneda, K., and Takahashi, H. (2009). Theoretical study on exciton recurrence motion in anthracene dimer using the ab initio MO-CI based quantum master equation approach. *Journal of Physical Chemistry A*, 113(18):5455–5462.

Kjellberg, P., Bruggemann, B., and Pullerits, T. (2006). Two-dimensional electronic spectroscopy of an excitonically coupled dimer. *Physical Review B*, 74(2):9.

Lambert, W. R., Felker, P. M., Syage, J. A., and Zewail, A. H. (1984). Jet spectroscopy of anthracene and deuterated anthracenes. *Journal of Chemical Physics*, 81(5):2195–2208.

Lee, H., Cheng, Y. C., and Fleming, G. R. (2007). Coherence dynamics in photosynthesis: Protein protection of excitonic coherence. *Science*, 316(5830):1462–1465.

Leggett, A. J., Chakravarty, S., Dorsey, A. T., Fisher, M. P. A., Garg, A., and Zwerger, W. (1987). Dynamics of the dissipative two-state system. *Reviews of Modern Physics*, 59(1):1–85.

Li, C. Q., Wagner, W., Ciocca, M., and Warren, W. S. (2007). Multiphoton femtosecond phase-coherent two-dimensional electronic spectroscopy. *Journal of Chemical Physics*, 126(16):164307.

Lin, H., Hunter, J. A., and Pfab, J. (1993). Laser-induced fluorescence spectroscopy of jet-cooled 2-methylanthracene s_1 $(\pi\,\pi^*)$ - evidence for methyl conformation change upon electronic excitation. *Chemical Physics Letters*, 210(1-3):38–44.

Manŏcal, T., Nemeth, A., Milota, F., Lukes, V., Kauffmann, H. F., and Sperling, J. (2010). Vibrational wave packet induced oscillations in two-dimensional electronic spectra. ii. Theory. *Journal of Chemical Physics*, 132(18):184515.

Martinez-Galicia, R. and Romero-Rochin, V. (2005). Molecular wave packet interferometry and quantum entanglement. *Journal of Chemical Physics*, 122(9):11.

Matro, A. and Cina, J. A. (1995). Theoretical study of time-resolved fluorescence anisotropy from coupled chromophore pairs. *Journal of Physical Chemistry*, 99(9):2568–2582.

Mercer, I. P., El-Taha, Y. C., Kajumba, N., Marangos, J. P., Tisch, J. W. G., Gabrielsen, M., Cogdell, R. J., Springate, E., and Turcu, E. (2009). Instantaneous mapping of coherently coupled electronic transitions and energy transfers in a photosynthetic complex using angle-resolved coherent optical wave-mixing. *Physical Review Letters*, 102(5):057402.

Migani, A. and Olivucci, M. (2004). Conical intersections and organic reaction mechanisms. In Domcke, W. Yarkony, D. R. and Köppel, H., editors, *Conical Intersections. Electronic Structure, Dynamics, and Spectroscopy*, Singapore. World Scientific.

Milota, F., Sperling, J., Nemeth, A., Manŏcal, T., and Kauffmann, H. F. (2009). Two-dimensional electronic spectroscopy of molecular excitons. *Accounts of Chemical Research*, 42(9, Sp. Iss. SI):1364–1374.

Mohseni, M., Rebentrost, P., Lloyd, S., and Aspuru-Guzik, A. (2008). Environment-assisted quantum walks in photosynthetic energy transfer. *Journal of Chemical Physics*, 129(17):174106.

Monshouwer, R., Baltuska, A., van Mourik, F., and van Grondelle, R. (1998). Time-resolved absorption difference spectroscopy of the LH-1 antenna of *rhodopseudomonas viridis*. *Journal of Physical Chemistry A*, 102:4360.

Mukamel, S. (1995). *Principles of Nonlinear Optical Spectroscopy*. Oxford University Press, New York.

Mukamel, S. (2000). Multidimensional femtosecond correlation spectroscopies of electronic and vibrational excitations. *Annual Review of Physical Chemistry*, 51:691–729.

Nakagaki, M., Nishi, E., Sakota, K., Nishi, K., Nakano, H., and Sekiya, H. (2005). Internal rotation of methyl group in 2-and 1-methylanthracene studied by electronic spectroscopy and DFT calculations. *Chemical Physics*, 316(1-3):178–184.

Nemeth, A., Milota, F., Mančal, T., Lukeš, V., Hauer, J., Kauffmann, H. F., and Sperling, J. (2010). Vibrational wave packet induced oscillations in two-dimensional electronic spectra. i. Experiments. *The Journal of Chemical Physics*, 132(18):184514.

Novoderezhkin, V., Monshouwer, R., and van Grondelle, R. (1998). Electronic and vibrational coherence in the core light-harvesting antenna of *rhodopseudomonas viridis*. *Journal of Physical Chemistry B*, 104(50):12056–12071.

Novoderezhkin, V., Monshouwer, R., and van Grondelle, R. (2000). Electronic and vibrational coherence in the core light-harvesting antenna of *rhodopseudomonas viridis*. *Journal of Physical Chemistry B*, 104(50):12056–12071.

Ohmori, K. (2009). Wave-packet and coherent control dynamics. *Annual Review of Physical Chemistry*, 60:487–511.

Ohmori, K., Katsuki, H., Chiba, H., Honda, M., Hagihara, Y., Fujiwara, K., Sato, Y., and Ueda, K. (2006). Real-time observation of phase-controlled molecular wave-packet interference. *Physical Review Letters*, 96(9):093002.

Ohmori, K., Sato, Y., Nikitin, E. E., and Rice, S. A. (2003). High-precision molecular wave-packet interferometry with HgAr dimers. *Physical Review Letters*, 91(24):243003.

Ohtsuki, Y., Kono, H., and Fujimura, Y. (1998). Quantum control of nuclear wave packets by locally designed optimal pulses. *The Journal of Chemical Physics*, 109(21):9318–9331.

Panitchayangkoon, G., Hayes, D., Fransted, K. A., Caram, J. R., Harel, E., Wen, J., Blankenship, R. E., and Engel, G. S. (2010). Long-lived quantum coherence in photosynthetic complexes at physiological temperature. *Proceedings of the National Academy of Sciences of the United States of America*, 107(29):12766–12770.

Parr, R. G. and Yang, W. (1991). *Density-Functional Theory of Atoms and Molecules in Chemistry*. Springer, New York.

Plenio, M. B. and Huelga, S. F. (2008). Dephasing-assisted transport: quantum networks and biomolecules. *New Journal of Physics*, 10:113019.

Pollard, W. T., Felts, A. K., and Friesner, R. A. (1996). The Redfield equation in condensed-phase quantum dynamics. 93:77–134.

Popescu, S., Short, A. J., and Winter, A. (2006a). Entanglement and the foundations of statistical mechanics. *Nature Physics*, 2(11):754–758.

Popescu, S., Short, A. J., and Winter, A. (2006b). The foundations of statistical mechanics from entanglement: Individual states vs. averages.

Rackovsky, S. and Silbey, R. (1973). Electronic energy transfer in impure solids i. Two molecules embedded in lattice. *Molecular Physics*, 25(1):61–72.

Ramos-Sanchez, S. and Romero-Rochin, V. (2004). Preparation and resolution of molecular states by coherent sequences of phase-locked ultrashort laser pulses. *Journal of Chemical Physics*, 121(5):2117–2124.

Rebentrost, P., Mohseni, M., and Aspuru-Guzik, A. (2009). Role of quantum coherence and environmental fluctuations in chromophoric energy transport. *Journal of Physical Chemistry B*, 113(29):9942–9947.

Renger, T. May, V. and Kuhn, O. (2001). Ultrafast excitation energy transfer dynamics in photosynthetic pigment-protein complexes. *Physics Reports*, 343:137.

Rhee, H., Joo, T., Aratani, N., Osuka, A., Cho, S., and Kim, D. (2006). Intramolecular and intermolecular energy transfers in donor-acceptor linear porphyrin arrays. *Journal of Chemical Physics*, 125(7):8.

Rice, S. A. and Zhao, M. (2000). *Optical Control of Molecular Dynamics*. John Wiley and Sons, New York.

Scherer, N. F., Carlson, R. J., Matro, A., Du, M., Ruggiero, A. J., Romero-Rochin, V., Cina, J. A., Fleming, G. R., and Rice, S. A. (1991). Fluorescence-detected wave packet interferometry: Time resolved molecular spectroscopy with sequences of femtosecond phase-locked pulses. *Journal of Chemical Physics*, 95(3):1487–1511.

Scherer, N. F., Matro, A., Ziegler, L. D., Du, M., Carlson, R. J., Cina, J. A., and Fleming, G. R. (1992). Fluorescence-detected wave packet interferometry. ii. Role of rotations and determination of the susceptibility. *Journal of Chemical Physics*, 96(6):4180–4194.

Scholes, G. D. (2003). Long-range resonance energy transfer in molecular systems. *Annual Review of Physical Chemistry*, 54(1):57–87.

Seibt, J., Renziehausen, K., Voronine, D. V., and Engel, V. (2009). Probing the geometry dependence of molecular dimers with two-dimensional-vibronic spectroscopy. *Journal of Chemical Physics*, 130(13):134318.

Shen, Y. C. and Cina, J. A. (1999). What can short-pulse pump-probe spectroscopy tell us about Franck-Condon dynamics? *Journal of Chemical Physics*, 110(20):9793–9806.

Silbey, R. and Harris, R. A. (1989). Tunneling of molecules in low-temperature media: An elementary description. *Journal of Physical Chemistry*, 93(20):7062–7071.

Smith, T. J. and Cina, J. A. (1996). Toward preresonant impulsive Raman preparation of large amplitude vibrational motion. *Journal of Chemical Physics*, 104(4):1272–1292.

Smith, T. J., Ungar, L. W., and Cina, J. A. (1994). Resonant short-pulse effects on nuclear motion in the electronic ground state. *Journal of Luminescence*, 58(1-6):66–73.

Soules, T. F. and Duke, C. B. (1971). Resonant energy transfer between localized electronic states in a crystal. *Physical Review B*, 3(2):262.

Spano, F. C. (2002). Absorption and emission in oligo-phenylene vinylene nanoaggregates: The role of disorder and structural defects. *Journal of Chemical Physics*, 116(13):5877–5891.

Spano, F. C. (2003). The fundamental photophysics of conjugated oligomer herringbone aggregates. *Journal of Chemical Physics*, 118(2):981–994.

Subramanian, V. and Evans, D. G. (2004). Excitation energy transfer in model light-harvesting antennae. *Journal of Physical Chemistry B*, 108(3):1085–1095.

Sugawara, M., Yoshizawa, S., and Yabushita, S. (2001). Coherent control of wavepacket dynamics by locally designed external field. *Chemical Physics Letters*, 350(3-4):253–259.

Tekavec, P. F., Dyke, T. R., and Marcus, A. H. (2006). Wave packet interferometry and quantum state reconstruction by acousto-optic phase modulation. *Journal of Chemical Physics*, 125(19):19.

Tekavec, P. F., Lott, G. A., and Marcus, A. H. (2007). Fluorescence-detected two-dimensional electronic coherence spectroscopy by acousto-optic phase modulation. *Journal of Chemical Physics*, 127:214307.

Tian, P. F., Keusters, D., Suzaki, Y., and Warren, W. S. (2003). Femtosecond phase-coherent two-dimensional spectroscopy. *Science*, 300(5625):1553–1555.

Ungar, L. W. and Cina, J. A. (1997). Short-time fluorescence stokes shift dynamics. *Advances in Chemical Physics*, 100:171–228.

Ungar, L. W. and Cina, J. A. (1998). The relaxation dynamics and short-time optical response of a multimode open system. *Journal of Physical Chemistry A*, 102(38):7382–7392.

Vaughan, J. C., Hornung, T., Stone, K. W., and Nelson, K. A. (1007). Coherently controlled ultrafast four-wave mixing spectroscopy. *Journal of Physical Chemistry A*, 111(23):4873–4883.

Walsh, A. M. and Loring, R. F. (1990). Quantum mechanical analysis of impulsive stimulated light scattering from phonons. *Journal of Chemical Physics*, 93(11):7566–7580.

Wefers, M. M., Kawashima, H., and Nelson, K. A. (1998). Optical control over two-dimensional lattice vibrational trajectories in crystalline quartz. *Journal of Chemical Physics*, 108(24):10248–10255.

Weiner, A. M., Leaird, D. E., Wiederrecht, G. P., and Nelson, K. A. (1990). Femtosecond pulse sequences used for optical manipulation of molecular motion. *Science*, 247(4948):1317–1319.

Werschnik, J. and Gross, E. K. U. (2007). Quantum optimal control theory. *Journal of Physics B: Atomic Molecular and Optical Physics*, 40(18):R175–R211.

Werst, D. W., Brearley, A. M., Gentry, W. R., and Barbara, P. F. (1987). s_1 torsional potentials of substituted anthracenes. *Journal of the American Chemical Society*, 109(1):32–40.

Womick, J. M. and Moran, A. M. (2009). Exciton coherence and energy transport in the light-harvesting dimers of allophycocyanin. *Journal of Physical Chemistry B*, 113(48):15747–15759.

Yamazaki, I., Akimoto, S., Aratani, N., and Osuka, A. (2004). Observation of coherent recurrence motion of excitons in anthracene dimers. *Bulletin of the Chemical Society of Japan*, 77:1959.

Yamazaki, I., Akimoto, S., Yamazaki, T., Sato, S., and Sakata, Y. (2002). Oscillatory excitation transfer in dithiaanthracenophane: Quantum beat in a coherent photochemical process in solution. *Journal of Physical Chemistry A*, 106(10):2122–2128.

Yan, Y. J. and Mukamel, S. (1990). Femtosecond pump-probe spectroscopy of polyatomic molecules in condensed phases. *Physical Review A*, 41(11):6485–6504.

Yang, M. and Fleming, G. R. (2002). Influence of phonons on exciton transfer dynamics: comparison of the Redfield, Förster, and modified Redfield equations. *Chemical Physics*, 282(1):163.

Zhang, W. M., Meier, T., Chernyak, V., and Mukamel, S. (1998). Exciton-migration and three-pulse femtosecond optical spectroscopies of photosynthetic antenna complexes. *Journal of Chemical Physics*, 108(18):7763–7774.

Zheng, J. (2010). *FRET and Its Biological Application as a Molecular Ruler*. Biomedical Applications of Biophysics. Humana Press Inc.